



University of HUDDERSFIELD

University of Huddersfield Repository

Papananias, Moschos

COMBINED NUMERICAL AND STATISTICAL MODELLING FOR IN-DEPTH
UNCERTAINTY EVALUATION OF COMPARATIVE COORDINATE MEASUREMENT

Original Citation

Papananias, Moschos (2018) COMBINED NUMERICAL AND STATISTICAL MODELLING FOR IN-DEPTH UNCERTAINTY EVALUATION OF COMPARATIVE COORDINATE MEASUREMENT. Doctoral thesis, University of Huddersfield.

This version is available at <http://eprints.hud.ac.uk/id/eprint/34836/>

The University Repository is a digital collection of the research output of the University, available on Open Access. Copyright and Moral Rights for the items on this site are retained by the individual author and/or other copyright owners. Users may access full items free of charge; copies of full text items generally can be reproduced, displayed or performed and given to third parties in any format or medium for personal research or study, educational or not-for-profit purposes without prior permission or charge, provided:

- The authors, title and full bibliographic details is credited in any copy;
- A hyperlink and/or URL is included for the original metadata page; and
- The content is not changed in any way.

For more information, including our policy and submission procedure, please contact the Repository Team at: E.mailbox@hud.ac.uk.

<http://eprints.hud.ac.uk/>

COMBINED NUMERICAL AND STATISTICAL MODELLING
FOR IN-DEPTH UNCERTAINTY EVALUATION OF
COMPARATIVE COORDINATE MEASUREMENT

MOSCHOS PAPANANIAS

A thesis submitted to the University of Huddersfield in partial
fulfilment of the requirements for the degree of Doctor of
Philosophy

The University of Huddersfield in collaboration with Renishaw plc.

March 2018

Copyright Statement

- i. The author of this thesis (including any appendices and/or schedules to this thesis) owns any copyright in it (the “Copyright”) and s/he has given The University of Huddersfield the right to use such Copyright for any administrative, promotional, educational and/or teaching purposes.
- ii. Copies of this thesis, either in full or in extracts, may be made only in accordance with the regulations of the University Library. Details of these regulations may be obtained from the Librarian. This page must form part of any such copies made.
- iii. The ownership of any patents, designs, trademarks and any and all other intellectual property rights except for the Copyright (the “Intellectual Property Rights”) and any reproductions of copyright works, for example graphs and tables (“Reproductions”), which may be described in this thesis, may not be owned by the author and may be owned by third parties. Such Intellectual Property Rights and Reproductions cannot and must not be made available for use without permission of the owner(s) of the relevant Intellectual Property Rights and/or Reproductions.

Abstract

Quality assurance at low cost needs a tight interaction between machining and inspection. For this reason, the modern view of quality control (QC) requires highly repeatable coordinate measuring systems (CMSs) capable of being integrated into the manufacturing process for in-process feedback. Using this method, it becomes possible to reduce scrap levels and production costs while increasing part throughput. CMSs such as coordinate measuring machines (CMMs) have been used for decades in traditional manufacturing industry to ensure that the size and form of a part conform to design specifications. Although CMMs are considered as powerful and accurate measuring systems, most can only maintain or guarantee their measurement capability in quality control rooms typically having environmental temperature control systems set to maintain a nominal 20°C and maximum variation typically limited to $\pm 2^\circ\text{C}$. However, shop floor environments have significant variability in ambient temperature.

The need in manufacturing for dimensional inspection on the shop floor has led to many technological advancements in manufacturing metrology during recent years. In particular, a recent development includes a parallel kinematic machine (PKM)-based automatic flexible gauge, which is the system under investigation for this thesis. In order to be able to determine the measurement capability of a measuring or gauging machine to dimension a part reliably, it is necessary to evaluate the measurement uncertainties. This thesis first employs the design of experiments (DOE) approach to implement a practical analysis of measurement uncertainty of the automated flexible gauge. Several experimental designs are applied to investigate the influence of various key factors and their interaction on the uncertainty associated with coordinate measurement in comparator mode, in which the geometry of a part is compared with that of a calibrated master part nominally of the same shape. The ISO 15530-3 method is applied to derive uncertainty budgets for the flexible gauging system. A comparison is then made between typical shop floor measurement methods namely hard gauging, on-machine probing (OMP) and the automated flexible gauge. A set of identical test pieces was manufactured and then measured repeatedly using each method, with process and operator variability added as necessary to include typical industrial conditions. The measurement uncertainty is then calculated and compared for each of the measurements. The results show the measurement uncertainty of the comparator technique, which are lower than would be expected from an absolute measurement under workshop conditions.

Finally, Markov chain Monte Carlo (MCMC) methods are applied to evaluate uncertainty associated with comparative coordinate measurement using a more realistic probability model to avoid repeating measurements. Samples are drawn from the unnormalized posterior using Gibbs sampling. Another feature of this thesis is the developed empirical method based on Bayesian regularized artificial neural networks (BRANNs) for estimating point coordinates and associated uncertainties when no satisfactory measurement model can be developed and large experimental designs are not practical. The effectiveness of the proposed method is demonstrated using two case studies.

Acknowledgements

This thesis has been prepared as a requirement of the Doctor of Philosophy (PhD) degree. This PhD project was carried out in the Centre for Precision Technologies (CPT) at the University of Huddersfield. I would like to express my great thanks to my sponsor Renishaw plc. I would also like to deeply thank the University of Huddersfield for offering me the 100% Fee Waiver Scholarship - Vice Chancellor's Initiative.

I would also like to thank Dr Simon Fletcher and Professor Andrew Peter Longstaff for giving me the opportunity to undertake this so interesting project and for their kind encouragement and immense patience in supervising the project. They provided me with continuous support and guidance throughout the duration of my PhD. I really appreciate it and am indebted to both of them. Thanks also to Mr Andrew Bell for both his technical expertise and encouragement and Dr Naeem Shaukat Mian for his professionalism and support whenever it was needed.

I am also deeply grateful to Dr Azibananye Mengot, Dr Blake Kendrick, and Dr Kevyn Jonas from Renishaw plc for their invaluable support and feedback for many aspects of the work. Their immense knowledge helped me in all the time of my PhD. Thanks also to Mr Robin Palmer for the training on the Renishaw Equator gauge and MODUS Equator software and other people from Renishaw plc for their support throughout my research.

It is also a pleasure to express my sincerest gratitude to Professor Alistair Barrie Forbes from National Physical Laboratory (NPL) for his crucial contribution to this research project. I owe much to him for his willingness to devote time and energy to my work, but words cannot describe how thankful I am. Thanks also to Mr Arthur Jeffcoate from NPL at the University of Huddersfield for the training on hard gauging.

Finally, I would like to take this opportunity to express my deepest gratitude to my family, friends and colleagues who have helped in many ways, both professionally and personally.

Moschos Papananias
Huddersfield
March 2018

Contents

Abstract.....	1
Acknowledgements	3
Contents	4
List of Figures.....	7
List of Tables	10
Glossary of Terms	12
Nomenclature	15

Chapter 1

Introduction.....	18
1.1 Motivation	21
1.2 Aims.....	22
1.3 Objectives	22
1.4 Novel contributions	22
1.5 Thesis outline.....	23

Chapter 2

Review of Previous Research	25
2.1 Measurement error and uncertainty	25
2.2 Dimensional inspection	27
2.3 Evaluating the measurement uncertainty	32
2.4 Coordinate metrology	37
2.4.1 Part alignment.....	39
2.4.2 Scanning versus touch-trigger probe data capture	41
2.4.3 CMM configurations	42
2.4.4 Uncertainty associated with coordinate measurement.....	44
2.5 Comparative metrology	50
2.5.1 Renishaw Equator comparator	53
2.6 Summary.....	57

Chapter 3

Evaluating the Uncertainty of Comparator Measurement Influenced by Misalignments using Full Factorial Designs	59
3.1 Comparator measurement.....	60

3.2 Experimental design for 2D angular misalignment	61
3.3 Comparator measurement uncertainty evaluation	65
3.4 Experimental design for advanced part misalignment.....	68
3.4.1 Preliminary experiments for probe configuration.....	69
3.4.2 Main experiment for advanced part misalignment.....	72
3.5 Managing the re-mastering process	80
3.6 Summary.....	84

Chapter 4

Evaluating the Comparator Uncertainty within the Whole Working Volume and Statistical Modelling	85
4.1 Comparative coordinate measurement based on TTP	85
4.1.1 Diameter uncertainties for all part locations using TTP	87
4.2 Comparative coordinate measurement based on scanning	89
4.2.1 Diameter uncertainties for all part locations using scanning.....	91
4.3 Statistical modelling of comparator measurement uncertainty.....	94
4.3.1 Comparator measurement uncertainties associated with circularity.....	95
4.4 Summary.....	99

Chapter 5

Flexible Gauging Comparative Study	100
5.1 On-machine measurement	100
5.2 Hard gauging	105
5.3 Equator - CMM Compare.....	108
5.4 Comparison.....	111
5.5 Summary.....	120

Chapter 6

A Bayesian Approach to Evaluate Uncertainty associated with Comparative Coordinate Measurement	121
6.1 Modelling comparator measurement uncertainty	121
6.2 Experimental comparator measurements.....	124
6.3 Bayesian framework	125
6.4 Gibbs sampling from the posterior distribution.....	127
6.5 Summary.....	131

Chapter 7

Estimating Point Coordinates and associated Uncertainties using Artificial Intelligence

Techniques	133
7.1 Motivation and methodology.....	133
7.1.1 Artificial neural networks	134
7.2 CMM measurement case study.....	137
7.2.1 Simulation results for CMM case study	138
7.3 Comparator measurement case study	139
7.3.1 Simulation results for comparator case study.....	140
7.4 Summary.....	142

Chapter 8

Conclusions and Suggestions for Further Work.....	143
8.1 Summary and conclusions	143
8.2 Contribution to knowledge	145
8.3 Suggested further work.....	146
8.4 Refereed papers	147
References	148

Appendix A

Renishaw Equator Specifications and Experimental Data	159
--	------------

Appendix B

Discrete-time Markov chains.....	183
---	------------

List of Figures

Figure 2.1: Diagram depicting the difference between measurement error and uncertainty...	25
Figure 2.2: (a) CMM, (b) AACMM and (c) hard gauges.	28
Figure 2.3: The normal distribution.	36
Figure 2.4: Common CMM configurations [50].....	42
Figure 2.5: Equator 300 gauging system [105].....	54
Figure 2.6: Working volume (a) front view and (b) right view [105].	54
Figure 2.7: Terminology for Equator gauging machine [105].....	55
Figure 2.8: Software/hardware communication [105].	56
Figure 3.1: Measurement uncertainty contributors for CMMs and comparators.	60
Figure 3.2: Test setup on Equator gauge for gauge block inspection.	62
Figure 3.3: Angular misalignment of the gauge block.	64
Figure 3.4: Normal probability plot of the measured length.	66
Figure 3.5: Main effects plots for expanded measurement uncertainties.	67
Figure 3.6: 3D offset by tilt for the conrod.	69
Figure 3.7: Test setup on Renishaw Equator for preliminary experiments.	70
Figure 3.8: Diameter of small circle versus probe configuration.	71
Figure 3.9: Length distance 2 versus probe configuration.....	71
Figure 3.10: Test setup on Renishaw Equator for main experiment.....	73
Figure 3.11: Sample of ambient temperature.....	73
Figure 3.12: Main effects plots for the uncertainties of small circle diameter.	75
Figure 3.13: Main effects plots for the uncertainties of medium circle diameter.....	75
Figure 3.14: Main effects plots for the uncertainties of large circle diameter.	76
Figure 3.15: Main effects plots for the uncertainties of length distance 1.....	76
Figure 3.16: Main effects plots for the uncertainties of length distance 2.....	77
Figure 3.17: Main effects plots for the uncertainties of length distance 3.....	77
Figure 3.18: The interaction plot of measurement mode and angular misalignment for the uncertainties of length distance 3.....	79
Figure 3.19: The interaction plot of CRF and angular misalignment for the uncertainties of length distance 3.	79
Figure 3.20: Boxplot of the diameter of small circle.	81
Figure 3.21: Boxplot of the diameter of medium circle.....	81
Figure 3.22: Boxplot of the diameter of large circle.....	82

Figure 3.23: Boxplot of the length distance 1.....	82
Figure 3.24: Boxplot of the length distance 2.....	83
Figure 3.25: Boxplot of the length distance 3.....	83
Figure 4.1 Test setup on Equator gauge for the clutch plate.	86
Figure 4.2 Clutch plate locations.	87
Figure 4.3: Main effects plots for the uncertainties of internal diameter.....	88
Figure 4.4 Main effects plots for the uncertainties of external diameter.	88
Figure 4.5: RESR ring part.	90
Figure 4.6 RESR ring locations.	91
Figure 4.7: Main effects plots for the uncertainties of diameter of large circle.....	92
Figure 4.8: Main effects plots for the uncertainties of diameter of medium hole.	92
Figure 4.9: Main effects plots for the uncertainties of diameter of small hole.....	93
Figure 4.10: Main effects plots for the uncertainties of Y_5	97
Figure 4.11: Main effects plots for the uncertainties of Y_{11}	97
Figure 4.12: Main effects plots for the uncertainties of Y_{13}	98
Figure 4.13: The interaction plot of scanning speed and sampling point density for the uncertainties of Y_5	98
Figure 4.14: The interaction plot of scanning speed and sampling point density for the uncertainties of Y_{13}	99
Figure 5.1: Test setup on a 5-axis CNC machining center.	102
Figure 5.2: CAD model of the measurement part.....	102
Figure 5.3: OMP combined expanded uncertainties.....	104
Figure 5.4: Sample of G6 temperature.....	104
Figure 5.5: Test setups using hard gauges.	106
Figure 5.6: Combined expanded uncertainties for G4 from hard gauging.	107
Figure 5.7: Combined expanded uncertainties for G6 from hard gauging.	107
Figure 5.8: Test setup on Equator gauge for CMM Compare method.	109
Figure 5.9: Sample of master part temperature.....	110
Figure 5.10: Equator combined expanded uncertainties.....	111
Figure 5.11: Comparison between OMP and Equator uncertainties for G2.....	112
Figure 5.12: Comparison between OMP and Equator uncertainties for G3.....	112
Figure 5.13: Comparison between OMP, hard gauging and Equator uncertainties for G4...	113
Figure 5.14: Comparison between OMP and Equator uncertainties for G5.....	113
Figure 5.15: Comparison between OMP, hard gauging and Equator uncertainties for G6...	114

Figure 5.16: Comparison between OMP and Equator uncertainties for G7.....	114
Figure 5.17: Comparison between OMP and Equator uncertainties for G8.....	115
Figure 5.18: Comparison between OMP and Equator residuals for G2.....	116
Figure 5.19: Comparison between OMP and Equator residuals for G3.....	116
Figure 5.20: Comparison between OMP, hard gauging and Equator residuals for G4.....	117
Figure 5.21: Comparison between OMP and Equator residuals for G5.....	117
Figure 5.22: Comparison between OMP, hard gauging and Equator residuals for G6.....	118
Figure 5.23: Comparison between OMP and Equator residuals for G7.....	118
Figure 5.24: Comparison between OMP and Equator residuals for G8.....	119
Figure 6.1: Comparator measurement uncertainty contributors.....	123
Figure 6.2: Test setup on Renishaw Equator flexible gauge.....	125
Figure 6.3: Trace plot of the Gibbs sampling chain after burn-in for measurand A.....	130
Figure 6.4: Bar graph for standard uncertainties.....	131
Figure 7.1 A perceptron.....	135
Figure 7.2: An MLP network architecture.....	136
Figure 7.3: The MLP network with five hidden neurons.....	138
Figure 7.4: Test set up on comparator gauge.....	140

List of Tables

Table 2.1: Number of contact points required per feature.	40
Table 2.2: Geometric errors in a 3-axis Cartesian machine.	45
Table 3.1: Factors and levels of the gauge block inspection.	64
Table 3.2: Values for the angular misalignment.	64
Table 3.3: Factors and levels of the conrod inspection.	69
Table 3.4: ANOVA results for the conrod inspection.	74
Table 3.5: Factors and levels for the DOE concerned with managing re-mastering.	80
Table 4.1: Factors and levels of the clutch plate inspection.	87
Table 4.2: Factors and levels of the RESR ring inspection.	90
Table 4.3: ANOVA results for the RESR ring inspection.	93
Table 4.4: ANOVA results for circularity.	96
Table 5.1: Measurands for flexible gauging comparative study.	103
Table 5.2: DOE for hard gauging.	105
Table 5.3: Implementation details for factor A.	106
Table 6.1: Measurands for probabilistic modelling.	125
Table 7.1: Performance of BRANN models.	139
Table 7.2: Performance of BRANN models with two hidden layers.	139
Table 7.3: Performance of MLP models for comparator data.	141
Table 7.4: Performance of Elman models for comparator data.	142
Table A.1: Equator machine specifications.	159
Table A.2: Operating conditions.	159
Table A.3: Equator controller specifications and electrical ratings.	160
Table A.4: Mean values and associated expanded uncertainties for $k = 2$ from the DOE with the gauge block.	161
Table A.5: Mean values from the DOE with the conrod part.	162
Table A.6: Expanded uncertainties for $k = 2$ from the DOE with the conrod part.	163
Table A.7: Mean values from the DOE for managing re-mastering.	164
Table A.8: Mean values and associated expanded uncertainties for $k = 2$ from the DOE with the clutch plate.	165
Table A.9: Mean values and associated expanded uncertainties for $k = 2$ from the DOE with the RESR ring.	166
Table A.10: Mean values for small-size holes from the DOE concerned with circularity.	167

Table A.11: Mean values for medium-size holes and large circle from the DOE concerned with circularity.	167
Table A.12: Expanded uncertainties for $k = 2$ for small-size holes from the DOE concerned with circularity.	168
Table A.13: Expanded uncertainties for $k = 2$ for medium-size holes and large circle from the DOE concerned with circularity.	168
Table A.14: OMP combined expanded uncertainties for $k = 2$	169
Table A.15: Hard gauging combined expanded uncertainties for $k = 2$ from operator 1 for G4.	170
Table A.16: Hard gauging combined expanded uncertainties for $k = 2$ from operators 2-7 for G4.	170
Table A.17: Hard gauging combined expanded uncertainties for $k = 2$ from operator 1 for G6.	171
Table A.18: Hard gauging combined expanded uncertainties for $k = 2$ from operators 2-7 for G6.	171
Table A.19: Equator combined expanded uncertainties for $k = 2$	172
Table A.20: CMM results for the comparative study.	173
Table A.21: OMP and Equator residuals for G2 and G3.	174
Table A.22: OMP, hard gauging, and Equator residuals for G4.	175
Table A.23: OMP and Equator residuals for G5.	176
Table A.24: OMP, hard gauging, and Equator residuals for G6.	177
Table A.25: OMP and Equator residuals for G7 and G8.	178
Table A.26: Testing, training, and MLP model 1 standard uncertainties for the comparator.	179
Table A.27: MLP model 2, 3, and 4 standard uncertainties for the comparator.	180
Table A.28: MLP model 5 and Elman model 1 standard uncertainties for the comparator. .	181
Table A.29: Elman model 2 and 3 standard uncertainties for the comparator.	182

Glossary of Terms

AACMM	Articulated Arm Coordinate Measuring Machine
AI	Artificial Intelligence
AMCM	Adaptive Monte Carlo Method
ANN	Artificial Neural Network
ANOVA	Analysis of Variance
BIPM	Bureau International des Poids et Mesures
BP	Back-Propagation
BRANN	Bayesian Regularized Artificial Neural Network
CMM	Coordinate Measuring Machine
CMS	Coordinate Measuring System
CNC	Computer Numerically Controlled
CPT	Centre for Precision Technologies
CRF	Coordinate Reference Frame
CTE	Coefficient of Thermal Expansion
DME	Dimensional Measuring Equipment
DMIS	Dimensional Measuring Interface Standard
DOE	Design of Experiment
DOF	Degrees of Freedom
DRF	Datum Reference Frame
DTI	Dial Test Indicator
GUF	GUM Uncertainty Framework
GUM	Guide to the expression of Uncertainty in Measurement
GUMS1	GUM Supplement 1
IGA	Improved Genetic Algorithm
ISO	International Organization for Standardization
JCGM	Joint Committee for Guides in Metrology

LSM	Least Squares Method
LTG	Linear Threshold Gate
MCM	Monte Carlo Method
MCMC	Markov Chain Monte Carlo
MCS	Machine Coordinate System
MLP	Multi-Layer Perceptron
MSE	Mean Squared Error
MZM	Minimum Zone Method
MZS	Minimum Zone Solution
NIST	National Institute of Standards and Technology
NPL	National Physical Laboratory
OLS	Ordinary Least Squares
OMM	On-Machine Measurement
OMP	On-Machine Probing
PCD	Pitch Circle Diameter
PCS	Part Coordinate System
PDF	Probability Density Function
PKM	Parallel Kinematic Machine
PSO	Particle Swarm Optimization
QC	Quality Control
QPSO	Quasi Particle Swarm Optimization
R&R	Repeatability and Reproducibility
RSS	Root Sum of the Squares
SI	International System of Units
TLU	Threshold Logic Unit

TTP	Touch-Trigger Probing
Type A	Method of evaluation of uncertainty by the statistical analysis of series of observations
Type B	Method of evaluation of uncertainty by means other than the statistical analysis of series of observations
UCC	Universal CMM Controller
UES	Uncertainty Evaluation Software
VCMM	Virtual CMM
2D	Two-dimensional
3D	Three-dimensional

Nomenclature

b	Systematic error
D_j	j th level of sampling point density
e	Systematic effects
e_{a_i}	Systematic effects associated with the ambient temperature
e_{w_i}	Systematic effects associated with the part temperature
ϵ_i	Random effects
f	Functional relationship
I	n -by- n identity matrix
$\text{IG}(\alpha_0, \beta_0)$	Inverse Gamma distribution with shape α_0 and scale β_0
k	Coverage factor
l	Measured dimension
L_r	The true length of the gauge block
n	Number of repeated observations
n_f	Number of contact points used to define each feature
$N(\mu, \sigma^2)$	Gaussian distribution with parameters μ and σ^2
N	Gibbs sample size
p	Probability
p_{ij}	Transition probabilities
$p(\boldsymbol{\theta})$	Prior distribution
$p(\boldsymbol{y})$	Prior predictive distribution
$p(\boldsymbol{\theta}, \boldsymbol{y})$	Joint PDF or probability mass function
$p(\boldsymbol{\theta} \boldsymbol{y})$	Posterior distribution
$p(\boldsymbol{y} \boldsymbol{\theta})$	Likelihood
$p(\tilde{\boldsymbol{y}} \boldsymbol{y})$	Posterior predictive distribution
$P(t, \nu)$	The PDF of the t -distribution
$r_{ij}(n)$	n -step transition probabilities
R^2	Percentage of the response variable variation explained by the regression model
s^2	Experimental variance
s	Experimental standard deviation
$s(\bar{x})$	Experimental standard deviation of the mean \bar{x}
\mathbf{S}	A finite set of possible states

S_i	i th level of scanning speed
$(SD)_{ij}$	Interaction between the i th level of first factor and the j th level of second factor
T	Average temperature of the calibrated part during measurement
$u(\mathcal{Y})$	Standard uncertainty in \mathcal{Y}
$u(x_{ij})$	Standard uncertainty of the measurement procedure associated with the i th level of first factor and the j th level of second factor
u_c	Combined standard uncertainty
U	Expanded uncertainty
U_{ij}	Expanded uncertainty associated with the i th level of first factor and the j th level of second factor
ν	Degrees of freedom of a t -distribution
\mathbf{V}_0	Symmetric positive definite matrix
w_i	Weight associated with the i^{th} input of a perceptron
w_0	Weight associated with the bias input of a perceptron
\bar{x}	Sample mean value
\bar{x}_{ij}	Sample mean value associated with the i th level of first factor and the j th level of second factor
x_f	The mathematical minimum number of points required to define a given feature
x_i	i th indication in a series
x_i	i th input of a perceptron
x_i	i th x -coordinate
x_i^*	i th nominal x -coordinate
\mathbf{X}	n -by- m matrix of predictors
\mathcal{Y}	Estimate of measurand Y
\mathcal{Y}_{ijn}	n th observed value of measurand Y for each i and j
\mathcal{Y}	Observed data
$\tilde{\mathcal{Y}}$	Future data
Y	A measurand
Υ	Output of a perceptron
α	The perpendicular distance of the projected sensing points from the calculated perpendicular to the surface
\mathbf{a}	m -by-1 vector of regression coefficients

γ	The angle between the calculated and actual perpendiculars
Γ	The gamma function
θ_i	i th unobservable quantity
μ or α	The true value or the expectation of the measurand
π_j	Steady-state probabilities
σ^2	Variance of a quantity characterized by a probability distribution
σ	Standard deviation of a quantity characterized by a probability distribution
σ_{pc}	Point coordinate error

Chapter 1

Introduction

In the manufacturing industry, manually-operated measurement devices such as micrometres, callipers, go/no-go gauges, and height gauges have been traditionally used for decades to assess whether a manufactured part is within tolerances or not. However, this inspection approach can be time consuming, it results in high measurement uncertainties, and, the repeatability, reproducibility, and part throughput depend on operators. Also, manual gauging tends to be inflexible to product design changes and can be costly due to the required calibration of each hard gauge.

With advances in machine automation over the last few decades, companies have been able use measurement systems as an alternative to operators performing manual measurements with custom hard gauging in order to reduce cycle times. Coordinate measuring systems (CMSs) such as coordinate measuring machines (CMMs) have been used extensively in manufacturing for a large range of measurement tasks because of their efficiency, flexibility and accuracy, assuming that they have been calibrated correctly and are being maintained in stable temperature controlled conditions, typically at 20°C. Evaluating the measurement uncertainty associated with CMM, however, is not straightforward since such systems are influenced by a large number of factors including both random and systematic effects, which are difficult to quantify [1]. In addition, as the need for shorter cycle times of measurement tasks and in-process feedback increases, serious attention has been paid to place the dimensional measurement equipment close to the machining process for close-to-manufacturing measurement while ensuring fast and precise dimensional control on the shop floor. Four basic CMM types can be distinguished: bridge, cantilever, horizontal arm, and gantry. Bridge machines are built in sizes ranging from 300 × 300 × 300 mm XYZ to 2000 mm × 5000 × 1500 mm. The accuracy of bridge machines is usually better than other types of machines, but they suffer from the limited accessibility to the part being measured due to their structure. The measuring range and accuracy of the CMM are critical selection criteria when selecting a CMM. The ISO 10360 series of standards addresses the accuracy testing and performance

verification of CMMs. Cantilever machines are generally used for measuring relatively small parts. Their accuracy is similar to that of bridge type or even higher. Horizontal arm machines are the least accurate of the four basic types CMMs, with most horizontal arm machines to perform to volumetric tolerances of 30 μm . Horizontal arm machines are usually used for measuring of large parts or parts, which have hard-to-reach features. The measuring range of horizontal arm machines usually vary from $2 \times 2 \times 1 \text{ m XYZ}$ to $4 \times 10 \times 3 \text{ m XYZ}$. Gantry machines are usually used for very large or heavy parts that require the precision of a bridge type machine. The measuring range of gantry machines usually varies from $1 \times 2 \times 1 \text{ m XYZ}$ to $4 \times 10 \times 3 \text{ m XYZ}$. Further details of CMM configurations are discussed in section 2.4.3. Over the years, enhanced CMMs, which are typically CMMs integrated with advanced thermal compensation techniques, have been proposed for shop floor dimensional inspection. However, enhanced CMMs increase the already high cost of such systems, and, in many practical applications, they are unable to reach the required inspection speeds while maintaining their repeatability due to their heavyweight structure.

Computer numerically controlled (CNC) machine tools can also be used as CMMs by exchanging the cutting tool for a touch-trigger probing (TTP) system. However, the level of measurement uncertainty achieved is often critically high since the same errors that influence the manufacturing process are also transferred to the inspection process. Consequently, this measurement approach requires supplementing with independent measurements for applications with high accuracy requirements due to the fundamental metrological limitations. Recently, parallel kinematic machines (PKMs) have been employed in the manufacturing industry for a wide range of applications such as machining, assembling and picking. PKMs are very lightweight and stiff (relative to the mass) in comparison to Cartesian machines and thus allowing for high repeatability at fast operating speeds.

Coordinate measurements can also be made in a gauging/comparator mode in which measurements of a production part are compared with those of a master part with known dimensions. The main advantage of operating in comparator mode is that the measurement system has only to provide relative measurements which are considered more accurate than absolute measurements. Another advantage is that many of the difficulties associated with evaluating the measurement uncertainties associated with CMMs operating in absolute mode are largely avoided since many of the systematic effects in the measurement system cancel out.

Motivated by the need for in-process feedback and the fact that one of the most critical factors affecting CMM performance on the shop floor is the variability in ambient temperature, Renishaw plc has developed a novel comparator gauging system called the Equator™ Gauge to fill the gap between CMM measurement and custom hard gauging. The Renishaw Equator is a variable gauge that employs the comparator principle through software to account for the influence of systematic effects associated with the measurement system. The Equator machine is constructed with a parallel kinematic constraint mechanism to minimise the machine's dynamic errors at high measurement speeds. To compensate for any change in temperature of the shop floor environment, the re-mastering process can be managed with the built-in temperature sensor and software configuration. So, a PKM-based flexible gauge provides all of the automation features of tactile CMMs, but it does so without actually requiring temperature controlled conditions due to the comparator principle. However, the traceability path is not as well defined due to comparator measurement results originating from indirect measurement. According to the manufacturer's specification, the comparison uncertainty is ± 0.002 mm and the maximum part weight, including the fixture plate, is 25 kg. The machine has a cylindrical working envelope with the dimensions XY $\phi 300$ mm and Z 150 mm. A detailed description of the comparator system is provided in section 2.5.1.

This thesis is focused on evaluating the measuring performance of PKM-based flexible gauges employed in shop floor conditions over traditional inspection methods. The Renishaw Equator 300 based in the Centre for Precision Technologies (CPT) at the University of Huddersfield is the automated flexible gauge under investigation. In this thesis, the design of experiments (DOE) approach is applied to investigate the effect of various key factors and their interaction on the comparator measurement uncertainty. The DOE method is used in many fields of science and engineering to assess the sensitivity of a process response (dependent variable) to a number of factors (independent variables) involved with the minimum calculation effort and cost. However, like CMMs, automated flexible gauges are multipurpose measuring/gauging systems. Therefore, the tests carried out during this work to quantify the comparator measurement uncertainties could not involve all the possible measurement tasks performed by such dimensional measurement systems. On the contrary, special attention was paid to a certain set of part features and characteristics to cover most of the common measurement tasks performed by flexible gauging systems. In addition, the experimental designs employed in this thesis are intended to be representative of the actual working conditions in which automated

flexible gauges are used. The Equator gauge has been designed for high speed comparative gauging on the shop floor with possibly wide temperature variation. Hence, the experiments are performed in both temperature controlled and uncontrolled environments. Therefore, multiple experimental runs (replicates) are used where required at different temperature conditions to decouple the influence of environmental effects and thus drawing more refined conclusions on the statistical significance.

Furthermore, a Markov chain Monte Carlo (MCMC) model is developed to evaluate the uncertainty associated with comparative coordinate measurement. Over the last three decades, the Bayesian approach to statistical inference has re-emerged due to the rapid developments in computing and demand in many fields of science and technology for modelling more realistically complex phenomena, systems or processes that have many parameters.

The hardware performance of a CMS is determined by the measurement uncertainties in the point coordinates. Due to the limitations and difficulties in implementation of currently used measurement uncertainty evaluation methods, a new method based on Bayesian regularized artificial neural networks (BRANNs) is developed to estimate the uncertainty of the coordinates of each measured point gathered by a CMS, operating either in absolute or comparator mode. The method is proposed to aid the determination of uncertainty contributors associated with a particular axis of a Cartesian CMS such as a CMM when no satisfactory mathematical model can be derived and enable very efficient implementations of geometric element best-fit algorithms implemented in CMM and comparator coordinate data.

1.1 Motivation

The demand in the manufacturing industry for increasing part quality while reducing inspection cycle times and manufacturing costs has been the driving force for many research projects. Over the last few years, various techniques and metrological instruments have been proposed to achieve fast and accurate dimensional inspection on the shop floor at low cost. An efficient solution that has been recently adopted for this complex task is to perform comparative coordinate measurement using a PKM based on the Delta robot architecture. In this way, parts can be independently inspected in the shop floor environment within a shorter time while also enabling feedback to the production loop. An essential part of assessing whether a measurement or gauging system meets its intended purpose is to estimate the measurement

uncertainties. This thesis employs several experimental designs to evaluate the performance of automated flexible gauge and applies computational Bayesian methods and nature-inspired computational methods to improve the assessment of uncertainty associated with comparative coordinate measurement.

1.2 Aims

- To evaluate the use of modern automated gauging in the production feedback loop.
- To produce efficient methods for evaluating uncertainty associated with comparative coordinate measurement.

1.3 Objectives

- Implement a practical analysis of uncertainty of measurement of the automated gauging system within its whole measuring volume in both temperature controlled and shop floor environments.
- Apply the DOE method to investigate the influence of various key factors and their interaction on the uncertainty associated with comparative coordinate measurement. In particular, induce known errors such as part setup offsets in the automated gauging process to investigate the impact of part misalignment from rotation between master and measure coordinate frames on the comparator measurement uncertainty.
- Perform a full analysis of measurement uncertainty of automated flexible gauge in comparison with traditional gauging systems and on-machine probing (OMP).
- Investigate and apply MCMC methods to evaluate uncertainty associated with comparative coordinate measurement according to Bayesian principles.
- Produce and assess an empirical method to estimate the uncertainty of measurement in the coordinates of each contact point.

1.4 Novel contributions

- Establishment of the influence of various key factors and their interaction on the uncertainty associated with comparative coordinate measurement through full factorial designs.

- Development of a statistical model for uncertainty associated with comparative coordinate measurement.
- The in-depth comparison between shop floor dimensional measurement systems in manufacturing.
- Application of MCMC methods to automated flexible gauging influenced by process variations for comparator measurement uncertainty evaluation.
- Development of a novel method based on BRANNs for estimating point coordinates and associated uncertainties.

1.5 Thesis outline

The work presented in this thesis is structured into eight chapters providing the necessary background material with the research contribution detailed in five relatively self-contained chapters. More specifically, a breakdown of the work presented in this thesis is as follows.

Chapter 2 reviews the state of the art literature in manufacturing metrology with the main focus on dimensional inspection methods, uncertainty associated with CMSs, and comparative metrology.

Chapter 3 is the first of the five chapters that present original contributions. It describes the experimental designs performed to investigate the influence of measurement strategy and part misalignment from rotation between master and measure coordinate frames on the uncertainty associated with comparative coordinate measurement.

Chapter 4 is concerned with the experimental designs performed to investigate the influence of part location on the comparator measurement uncertainty. This chapter is also concerned with the development of a statistical model for uncertainty associated with comparative coordinate measurement through analysis of variance (ANOVA) techniques.

Chapter 5 presents a comparative study between automated flexible gauging, hard gauging, and OMP. The work uses a broad range of repeated measurements on nominally identical parts to support the statistical evaluation of the uncertainty for common characteristics.

Chapter 6 applies computational Bayesian methods to evaluate uncertainty associated with comparative coordinate measurement. Alternating conditional sampling (Gibbs sampling) is applied to generate samples from the posterior distribution using experimental comparator measurements.

Chapter 7 develops a new method based on BRANNs to estimate point coordinates and associated uncertainties. The method is first introduced using simulated coordinate data representing CMM measurements and then using experimental comparator coordinate data.

Chapter 8 summarises the results obtained throughout this thesis and draws conclusions. It also suggests some points for further research.

Chapter 2

Review of Previous Research

This chapter provides the literature review of manufacturing metrology relevant to this thesis. It commences by describing measurement uncertainty and providing an overview of different measurement principles and inspection approaches. Then, a comprehensive review of the major approaches to measurement uncertainty evaluation is conducted. This is followed by discussion of coordinate metrology with the main focus on the uncertainty associated with CMM measurement. The chapter ends with comparative metrology and automated flexible gauging as well as a brief summary of the literature review.

2.1 Measurement error and uncertainty

Metrology is the science that deals with measurement and its application [2, 3]. It is essential not to confuse, in a measurement result, the terms *error* and *uncertainty*. Measurement error is the measurement result minus the true value of the measurand (physical quantity intended to be measured). Any error that is not recognized gives rise to measurement uncertainty; it is a quantification of the doubt about the validity of the result of any measurement. Figure 2.1 illustrates the difference between measurement error and measurement uncertainty as depicted in [4].

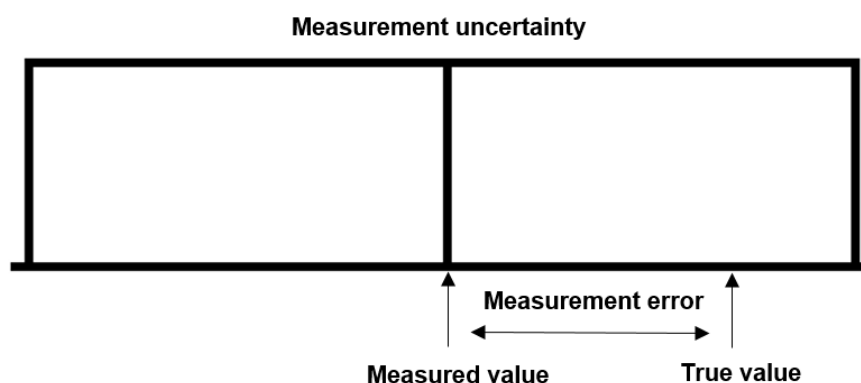


Figure 2.1: Diagram depicting the difference between measurement error and uncertainty.

The doubt about a measurement result has two aspects. One is the interval (confidence interval or coverage probability) that states the width of the margin, or in other words, the margin within which the true value being measured can be said to lie, with a given confidence level. The other aspect is the confidence level expressing the degree of confidence that the result lies within that margin. Sources of uncertainty in measurement can arise from a random component, where repeating the measurement gives a randomly different result, and a systematic component where the same influence has a predictable impact on the result for each of the repeated measurements [5].

In order to calculate the uncertainty of a measurement [6], the first step is to identify the sources of uncertainty in the measurement and then to estimate the size of the uncertainty from each source. Finally, all the individual uncertainties are combined to give an overall figure. There are two ways to estimate uncertainties regardless of any sources:

- Type A: Evaluation of uncertainty by statistical methods.
- Type B: Evaluation of uncertainty by non-statistical methods.

Uncertainty contributions must be expressed in similar terms before their combination. This means that, the same units and confidence level must be used for expressing all the contributing uncertainties, called the standard uncertainties. A standard uncertainty is usually shown by the symbol u or $u(y)$ (the standard uncertainty in y) and considered to be a margin whose size can be assumed as plus or minus one standard deviation.

To give an overall figure, individual standard uncertainties that have been calculated either by Type A evaluation or Type B evaluation can be combined validly by a variety of functions such as summation in quadrature, also known as the root sum of the squares (RSS) method. The combination of standard uncertainties results in the combined standard uncertainty that may be also thought of as equivalent to one standard deviation and is usually shown by the symbol u_c or $u_c(y)$. After having calculated the combined standard uncertainty, an overall uncertainty stated at another confidence level can be achieved by multiplying the combined standard uncertainty by a coverage factor k , which is a numerical factor that typically varies from two to three. This re-scaling of the combined standard uncertainty gives the expanded uncertainty usually shown by the symbol U .

2.2 Dimensional inspection

Dimensional metrology is that branch of metrology which is concerned with the measurement or gauging of a number of part characteristics in order to ensure that the size and form of the part conform to design specifications. The difference between a measuring system and a gauging one is that the latter is used for measuring the magnitude and direction of the geometric deviation between a test part and a calibrated master part nominally of the same design. Therefore, a gauging system holds the advantage of providing relative (comparative) measurements, while a measuring system provides absolute or direct measurements since an unknown quantity is compared directly against a known standard. Comparative measurements benefit from the fact that constant systematic effects associated with the measurement system cancel out. Gauges fall into two general categories: hard gauges and variable gauges. A hard gauge such as a go/no-go gauge is a simple mechanical object which is easy to use for evaluating only whether a part is within tolerance or out of tolerance. Unlike a hard gauge, a variable gauge is capable of quantifying and displaying the amount of deviation between the parts. In addition, variable gauges are further subdivided into fixed and adjustable. A fixed variable gauge is designed to inspect a specific dimension while an adjustable variable gauge, as the name suggests, can be adjusted (mastered) to measure a variety of part sizes [7]. Examples of fixed variable gauges include mechanical and air plug gauges. The Equator system is an adjustable variable gauge.

Following the inspection, a decision must be taken on whether or not the part meets its specification. However, the assessment from the examination of the part may lead to more than two actions [8, 9]. For example, an acceptable part may be graded as a high-, medium- or low-quality part to be used for different applications or for selective assembly. On the other hand, the decision associated with an unacceptable part may result in reworking of the part and/or in some positive action for feedback to the production loop. The latter is of extreme importance because corrective actions will minimize the number of future defective parts.

Dimensional inspection can be accomplished either by using labour-intensive methods such as hard gauges and articulated arm coordinate measuring machines (AACMMs) or by using automated systems such as CMMs, which is a particular type of CMSs (see Figure 2.2). Certainly there are major differences between manual inspection and automated inspection. In particular, CMMs are accurate measuring systems and potentially more versatile and flexible

than custom hard gauges. However, they are very costly and require environmental conditions that are unlikely to be met in a shop floor environment. Consequently, this approach proves unsuitable for effective feedback to the production loop. Also, the time required for the inspection cycle can often be longer than the manufacturing cycle itself. This is because of the need to transfer the manufactured parts to the quality control room after the machining process is finished and thermally stabilize them. In addition, the determination of measurement uncertainty of CMMs is not straightforward due to the wide range of multivariate influencing factors such as probing effects, kinematic errors and environmental effects [1, 10]. AACMMs are portable and flexible instruments consisting of a number of articulated links equipped with angular encoders, but they are much less accurate than CMMs [4, 11]. As with CMMs, they are also thermally sensitive, though they have a much simpler construction. In addition, unlike automated inspection systems, the manual control of AACMMs adds a non-predictable error source, the operator, and thus can produce worse values of repeatability and reproducibility [12]. A detailed description of the errors of AACMMs is outside the scope of this work, but interested readers are referred to [13-15]. Finally, dedicated gauging is time consuming and costly, since traceable calibration is required for each hard gauge, and similarly with AACMMs, the repeatability and reproducibility are dependent on operators. Also, hard gauges require a level of re-engineering when the design of the parts to be measured changes and thus potentially increasing production bottlenecks.

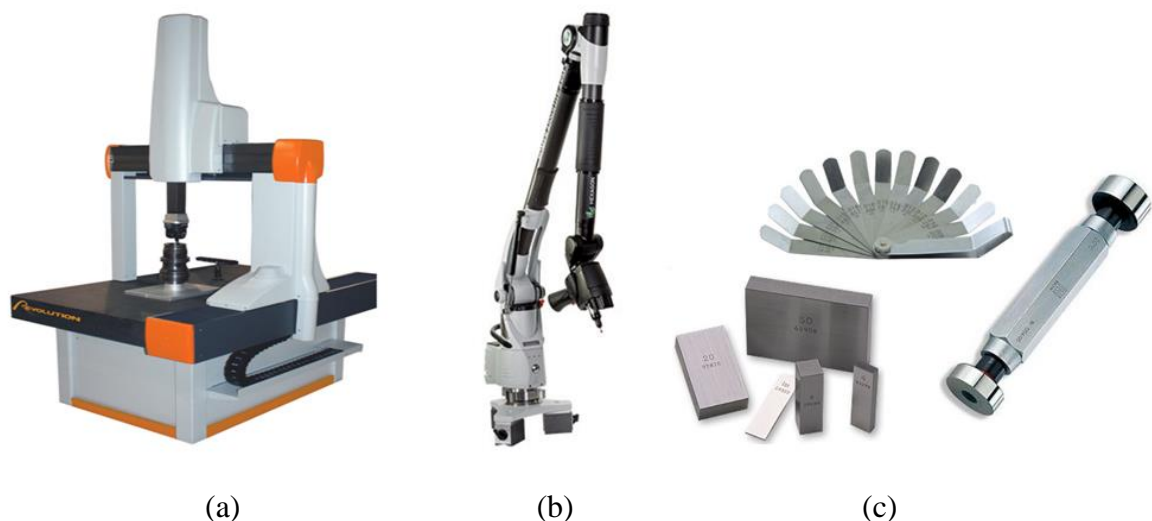


Figure 2.2: (a) CMM, (b) AACMM and (c) hard gauges.

OMP has been used extensively as part of the machining cycle to avoid or reduce hard gauging. The accuracy and repeatability of the CNC machine tool depend on the performance of the motion control system, which is affected by many factors [16]. Therefore, a number of research works have considered existing methods for modelling and simulating the dynamic behaviour of CNC machine tool feed drives. In particular, mechatronic modelling, which considers the coupling of elastic mechanical structure with the control system, has been of special importance and recently has become an advanced tool in machine tool industry [17, 18].

Although CNC machine tools can be used in the same way as CMMs, the level of measurement uncertainty achieved is significant because the same errors that influence the machining process are also transferred to the inspection process. Consequently, this measurement approach is not suitable for applications with high accuracy requirements and strict traceability. In particular, as stated by Saunders et al. [19], CNC machine tools used as CMMs will have the same errors sources as CMMs; differences may be observed in the relative magnitude and dynamics of those errors. These authors repurposed CMM-based uncertainty evaluation software (UES) to OMP. However, the UES uncertainty predictions did not compare well with the uncertainty calculated from physical measurements on the CNC machine tool.

Test procedures required to evaluate the measurement performance of TTP systems integrated with a CNC machine tool are specified in ISO 230-10 [20]. Therefore, the evaluation of the performance of the CNC machine tool used as a CMM shall, in addition to ISO 230-10, be evaluated according to ISO 10360-2 [21] and 10360-5[22]. Verma et al [23] tested the measurement capability of multi-axis CNC machine tools under various working conditions. They found that the repeatability of machine tool may be affected by critical performance variables such as machine tool warm-up and tool-change cycles.

The requirement for an increasingly accurate measurement in a reduced time span has produced the need for new measurement methods. One commonly used approach involves hybrid systems (multi-sensor CMMs) based on cooperative integration of multiple sensors (contact and noncontact) mounted on the heads of traditional CMMs or CNC machine tools in the case of on-machine measurement (OMM). Although multi-sensor measuring systems overcome the limitations of tactile and optical sensing technologies when used separately, a problem that arises when they are combined is that of coordinate system unification as a change in the configuration of any of the systems requires the repetition of unification process [24]. Also,

despite the fact that currently developed methods for coordinate unification such as in [25] have been found to perform well, alternate measurement methods are still required in terms of cost, inspection time, flexibility and efficiency to fill the gap between CMM measurement and custom hard gauging.

Manual inspection is usually used for production situations where only one part is produced and inspected or for sampling inspection in which only a small sample size of parts taken from the population is inspected. Automated inspection systems are more common for screening inspection (100% inspection) in mass production. The disadvantage of sampling inspection is that defective parts may slip through the inspection process [26]. However, this does not imply that the screening automated inspection is error-free. Both the manual inspection and the automated inspection are subject to the so-called Type I and Type II errors that occur during the examination and decision steps. A Type I error occurs when a good quality product is incorrectly classified as being defective. On the other hand, a Type II error takes place when a part of poor quality is mistakenly classified as being good [8, 27]. Forbes [9] applied Bayesian decision-making approaches to conformance assessment for both types of error using a loss function. He concluded that the behaviour of the expected loss depends on the magnitude of systematic effects associated with the measurement system. Therefore, a measurement system which accounts for the influence of systematic effects can significantly reduce the actual cost of making a wrong decision.

Quality Control (QC) is a process intended to detect poor quality in manufactured parts and take corrective actions for eliminating it. However, QC is often limited only to inspection of the product and its components and determination of whether the dimensions and other features meet their specification [8]. The principal standard devoted to QC is the ISO 9000, which is a set of international standards on quality. The ISO 9000 family of standards addresses a variety of aspects of quality management and aims to assist organizations to implement and operate efficient quality systems. In QC, the time interval between the inspection procedure and the manufacturing process is of great importance. In particular, three main different cases can be distinguished [8, 28]:

1. Off-line inspection
2. On-line/in-process inspection
3. On-line/post-process inspection

The first case is concerned with inspections performed away from the manufacturing process and after a considerable time delay once the manufacturing process is complete. The main disadvantage of off-line inspection is that compensating adjustments cannot be made in the manufacturing process in order to reduce variability. In this case, manual methods and statistical sampling are common. The last two situations are related to inspections which are performed either when the parts are made or immediately afterward. The on-line/in-process inspection takes place during the manufacturing process and therefore quality can be improved. Manual methods or OMM using touch-trigger probes integrated with a CNC machine tool are common. OMM using scanning probes is rare, because there are many significant sources of machine tool error that contribute to component errors such as thermal errors, geometric errors, cutting forces, kinematic errors, vibrations, etc. [19, 23, 28]. Therefore, the level of measurement uncertainty is critically high. The on-line/post-process inspection is the most common case and can be performed as either a manual procedure or an automated one. Although with post-process inspection, the measurement or gauging procedure in most cases is performed immediately following the manufacturing process, it is still considered an on-line method because its results can influence the production of subsequent parts. Its disadvantage however is that there can be no correction that will influence the processing of the part being gauged or measured since it has already been produced. Therefore, automated cells consisting mainly of manufacturing equipment, inspection equipment, and handling robots are being increasingly employed for shortening of feedback loops. In this way, data such as coordinates can be immediately fed back to the preceding machining process to correct process parameters on future parts [28]. However, this approach requires automated inspection systems capable of performing repeatable measurements in a short time on the factory floor. Also, another category of measurement methods that can be placed between in-process and post-process inspection includes process-intermittent measurements which can be performed either on or off the machine. In any case, the manufacturing process is halted for a relatively short time in order to perform measurements of the part, and those measurements are then used for process correction [28]. This thesis focuses on the latter two cases.

CMMs have been the most effective measuring systems in traditional manufacturing for form, size, position and orientation assessment. However, for the aforementioned reasons of increased efficiency and control, the modern approach to dimensional inspection requires that the measuring equipment is placed close to the manufacturing equipment. Although there are

various CMM configurations (see section 2.4.3), there are many factors affecting their accuracy such as geometric errors, thermal errors, probing system errors and environmental effects (see section 2.4.4). Also, the heavyweight structure of CMMs causes hysteresis error and leads to practical limitations in terms of inspection speed in order to maintain accuracy at high levels [29].

Over the years, enhanced CMMs have been proposed to address inspection challenges in a shop floor environment. However, such CMMs use compensation techniques in order to account for the influence of thermally induced structural deformations, which increase the already high cost of the CMM measurement approach to industrial dimensional metrology. CMSs can also be used in comparator mode in which measurements of a production part are compared with those of a master part nominally having the same geometry and many of the difficulties associated with evaluating the measurement uncertainties are avoided since many of the systematic effects cancel out. Although the comparative approach to dimensional inspection may be particularly attractive, it is not the ideal solution in terms of inspection speed since comparative measurements require additional measurements on the master part.

PKMs can often move very fast while maintaining their precision. In particular, compared to Cartesian structures, parallel kinematic structures have a higher stiffness-to-mass ratio, lower inertial effects, better dynamic performance, no bending forces, and allow for higher working speeds [30]. However, their workspace size is considerably limited in comparison to Cartesian machines. Recently, Renishaw plc has developed a software-driven comparative gauging system constructed with a parallel kinematic constraint mechanism [1, 31]. The Renishaw Equator based on the Delta robot architecture is an automated flexible gauge used to perform comparative coordinate measurements on the shop floor (see section 2.5.1).

2.3 Evaluating the measurement uncertainty

The evaluation of measurement uncertainties is a necessary process for the quality of measurements. All measurement processes have uncertainty to some degree and therefore, when a measurement result is reported, the measurement uncertainty that characterizes the reliability of the results needs to be provided. Measurement uncertainty can result from the measurement equipment, the item being measured, the measurement environment and the operator including the measurement strategy [10, 32, 33].

Over the years, concepts that involve metrology and reliability of measurements have been established and harmonized by international organizations for bringing uniformity to the evaluation of measurement uncertainty. The International Organization for Standardization (ISO) and the Bureau International des Poids et Mesures (BIPM) created a guide to the expression of uncertainty in measurement (GUM). This guide was published as an ISO standard [34] and as a Joint Committee for Guides in Metrology (JCGM) guide [5], which are a reissue of the 1995 version of the GUM, with minor corrections. The GUM provides a framework to determine the best estimate y of an unknown quantity Y and its associated standard uncertainty $u(y)$ from available information such as experimental data. The GUM uncertainty framework (GUF) uses linearizing approximations (first-order Taylor series) that can limit the validity of the results and fails when the required assumptions are not valid [35]. In order to overcome the limitations of GUF, recently, measurement uncertainty evaluation has been proposed on the basis of probability density functions (PDFs) using a Monte Carlo method (MCM) that actually combines and propagates distributions rather than propagating uncertainties as in the GUF. The MCM described in the GUM supplement 1 (GUMS1) [36] uses the distribution functions of each uncertainty contributor as input and runs regardless of the complexity of the measurement process or its mathematical model. However, an important drawback of both the GUM and GUMS1 approaches is that any prior information about the unknown quantity is not taken into account [37].

The GUF recommends the t -distribution (Student's distribution) approach when dealing with a small data set that follows a Gaussian (normal) distribution. However, the information on the parent PDF cannot be inferred from a small amount of repeated measurements. The bootstrap approach [38], which is a very general resampling procedure for estimating the probability distributions based on independent observations, is an alternative to the standard Type A uncertainty evaluation. Unlike the GUF, it requires no information on the PDF from which the actual measurements are drawn. It has been found to be successful in many situations, especially for estimating the reliability of estimators and their uncertainty when large sample sizes are available for any PDF [39]. However, although it is better than some other asymptotic methods, some counterexamples have shown that the bootstrap method provides incorrect solutions [40]. In addition, the bootstrap approach requires more effort to calculate the expanded uncertainty in comparison to GUF and its performance has not been specified yet for

small data sets, when the parent PDF is of a skewed type [41] and generally this is a controversial issue in the literature and is outside of the scope of this thesis.

The normal PDF is [5]:

$$f(x) = \frac{1}{\sigma\sqrt{2\pi}} e^{-\frac{(x-\mu)^2}{2\sigma^2}} \text{ for } -\infty < x < +\infty \quad (2.1)$$

where μ is the true value of the measurand or the expectation to be more precise since a unique true value could be obtained only by a perfect measurement and therefore it is only an idealized concept and σ is the standard deviation of the normal distribution defined accordingly by:

$$\mu = \frac{1}{n} \sum_{i=1}^n x_i \text{ and } \sigma = \sqrt{\frac{1}{n} \sum_{i=1}^n (x_i - \mu)^2}. \quad (2.2)$$

For a small number of repeated measurements n , and in the case where the PDF for the measured input quantity is a Gaussian, the GUM approach [5] uses the sample mean value \bar{x} as the expectation of x and the experimental standard deviation of the mean

$$s(\bar{x}) = \frac{s}{\sqrt{n}} \quad (2.3)$$

as uncertainty $u(x)$ associated with that mean, and infers the expanded uncertainty from a t -distribution with $\nu = n - 1$ degrees of freedom (DOF). Note that, the sample mean value \bar{x} and the sample (experimental) standard deviation s are defined accordingly by:

$$\bar{x} = \frac{1}{n} \sum_{i=1}^n x_i \text{ and } s = \sqrt{\frac{1}{n-1} \sum_{i=1}^n (x_i - \bar{x})^2}. \quad (2.4)$$

So, the sample mean value \bar{x} gives the most likely estimate of the true mean value μ . Therefore, let us suppose that a simple random sample of size n is taken from a population. If the population from which the sample is drawn forms a normal distribution, the distribution of

$$t = \frac{\bar{x} - \mu}{s(\bar{x})} \quad (2.5)$$

follows the t -distribution with $\nu = n - 1$ DOF. The PDF of the t -distribution is:

$$P(t, \nu) = \frac{1}{\sqrt{\pi\nu}} \frac{\Gamma\left(\frac{\nu+1}{2}\right)}{\Gamma\left(\frac{\nu}{2}\right)} \left(1 + \frac{t^2}{\nu}\right)^{-(\nu+1)/2}, \quad -\infty < t < +\infty \quad (2.6)$$

where Γ is the gamma function and $\nu > 0$. The expectation μ of the t -distribution is equal to zero and its variance is equal to $\nu/(\nu - 2)$ for $\nu > 2$. Therefore, as $\nu \rightarrow \infty$, the t -distribution approaches a normal distribution with expectation $\mu = 0$ and standard deviation $\sigma = 1$. Figure 2.3 shows the normal (bell-shaped curve) distribution and the associated levels of confidence for one, two, and three standard deviations of the mean. The true variance and the sample (experimental) variance are defined accordingly by:

$$\sigma^2 = \frac{1}{n} \sum_{i=1}^n (x_i - \mu)^2 \quad \text{and} \quad s^2 = \frac{1}{n-1} \sum_{i=1}^n (x_i - \bar{x})^2. \quad (2.7)$$

The basis for estimating measurement uncertainties is measurement traceability [42]. Demonstrating traceability to national standards is required to ensure confidence in the measurements. By definition [2], the metrological traceability is the “property of a measurement result relating the result to a stated metrological reference through an unbroken chain of calibrations of a measuring system or comparisons, each contributing to the stated measurement uncertainty.” Besides the importance of measurement uncertainty in traceability, the measurement uncertainty also plays a key role in conformity assessment, in particular, in setting acceptance limits [43, 44].

The last few years have seen an increase in the use Bayesian approaches to evaluating measurement uncertainty [45, 46]. The reason for that is because Bayesian methods can leverage prior knowledge of the measurement process and are particularly useful for inference given small sample sizes or missing data [47]. Also, developments in computing have made Bayesian statistical methods very attractive to apply in metrology to determine parameter

estimates and associated uncertainties [48]. Bayesian methods easily combine expert knowledge with experimental data while considering uncertainty. They use a full probability model providing a joint probability distribution for all observable and unobservable quantities and usually require MCMC methods to generate samples distributed according to the target posterior distribution. MCMC methods combine Monte Carlo sampling and Markov chain theory (see Appendix B for discrete-time Markov chains). Well-known MCMC methods include the Metropolis algorithm, the Metropolis-Hastings algorithm, and the Gibbs sampler, also called alternating conditional sampling. In particular, the latter has been found very useful in a large number of multidimensional problems [49]. Although computational Bayesian methods such as MCMC are straightforward to use to generate samples from the posterior distribution of interest which may otherwise be difficult to generate samples from, prior knowledge may be difficult to elicit in probabilistic form.

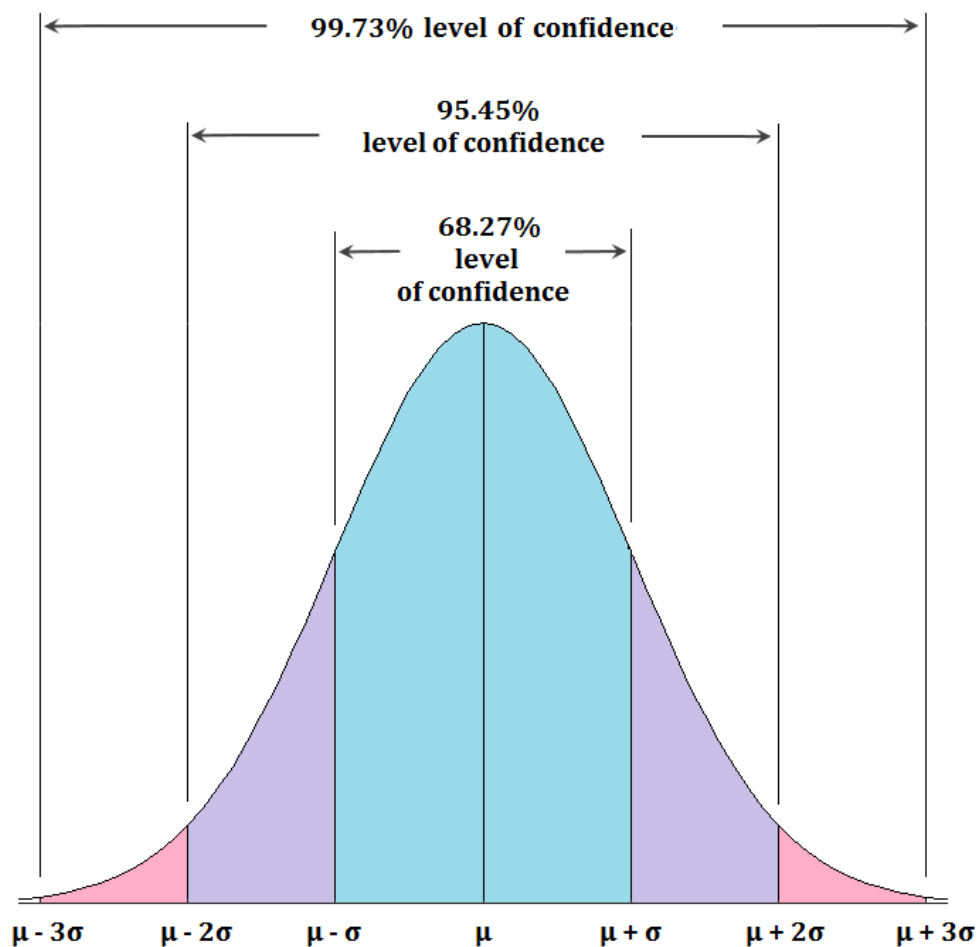


Figure 2.3: The normal distribution.

2.4 Coordinate metrology

Coordinate metrology has become fundamental for manufacturing metrology. In order to perform coordinate metrology, a CMS such as a CMM is employed to: a) measure the actual form and dimensions of a part, b) compare them against the desired form and dimensions as specified by a technical drawing or computer-aided design (CAD) specification, and c) evaluate the metrological information of interest [50]. A CMS utilizes a sensing device called a probe to collect point coordinates on part surface at certain areas. Its software then processes these point coordinates in order to produce a geometric result or to establish a local coordinate system from datum features. Various probe designs are available and compatible with most of the CMMs used in industry in order to meet the requirements of each application as best as possible. In particular, two basic types of probing systems can be distinguished:

- Contact or tactile probing systems
- Noncontact or nontactile probing systems

Noncontact probes are capable only of measuring visible features on the exterior of a part and require a cleaner measurement environment than contact probes. They are usually used for applications which involve small and flexible parts since no physical contact is made between the part and the sensor, or where very high scanning speeds are required. Unlike noncontact probes, contact probes gather coordinate data by physically touching the part and therefore inspection cycle times may be slower. They are common for parts with complex geometries and measurements tasks with high accuracy requirements. This is because noncontact probing systems such as optical ones generally provide higher measurement uncertainty of each probed point [51]. Contact probes fall into three general categories:

- Hard probes
- Touch-trigger probes
- Analogue scanning probes

Hard probes are used in conjunction with manual CMMs for measurement tasks with typically low accuracy requirements [52]. Touch-trigger probes can be positioned to contact the part surface either manually by an operator or automatically via direct computer control (DCC). Both hard probes and touch-trigger probes measure discrete points. However, the latter ones

always measure dynamically (detection of a surface point while the machine is moving with constant velocity), while with hard probes the readout of the coordinate axes is triggered manually. Analogue scanning probes can keep contact with the part surface and measure either dynamically or statically [51, 53]. They are common for automated inspection, though manual inspection can also profit from the advantages offered by this newest technology. Unlike TTP systems which are suitable for measuring standard geometric features, scanning probing systems can acquire several hundred points each second on their path along the part surface, enabling measurement of form characteristics and free-form surfaces. Scanning probing systems have also the possibility for scanning both known and unknown parts. Therefore, two types of continuous scanning methods can be distinguished: open loop and closed loop [54]. Open loop scanning is a high-speed technique used for parts with known geometry, while closed loop scanning is particularly useful for measuring unknown parts, including reverse engineering.

Furthermore, the trend in sensor development over recent years has been directed toward 5-axis probing systems (three machine axes and two rotary axes of the head) [54]. The 5-axis measurement technology, which utilises an articulating head that moves in two rotary axes as it measures, can be used to minimise machine's dynamic errors at very high measurement speeds. Two examples of 5-axis systems are the Renishaw REVO 5-axis measurement system capable of performing multi-sensor coordinate metrology and the Renishaw PH20 5-axis touch-trigger system for touch-trigger measurement.

In the domain of coordinate metrology, a significant amount of research work has been conducted to quantify the measurement accuracy of CMMs and increase it by improvements in hardware, software, and general measurement strategy. In order to ensure that the measurements are accurate, the calibration of the CMM needs to be traceable to the international system of units (SI), in particular, to the international standard of length with known measurement uncertainty [55]. In fact, the definition of metrological traceability has achieved global acceptance in the metrology community [2]. Traceability is the comparison of a measurement system to a standard of higher accuracy. However, CMMs are multi-purpose measuring systems and therefore demonstrating traceability to national standards and, ultimately, to the international standard is not straightforward. Therefore, the only practical way of ensuring that the CMM measurements are accurate is to provide measurement-task-specific traceability statements [55, 56]. As a matter of fact, the uncertainty associated with the

measurement of a specific feature through a specific measurement strategy is usually referred to as task-specific uncertainty. An excellent review for uncertainty sources and methodologies developed to model and assess task-specific uncertainty for coordinate measurements is provided by Wilhelm et al. [10]. The evaluation of measurement uncertainty associated with CMSs is further discussed in section 2.4.4.

2.4.1 Part alignment

In coordinate metrology using CMMs or automated flexible gauges, there are two basic types of coordinate systems: the machine coordinate system (MCS) which defines the XYZ position on the CMS with respect to the 'HOME' or 'START' position; and the part coordinate system (PCS) which determines the position and orientation of the part in relation to the MCS. PCSs are specific to each part and therefore, when using a CMS it is necessary to establish the PCS and relate it to the MCS. The process of assigning a reference coordinate system on the part is called part alignment or simply alignment. In order to establish correctly an alignment, at least two PCSs are required to be generated; the first is used to establish the approximate position of the part within the CMS's working volume, while the second for the inspection of the part.

As any unrestrained rigid body, a part in space has six DOF: three translational DOF and three rotational DOF. Therefore, for the inspection of a rectangular part with flat surfaces the minimum number of probing points required to establish the PCS is six. Three contact points are required to define the primary datum A (a plane) which controls three DOF (two rotational and one translational degree of freedom); two contact points are required to define the secondary datum B (a line) which controls two translational DOF; and one contact point to define the tertiary datum C which controls the remaining rotational degree of freedom [57, 58].

The features used to define the PCS are called datum features and usually required to have good form so that the measurement uncertainty associated with the PCS or datum reference frame (DRF) can be kept low [59]. The DRF is that coordinate system against which the geometric dimensions and tolerances of a part are defined and can be different from the PCS. The tolerances on datum features should be tight because the form errors on datum features affect the datum measurement uncertainty. Datum uncertainties have to be taken into account for features which are evaluated with respect to datums such as true position. These

uncertainties are determined as follows since each datum controls a different number of DOF, [60]:

$$u_{datum} = \sqrt{\frac{3}{6} \times u_{primary}^2 + \frac{2}{6} \times u_{secondary}^2 + \frac{1}{6} \times u_{tertiary}^2} \quad (2.8)$$

where the uncertainty for each datum is its own feature uncertainty calculated as follows:

$$u_{sampling} = \frac{\sigma_{pc}}{\sqrt{n_f - x_f}} \quad (2.9)$$

where σ_{pc} is the point coordinate error, n_f is the number of contact points used to define the feature, and x_f is the mathematical minimum number of contact points required to define a given feature. Table 2.1 provides the mathematical minimum and the recommended minimum number of contact points required for various geometric features [57, 61].

Table 2.1: Number of contact points required per feature.

Geometric feature	Mathematical minimum number of contact points	Recommended minimum number of contact points
Line	2	5
Plane	3	9
Circle	3	7
Sphere	4	9
Cone	6	12 for straightness or 15 for roundness
Ellipse	4	12
Cylinder	5	12 for straightness or 15 for roundness
Cube	6	18

Both the DRF and substitute geometries are determined by the point coordinates gathered by the CMS through its software. For an ideal CMS (having no measurement uncertainty in the point coordinates) and an ideal part (having no form error), sets of point coordinates arising from alignment strategies based on different datum features will lead to identical computed results. However, in real part measurements (where both the CMS and the part are imperfect),

sets of point coordinates representing different measurement strategies will result in different definitions of the DRF and thus, in different estimates, for example of the positions of other geometric features or profile tolerances constrained with respect to datums associated with the part [62]. In addition, poor sampling strategies can lead to large differences in computed results even though the difference in point coordinates are small [4]. Approaches for evaluating the effect of form error associated with datum features on the uncertainties associated with geometric features have been described by Forbes et al. [62].

2.4.2 Scanning versus touch-trigger probe data capture

Compared to TTP systems, scanning probing systems perform faster measurements, gather larger amounts of data, and provide greater coverage of the feature under inspection [54, 63]. However, the measurement uncertainty associated with the position of a single point is generally higher in scanning due to dynamic influences [51]. Scanning probing systems can also be used to acquire discrete points, but TTP systems measure discrete points faster than scanning probing systems. Also, in scanning CMMs, machine dynamics limit measurement accuracy at higher speeds. Therefore, conventional scanning probes can achieve measurement accuracy at relatively low scanning speeds where inertial forces are trivial. In fact, while in TTP inertial forces are negligible, in scanning, acceleration and as a consequence inertial loads are always present. In particular, as the machine is moving faster, the accelerations typically increase by the square of scanning speed [64]. For this reason, dynamic compensation measurement techniques have received much attention in recent years [63, 64].

Renishaw developed a new dynamic error compensation method called Renscan DC (dynamic compensation) to enhance CMM measurement performance. This is a feature-based compensation method in which each feature on a part is first scanned slowly and then it is re-measured with a higher velocity so that the errors introduced by the greater speeds can be taught. In particular, the differences between the measurement results are used by the universal CMM controller (UCC) to compute a dynamic compensation ‘map’ for each feature. Once this process has been derived, all subsequent parts nominally of the same size and located in the same part of the machine can be measured at high speed, but with the accuracy of slow speed scanning [53, 64].

Pereira and Hocken [63] proposed two scanning error compensation models to improve the performance of a CMM when scanning internal circular features at any scanning speed and radius combination. For diameters smaller than 50 mm the first model achieved an error reduction of more than 38% while for diameters larger than 50 mm the second model achieved an error reduction of 49%.

Some studies have been conducted to determine the difference obtained in measurement accuracy between scanning and touch-trigger probe technologies. Ollison et al. [65] employed an experimental design and determined statistically that there is a significant difference in cylindricity accuracy between scanning and touch-trigger probe measurements of 3D-printed parts. In general, it can be concluded that the higher the number of contact points, the more accurate the results due to the smaller sampling effects.

2.4.3 CMM configurations

A CMM is a complex mechatronic system consisting mainly of a probe head and probing system along with the stylus/styli, a mechanical structure, a worktable, drive systems, displacement transducers, control systems, and a computer with peripheral equipment and application software. There are various CMM configurations (see Figure 2.4) such as moving bridge, fixed bridge, cantilever, horizontal arm, and gantry, each one having its own advantages and disadvantages [50].

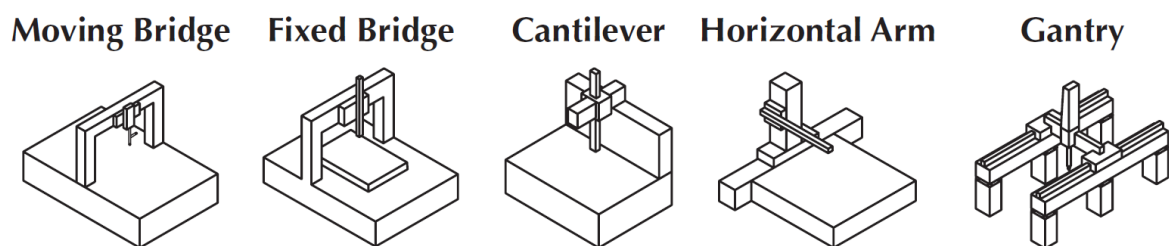


Figure 2.4: Common CMM configurations [50].

The most commonly used configuration is the moving bridge, which has a stationary table and a moving bridge. This design has a small to medium measuring range and is affected by yawing. Therefore, although it provides relatively small measurement uncertainties, the measurement accuracy depends on part location within the CMM's measuring volume. The ring bridge

configuration, which is another category of moving bridge machines not mentioned so far in this thesis, enhances the structural rigidity. With this design, the Abbe offset error is reduced and the measurements are not affected by the mass of the part. The fixed bridge configuration is characterised by its high rigidity and high accuracy. In this design, the bridge is rigidly fixed to the machine bed and the table, which supports the part to be measured, provides one axis of motion. However, this adds a limitation to the operating speed and the maximum allowable part weight because the moving table is heavy. As a result, a major disadvantage of this configuration is the lower part throughput. Cantilever CMMs have a moving cantilever arm and a fixed table upon which the part to be measured is mounted. The cantilever arm supports a carrier to move in and out, which in turn supports the probe arm for the vertical movement. This design can support heavier parts and allows higher part throughputs because it has a low moving mass structure for a given working volume. The disadvantages of cantilever configuration over the moving bridge are the bending effect and the lower system natural frequency, limiting the machine size. However, cantilever CMMs are ideal for general measurement applications as well as long, thin parts due to their design. Horizontal arm CMMs are particularly suitable for measuring automobile bodies or other parts with similar size and tolerances. There are numerous horizontal arm configurations such as moving ram, moving table, and dual-arm designs. In the case of moving table horizontal arm CMMs, like all other such machines, the measurement speed and accuracy depend on the size and weight of the part. Regarding moving ram configurations, the cantilevered design lead to low dynamic stiffness and considerably Abbe offsets. Dual-arm configurations result in higher part throughput because they allow the simultaneous measurement of both part sides. Horizontal arm machines in any configuration are characterised by exceptional part accessibility, large measuring ranges (up to 25 m for moving ram configurations in the long axis), high measurement speeds, and small measurement accuracy with the levels of measurement uncertainties to vary significantly. Gantry CMMs are ideal for measuring very large parts with relatively tight tolerances. For convenient control of large mechanisms such as gantry machines [17, 18], two motors may be required to drive a single axis. Dual-drive systems have also been adopted by CMMs for the gantry drive. The split-axis feature (master and slave) automatically coordinates the drive of the two motors that receives coordinated commands to keep the mechanism properly aligned and thus, avoiding the yawing of the traveling beam. The main advantages of gantry CMMs are the large measuring volume and excellent part accessibility. For more details about Cartesian CMMs, interested readers are referred to [50]. Most of the aforementioned CMMs have significant moving mass to maintain rigidity and significant Abbe offset, therefore this

limits the accelerations speeds, even with dynamic compensation methods. This is one of the main driving forces behind the PKM design in the Renishaw Equator system described later in section 2.5.1.

2.4.4 Uncertainty associated with coordinate measurement

Measurement uncertainty in CMSs comes from a large number of sources. Methods for evaluating task-specific uncertainty in coordinate measurement were reviewed by Wilhelm et al. [10]. These authors divided uncertainties associated with CMSs into five main categories: hardware, part, extrinsic factors, sampling strategy, and fitting and evaluation algorithms. Weckenmann and Knauer [32] focused on the last two factors and showed that the way the CMM operator defines the measurement strategy has a strong influence on the CMM measurement uncertainty. In particular, factors that could affect the accuracy of CMM measurements are:

- Environmental effects
- Machine repeatability
- Machine thermal errors
- Machine geometry errors
- Kinematic errors
- Scale errors
- Probing system errors
- Machine dynamics
- Vibrations
- Measurement strategy
- Measurement part
- Fixturing variability
- Software errors

Thermal errors arise from thermal deformations of the machine elements and should be compensated by real-time error compensation techniques [66-68]. Kinematic and geometric errors are inter-related [69]. The geometric errors are systematic and can be compensated by non-real-time error compensation techniques. They affect the machine repeatability and

kinematic accuracy. For a 3-axis Cartesian machine, there are 21 parametric errors (see Table 2.2). In particular, each axis is characterised by six geometric errors; three translation errors (linear positioning and two straightness errors) and three rotation errors (roll, pitch, and yaw). In addition to the six geometric error components along each axis, three squareness errors between them can be identified [4, 16].

Table 2.2: Geometric errors in a 3-axis Cartesian machine.

Errors	Number per axis	Total
Linear position	1	3
Straightness	2	6
Angular	3	9
Squareness	-	3
Total	6	21

Although the GUM for univariate measurement models [5] or for multivariate measurement models [70] can be put in an application for CMM measurement [71] (the second part of ISO 14253 is of special importance in relation to ISO 9000 quality assurance systems), a correct measurement uncertainty statement remains a difficult task to achieve due to the various complex multivariate influencing factors [72]. Wilhelm et al. [10] surveyed different approaches used to model and evaluate task-specific uncertainty for CMMs using contacting probes as listed below:

- Sensitivity analysis
- Expert judgment
- Substitution method
- Simulation
- Statistical estimations from measurement history
- Hybrid methods

Sensitivity analysis is used when a precise mathematical model for the measurement process can be derived. In such a case, it is relatively straightforward to follow the GUM approach [5] for estimating measurement uncertainties using the law of propagation of uncertainties (LPU). However, the GUM approach based on the LPU and the characterization of the output quantity

by a Gaussian distribution or a scaled and shifted t -distribution is based on a number of assumptions that are not always valid [35]. Therefore, methods depending on the propagation of distributions have been applied to metrology to overcome the limitations of the GUF. The MCM presented in the GUMS1 [36] uses the probability distribution functions of each uncertainty contributor as input and runs regardless of the complexity of the measurement process. In Monte Carlo simulation, a computer simulates the actual measurement process a predefined, large number of times and each time, different values are randomly chosen for each uncertainty contributor from the corresponding input distributions. Thus, the number of measurement results is equal to the number of Monte Carlo trials, which has to be sufficient for achieving a representative error distribution.

Expert judgment is a Type B uncertainty evaluation. This technique has been used extensively by experienced metrologists for decades due to the lack of other tools. However, it is now recommended only when measurement data are not available or a precise mathematical model for the measurement process and/or for the CMM itself cannot be derived.

The substitution method [73] involves the regular measurement of an additional traceable reference part and the comparison between its calibrated value and the measured value obtained by the CMM to derive a correction value, Δ_i , which is then applied to the measurement of the production parts. This measurement strategy also referred to as the *Comparator Principle* can achieve high accuracy and is relatively straightforward [5, 57].

Simulation is considered the state of the art approach for task-specific CMM uncertainty evaluation. Over the recent years, various methods based on Monte Carlo simulation have been developed to deal with this task e.g. the virtual CMM (VCMM) [74], simulation by constraints [75] and the expert CMM [76]. Such methods simulate certain characteristics of CMMs to estimate the task-specific measurement uncertainty for a specific CMM or facilitate CMM inspection planning.

Statistical estimations from measurement history are common when a large number of measurement data are available. An efficient way to plan and conduct experiments is the method of DOE. This is a systematic approach used extensively for analysing and optimising complex processes. In dimensional metrology, the DOE method assesses the sensitivity of the

measurand to various factors that comprise the measurement process. Also, based on the type of the DOE technique used, the interactions between the factors involved can be studied.

Hybrid methods are those methods that involve at least two of the methods (or part of them) described previously. Hybrid methods are common due to practical limitations or difficulties when employing only one approach.

D'Amato et al. [77] presented a paper concerning the calculation of the uncertainty associated with the indirect measurement of angles using a moving bridge CMM located in a temperature controlled environment of $20^{\circ}\text{C} \pm 1^{\circ}\text{C}$. They used two different behavioral models for the CMM; a linear statistical model and a Mitutoyo model based on the work of Phillips et al. [75] to determine the values of the angles and Monte Carlo simulation to calculate their associated uncertainties. The results showed that the Mitutoyo model provides more conservative uncertainty values than the linear statistical model.

Osawa et al. [78] described a method based on the combination of multiple orientation and substitution techniques to compensate all geometrical errors of a CMM, systematic probing effects, and the bending of the artefact due to gravity for cylinder measurements. They employed the VCMM software [79] installed on the CMM to evaluate the task-specific uncertainties. Their method reduced the uncertainty of measurement by a factor of 5-10 and the VCMM was able to account for the effects associated with the error elimination.

Limited sampling in combination with feature form deviations is usually the most important source of uncertainty in CMM measurement. Thus, when measuring features with a limited number of contact points, the influence of feature form deviations on the measurement uncertainty need to be considered. However, this is not straightforward using traditional uncertainty evaluation methods because the magnitude of the true form deviation is not known in advance (since it is one of the parameters to be measured). Although expert knowledge is often used to specify an upper limit of the true form deviation, the measurement uncertainty statements are still not reliable. Kruth et al. [33] have proposed an alternative method based on Monte Carlo simulation and a profile database of realistic form profiles to determine uncertainties for CMM measurements with limited sampling.

In the reviewed literature, numerous studies have been reported in evaluating the uncertainty associated with coordinate measurement through the DOE method [80]. There are various DOE techniques such as factorial designs, response surface designs, Taguchi orthogonal array designs, etc. [81, 82]. The objectives of the experiment and the number of factors of interest usually determine which type of experimental design to apply. In the manufacturing industry, the most commonly used approach includes factorial designs [83]. Factorial designs fall under two main categories: full factorial designs and fractional factorial designs. Fractional factorial designs are an alternative to full factorial designs when the number of factors is large because they use fewer runs than the full factorial designs. However, only the full factorial designs include all possible combinations of every level of every factor so that all the possible interactions among the factors can be examined. Response surface designs are usually used to refine models after the important factors have been determined using factorial designs [84]. Taguchi orthogonal array design is a type of general fractional factorial design and therefore interactions between the factors are normally not taken into consideration [85, 86].

Barini et al. [87] described a study associated with point-by-point sampling of complex surfaces using a tactile CMM. They carried out a completely randomized full factorial experiment with four factors at two levels each and concluded that the analysis of factorial experiments can help determine the statistically important factors. Similar conclusions, but for length type features of ball bar gauges, were made by Piratelli-Filho and Giacomo [88] who applied a 3^2 factorial design for carrying out a performance test using a ball bar gauge and for investigating CMM errors associated with orientation and length in the work volume. Feng et al. [89] employed a sequential experimentation approach through fractional factorial designs for the measurement uncertainty evaluation of the location of a hole measured by a CMM equipped with a Renishaw TP2 touch-trigger probe. They concluded that, the interaction of speed and probe ratio (the ratio between the diameters of the probe and the ring gauge) is of statistical significance and the uncertainty is minimized when highest speed is used, the stylus length is shortest, and the probe ratio and number of pitch points are largest. Lobato et al. [90] presented a non-fully randomized experimental study due to practical considerations using a CMM located in a temperature controlled room with different levels of room temperature to simulate measurement tasks performed in workshop environments. The factors of interest were: the environment temperature; number of probing points; feature type; probe extension; and stylus length. They concluded that all studied factors were found to be statistically

significant as well as the two-factor interactions of environment temperature with feature type, number of probing points with feature type, and probe extension with stylus length.

The coordinate data gathered by the probe of a CMM on part surface are analyzed using appropriate algorithms through its software in order to calculate the associated geometric features. Nowadays, minimum zone methods (MZMs) of various form errors evaluation have received much attention, because the CMM software is usually based on least squares method (LSM) that does not guarantee the minimum zone solution (MZS) specified in ISO 1101:2012 [91]. Dhanish and Mathew [92] studied the effect of CMM point coordinate uncertainty on uncertainties of parameters of a non-ideal form circular feature using Monte Carlo simulation for four different criteria including the LSM, the MZM, the maximum inscribed and the minimum circumscribed. They showed that the distribution associated with the estimates of the circularity may be non-normal and the measurement uncertainty is due to finite sampling and random effects.

Wen et al. [93] formulated the mathematical model of flatness error MZS and proposed an improved genetic algorithm (IGA) to implement flatness error minimum zone evaluation. Wen et al. [94] established the mathematical model of cylindricity error based on the minimum zone condition and proposed a quasi particle swarm optimization (QPSO) for searching the cylindricity error. Both models were nonlinear and therefore the authors considered that it is necessary to investigate the validity of the GUM for the uncertainty evaluation of flatness and cylindricity error, respectively. GUM and Monte Carlo approaches were selected to estimate the uncertainty of the minimum zone flatness error. In order to overcome the problem that the number of Monte Carlo trials is required to be defined in advance, adaptive Monte Carlo method (AMCM) can be used. In AMCM, a procedure that selects the number of trials adaptively takes place until the results have stabilized in a statistical sense. Therefore, Wen et al. [94] used AMCM and GUM approaches for the evaluation of measurement uncertainty of cylindricity error and the results showed that considering only the first-order terms in the Taylor series approximation, the GUM does not reach the required precision to assess the uncertainty of measurement of cylindricity error. The cylindricity errors of MZM were much smaller than those of LSM as shown by the comparison. Wen et al. [93] also used particle swarm optimization (PSO) to calculate the flatness errors of MZM, but the IGA was found to be more suitable to calculate the flatness error of MZS than PSO.

Ordinary least squares (OLS) is the most common fitting criterion used to fit a geometric surface to coordinate data. Least squares algorithms for lines, planes, circles, spheres, cylinders, and cones have been described by Forbes [95]. This algorithm is appropriate if the covariance matrix associated with the measured coordinate data is a diagonal matrix. Nevertheless, in recent years, much research work in the domain of coordinate metrology has dealt with developing more realistic uncertainty models for coordinate data. Therefore, fitting algorithms that can consider more realistic uncertainty structures associated with the measured coordinates have also been developed [96-98].

Although a mathematical model of the measurement system is required to assess the uncertainty associated with the coordinate data, most systems are complex and thus, developing an accurate mathematical model for the measurement system is very difficult. In this thesis, data-driven models, and, in particular, artificial neural networks (ANNs) are developed to estimate point coordinates and associated uncertainties (see chapter 7).

2.5 Comparative metrology

Comparative measurements involve the comparison of a quantity between a test part and a calibrated (master) part or reference standard. A fundamental issue in comparative measurements is the problem of temporal drift (a time-dependent bias). Therefore, various approaches have been used to make the comparison sequence insensitive to drift [99-102].

Sutton and Clarkson [99] presented a general approach to comparisons affected by a temporal drift and discussed comparison sequences for linear, quadratic, and cubic drift. They used a matrix least squares model in order to obtain information about the drift, the item differences, and their uncertainties. In their study on mass comparisons, in which the dominant drift was in the balance zero, the analysis of different comparison sequences showed that the best performance is achieved when three to five items are involved in each comparison. Gläser [103] was concerned with the cycles of comparison measurements to determine which measurement sequence leads to the smallest measurement uncertainty. Lira [102] discussed the least squares estimation method for evaluating comparison measurements. He presented two algorithms to show that this method results in a considerably more convenient framework in comparison to GUM [5] for analyzing different sequences of repeated measurements (cycles) of comparison measurements. Although the algorithms differ from each other in modelling

drift as the second algorithm leads directly to estimates of the differences of interest without an explicit drift model as opposed to the first one, an illustrative example for mass comparisons taken from [99] showed that both algorithms yield similar results.

Although various research works such as [99, 101, 104] have discussed schemes which eliminate the drift effects for simultaneous comparisons, there are cases, especially in dimensional metrology, where the comparisons cannot be done simultaneously. For dimensional measurements, the instrument drift is due most often to temperature effects and therefore, it cannot be minimized by repeated measurements [100]. Drift effects on calibrations by comparison have been extensively studied at the National Institute of Standards and Technology (NIST). In particular, Doiron [100] presented schedules for non-simultaneous comparison calibrations eliminating the bias from drift and simultaneously providing a numerical approximation of the magnitude of drift. Drift eliminating designs for simultaneous comparison calibrations can be found in Cameron and Hailes [101].

Although comparison schemes where the drift effects are measured for applying a correction are less common [99], the particular interest of this thesis, concerning with comparative coordinate measurements in which the dominant drift is due to changes in temperature, falls under this category. The system under investigation can cope with temperature changes in a shop floor environment by re-zeroing the gauging system through the principle of mastering. This means that re-mastering will ‘zero’ any thermal effects when the environment temperature changes and thus, the measurement results start to drift.

In a shop floor environment, the traditional approach to dimensional inspection is based on manually-operated devices such as micrometres, callipers, go/no-go gauges, etc., because CMMs often require temperature controlled rooms to adequately meet their measurement capability. Nevertheless, the influence of systematic effects associated with the CMM can be much reduced in comparator mode in which a machine having high repeatability is required [1, 31]. In particular, the substitution method [73], where the CMM is used as a comparator, generally decreases the measurement uncertainty and is used extensively, especially for measurement tasks with high accuracy requirements such as in the field of gauge calibration. In fact, the comparison between the calibrated value of the working standard and the indication of the CMM shows the systematic deviations of the CMM that can be subsequently used to correct the measurement results of production parts. Therefore, the problem of performing an

uncertainty budget for comparator measurements is much simpler than CMM measurements [5].

Substitution as well as non-substitution measurements on CMMs are covered by the third part of ISO 15530 [73]. To calculate the measurement uncertainty associated with CMM using calibrated parts or measurement standards, four uncertainty contributors should be considered. These uncertainty contributors are described by the following standard uncertainties:

- The standard uncertainty, $u(cal)$, of the calibrated part.
- The standard uncertainty, $u(p)$, of the measurement procedure.
- The standard uncertainty, $u(b)$, of the systematic error, b .
- The standard uncertainty, $u(w)$, from the manufacturing process.

Therefore, the expanded measurement uncertainty, U , of any measurand is calculated as follows:

$$U = k \times \sqrt{u^2(cal) + u^2(p) + u^2(b) + u^2(w)} + b \quad (2.10)$$

The standard uncertainty, $u(cal)$, is determined from the expanded measurement uncertainty, $U(cal)$, given in the calibration certificate of the calibrated part as follows:

$$u(cal) = \frac{U(cal)}{k} \quad (2.11)$$

The standard uncertainty, $u(p)$, is determined by Equation 2.3. The systematic error, b , is obtained by the difference between the mean of the measured values of the CMM, \bar{x} , and the calibrated value of the calibrated part, y_{cal} , and thus, $b = |\bar{x} - y_{cal}|$. Therefore, the standard uncertainty, $u(b)$, is evaluated by the repeated measurements on the calibrated part. The minimum number of repeated measurements is 20. Hence, this uncertainty component is usually neglected unless it is not very small. However, the standard uncertainty associated with the systematic error also includes the effect of the uncertainty in the coefficient of thermal

expansion (CTE) value for the calibrated part. This quantity is not negligible and is calculated by:

$$u(b) = (T - 20^{\circ}\text{C}) \times u(a) \times l \quad (2.12)$$

where T is the average temperature of the calibrated part during measurement, $u(a)$ is the standard uncertainty of the expansion coefficient of the calibrated part, and l is the measured dimension. Finally, the standard uncertainty, $u(w)$, includes two uncertainty quantities associated with the uncalibrated parts: the standard uncertainty, $u(wp)$, which covers the influences associated with the variations of form errors and roughness and the variations in elasticity; and the standard uncertainty, $u(wt)$, which covers the influence associated with the variation of the CTE of the measured parts. The latter uncertainty quantity is calculated by Equation 2.12, but considering the uncalibrated parts. Therefore, the standard uncertainty, $u(w)$, is obtained by:

$$u(w) = \sqrt{u^2(wp) + u^2(wt)} \quad (2.13)$$

2.5.1 Renishaw Equator comparator

The Renishaw Equator comparative gauging system has been designed to be a versatile alternative to custom hard gauging. In particular, the Equator is not an absolute measuring machine like a CMM, but it is a high speed comparative gauge, which aims at medium to high volume gauging applications on the shop floor, alongside the manufacturing equipment. Its gauging technology is based on the traditional comparison of a test part to a master part with dimensions having a high level of confidence through a software, called RenCompare. The re-mastering process can be managed with the built-in sensor and software configuration and is required to compensate for any change in thermal conditions.

The Equator gauging system has been on the market since 2011. It comprises the Equator gauging machine, the Equator controller, and the SP25 3-axis analogue scanning probe (see Figure 2.5). In particular, the SP25M (25 mm diameter scanning probe with scanning and touch-trigger modules) comprises two sensors in a single housing in order to function either as a scanning probe to gather several hundred surface points each second or as a touch-trigger

probe to acquire discrete points on the part surface. The Equator is a parallel kinematic machine (PKM) and weighs about 25kg. The Equator gauging machine is powered directly from its controller which requires single phase power. The Equator controller is a powerful dedicated control system that contains all the software required to run the system. Therefore, an additional computer is not required to operate the Equator. The Equator, as standard and used in this research, has a cylindrical working envelope with the dimensions $\varnothing 300 \text{ mm} \times 150 \text{ mm}$ (XY $\varnothing 300 \text{ mm}$ and Z 150 mm) as shown in Figure 2.6. Other models with larger working volumes are also now available.

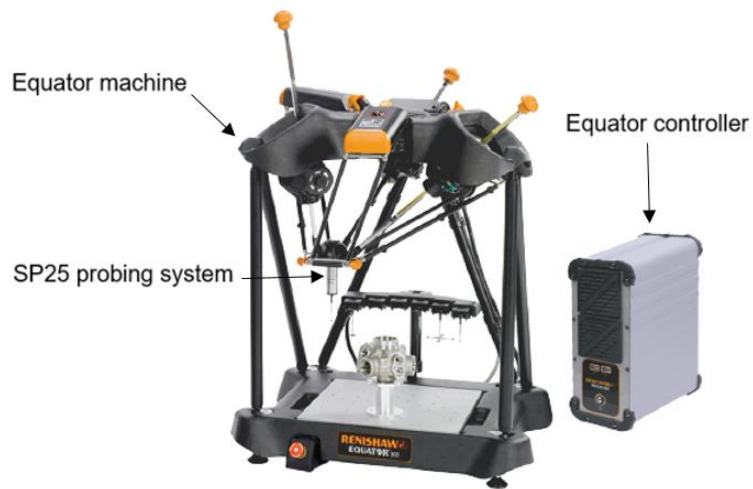


Figure 2.5: Equator 300 gauging system [105].

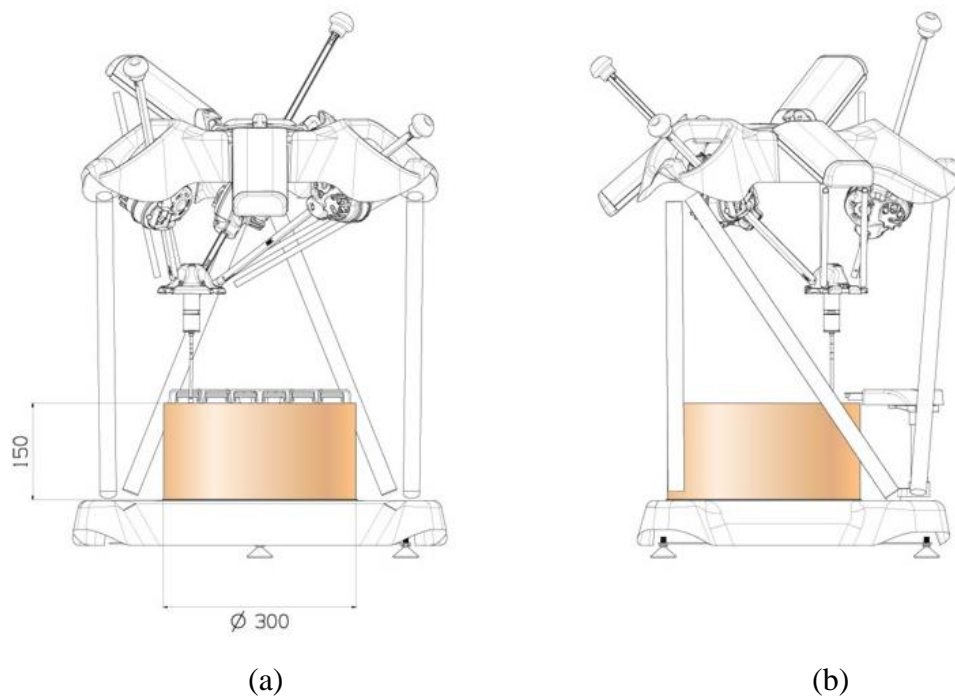


Figure 2.6: Working volume (a) front view and (b) right view [105].

The Equator machine is composed of three linear drive struts separated by an angle of 120° with respect to each other. Each drive strut is equipped with a linear encoder and is mounted on the Hooke's joint on the fixed top casting. The probe (movement) platform of the Equator is constrained by a parallel kinematic constraint mechanism so that it can remain parallel to the fixture plate or fixed base casting. Figure 2.7 provides the terminology for the Equator gauging machine.

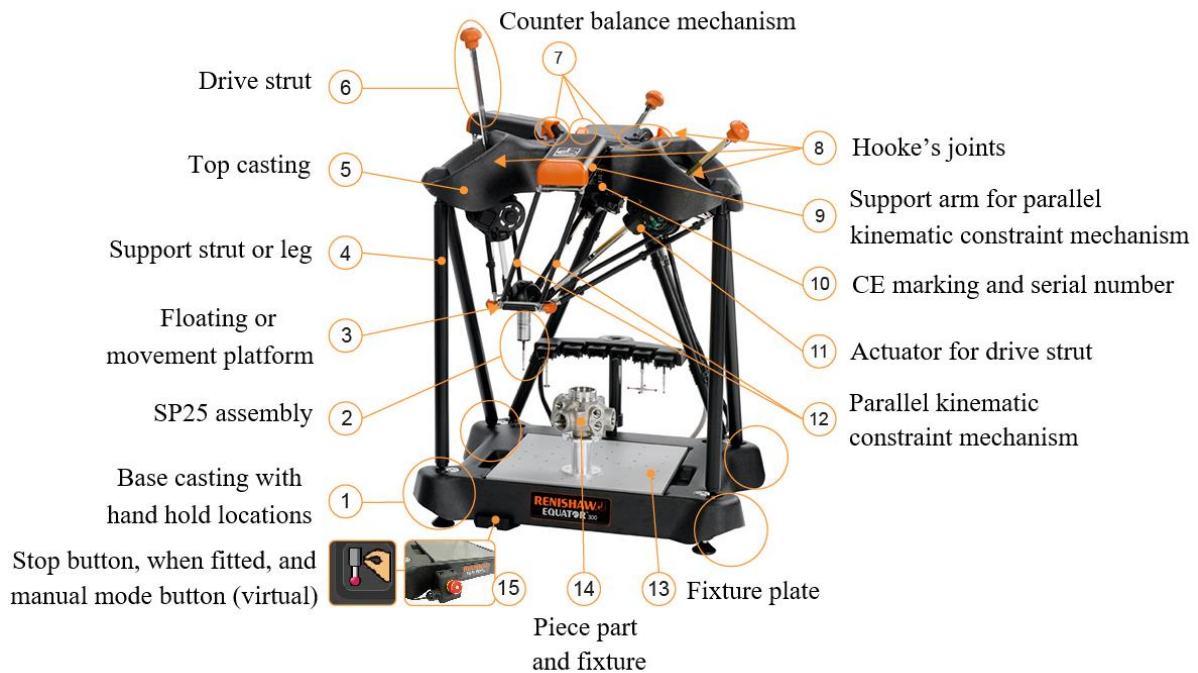


Figure 2.7: Terminology for Equator gauging machine [105].

The Renishaw MODUS Equator software has three modes: the operator mode; the programmer mode; and the administrator mode. The operator mode can be used by operators to run gauging routines and generate results using the front-end software MODUS Organiser. The operator software communicates with MODUS Gauge (see Figure 2.8) which is a version of MODUS, especially developed for gauging. MODUS Gauge communicates with RenCompare via an I++ dimensional measuring equipment (DME) interface. RenCompare software performs the comparative analysis of the metrology data and communicates with UCCserver Equator which commands the Equator and at the same time registers the probe position in space.

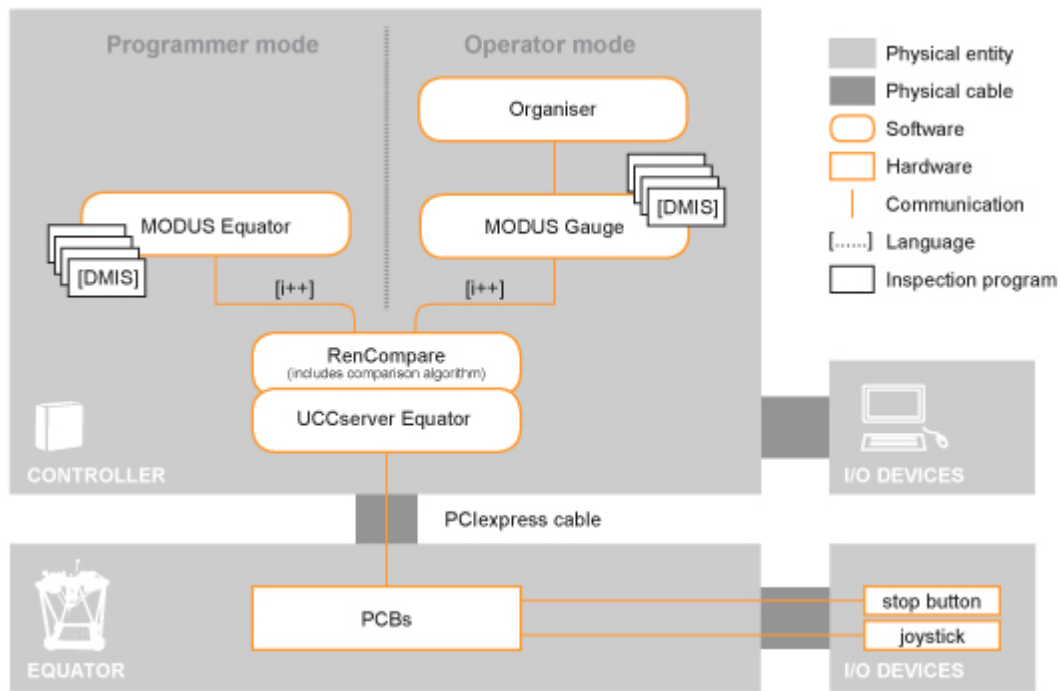


Figure 2.8: Software/hardware communication [105].

The programmer mode contains the MODUS Equator programming software which is used by production engineers to program inspection routines using the internationally recognised dimensional measuring interface standard (DMIS) language. Programming capabilities can be activated by the use of a USB security device (dongle). The administrator mode can be just used to set up the system for operator use and is only available for administrators.

In order to generate a master data set, a master part is measured using the same measurement routine produced to measure each test part. Each test data set is then compared to the master data set to determine the actual size of the test part and assess its conformance to the engineering drawing. Three different comparison methods can be distinguished:

- CMM Compare
- Feature Compare
- Golden Compare

CMM Compare is the most accurate method of using an Equator flexible gauge. It does not require a reference master part to calibrate the Equator. With CMM Compare, a test part produced close to drawing nominals can be used as a master part. However, it requires to

calibrate the “marked” master part on an accurate CMS such as a CMM in order to generate a calibration (.cal) file, which is then transferred to the Equator and read during mastering to enable the individual points of a master data set to be compared with that of test data sets. Therefore, with this compare method, the calibrated absolute accuracy of the CMM located in a temperature controlled environment can be extended onto the shop floor to provide calibrated traceability to Equator measurements.

Feature Compare is an alternative to CMM Compare that simplifies the calibration process of the master part. With Feature Compare, the inspector can manually enter the actual values for each feature’s size, position or orientation of the master part.

Golden Compare differs from the other compare methods in that there is no requirement to first calibrate the master part, for example on a CMM. However, it requires a reference master part to calibrate the Equator and presumes that the master part is produced to drawing nominals. Therefore, with this compare method, any deviation of the master part to drawing nominals will be included in the measurements. This thesis focuses on Golden Compare and CMM Compare methods.

2.6 Summary

In traditional manufacturing industry, hard gauges and CMMs have been used for many years to assess whether the dimensions of a manufactured part conform to design specifications. However, inspecting manufactured parts using hard gauges: i) is time consuming and inflexible, ii) is characterised by costly hardware changes when the design of the production parts changes, and, iii) requires highly skilled operators to assure confidence on the measurement results. Modern manufacturing requires CMSs capable of performing complex inspection tasks with low measurement uncertainty in a shop floor environment and within a very short time. CMSs such as conventional CMMs are very accurate and flexible measuring systems. However, they require stable environmental temperature conditions to ensure accurate measurement results. As a result, hard gauges or more rarely AACMMs are usually preferred on the shop floor though they are also thermally sensitive. AACMMs are manual CMMs based on a non-Cartesian structure. Compared to CMMs, they are of lower cost and weight, portable, and more flexible since they may have more than six DOF. However, their manual operation, low accuracy and frequent calibration required to reduce their errors make them not suitable

for most applications in precision manufacturing. Therefore, the traditional approach to dimensional inspection on the shop floor is based on manual gauging.

The demand for lightweight CMSs operating at higher speeds with reduced inertial effects on the shop floor has forced manufacturers to consider automated comparator gauges based on a PKM in order to achieve accurate shop floor dimensional inspection at low cost. Therefore, the Equator gauge has been recently adopted for flexible dimensional inspection on the shop floor to help bridge the divide between CMM measurement and hard gauging. Identifying defective parts immediately after they have been manufactured is of special importance because it enables effective in-process feedback from dimensional inspection on the shop floor, reduction of inspection scrap and bottlenecks since defective parts can be excluded immediately without the need for further processing, etc. However, inspection devices such as CMMs and comparator gauges are complex mechatronic systems and therefore, an accurate mathematical model for the measurement system is difficult to develop. In this thesis, artificial intelligence (AI) techniques are applied to predict CMS coordinate data.

While research has been performed on evaluating uncertainty of coordinate metrology using comparative mode, there is no academic research into uncertainty for high speed PKM configuration. Classical uncertainty evaluation methodologies usually require many repeated measurements and ignore any prior knowledge about the inspection process. On the other hand, computational Bayesian methods such as MCMC are straightforward to use to generate samples from the posterior distribution, but prior knowledge may be difficult to specify in probabilistic form.

Chapter 3

Evaluating the Uncertainty of Comparator Measurement Influenced by Misalignments using Full Factorial Designs

This chapter is concerned with evaluating the uncertainty associated with comparative coordinate measurement using the DOE approach. For the Equator gauge, the fixturing requirement of each production part to the master part is approximately ± 1 mm for a comparison process with a stated uncertainty of ± 2 μ m. Therefore, a number of experimental designs are applied with the main focus on the influence of part misalignment from rotation between master and measure coordinate frames on the comparator measurement uncertainty. Other factors considered include measurement mode mainly in scanning and TTP and alignment procedure used to establish the coordinate reference frame (CRF) with respect to the number of contact points used for each geometric feature measured.

The measurement uncertainty analysis of the comparator technique used by the Equator gauge in Golden Compare commences with a simple measurement task using a gauge block to evaluate the three-dimensional (3D) uncertainty of length comparative coordinate measurement influenced by an offset by tilt in one direction (2D angular misalignment). Then, a specific manufactured measurement object is employed so that the comparator measurement uncertainty can be assessed for numerous measurement tasks within a satisfactory range of the working volume of the versatile gauge. Furthermore, in the second case study, different types of part misalignment including both 2D and 3D angular misalignments are applied. The time required for managing the re-mastering process is also examined. A task-specific uncertainty evaluation is completed using DOE. Also, investigating the effects of process variations that might be experienced by such a device in workshop environments. Most of this work has been published in [31] and [106].

3.1 Comparator measurement

Comparator measurements are mainly subject to random effects since constant systematic effects associated with the measurement system cancel out through the principle of mastering. The re-mastering process is required to efficiently calibrate the comparator system for a specific measurement task. Figure 3.1 shows the measurement uncertainty contributors for CMMs and comparators. The main uncertainty contributors for comparator measurement can be considered to be: environmental effects, calibrated master part, measurement part, machine repeatability, part fixturing, sampling strategy, and geometric element best-fit algorithms.

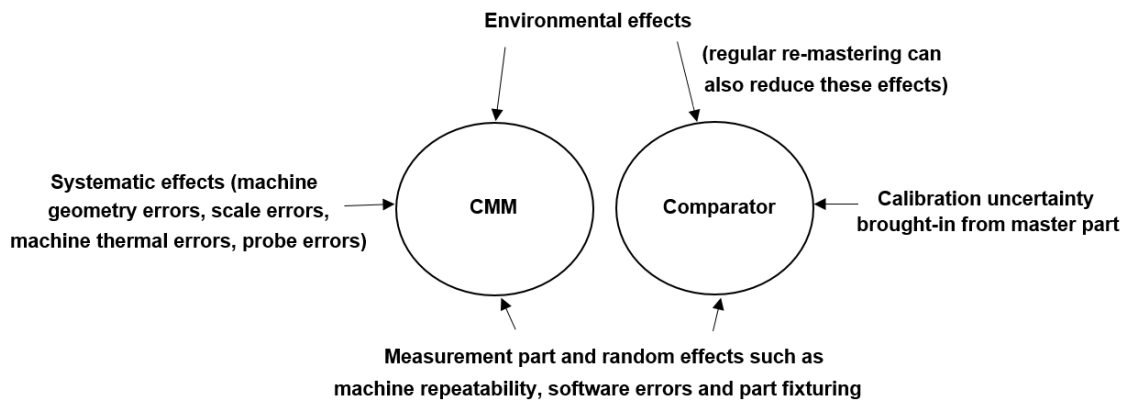


Figure 3.1: Measurement uncertainty contributors for CMMs and comparators.

The principle of operation of the Equator is to gauge or compare data/components. As has been discussed in section 2.5.1, the Equator gauge provides various compare methods, the main ones being “CMM Compare” and “Golden Compare”. In CMM Compare, the calibrated absolute accuracy of the CMM located in a temperature controlled room can be transferred to the shop floor to provide calibrated traceability to Equator measurements. The Golden Compare uses a master part (golden master) to calibrate the Equator and differs from the CMM compare procedure in that there is no requirement to measure the master part on a CMM. The Golden Compare method assumes that the master part is produced at drawing nominals and therefore, any deviation of golden master part to drawing nominals will be included in the measurements. However, measurements need to be obtained by traceable measuring systems and therefore, when employing a comparator that uses a production part as a master part, traceability to national standards needs to be established. The Golden Compare procedure consists of the following steps:

- i. Obtain a master part.
- ii. Generate the required part program on the Equator, including the commands COMPARE/ON and COMPARE/OFF.
- iii. Run the part program using the master part in master mode to generate an Equator master file.
- iv. Run the part program using the master part in measure mode (verification step).
- v. Remove the master part and replace with the production parts to be measured.

The methodology for this chapter is therefore to conduct a DOE with the factors listed in Figure 3.1, excluding the, “calibration uncertainty brought-in from master part.” The reason for this exclusion is that this chapter studies the performance of the comparator gauge and thus, it concerns only the verification step of the mastering process. In addition, the application of the CMM to the master part and determination of uncertainty is an established methodology [73].

3.2 Experimental design for 2D angular misalignment

In the first stage of this thesis, a general full factorial design using a gauge block of 100 mm was employed to evaluate the 3D uncertainty of length comparative coordinate measurement influenced by a 2D angular misalignment. Gauge blocks are simple mechanical artefacts with accurately known length between their two flat and parallel end faces and one of their primary applications is that of calibration [107]. The performance of the comparator gauge was evaluated at $24^{\circ}\text{C} \pm 0.5^{\circ}\text{C}$ temperatures (uncontrolled temperature conditions) because ideal laboratory conditions do not encompass uncontrollable factors and as a consequence, do not represent those conditions in which the comparator gauge is likely to be deployed. The stylus used was a typical 21 mm long stylus with stainless steel stem and a 5 mm diameter ruby ball. A general overview of the experimental setup is shown in Figure 3.2.

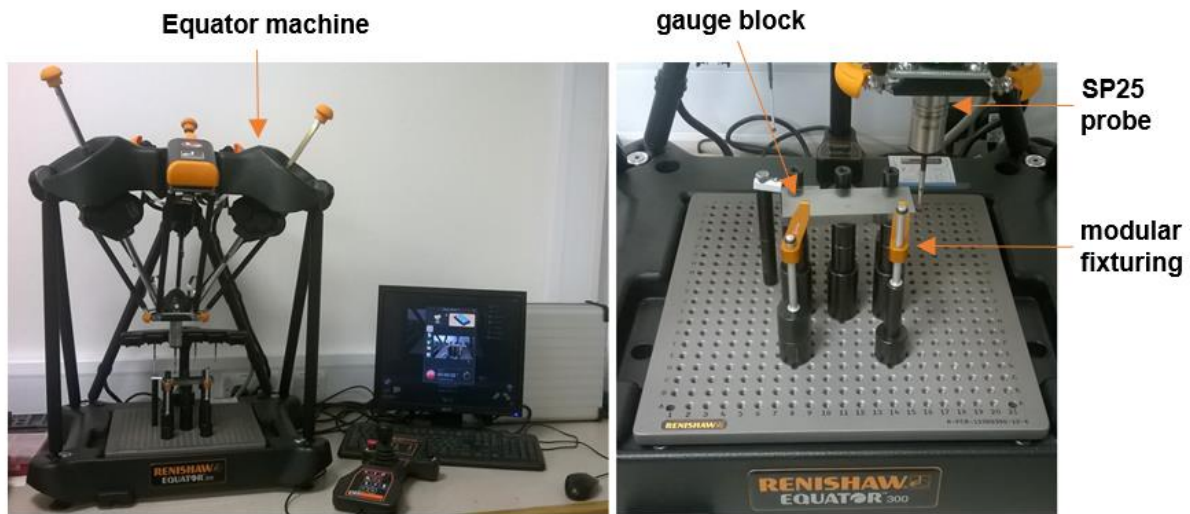


Figure 3.2: Test setup on Equator gauge for gauge block inspection.

Beyond TTP which is slow because the probe must traverse the measurement object point-to-point, scanning is being increasingly used in a large number of measurement tasks. Therefore, a number of studies have been concerned with the comparison of scanning versus touch-trigger probe measurement in absolute mode [65, 108]. However, no prior studies were found that compared scanning and touch-trigger probe measurement in comparator mode. The Equator 300 gauge used in this thesis is a PKM. Parallel kinematic mechanism-based machines have many advantages over serial structured ones such as improved repeatability and reduced inertial effects at high working speeds [109-111]. However, they suffer from a limited operational workspace and nonlinear force transmission and stiffness characteristics [112]. The Equator gauge is supplied with the industry standard SP25 3-axis analogue scanning probe. The SP25M comprises two sensors in a single housing in order to function either as a scanning probe to gather several hundred surface points each second or as a touch-trigger probe to acquire discrete points on the surface. Therefore, this study sought to investigate the difference obtained in length accuracy between scanning and touch-trigger probe measurement in comparator mode and their impact on measurement uncertainty. In order to investigate the influence of high-speed scanning on the comparator measurement uncertainty, the speed used for scanning was 100 mm/s, which is the maximum recommended for the specific comparator gauge. For TTP, a relative small number of contact points were taken because it was only to evaluate the length of a simple object consisting of two parallel planes of equal sizes, i.e. gauge blocks.

One critical factor affecting CMM performance is the part-alignment procedure used to define the coordinate system or frame of reference (CRF). In addition, estimating the measurement uncertainty contributed by the misalignment of the gauge block depends upon the alignment procedure [113]. While some recommendations for aligning gauge blocks are given in [113], there is no completely general method. However, due to the fact that in many practical applications the inspection cycle time is crucial, especially for inspections performed by the Equator which is aimed at medium to high volume gauging, two alignment procedures were chosen to highlight the influence of this factor on the uncertainty of comparator-mode measurement; 1) the non-time-saving alignment in which a sufficient number, based on good measurement practices, of discrete points were taken for each geometric feature measured and 2) the time-saving alignment where the number of contact points required for various geometric features was the mathematical minimum.

In coordinate measurement, an improper part fixturing setup affects measurement accuracy and part throughput. On the Equator, when each part is fixtured to within 1 mm relative to the master part, size and position measurements made immediately following re-mastering have a comparison uncertainty, according to the system specification, of $\pm 2 \mu\text{m}$ relative to the certified measurements of the master part. Angular misalignments [7] can largely be avoided by using an appropriate fixture arrangement for part holding. However, holding the parts to be inspected in proper position and orientation is not always an easy task. In some cases, this is not even feasible from a practical point of view e.g. in automated presentation of parts by a robot with limited repeatability or by using a non-repeatable fixturing setup or both. In this test, the alignment error leads to a cosine error [114] ($0.5\gamma L_r$), where γ is the angle between the calculated and actual perpendiculars and L_r the true length of the gauge block, and a first-order error ($\gamma\alpha$), which is negligible for measurement under computer control, since in this case α , which is the perpendicular distance of the projected sensing points from the calculated perpendicular to the surface, can be chosen to be very small [113]. Cosine error is the least of the errors caused by misalignment despite the fact that, this type of error often receives the most attention [115]. Figure 3.3 shows the misalignment of the gauge block by tilt along y-axis and Table 3.1 shows the factors and levels of the gauge block inspection. The length and width of the gauge block are 100 mm and 35 mm, respectively. So, for example, for an angle $\hat{\omega} = 8.627^\circ$ ($AB = 15 \text{ mm}$), the angle $\hat{\theta}$ is equal to 81.373° and therefore, based on Pythagorean

Theorem, $\Gamma\Delta = 5.25$ mm. In order to investigate if the measurement accuracy degrades as the angle value $\hat{\omega}$ increases, seven levels were used for this factor (see Table 3.2).

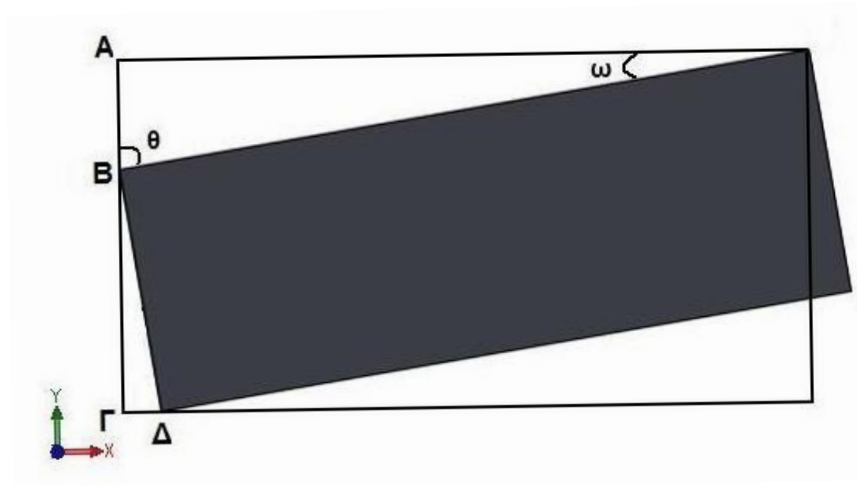


Figure 3.3: Angular misalignment of the gauge block.

Table 3.1: Factors and levels of the gauge block inspection.

Factors	Levels						
	1	2	3	4	5	6	7
(A) Measurement mode	Scanning	TTP					
(B) CRF	Non-time-saving	Time-saving					
(C) Angular misalignment	a	b	c	d	e	f	g

Table 3.2: Values for the angular misalignment.

Levels	$\hat{\omega}$	$\hat{\theta}$	AB	$\Gamma\Delta$
a	0.000°	90.000°	0.000 mm	0.000 mm
b	0.573°	89.427°	1.001 mm	0.350 mm
c	1.146°	88.854°	2.000 mm	0.700 mm
d	2.292°	87.708°	4.000 mm	1.400 mm
e	4.014°	85.986°	7.000 mm	2.450 mm
f	5.739°	84.261°	10.000 mm	3.500 mm
g	8.627°	81.373°	15.000 mm	5.250 mm

It is worth mentioning that, the use of randomization technique for balancing the effect of extraneous or uncontrollable conditions that can impact the measurement results is not required in this work because the flexible gauge is calibrated by mastering. In addition to that, the presented work is designed to be representative of the actual working conditions in which the flexible gauge is used. The Equator comparator has been designed for shop floor gauging with possibly wide temperature variation. Shop floor conditions mostly differ from ideal laboratory conditions in the fact that they have more random and systematic effects. It is usually difficult to distinguish between these effects very clearly [116]. Consequently, the concerns of randomization issues due to practical considerations [90] and/or the need of mixed-effects models [117] in statistical data analyses are largely avoided.

3.3 Comparator measurement uncertainty evaluation

In order to avoid misleading conclusions mainly due to the random effects of shop floor environment and achieve a good level of confidence, the measurement of the gauge block was followed immediately after mastering and repeated ten times without re-mastering so in total, 280 lengths were determined. For each set of ten repeated measurements, the comparison measurement uncertainty was determined following the uncertainty evaluation methodology given in ISO 15530-3:2011 [73] concerned with substitution measurement. At present, there is no standard specifically concerned with uncertainty evaluation associated with scanning measurement in comparator mode. ISO 15530-3 provides an experimental technique for evaluating uncertainty associated with discrete-point probing. By capturing points by scanning, a high spatial density is achieved. Consequently, through the combination of oversampling and the application of the same measurement routine for master and production parts, the individual probing points are sufficiently coincident to permit the use of this standard for uncertainty evaluation. Therefore, the expanded uncertainty, U , was calculated by Equation 2.10 (in section 2.5) considering only the standard uncertainty associated with the measurement procedure. In such a measurement system, all actual features on the master part are set to their drawing/part program nominal values during the master procedure.

In order to evaluate the fit of a given distribution (such as the normal distribution in this case) to the data set, a histogram and a normal probability plot of the measurand values were produced. However, to easily assess substantive departures from normality, Figure 3.4 shows the normal probability plot of the measurand because histograms require more data in order to

effectively identify which standard distribution to select. Also, although a probability plot serves a similar function as an empirical cumulative distribution function plot, with a probability plot the distribution fit is easier to be judged by viewing how the data points fall about the line because deviations from the straight line indicate departures from normality.

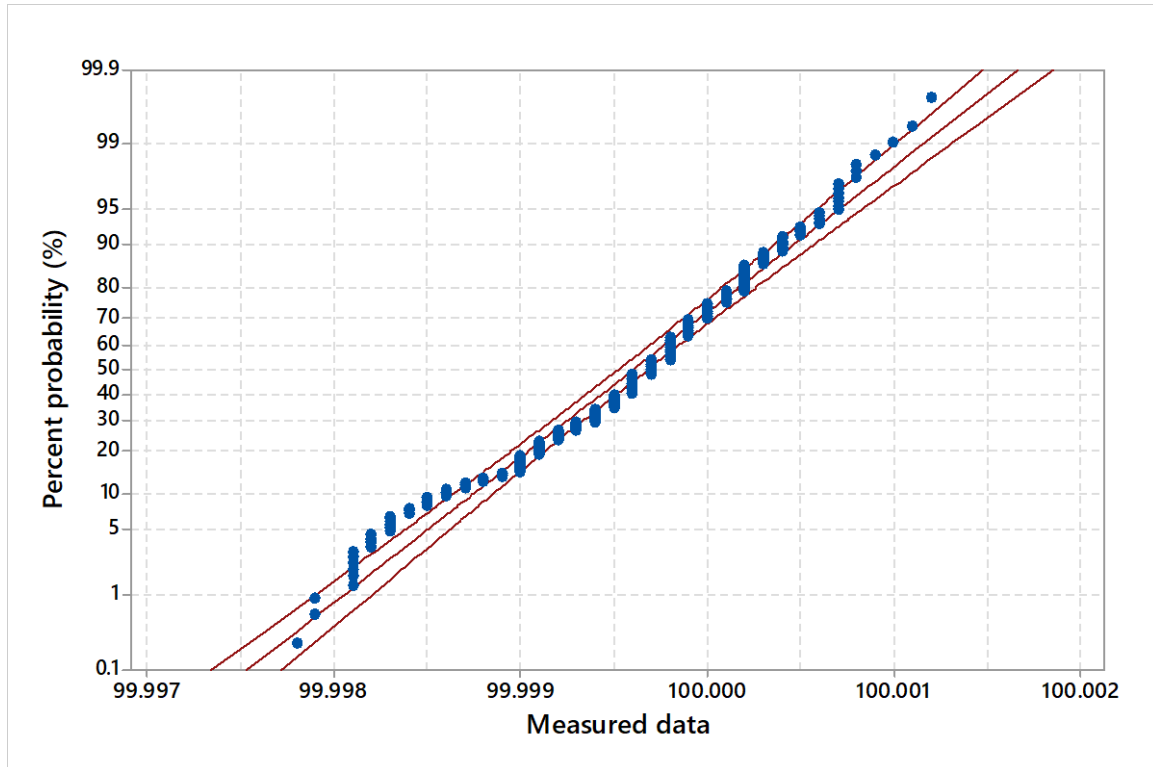


Figure 3.4: Normal probability plot of the measured length.

As can be seen from Figure 3.4, the measurement results follow a normal distribution with negligible departures from normality. For a normal distribution, the interval that contains only one standard deviation provides a confidence level of 68.27%. A confidence level of 95.45% is achieved by using a coverage factor $k = 2$ (two standard deviations of the mean) [5]. Figure 3.5 shows the main effects plots of the factors for the expanded measurement uncertainties U for $k = 2$ and a 95.45% confidence level.

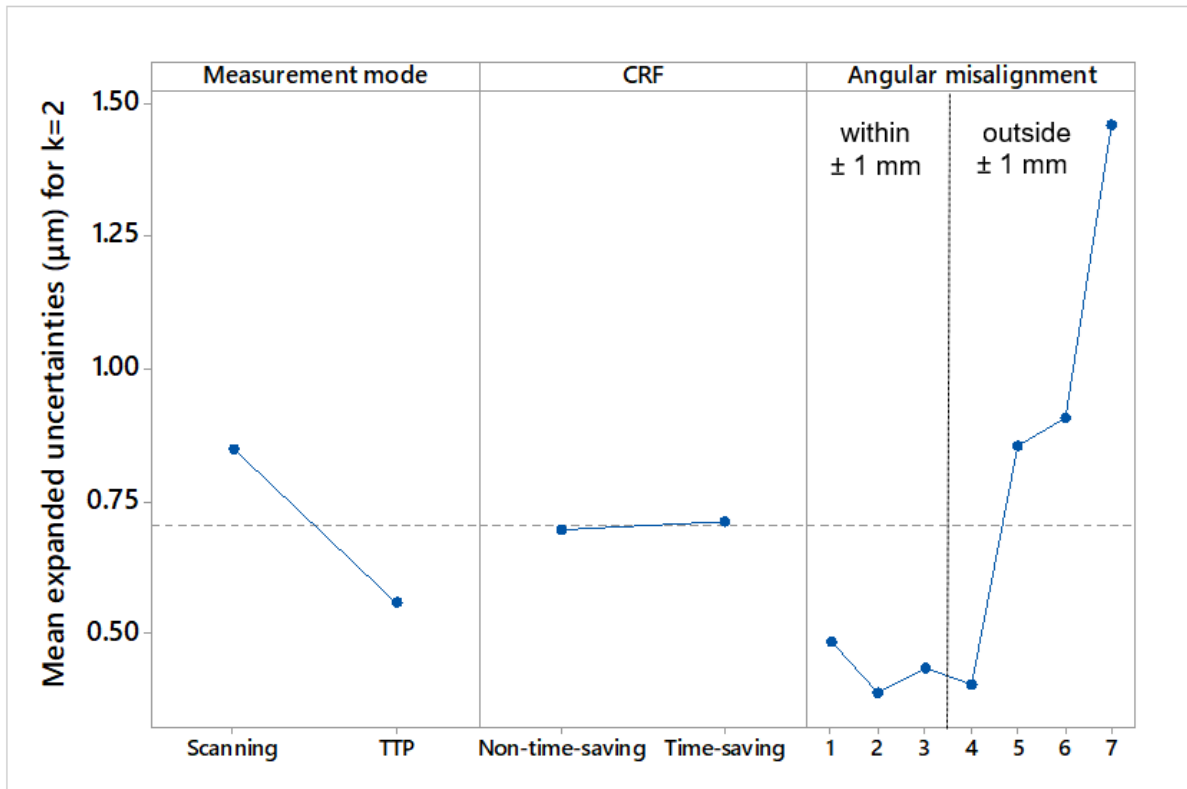


Figure 3.5: Main effects plots for expanded measurement uncertainties.

The results in Figure 3.5 show the measurement uncertainty of the comparator technique, which is well within specification. As can be seen, for this measurement task: the comparator measurement uncertainty is smaller in TTP mode than scanning mode though the difference in uncertainty between scanning and TTP is less than 0.5 µm; the number of probing points used to establish the CRF above the mathematical minimum have no statistically significant influence on the comparator measurement uncertainty; and the comparison uncertainty becomes larger as the angular misalignment exceeds the ± 1 mm fixturing requirement in the Equator specification but enabled any sensitivity and relationship to be identified. As previously stated, this test takes the misalignment well beyond the device's specification. In addition, the interaction plots including all the possible interactions of the factors for the length comparator measurement uncertainties were produced. However, they are very small (< 2 µm) under all combinations of factors and therefore, factor interactions are shown only for the second experimental design.

Sections 3.2 and 3.3 have provided a methodology for investigating, in an effective way, the effect of angular misalignment on the comparator measurement uncertainty using simple measurement objects such as gauge blocks. Section 3.4 follows the same procedure for

different measurement tasks on a representative part in order to make an adequate statement about the measurement capability of the flexible gauge using the Golden Compare method. In addition, both 2D and 3D angular misalignments are applied.

3.4 Experimental design for advanced part misalignment

For the second experimental work, a connecting rod (conrod) was designed using CAD software and then manufactured using a CNC machine tool so that the uncertainty of comparator-mode measurement can be assessed for different types of measurement (different features and characteristics) within a satisfactory range of the Equator working volume. Therefore, the probe configuration was based on preliminary experiments that involved four different probe configurations, multiple point alignment and minimal point alignment procedures, and measurement mode in scanning and TTP. Also, in order to investigate if a lower speed in scanning and a larger number of contact points in TTP improve or degrade measuring accuracy, two different speeds were used for scanning and two different numbers of discrete points were selected to be taken for each feature in TTP; one using a relatively large number of contact points and one using a relatively small number of contact points for that particular features according to good measurement practices. Then, based on the results of preliminary experiments, angular misalignments were applied with one probe configuration so that the emphasis is on the effects and interactions of angular misalignment with measurement mode and alignment procedure used to define the CRF on the comparator measurement uncertainty. Also, it was argued, if the distribution of points with TTP should follow the same path used for scanning. To avoid the influence of feature form deviations and be able to draw more refined conclusions about the effect of these factors and their interactions on comparator measurement uncertainty, the same path was used for both measurement modes. CMM measurement strategies, including the selection of the number and distribution of contact points, are outlined in the NPL good practice guide [57].

This chapter concentrates on diameter and length measurement. The levels considered for the angular misalignment after mastering were: no offset by tilt in any direction; 2.5 mm offset by tilt along z -axis; 3 mm offset by tilt along y -axis; and the resulting 3D angular misalignment with the simultaneous combination of both (see Figure 3.6). As described above, angular misalignments with unknown magnitude are common in practical applications. Therefore, investigating their influence on the uncertainty associated with comparative coordinate

measurement is of great importance. Table 3.3 shows the factors and levels of the conrod inspection.

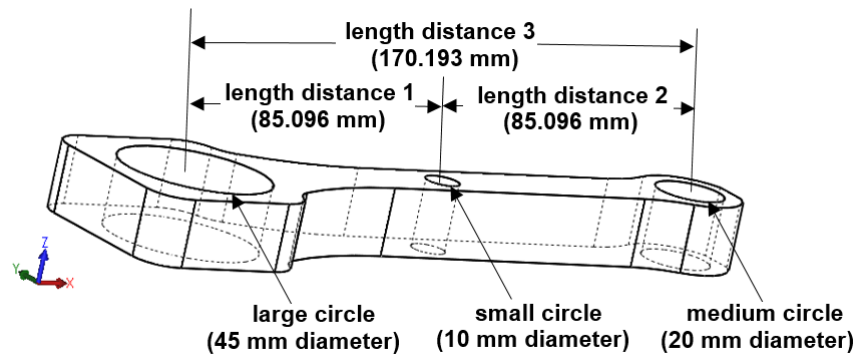


Figure 3.6: 3D offset by tilt for the conrod.

Table 3.3: Factors and levels of the conrod inspection.

Factors	Levels			
	1	2	3	4
(A) Measurement mode	Scanning 100 mm/s	Scanning 50 mm/s	TTP Many points	TTP Few points
(B) CRF	Non-time-saving	Time-saving		
(C) Angular misalignment	0 mm	2.5 mm along z-axis	3 mm along y-axis	3D
(D) Probe configuration	Stylus 21×5	Stylus 50×5	Stylus 40×2	Stylus 30×4

3.4.1 Preliminary experiments for probe configuration

A full factorial design was applied to assess the influence of the factors on the comparator measurement uncertainty. The factors of interest in the preliminary experiments were measurement mode, alignment procedure used to establish the CRF, and probe configuration including the following styli: 1) a 21 mm long stylus with stainless steel stem and a 5 mm diameter ruby ball; 2) a 50 mm long stylus with ceramic stem and a 5 mm diameter ruby ball; 3) a 40 mm long stylus with tungsten carbide stem and a 2 mm diameter ruby ball; and 4) a 30 mm long stylus with tungsten carbide stem and a 4 mm diameter ruby ball. The room temperature was set to $20^{\circ}\text{C} \pm 0.5^{\circ}\text{C}$ because choosing the right probe configuration for an inspection process required the minimization of environmental effects. The measurement of the conrod was followed immediately after mastering and repeated ten times without re-

mastering. 80 measurement results were determined for each measurand and for each stylus used. A general overview of the experimental setup is shown in Figure 3.7.

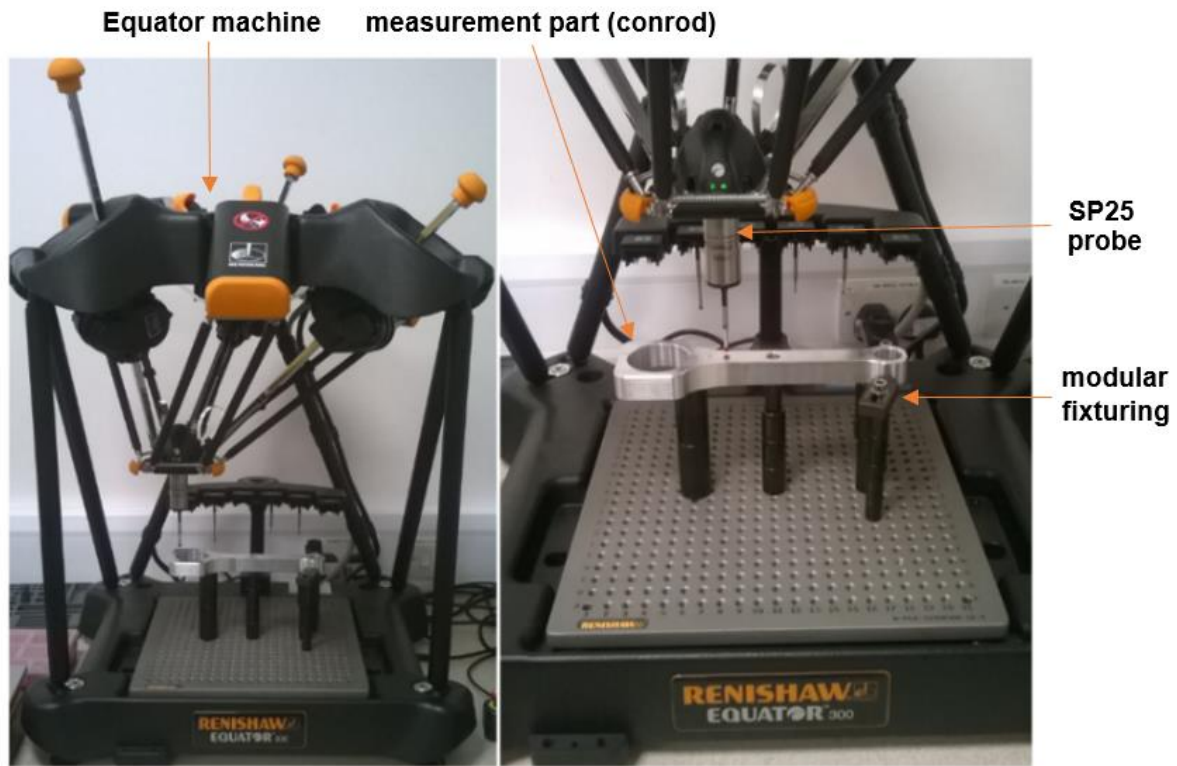


Figure 3.7: Test setup on Renishaw Equator for preliminary experiments.

To illustrate both a measure of central tendency and variability of the data against probe configuration, an interval plot was produced for each measurand. Due to the large number of measurands, only representative figures are presented. Figures 3.8 and 3.9 show one interval plot for diameter measurement and one interval plot for length measurement. Based on the interval plots and the associated standard uncertainties for all the measurands, the best results were obtained from the 21×5 and the 40×2 probe stylus. However, the 21×5 probe stylus was selected for the main experiment because a short straight stem configuration is more rigid and generally provides better results. The longer stylus with ceramic stem provided measurement data having the highest standard deviation and the least probable estimate of the true mean value, while the 30×4 probe stylus provided results with higher uncertainties in comparison to that obtained by the 21×5/40×2 probe styli.

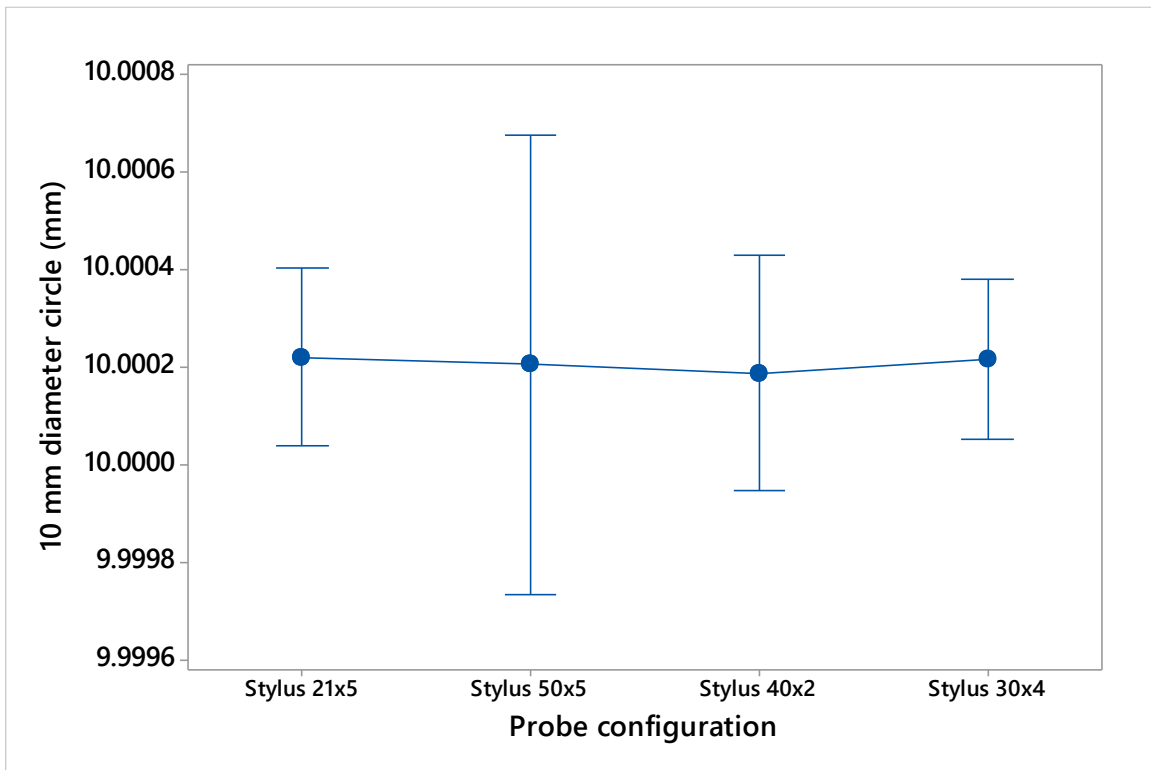


Figure 3.8: Diameter of small circle versus probe configuration.

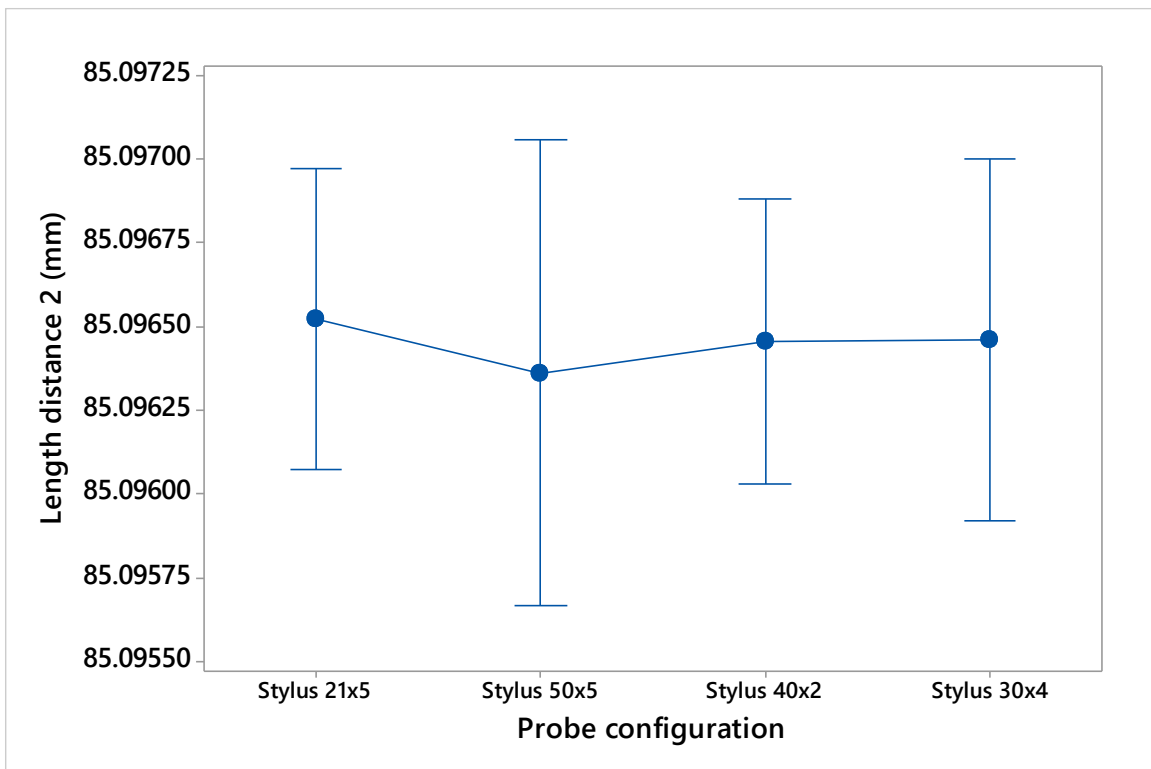


Figure 3.9: Length distance 2 versus probe configuration.

3.4.2 Main experiment for advanced part misalignment

A full factorial design was applied under workshop conditions for the main experiment using the first stylus and involving the factors: measurement mode, alignment procedure used to establish the CRF, and angular misalignment (part misalignment from rotation between master and measure CRFs). After mastering, ten repeated measurements were performed without re-mastering so 320 measurement results were determined for each measurand.

Furthermore, temperature readings were recorded during the main experiment to record the temperature variation of shop floor conditions. One temperature sensor was used for the ambient temperature, three for the temperature of the measuring machine, and four for the part. Although the flexible gauge is insensitive to ambient temperature changes due to the comparison method of mastering, the accuracy of inspection results is dependent on the influence of temperature on the parts to be measured, unless the flexible gauge has been calibrated using a master part having the same temperature with that of production parts or multiple master files have been used. Figure 3.10 shows the experimental setup and location of the temperature sensors. The accuracy of the temperature sensors is $\pm 0.5^{\circ}\text{C}$. The part is made of aluminium, which is a material with high thermal conductivity and high expansion coefficient making it sensitive to temperature gradients with rapid response to variation in the temperature of the environment. In the case of manual loading of parts into the machine, the temperature distribution on the part can be dependent on operator handling. Figure 3.11 shows a representative sample of the ambient temperature under which the experiment took place (temperature readings were taken every ten seconds).

The fixturing arrangement was slightly modified for the main experiment in order to attach the temperature sensors on the bottom plane of the part. It is also worth mentioning that, an important contribution to the overall measurement uncertainty may owe to the fixturing variability due to the simple fixture arrangement used so that the angular misalignments can be easily applied. However, this is taken into account by the uncertainty contribution associated with the measurement procedure and shall not be considered separately.

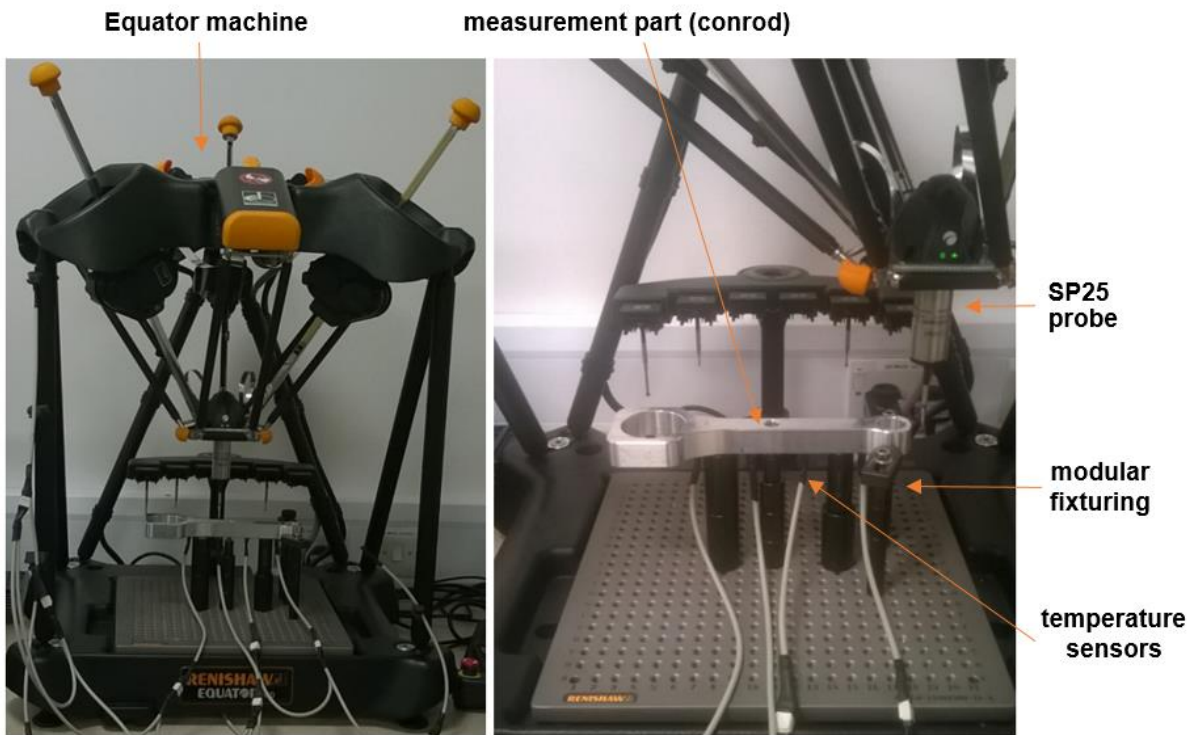


Figure 3.10: Test setup on Renishaw Equator for main experiment.

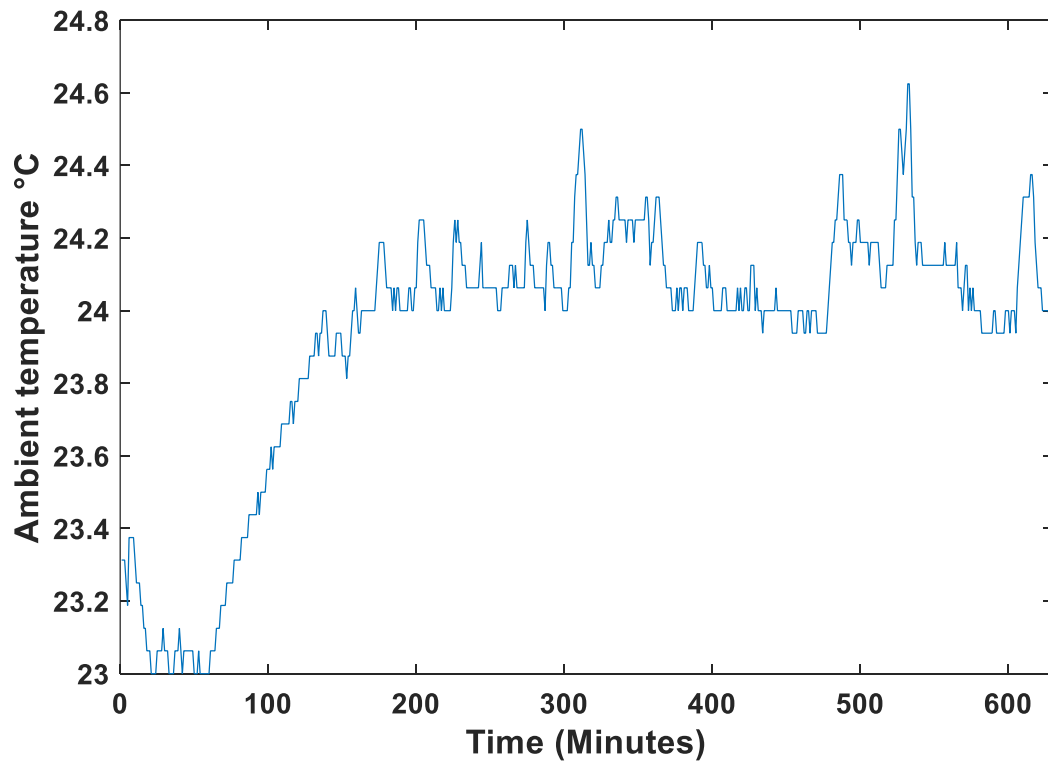


Figure 3.11: Sample of ambient temperature.

As with the gauge block inspection, for each set of ten repeated measurements, the comparison measurement uncertainty was determined following the uncertainty evaluation methodology given in ISO 15530-3:2011 [73]. For each measurand, a normal probability plot was produced for assessing substantive departures from normality and all were judged to be satisfactory for 95% confidence level. Table 3.4 shows the results obtained by the ANOVA procedure based on a least squares regression approach.

Table 3.4: ANOVA results for the conrod inspection.

Measurands	p-values						R^2
	A	B	C	A*B	A*C	B*C	
Small circle diameter	0.040	0.528	0.729	0.733	0.975	0.768	68.05%
Medium circle diameter	0.052	0.183	0.116	0.305	0.381	0.336	81.81%
Large circle diameter	0.923	0.536	0.087	0.493	0.368	0.709	73.76%
Length distance 1	0.853	0.222	0.013	0.498	0.481	0.449	80.20%
Length distance 2	0.043	0.178	0.000	0.088	0.154	0.147	92.13%
Length distance 3	0.253	0.448	0.000	0.297	0.582	0.707	90.11%

Based on the ANOVA results, the statistically significant factors and second order factor interactions for 95% confidence level (p -values < 0.05) are: measurement mode (A) for the small circle; angular misalignment (C) for length distance 1 and 3; and measurement mode (A) and angular misalignment (C) for length distance 2. Note that, R^2 is the percentage of the response variable variation explained by the linear regression model in Minitab [118]. Figures 3.12-3.17 show the main effects plots for the expanded measurement uncertainties U for $k = 2$ and a confidence level of 95.45%.

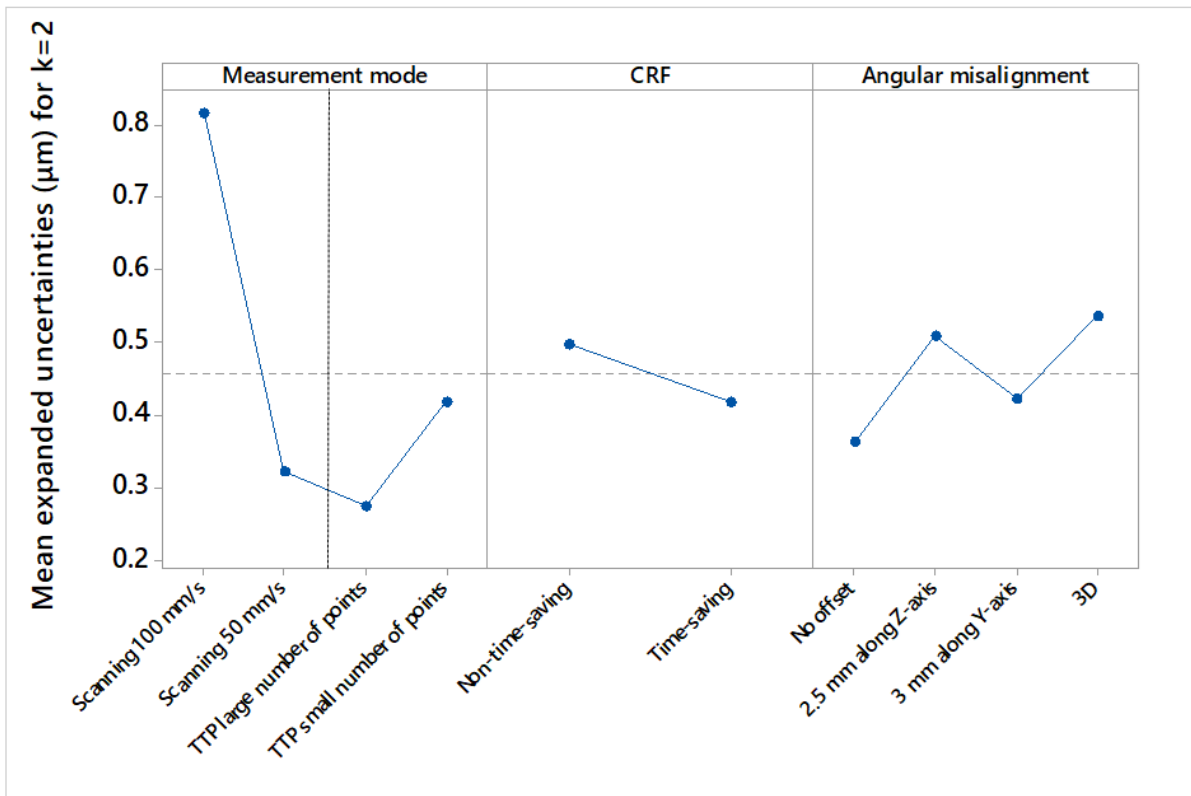


Figure 3.12: Main effects plots for the uncertainties of small circle diameter.

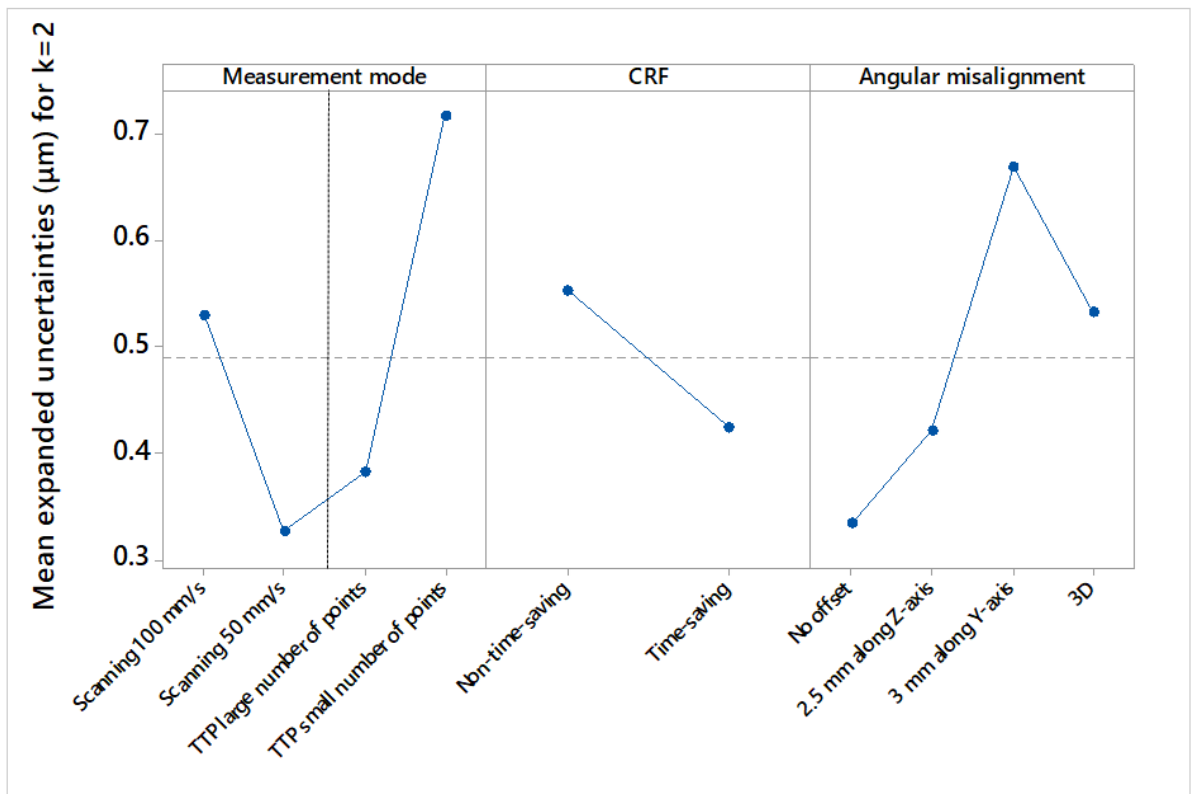


Figure 3.13: Main effects plots for the uncertainties of medium circle diameter.

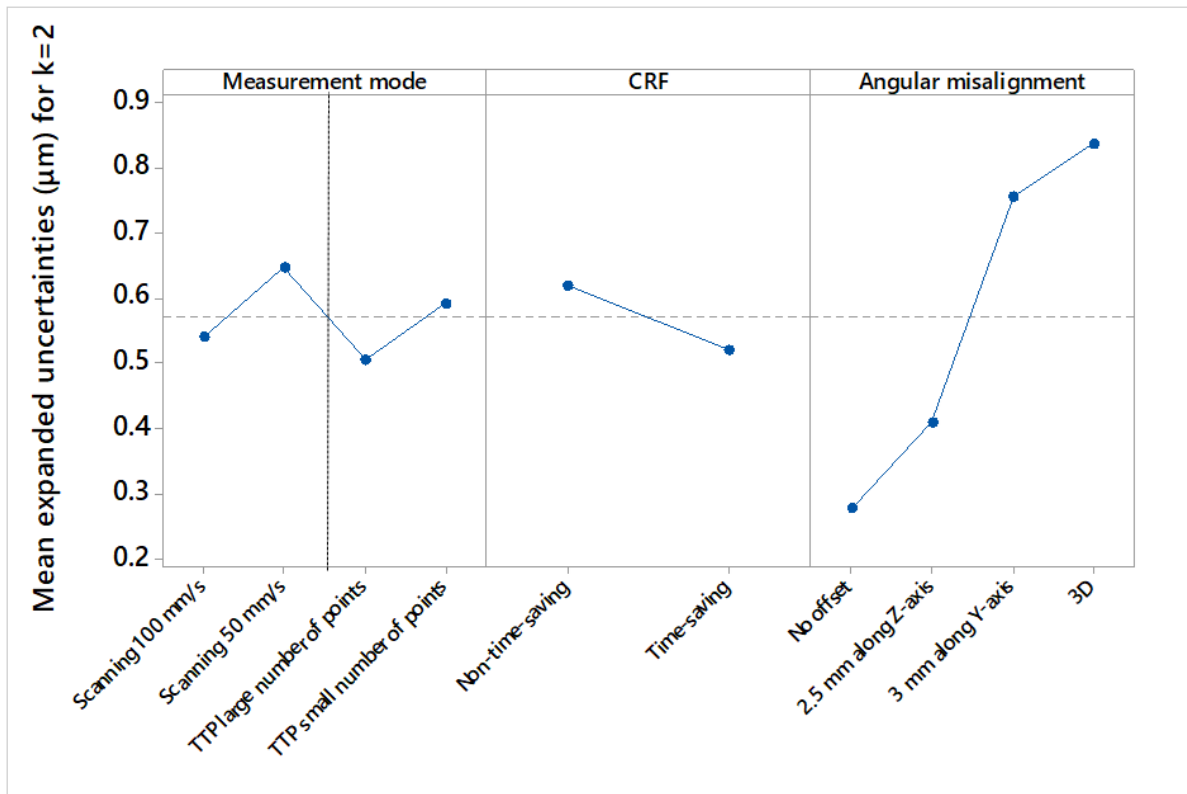


Figure 3.14: Main effects plots for the uncertainties of large circle diameter.

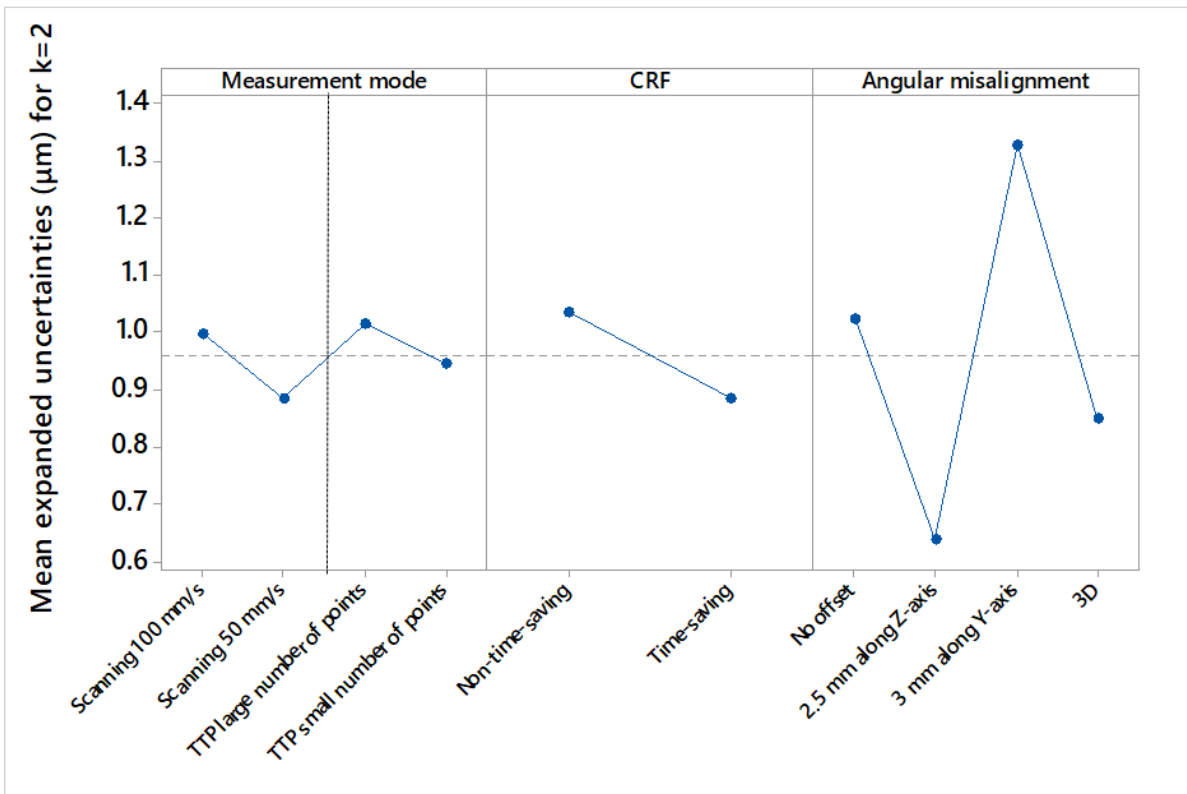


Figure 3.15: Main effects plots for the uncertainties of length distance 1.

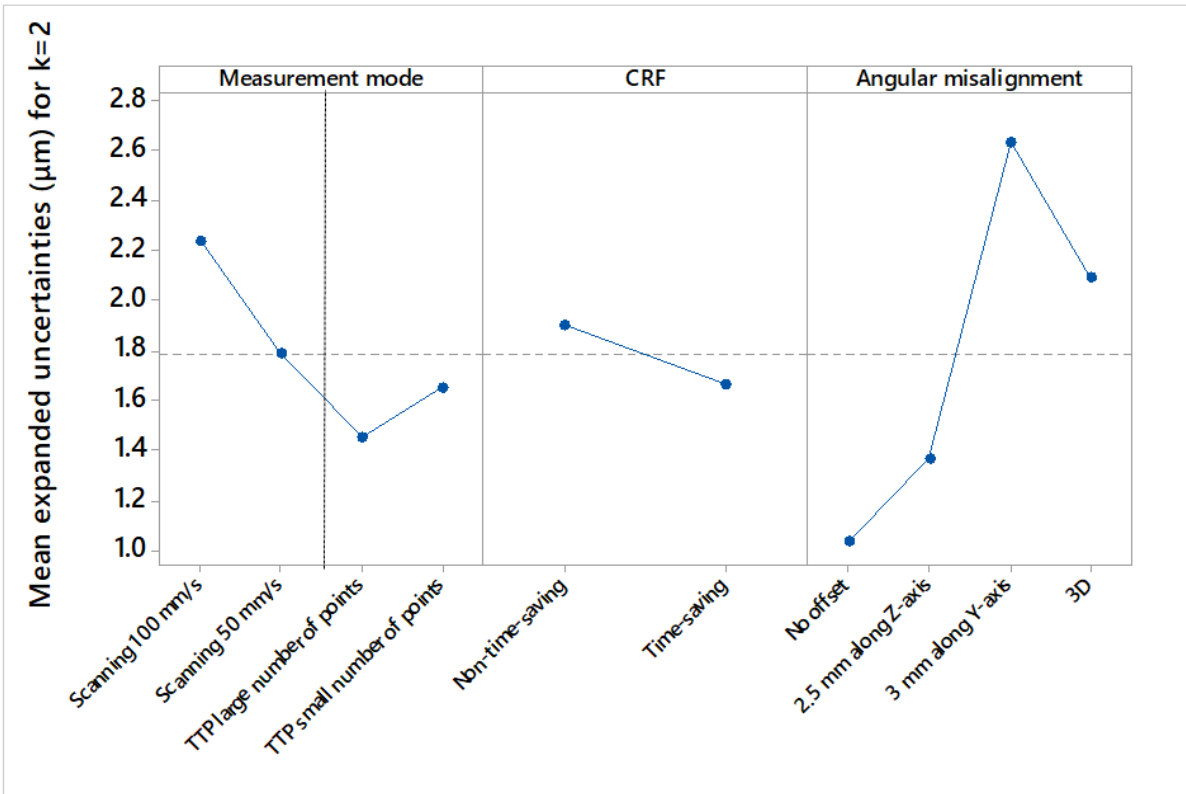


Figure 3.16: Main effects plots for the uncertainties of length distance 2.

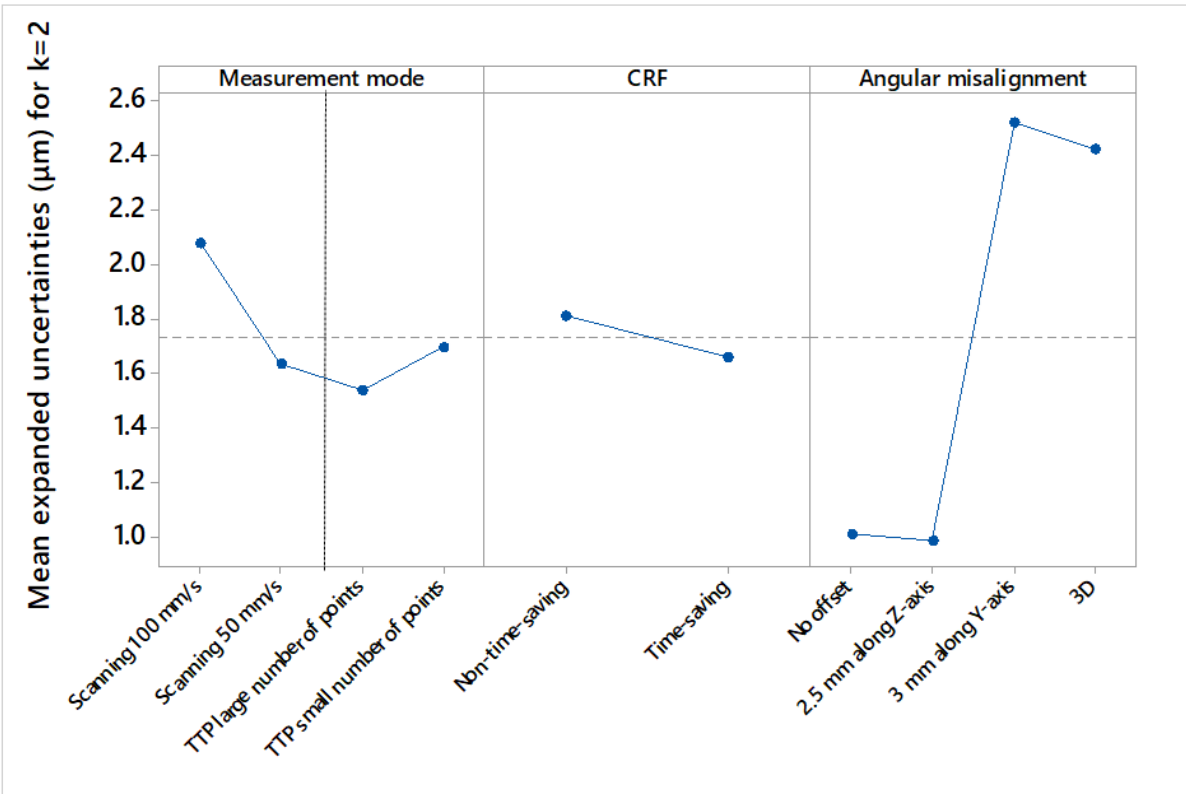


Figure 3.17: Main effects plots for the uncertainties of length distance 3.

Based on the main effects plots shown in Figures 3.12-3.17, the following conclusions can be made for the specific flexible gauge, part and test conditions:

1. The comparator measurement uncertainty is not significantly influenced by a time-saving alignment procedure so a considerable saving of time can be achieved by performing a quick alignment procedure without increasing uncertainty. However, datum uncertainties have to be taken into account for features which are evaluated with respect to datum's such as true position [60].
2. Careful consideration needs to be paid for the scanning speed used for the inspection of each feature because this is proportional to the traversed radius. As a consequence, a very high scanning speed will result in increasing the comparator measurement uncertainty (see Figures 3.12 and 3.13 and Figures 3.15-3.17). However, a typical Cartesian CMM without compensation techniques normally requires lower scanning speeds to meet its measurement capability and thus, such low uncertainty values.
3. A relatively large number of contact points provides smaller measurement uncertainties in comparison to limited sampling (see Figures 3.12-3.14 and Figures 3.16 and 3.17).
4. The difference in comparator measurement uncertainty between scanning and TTP measurement is associated with the scanning speed used for scanning and the number of probing points used for TTP for a given feature, but was found to be less than 1 μm for all cases tested.
5. The diameter measurement uncertainties remain below $\pm 2 \mu\text{m}$ even when exceeding the specified alignment conditions.
6. The length measurement uncertainties remain below $\pm 2 \mu\text{m}$ under specified conditions and when exceeding the specified conditions only along z-axis for this experimental setup.

Departures from the specified part fixturing requirement of the flexible gauge show that the comparator measurement uncertainty is associated with the measurement task, feature size, measurement strategy used, and magnitude and direction of offset angles in relation to the reference axes of the machine. Figures 3.18 and 3.19 show the factor interactions at the 95% confidence level for the expanded measurement uncertainties of length distance 3 to illustrate that the degree of interaction is high for length measurement only when the misalignment includes a 3 mm offset by tilt along y-axis, which exceeds to a great extent the specified conditions of the system.

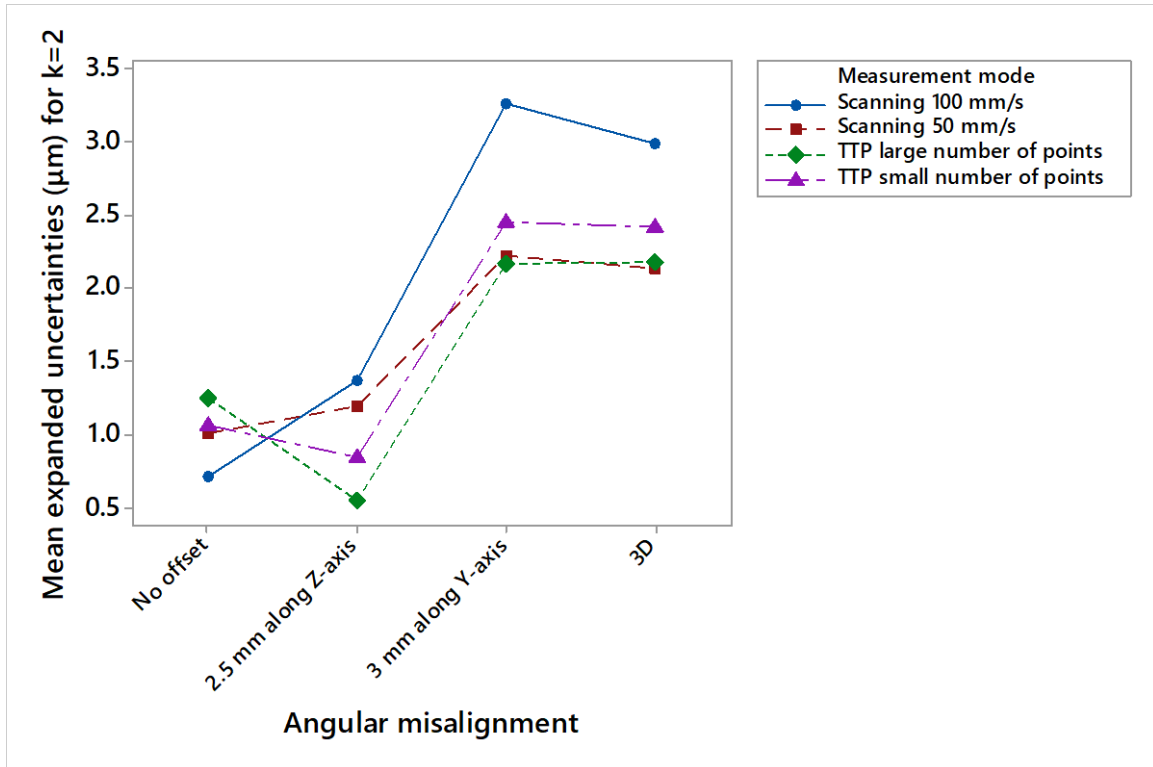


Figure 3.18: The interaction plot of measurement mode and angular misalignment for the uncertainties of length distance 3.

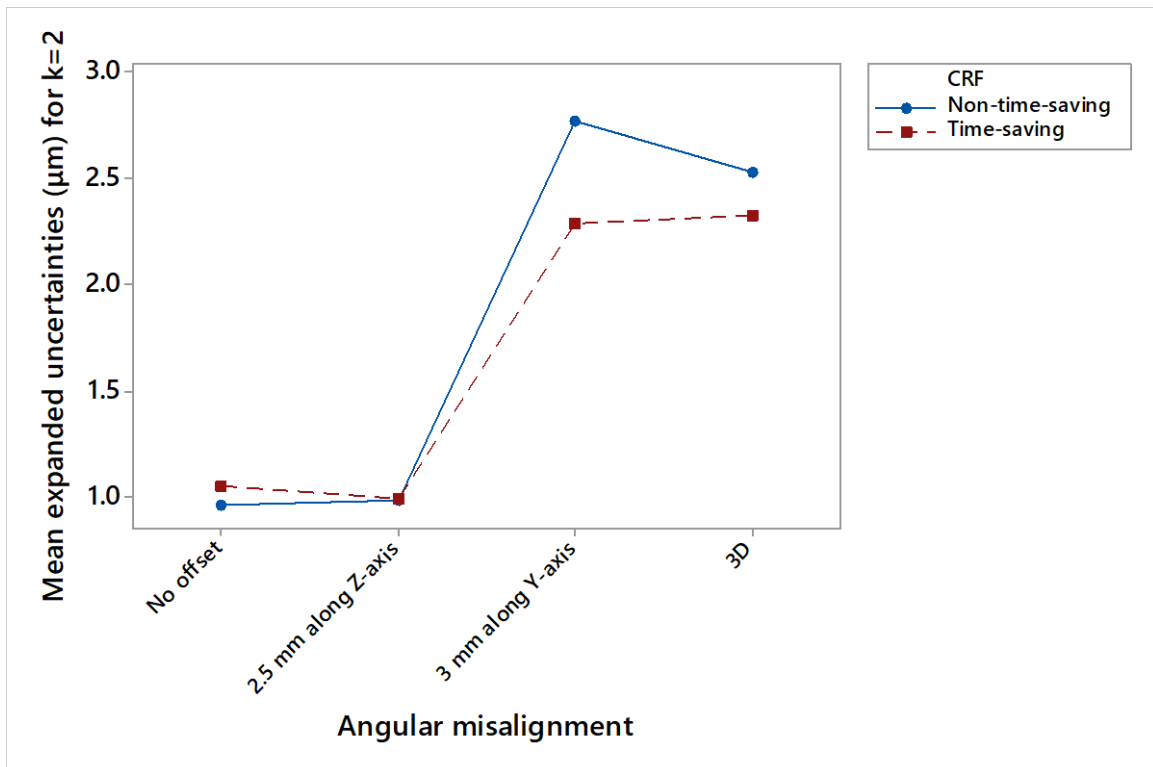


Figure 3.19: The interaction plot of CRF and angular misalignment for the uncertainties of length distance 3.

3.5 Managing the re-mastering process

Another DOE was employed to examine the time required for managing the re-mastering process in shop floor conditions. The factors were: i) temperature in different levels for two different cases and ii) scanning speed in two levels (100 mm/s and 50 mm/s), as previously, for the main experiment. In the first case, the comparator gauge was used to measure the circular features of the part ten times at both scanning speeds immediately after mastering for different ambient conditions (21.5°C, 24°C, 26.5°C, and 29°C). In the second case, the comparator gauge was mastered at 21.5°C ± 0.5°C and then employed to measure the circular features of the part ten times at both scanning speeds without re-mastering in each case (24°C*: Master at 21.5°C/Measure at 24°C, 26.5°C*: Master at 21.5°C/Measure at 26.5°C, and 29°C*: Master at 21.5°C/Measure at 29°C). Table 3.5 shows the factors and levels for the DOE concerned with managing the re-mastering process. The results obtained from this experimental design are shown in Figures 3.20-3.25.

Table 3.5: Factors and levels for the DOE concerned with managing re-mastering.

Factors	Levels						
	1	2	3	4	5	6	7
(A) Temperature	21.5°C	24°C	26.5°C	29°C	24°C*	26.5°C*	29°C*
(B) Scanning speed	100 mm/s	50 mm/s					

The CTE describes how the size of a part material changes with a change in temperature. For a typical material such as aluminium in this case this is expressed as $23.1 \times 10^{-6} \text{ }^\circ\text{C}^{-1}$. To correct a length to 20°C, consider the following equation:

$$l_{20} = l_T + (20 - T) \times a \times l_T \quad (3.1)$$

where l is the measured length, T is the average temperature at which the length was measured, and a is the CTE. Without re-mastering the behaviour of the comparator system is similar to that of CMMs, which are sensitive to environmental effects. Temperature changes cause the machine components and parts being measured to expand, contract, and, in certain cases, distort in a nonlinear manner. Thus, the coefficient of linear thermal expansion may not be accurate.

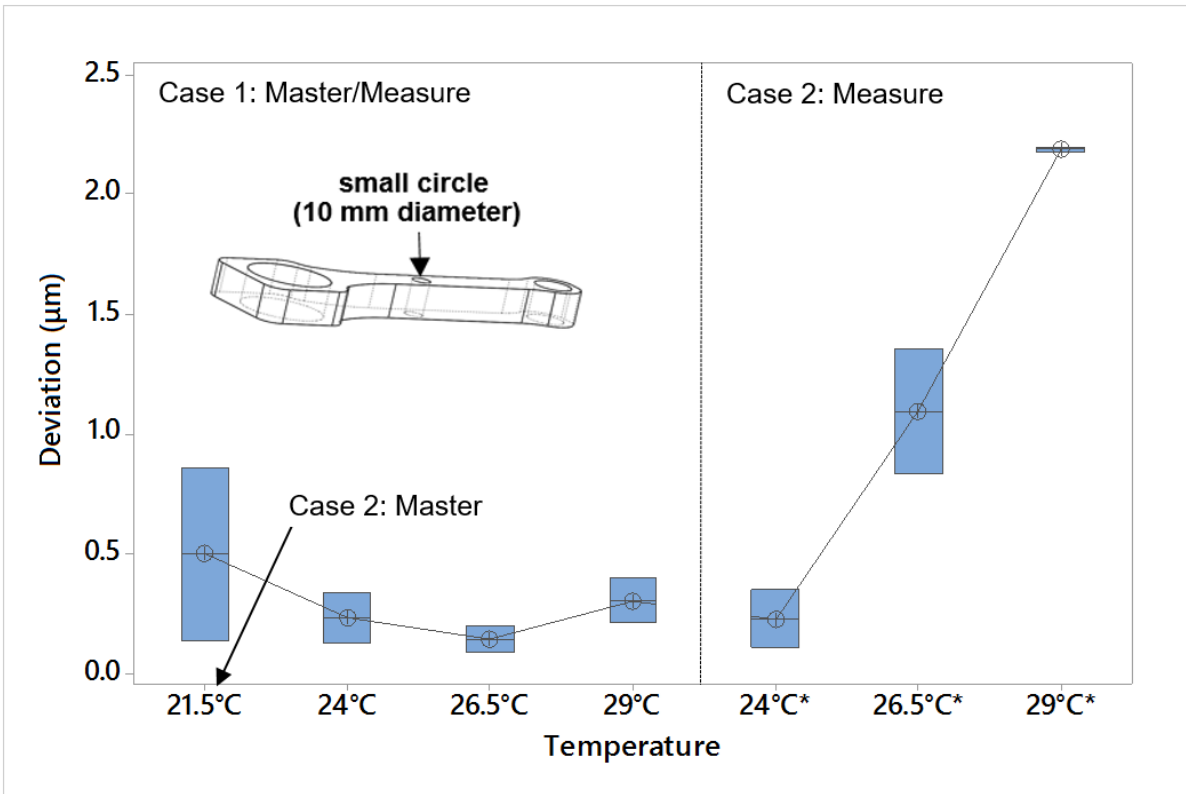


Figure 3.20: Boxplot of the diameter of small circle.

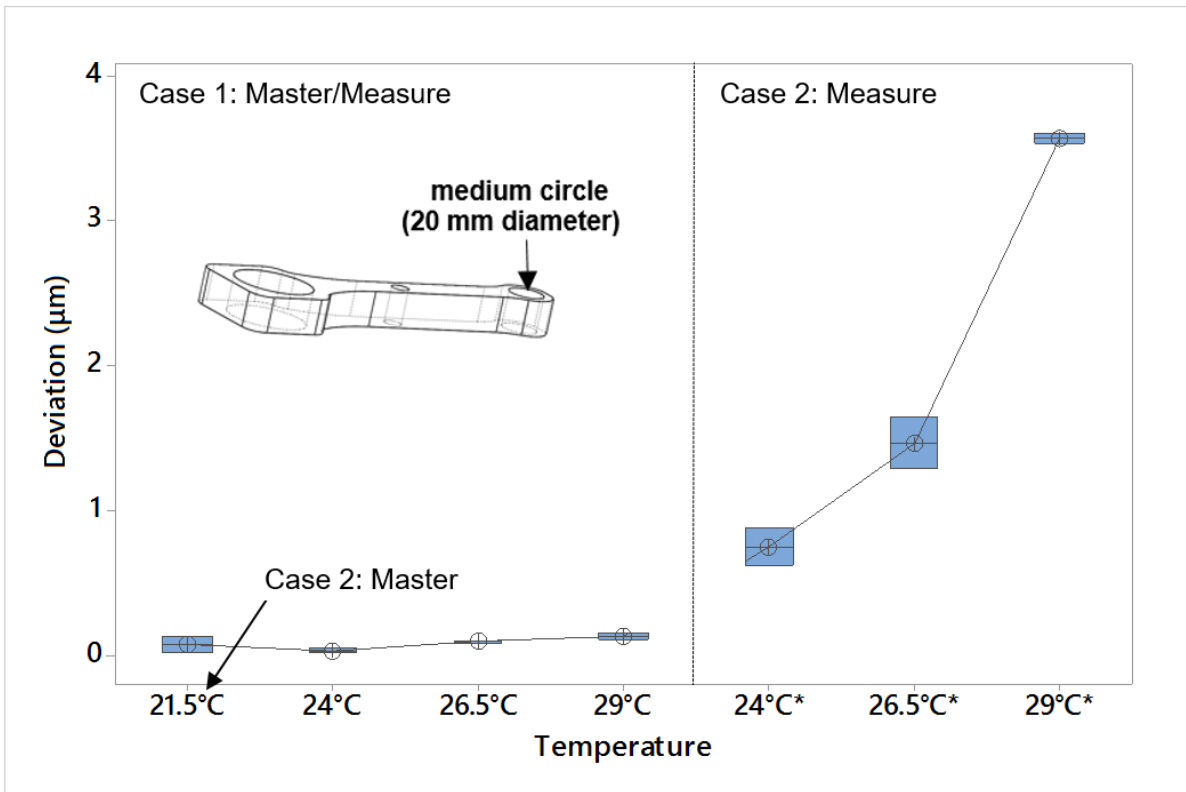


Figure 3.21: Boxplot of the diameter of medium circle.

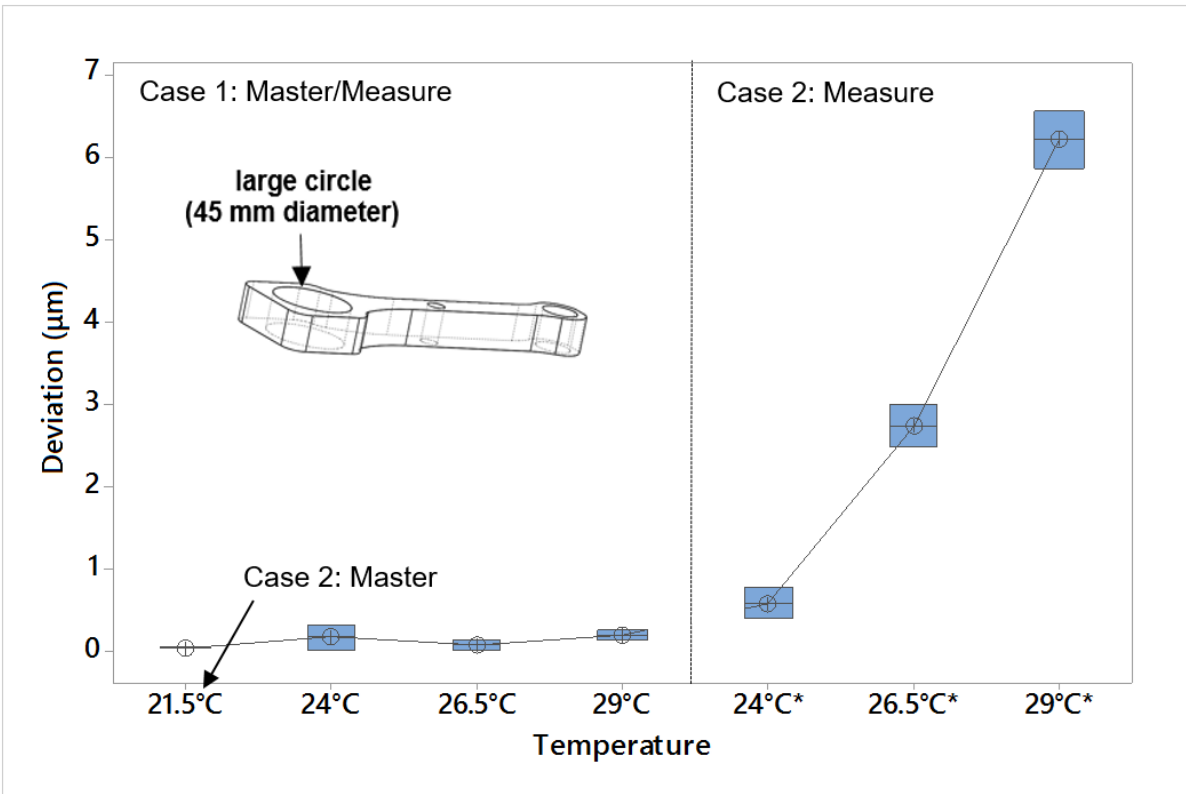


Figure 3.22: Boxplot of the diameter of large circle.

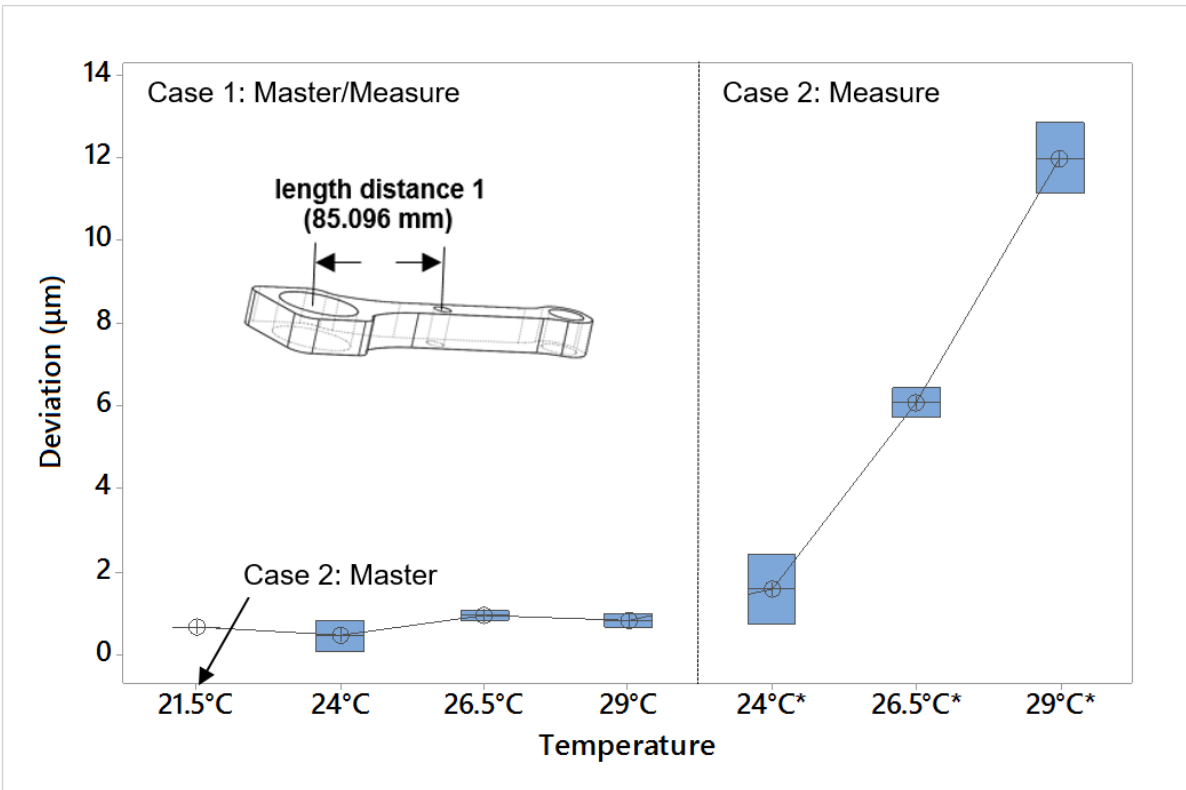


Figure 3.23: Boxplot of the length distance 1.

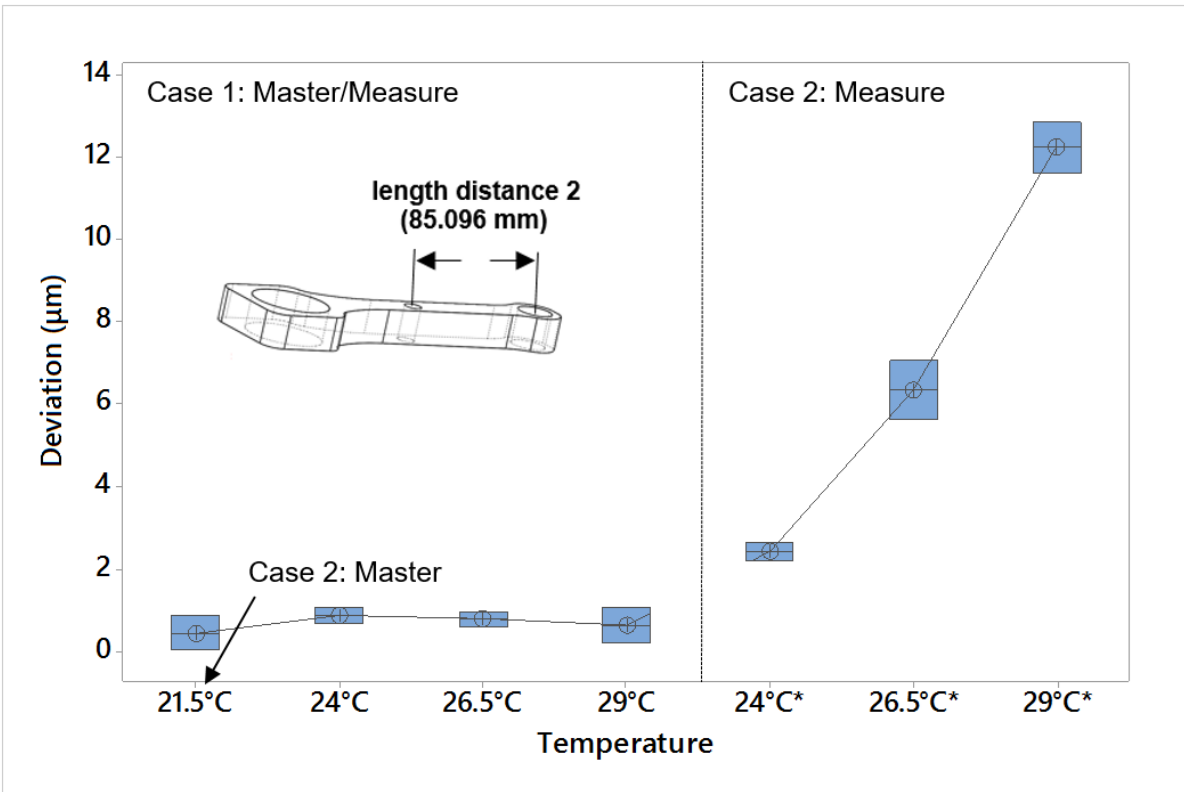


Figure 3.24: Boxplot of the length distance 2.

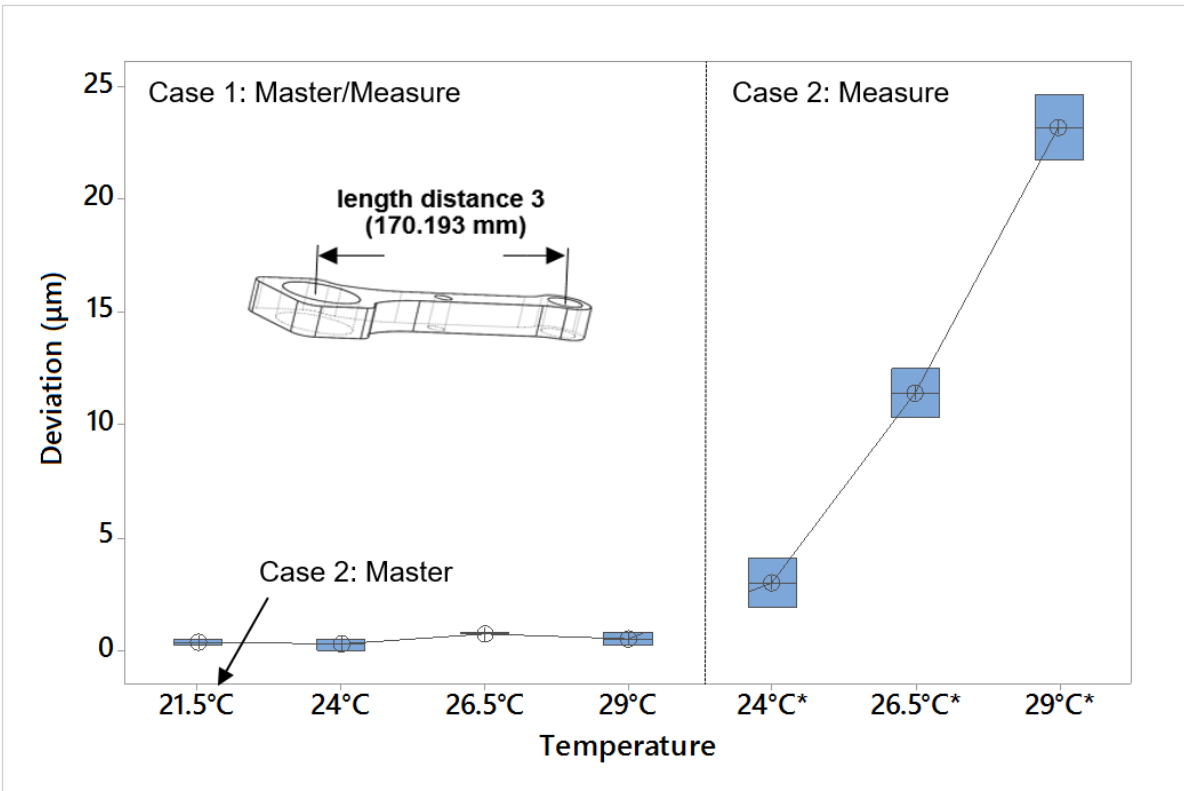


Figure 3.25: Boxplot of the length distance 3.

As shown in Figures 3.20-3.25, the uncertainty requirements of the application will determine the time of re-mastering because environmental effects cause linear and nonlinear strains and deformations of the part being measured as well as the CMS. For higher accurate measurements, the effect of environmental conditions on the comparative measurement can be managed by setting a more restricted upper and lower temperature drift limit by means of built-in sensor feature of Equator. Finally, it is important to note that in Figure 3.20, the large data variability owes to the high scanning speeds used for measuring the small circle of 10 mm diameter. However, based on the results, it can be concluded that a PKM-based flexible gauge maintains its accuracy at high speeds.

3.6 Summary

As the need in manufacturing for in-process feedback increases, many efforts have been made to place the measuring equipment close to the machining process and, at the same time, to achieve repeatable measurements with relatively low measurement uncertainty and within a very short time. Renishaw has developed a new adjustable variable gauge, called Equator. However, there are practical applications in which fixture arrangements are restricted to setups of low repeatability, thus inducing errors in the measurement process. For this reason, full factorial designs have been employed to evaluate the influence of 2D and 3D angular misalignments between master and measure coordinate frames on the comparator measurement uncertainty. It has been demonstrated that for this PKM-based flexible gauge and test conditions there is no significant effect on system repeatability associated with diameter measurement in comparator mode even when the fixturing requirement is exceeded by the studied misalignment values. In particular, it is associated with the feature size, measurement strategy used, and magnitude and direction of offset angles in relation to the reference axes of the machine. However, for length measurement, fixtures/components should relocate within the versatile gauge's volume to an approximate tolerance of ± 1 mm (fixturing requirement according to the system specification) to ensure a successful comparison process. The comparator measurement uncertainty is dependent on the number of probing points used to measure each feature in TTP mode and on the scanning speed used in scanning mode, but not on the number of probing points taken for establishing the CRF. Lastly, the accuracy requirements of the application and task-specific uncertainty evaluation are required for managing the re-mastering process.

Chapter 4

Evaluating the Comparator Uncertainty within the Whole Working Volume and Statistical Modelling

This chapter employs the DOE approach to investigate the influence of part location, measurement strategy and environmental effects on the comparator measurement uncertainty. Therefore, two full factorial designs are applied to perform a practical analysis of measurement uncertainty of the PKM-based flexible gauge within its whole measuring volume. The Equator is used in Golden Compare mode under shop floor conditions and in both TTP and scanning mode in order to investigate the behaviour of the comparator system within its whole measuring volume in both measurement modes. In addition, this chapter is concerned with the development of a statistical model for uncertainty associated with comparative coordinate measurement. Therefore, another full factorial design is employed using two replicates at different temperature conditions in order to decouple the influence of environmental effects. The concepts and key results from this work have been published in [119] and [120].

4.1 Comparative coordinate measurement based on TTP

A full factorial design was employed using discrete probing to investigate the effect of part location and ambient temperature on comparator measurement uncertainty. The part used is a clutch plate with a nominal internal diameter of 77 mm and an external diameter of 98.4 mm. The stylus used is a typical 21 mm long stylus with stainless steel stem and a 2 mm diameter ruby ball. A general overview of the experimental setup is shown in Figure 4.1.

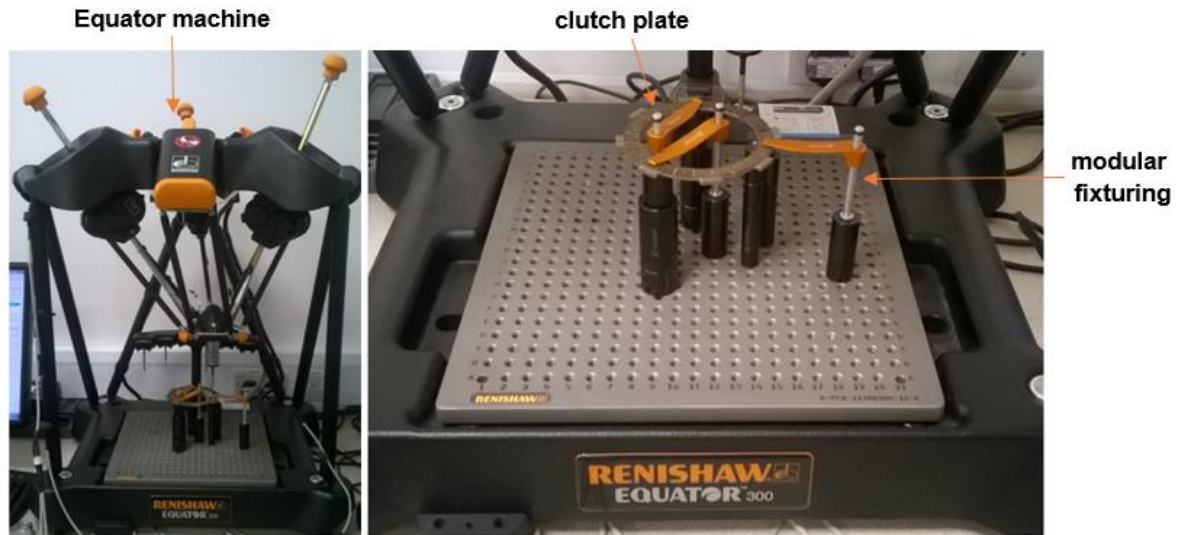


Figure 4.1 Test setup on Equator gauge for the clutch plate.

The part was placed in nine different locations within the Equator’s measuring volume in order to cover a significant portion of the total working volume. For consideration of ambient temperature effects, two conditions were represented; 1) typical metrology room temperature control of 20-22°C and 2) typical uncontrolled workshop temperature of 27-29°C. The actual temperature varied a little depending on the part location but never exceeding a difference in temperature between master and measure larger of more than 1°C and, in both cases, the part had been thermally stabilized at each temperature before mastering. Temperature readings were recorded during the experiment using additional temperature sensors to record the temperature variation of the environment. The measurands were the internal and external diameters. For both diameters seven points were selected to be taken as such a sample size of contact points is practical for many applications. The measurement of the clutch plate was followed immediately after mastering and repeated 20 times without re-mastering and without moving the part. Therefore, in total, 720 diameters were determined; 360 internal diameters and 360 external diameters. Table 4.1 shows the factors and levels for the DOE with the clutch plate. Figure 4.2 depicts the nine different locations where the part was placed.

Table 4.1: Factors and levels of the clutch plate inspection.

Factors	Levels								
	1	2	3	4	5	6	7	8	9
(A) Ambient temperature	20-22°C	27-29°C							
(B) Part location	1	2	3	4	5	6	7	8	9

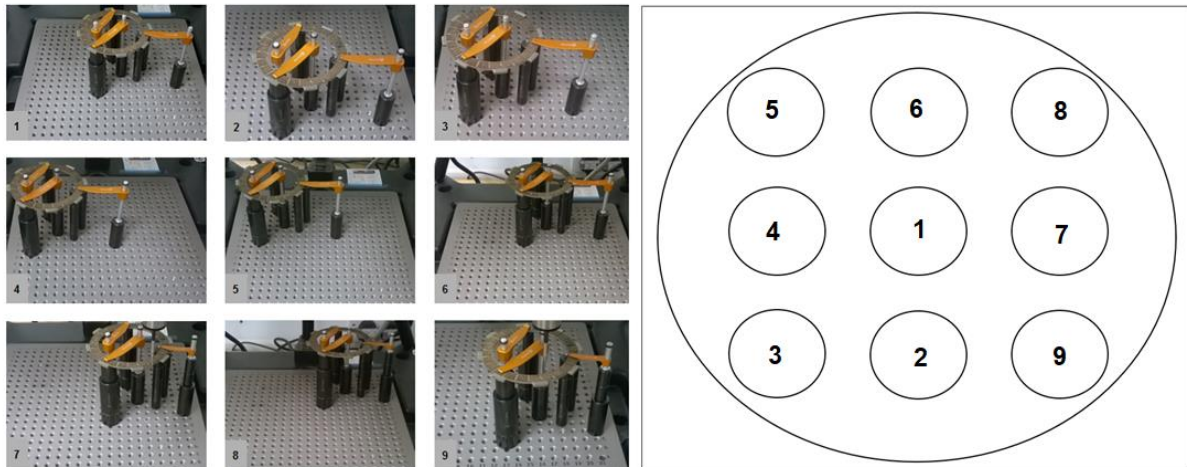


Figure 4.2 Clutch plate locations.

4.1.1 Diameter uncertainties for all part locations using TTP

For each set of 20 repeated measurements, the expanded comparator measurement uncertainty was determined following the uncertainty evaluation methodology given in ISO 15530-3:2011 [73]. In addition, a normality test was performed for each measurand to determine whether the measurement data followed a normal distribution, and all were judged to be satisfactory for a significance level of 0.05. Therefore, Figures 4.3 and 4.4 show the main effects plots for the expanded measurement uncertainties U of the internal and external diameters of clutch plate, for $k = 2$ and a confidence level of 95.45%, where the Equator is used in TTP mode.

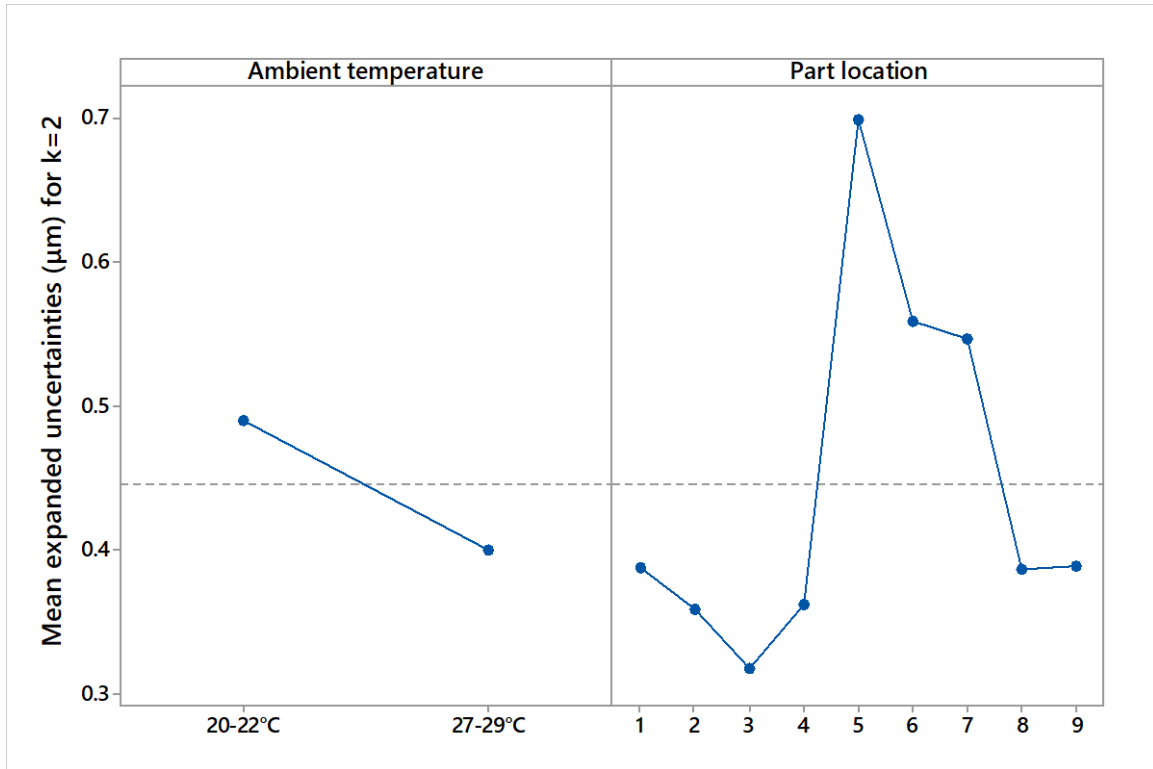


Figure 4.3: Main effects plots for the uncertainties of internal diameter.

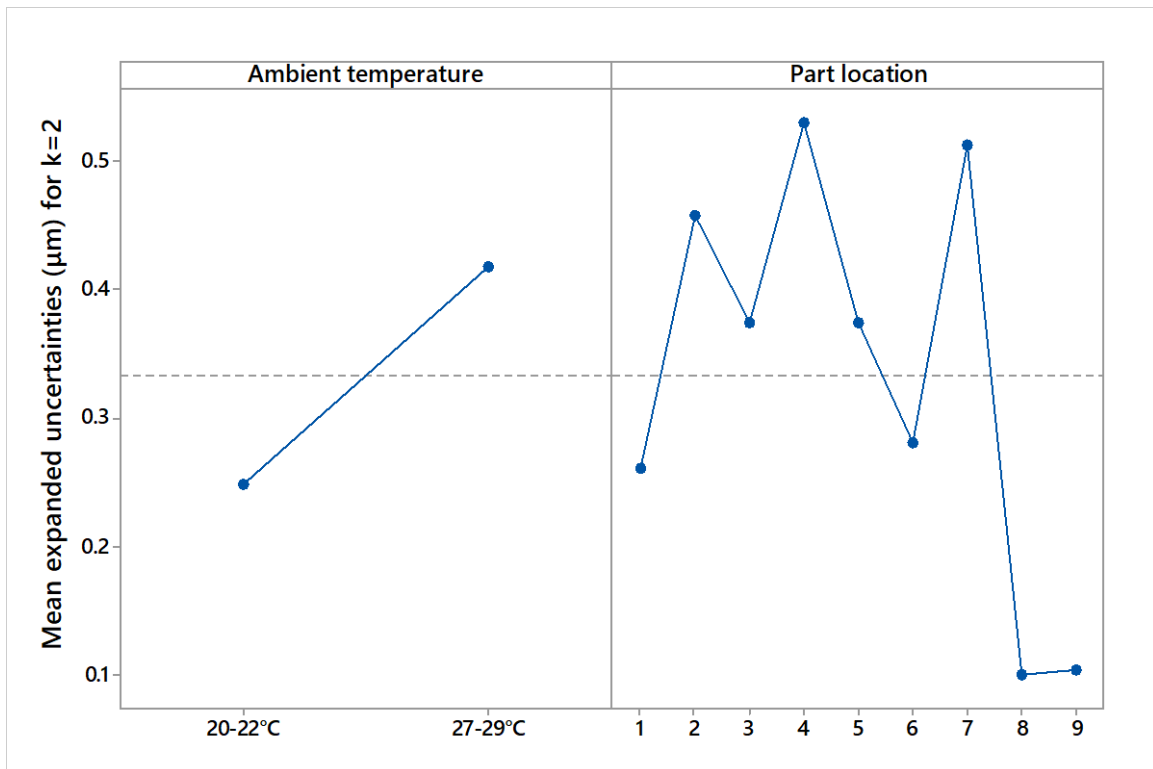


Figure 4.4 Main effects plots for the uncertainties of external diameter.

The results in Figures 4.3 and 4.4 show that the comparator measurement uncertainty is less than 1 μm within the whole measuring volume of the versatile gauge in TTP mode and under both temperature controlled and example shop floor conditions.

4.2 Comparative coordinate measurement based on scanning

An additional full factorial design was employed to investigate the effect of (A) scanning speed, (B) sampling point density, and (C) part location on comparator measurement uncertainty when scanning. The part used for this study is a production part (RESR ring) for an encoder that has thirteen circular features: six small-size holes with a nominal diameter of 3.6 mm, six medium-size holes with a nominal diameter of 6 mm, and a large circle with a nominal diameter of 80 mm. The measurands of interest in this case study were the internal diameter of the large circle, the diameter of one of the medium-size holes (the hole at 150° according to the CRF) and the diameter of one of the small-size holes (the hole at 0° according to the CRF). The stylus used for this experimental design is the same (21 \times 2) with that used for the previous study concerning TTP.

As has been discussed in previous chapters, in scanning CMMs, a major limitation at higher scanning speeds is the high measurement uncertainties due to dynamic influences [64]. Therefore, this study sought to evaluate the uncertainties associated with automated flexible gauging at high scanning speeds for different part locations. Hence, three levels were used for the scanning speed. The first level corresponds to: 5 mm/s for the small-size holes, 10 mm/s for the medium-size holes, and 25 mm/s for the large circle. Levels 2 and 3 are, respectively, the double and quadruple values of the scanning speeds used for level 1. So, they are 10 mm/s, 20 mm/s, and 50 mm/s for level 2 and 20 mm/s, 40 mm/s, and 100 mm/s for level 3. Regarding the factor of sampling point density, two levels were used; level 1 corresponds to a sampling distance (the distance between sample points on the scan path, in the current units) of 0.5 and level 2 to a sampling distance of 0.1. Table 4.2 shows the factors and levels for the DOE with the RESR ring part. The RESR ring part is shown in Figure 4.5 and the part locations are shown in Figure 4.6.

Table 4.2: Factors and levels of the RESR ring inspection.

Factors	Levels				
	1	2	3	4	5
(A) Scanning speed	5, 10, 25 mm/s	10, 20, 50 mm/s	20, 40, 100 mm/s		
(B) Point density	0.5	0.1			
(C) Part location	1	2	3	4	5

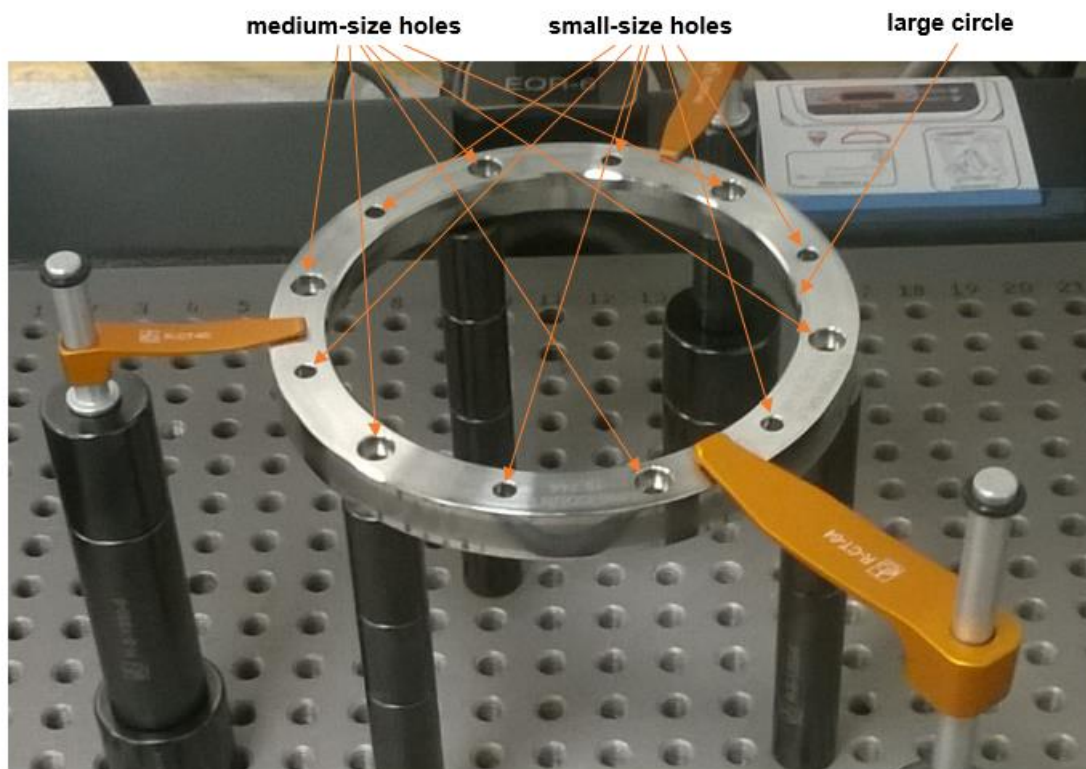


Figure 4.5: RESR ring part.

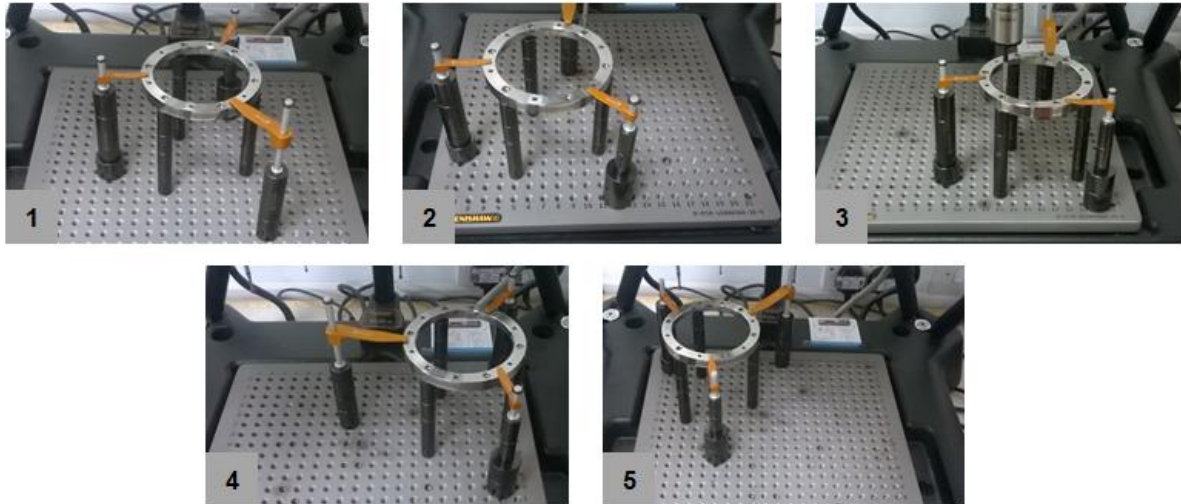


Figure 4.6 RESR ring locations.

20 repeated measurements were performed immediately after mastering on the same part at a temperature of 28-29°C without re-mastering in order to investigate the performance of the comparator gauge at high temperatures. The measurement part had been thermally stabilized at these temperature conditions before mastering. In total, 600 diameters were determined for each feature.

4.2.1 Diameter uncertainties for all part locations using scanning

As with section 4.1.1, Figures 4.7-4.9 show the main effects plots for the expanded measurement uncertainties U of the diameters of features of interest for $k = 2$ and a confidence level of 95.45% where the versatile gauge is used in scanning mode.

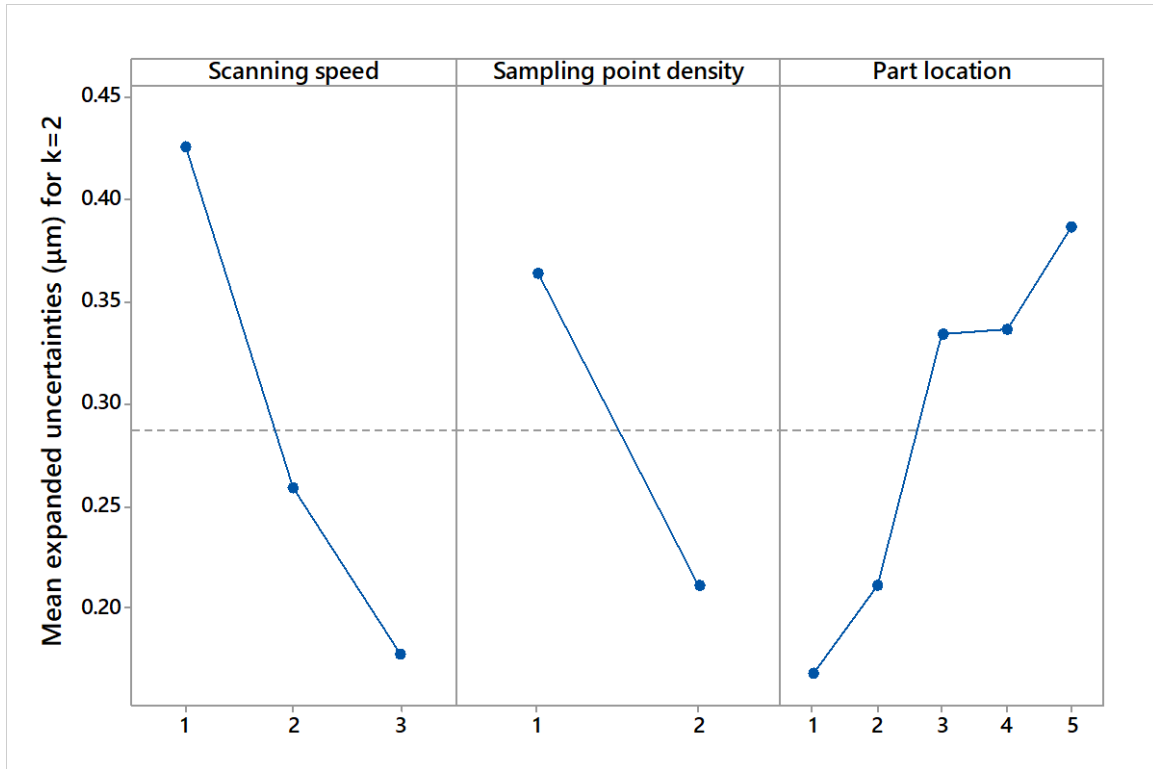


Figure 4.7: Main effects plots for the uncertainties of diameter of large circle.

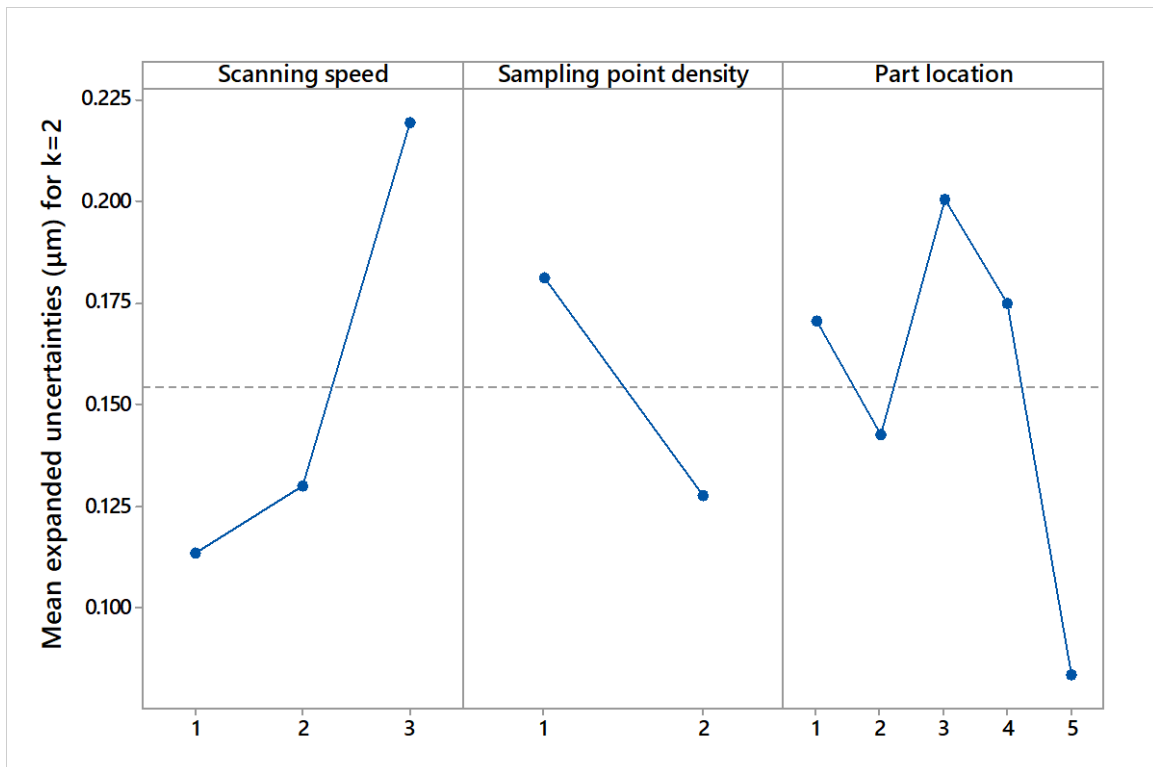


Figure 4.8: Main effects plots for the uncertainties of diameter of medium hole.

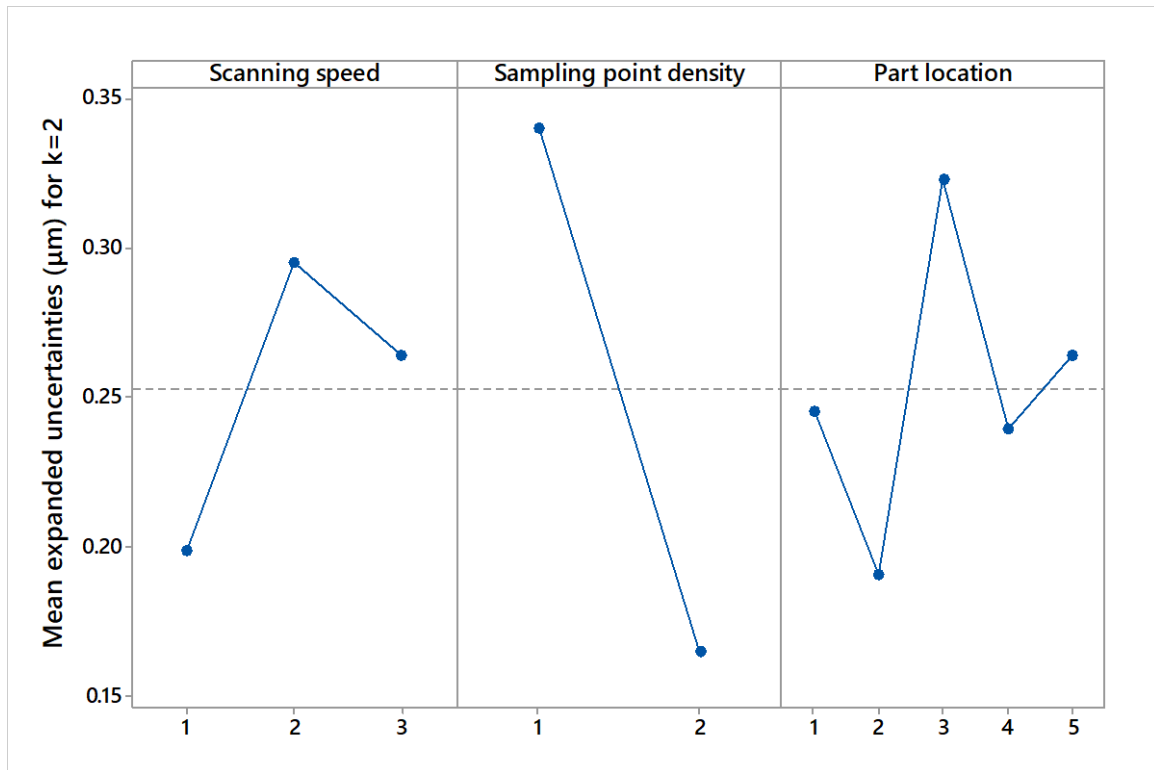


Figure 4.9: Main effects plots for the uncertainties of diameter of small hole.

The results in Figures 4.7-4.9 show that: the machine dynamics do not limit the accuracy of size measurement at higher scanning speeds; the higher the sampling point density, the lower the comparator measurement uncertainty; and, the comparator measurement uncertainty is less than 0.5 μm within the whole measuring volume of the versatile gauge in scanning mode and under example shop floor conditions (28-29°C). Table 4.3 shows the results obtained by the ANOVA procedure based on ordinary least squares (OLS) regression for 95% confidence level using Minitab.

Table 4.3: ANOVA results for the RESR ring inspection.

Measurands	p-values						R^2
	A	B	C	A*B	A*C	B*C	
Diameter of large circle	0.073	0.079	0.382	0.033	0.811	0.562	81.14%
Diameter of medium hole	0.019	0.067	0.126	0.377	0.527	0.231	84.88%
Diameter of small hole	0.507	0.029	0.788	0.881	0.510	0.778	71.51%

Based on the ANOVA results, the statistically significant factors and their interactions for 95% confidence level are:

1. The interaction of scanning speed and sampling point density for the diameter of large circle where the model explains 81.14% of the variance.
2. The scanning speed for the diameter of medium hole where the model explains 84.88% of the variance.
3. The sampling point density for the diameter of small hole where the model explains 71.51% of the variance.

4.3 Statistical modelling of comparator measurement uncertainty

Another full factorial design was performed, using the Renishaw Equator to investigate the influence of scanning speed and sampling point density and their interaction on the comparator measurement uncertainty when evaluating circularity. The measurands of interest were the circularity of all circular features of the RESR ring part (see Figure 4.5): the circularity of small-size holes Y_1, \dots, Y_6 , the circularity of medium-size holes Y_7, \dots, Y_{12} , and the circularity of large circle Y_{13} . The factors of interest were the same with that described in section 4.2 apart from the factor of part location since it has no statistical significant influence on the comparator measurement uncertainty for 95% confidence level. The measurement of the part was followed immediately after mastering and then repeated 20 times, without re-mastering used to compensate for any shop floor temperature change. To decouple the influence of environmental effects two replicates were used. The first experimental run was performed at $28.5^\circ\text{C} \pm 0.5^\circ\text{C}$ while the second at $22.5^\circ\text{C} \pm 0.5^\circ\text{C}$, representing the typical uncontrolled and controlled states discussed previously.

The three different scanning speeds can be labelled as $S_i (1 \leq i \leq 3)$ and the two different sampling point densities as $D_j (1 \leq j \leq 2)$. Consequently, six different sample mean values $\bar{x}_{ij} (i = 1, \dots, 3; j = 1, 2)$ and associated standard uncertainties $u(x_{ij}) = s(\bar{x}_{ij}) = \frac{s}{\sqrt{n}}$, where s is the sample standard deviation and n is the number of repeated measurements for each i and j , can be obtained for each replicate and measurand $Y = \{Y_1, \dots, Y_{13}\}$. However, \bar{x}_{ij} is a random variable due to the random effects $\epsilon \sim N(0, \sigma^2)$. In particular, S_i and D_j are the controlled factors, while ϵ is an uncontrolled or unassigned factor. In order to investigate

whether S_i and D_j have a significant influence on the measurand Y , consider the following model:

$$\psi_{ijn} = \mu + S_i + D_j + (SD)_{ij} + \epsilon_{ijn} \quad (4.1)$$

where ψ_{ijn} is the n th observed value of each measurand for each i and j , μ is the population mean value and $(SD)_{ij}$ is the effect of the interaction between the factors. Consequently, ψ_{ijn} is also Gaussian (at least for a relatively large number of repeated measurements n), and this was verified by performing a normality test for each measurand. Considering the uncertainty evaluation methodology for substitution measurement [73], the statistical model for the uncertainty component associated with the measurement procedure can be obtained by:

$$u(x_{ij}) = \frac{\sqrt{\frac{1}{n-1} \sum_{r=1}^n (x_{ijr} - \bar{x}_{ij})^2}}{\sqrt{n}} \quad (4.2)$$

Therefore, the expanded combined uncertainty can be given by:

$$U_{ij} = k \sqrt{u^2(x_{ij}) + u^2(cal) + u^2(b) + u^2(w_{ij}) + |b|} \quad (4.3)$$

where k is the coverage factor, $u(cal)$ is the standard uncertainty obtained by the calibration of the master artefact, $u(b)$ is the standard uncertainty associated with the systematic error $b = \bar{x}_{ij} - \psi_{cal}$, and $u(w_{ij})$ is the standard uncertainty associated with material and manufacturing variations.

4.3.1 Comparator measurement uncertainties associated with circularity

Considering the standard uncertainty of the mean value of the measurements for $k = 2$, Table 4.4 includes the ANOVA results. The statistically significant factors and second order factor interactions for 95% confidence level are highlighted in bold. Based on the ANOVA results shown in Table 4.4, it can be concluded that the scanning speed has a higher influence on the

comparator measurement uncertainty than the sampling point density and that their interaction is of less statistical significance.

Table 4.4: ANOVA results for circularity.

Measurands	p-values			R^2
	S_i	D_j	$(SD)_{ij}$	
Y_1	0.000	0.002	0.020	98.28 %
Y_2	0.001	0.097	0.020	92.71 %
Y_3	0.001	0.020	0.843	92.31 %
Y_4	0.011	0.030	0.730	83.37 %
Y_5	0.000	0.000	0.007	98.55 %
Y_6	0.000	0.002	0.024	99.04 %
Y_7	0.000	0.005	0.597	93.78 %
Y_8	0.002	0.032	0.431	89.71 %
Y_9	0.000	0.010	0.333	94.33 %
Y_{10}	0.000	0.003	0.092	97.55 %
Y_{11}	0.000	0.000	0.602	98.34 %
Y_{12}	0.000	0.019	0.412	95.00 %
Y_{13}	0.000	0.642	0.033	98.47 %

The main effects plots for all the measurands showed that the comparator measurement uncertainty associated with circularity increases as the scanning speed and sampling point density increase. For example, Figures 4.10-4.12 show the main effects plots for Y_5 , Y_{11} and Y_{13} , respectively. Figures 4.13 and 4.14 show representative results for the factor interactions; the interaction plots for Y_5 and Y_{13} . As can be seen from Figures 4.13 and 4.14, the highest scanning speed (level 3) leads to the highest measurement uncertainty and this is higher for a sampling distance of 0.1.

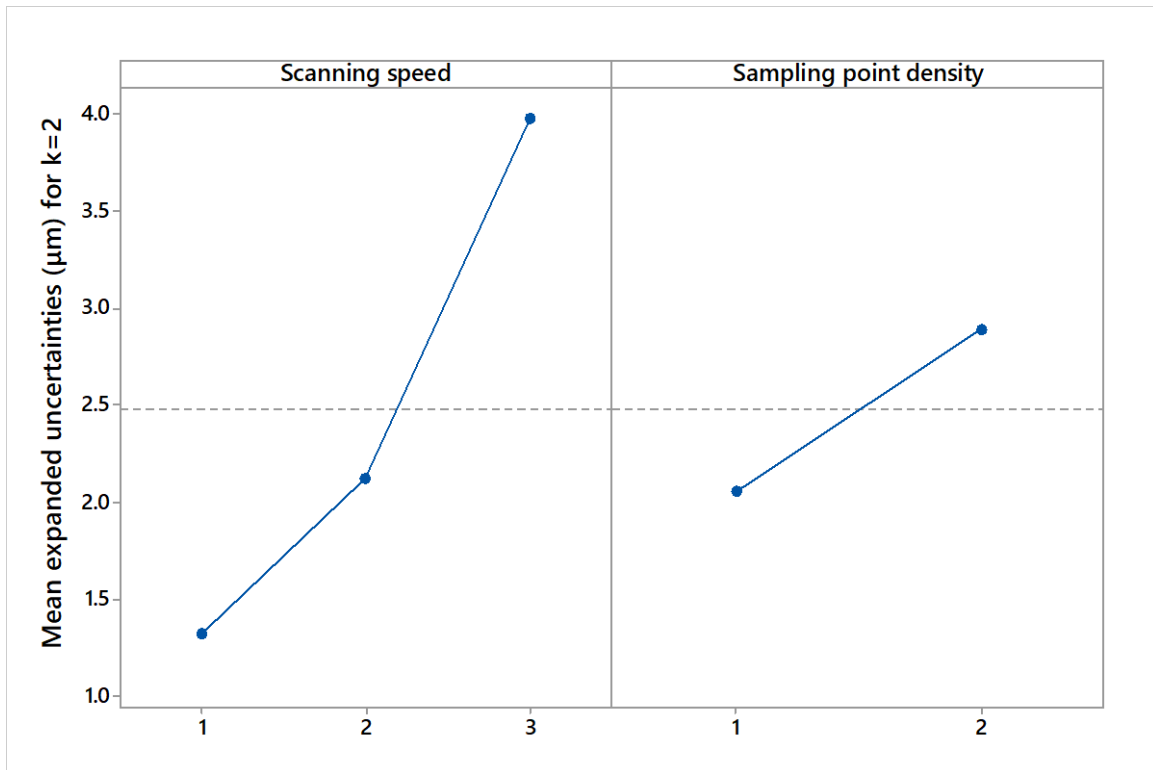


Figure 4.10: Main effects plots for the uncertainties of Y_5 .

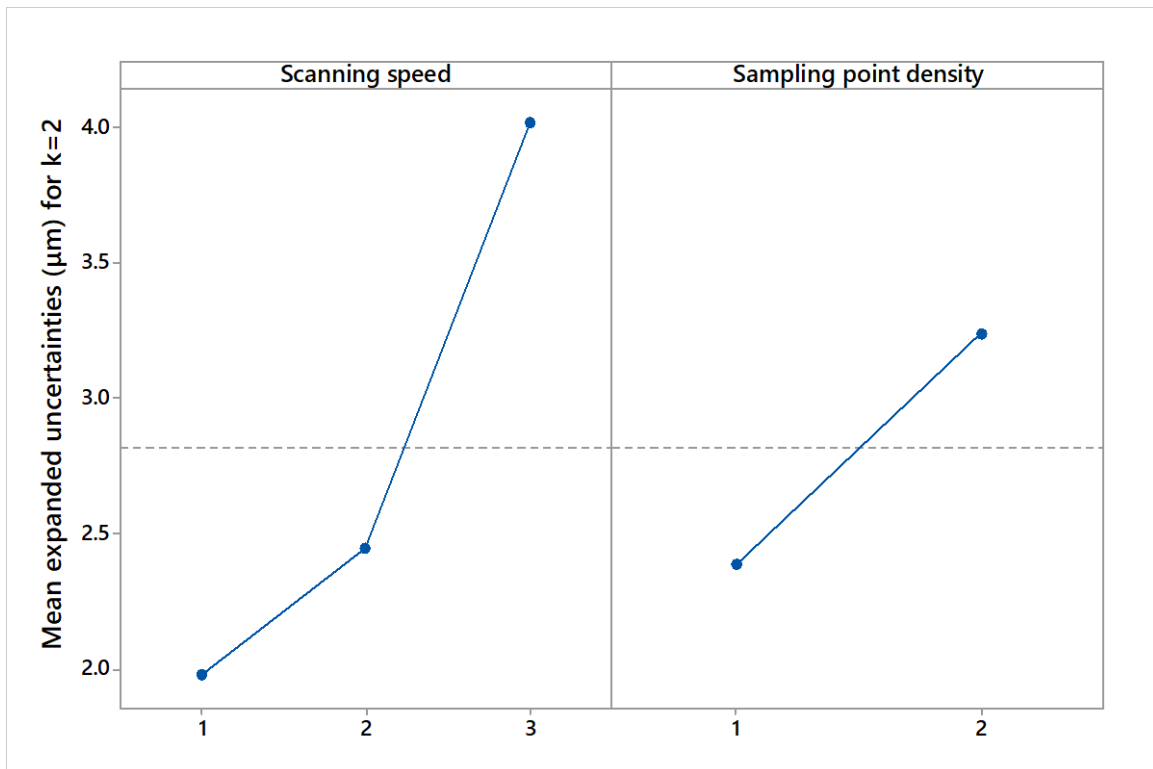


Figure 4.11: Main effects plots for the uncertainties of Y_{11} .

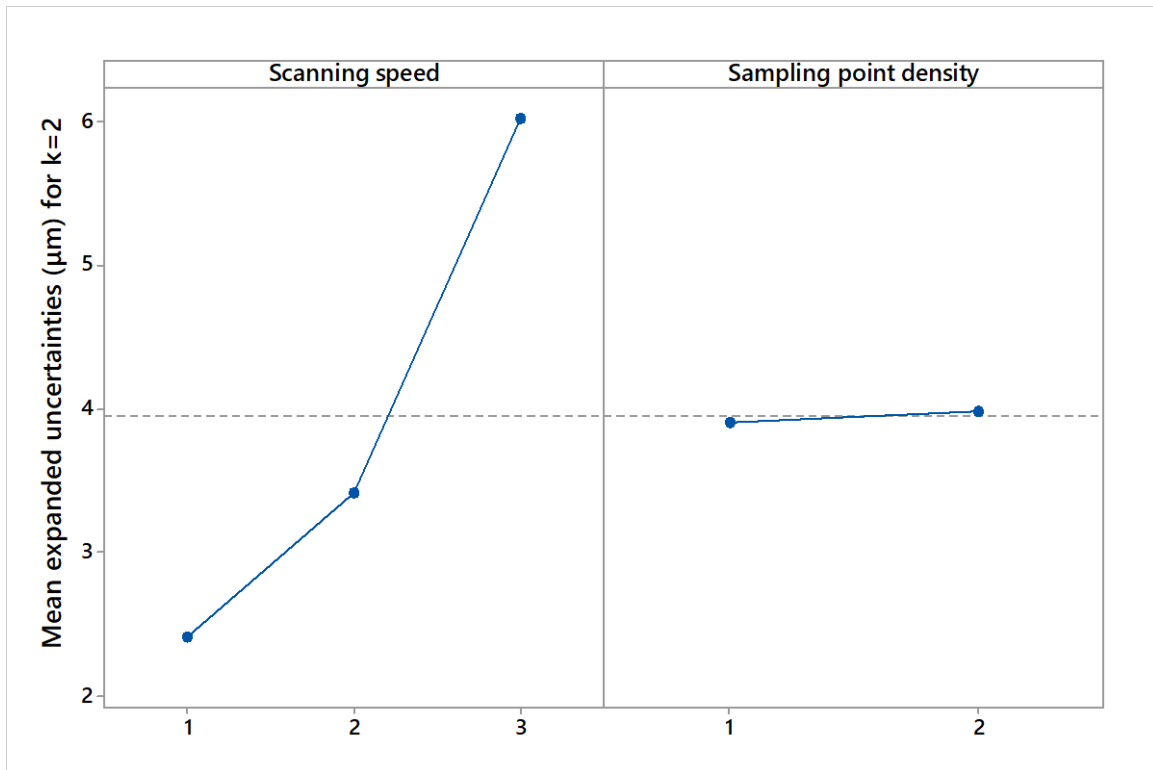


Figure 4.12: Main effects plots for the uncertainties of Y_{13} .

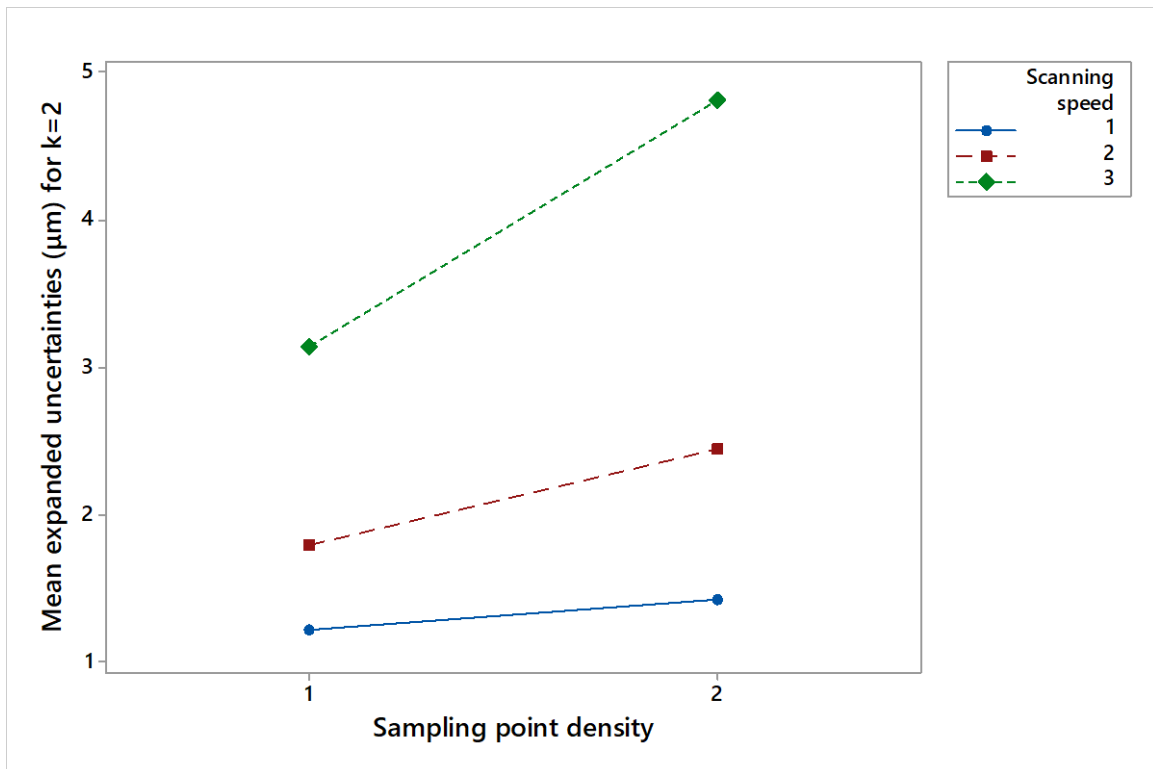


Figure 4.13: The interaction plot of scanning speed and sampling point density for the uncertainties of Y_5 .

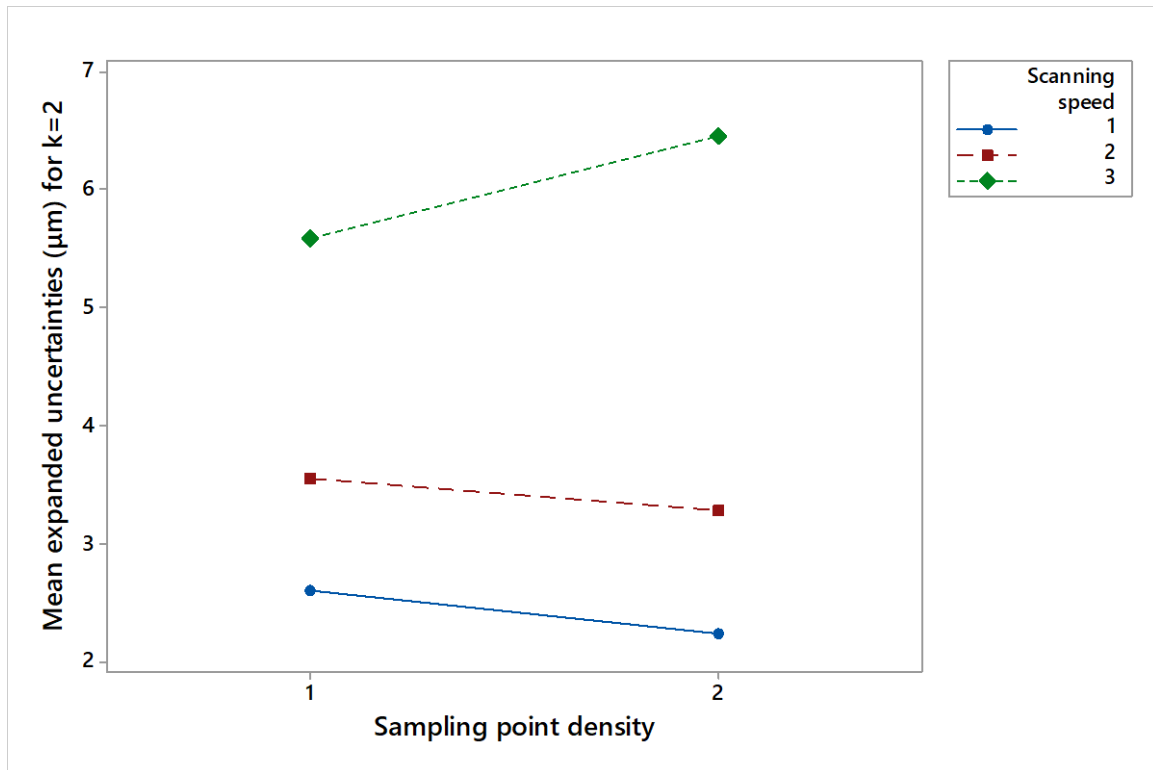


Figure 4.14: The interaction plot of scanning speed and sampling point density for the uncertainties of Y_{13} .

4.4 Summary

In this chapter, the DOE approach has been employed to perform a practical analysis of uncertainty of measurement of the Equator gauging system, in discrete-point probing and scanning measuring modes (especially at high scanning speeds), within a significant portion of the whole measuring volume and under workshop conditions. It has been demonstrated that the accuracy of shop floor dimensional inspection based on automated flexible gauging is not affected by part location for both measurement modes, even at high scanning speeds. In addition, a statistical model has been developed for comparator measurement uncertainty associated with circularity. Replicates, subject to the same sources of variability, were used to decouple the influence of environmental effects. It can be concluded that the uncertainty of form measurement is affected by dynamic effects. Therefore, more conservative scanning speeds should be used to reduce the dynamic effects for form measurement.

Chapter 5

Flexible Gauging Comparative Study

This chapter presents a comparative study of different dimensional inspection methods including OMM, automated flexible gauging, and hard gauging. For this purpose, eight parts (gears), two made of aluminium and six made of steel, were machined on a 5-axis CNC machining center and then measured by each inspection approach to evaluate various tolerances. Special attention was paid to ensure that the parts were measured as far as was possible at the same surface points. Each inspection approach is discussed separately and the measurements uncertainties are evaluated for each measurand and inspection approach.

5.1 On-machine measurement

A modern CNC machine tool is capable of producing parts with tight tolerances at high speed. More often, they are also equipped with probing systems to automate part setup and in some cases for verification or even inspection. Here are significant issues to consider for the latter two applications because the many of the errors present during machining, are also present during use of the probe. In addition, and sometimes the most significant influence, is the uncertainty due to temperature effects. Often, the machine is not in a temperature controlled environment and the machine has likely been performing work prior to probing which means there are significant transient effects from internally generated heat. Such changes occurring during transitions from machining and idle modes are sometimes well understood and warm-up cycles often precede production to improve stability. An inverse problem exists for post-production measurements, therefore the influence of which can vary significantly depending on the sequence and timing of the various operations. In this work, a wide variety of measurement have been completed with such variability considered by adding process variation to the probing routines. The first two parts, “G1” and “G2”, are made of aluminium while the other six parts, “G3”, “G4”, “G5”, “G6”, “G7”, and “G8”, are made of steel. The first part, “G1”, was the test gear for the program and probing routines. Therefore, measurement results for this gear are not included. The probe system used was the Renishaw RMP60. A

general overview of the experimental setup for OMP is shown in Figure 5.1. The DOE for OMP is described below:

- The second part, “G2”, was first probed immediately after machining with no datum reset. The probe had been calibrated just prior to the measurements. The part was then re-probed two times after 1.5 hours in both cases.
- The third part, “G3”, was first probed immediately after machining. It was then re-probed twice where in the second time after a warm up cycle.
- The fourth part, “G4”, was first probed immediately after machining. It was then re-probed twice after the machine had cooled to include reduced transient effects. Typically, it takes at least 30 minutes for the rate of change of spindle thermal error to become negligible after a significant change in spindle speed.
- The fifth part, “G5”, and the sixth part, “G6”, were first probed immediately after machining, then re-probed twice before warming the machine up, and then re-probed again after running the machine through a typical warm up cycle.
- The seventh part, “G7”, was first probed immediately after machining, then re-probed twice, and then re-probed again after running the machine through a typical warm up cycle.
- The eighth part, “G8”, was first probed immediately after machining and then re-probed twice after running the machine through a typical warm up cycle.

For analysing the CNC probing points and fitting the features to those points, the ZEISS CALYPSO software was used. Such fitting of probing points was necessary in order to assess the various characteristics of interest in a standard way as per CMS software. Figure 5.2 shows the CAD model of the measurement part and labels the features. Table 5.1 shows the measurands considered for this work.

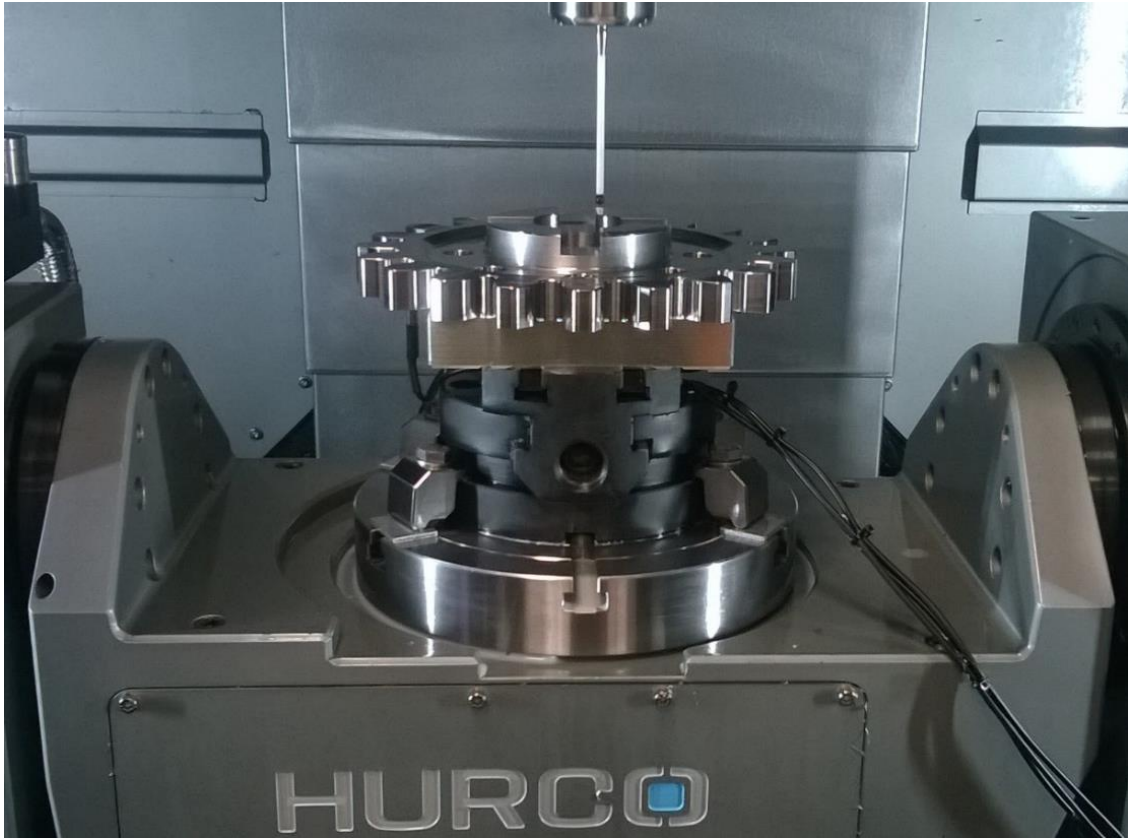


Figure 5.1: Test setup on a 5-axis CNC machining center.

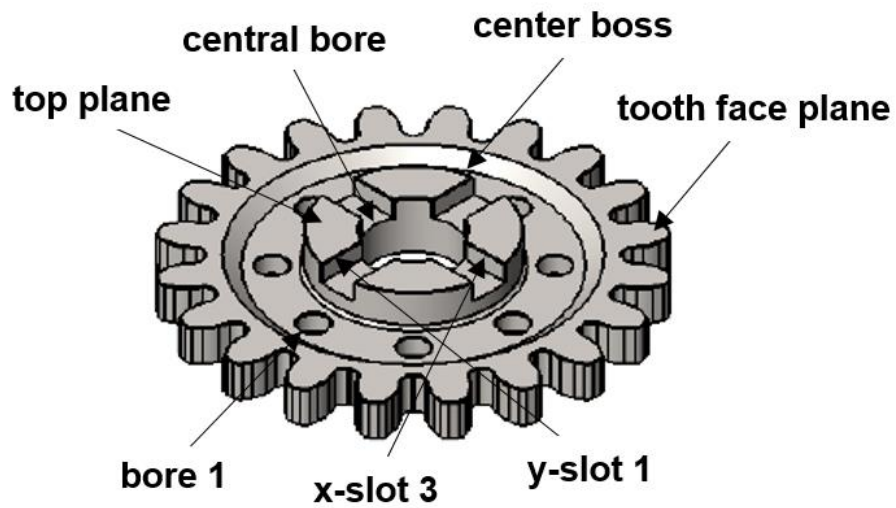


Figure 5.2: CAD model of the measurement part.

Table 5.1: Measurands for flexible gauging comparative study.

Measurands		Measurands	
A	Diameter of central bore (50 mm)	M	Width of x-slots 4-1 (20 mm)
B	Diameter of center boss (100 mm)	N	Width of y-slots 3-2 (20 mm)
C	Diameter of Bore 1 (16 mm)	O	Width of y-slots 4-1 (20 mm)
D	Diameter of Bore 2 (16 mm)	P	Teeth face flatness
E	Diameter of Bore 3 (16 mm)	Q	Perpendicularity of y-slot 1 to datum B
F	Diameter of Bore 4 (16 mm)	R	Perpendicularity of y-slot 2 to datum B
G	Diameter of Bore 5 (16 mm)	S	Perpendicularity of y-slot 3 to datum B
H	Diameter of Bore 6 (16 mm)	T	Perpendicularity of y-slot 4 to datum B
I	Diameter of Bore 7 (16 mm)	U	Parallelism of x-slot 1 to datum B
J	Diameter of Bore 8 (16 mm)	V	Parallelism of x-slot 2 to datum B
K	Pitch circle diameter (129 mm)	W	Parallelism of x-slot 3 to datum B
L	Width of x-slots 3-2 (20 mm)	X	Parallelism of x-slot 4 to datum B

Note that, the x-slot 1 is the perpendicular surface to y-slot 1 shown in Figure 5.2. The bores and y-slots are numbered clockwise while the x-slots are numbered anticlockwise. Datum A (XY) is defined at the center of the central bore, datum B is defined by a line perpendicular to y-slot1 for the 2D rotation, and datum C is defined by a plane on the top surface of the part (top plane) for the 3D rotation. Perpendicularity is a tolerance applied to features that must be 90° apart [59, 121]. Figure 5.3 is the bar graph for the combined expanded uncertainties due to the probing procedure and thermal expansion of the part for the size measurements for $k = 2$ and a 95.45% confidence level from OMP. Note, the measurand P has not been considered in this case because it is not realistic to evaluate flatness using OMP. As can be seen, the measurement results for each gear are different due to varying manufacturing and measurement conditions. A representative sample of temperature conditions is shown in Figure 5.4 (temperature readings were taken every ten seconds).

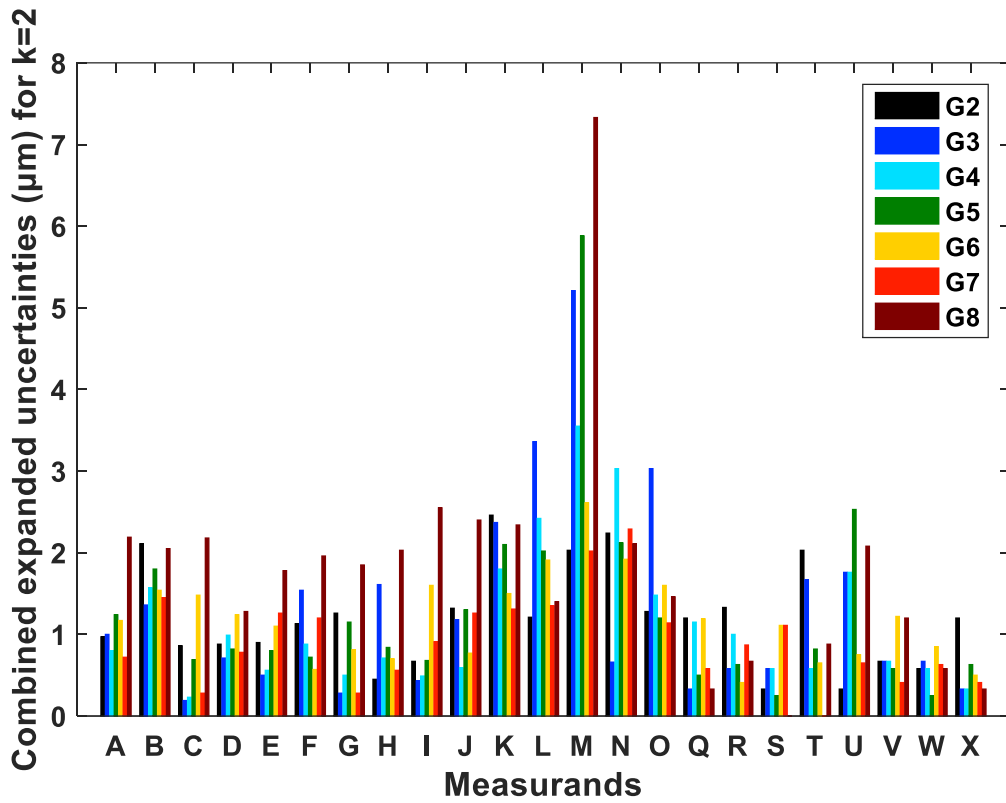


Figure 5.3: OMP combined expanded uncertainties.

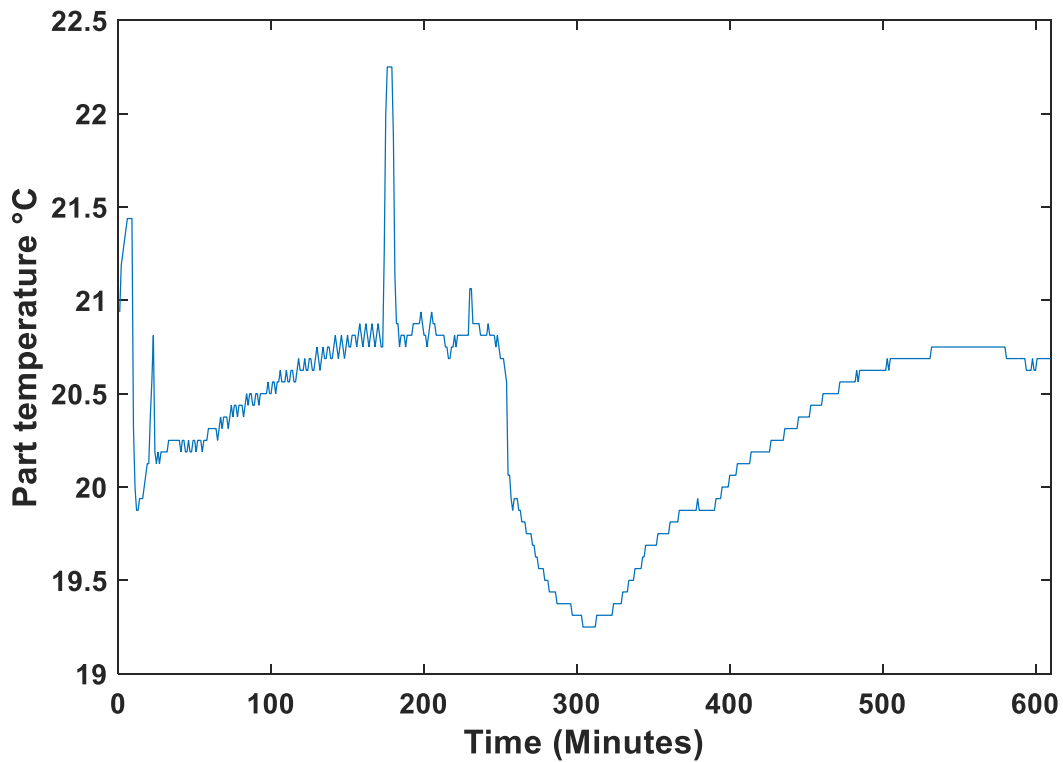


Figure 5.4: Sample of G6 temperature.

5.2 Hard gauging

As has been discussed in previous chapters, the disadvantages of inspecting manufactured parts using hard gauges include wear, cost, maintenance, etc [121]. In this thesis, the manual inspection approach was based on: (1) a measurement technique involving a dial test indicator (DTI) attached on a height gauge and gauge blocks to provide the height values (alternatively, a height micrometer could be used), (2) two bore gauges of 16 mm – 20 mm and 37 mm – 51 mm, (3) an outside micrometer of 100 mm – 125 mm, and (4) gauge blocks. Different operators will provide different results based on their training, experience, fatigue, etc. Therefore, various operators with different level of training, experience and educational background including mechanical, electrical, and control engineering were employed. Only two gears (G4 and G6) were considered for hard gauging due to the much time required to measure the features of interest using this inspection method. It is important to note that the formal sequence and measurement locations were designed in collaboration with the NPL to ensure correct methodology. The variable comes from the application of the measurement after training. In total, seven operators carried out the measurements on a surface plate in shop floor conditions at various temperatures resulting from the natural variability of the workshop over several days of testing rather than by forced conditions. The flatness of the surface plate was evaluated using a CMM in TTP mode, $0.020 \text{ mm} \pm 0.002 \text{ mm}$ for $k = 2$ and a 95.45% confidence level. Tables 5.2 and 5.3 describe the DOE performed for hard gauging.

The first measurement technique was employed for evaluating pitch circle diameter (PCD) and flatness. The second (bore gauges) for the diameters of eight small bores and central bore. The third (outside micrometer) for the diameter of center boss. The fourth (gauge blocks) for the width of slots. It is worth mentioning that the first measurement technique was very time consuming due to the part alignment procedure and nature of measurement technique itself. A general overview of the experimental setups for the hard gauging is shown in Figure 5.5.

Table 5.2: DOE for hard gauging.

Factors	Levels						
(A) Operator	1	2	3	4	5	6	7
(B) Measurement technique	1	2	3	4			
(C) Shop floor temperature	Low	High					

Table 5.3: Implementation details for factor A.

Operators	Repetitions	Replicates	G4 Temperature (°C)	G6 Temperature (°C)
1	20	a	20.5-21	20.5-21
1	20	b	25.6-27	23-24.9
1	5	c	20.3-21.5	20.5-21
1	5	d	24.3-25.1	22.7-23.5
2	5		24-25	23-25
3	5		20-21.5	22.9-23.6
4	5		22.9-26.4	22.5-23.4
5	5		26.2-26.4	24.3-25.2
6	5		26.4-27	24.2-25.2
7	20		25.6-26.5	24.3-24.5

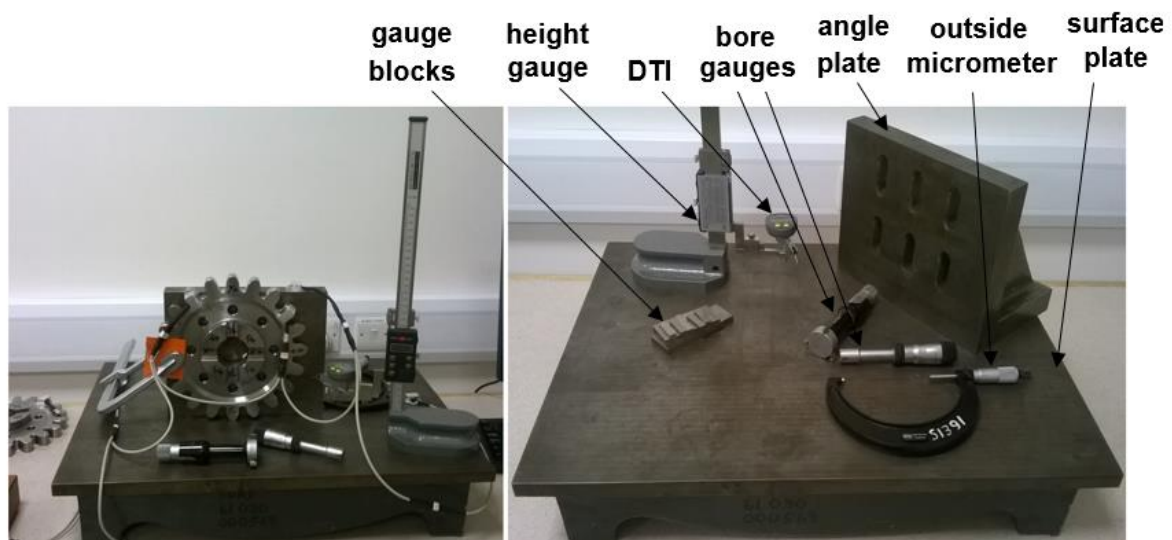


Figure 5.5: Test setups using hard gauges.

Figures 5.6 and 5.7 show the bar graphs for the combined expanded uncertainties from hard gauging for G4 and G6, respectively. The measurement uncertainties vary for each measurand due to different operators and measurement conditions. These measurement uncertainties are the combined expanded uncertainties due to the measurement procedure and thermal expansion of the part for the size measurements and flatness error of the surface plate for the form measurements for $k = 2$ and a 95.45% confidence level.

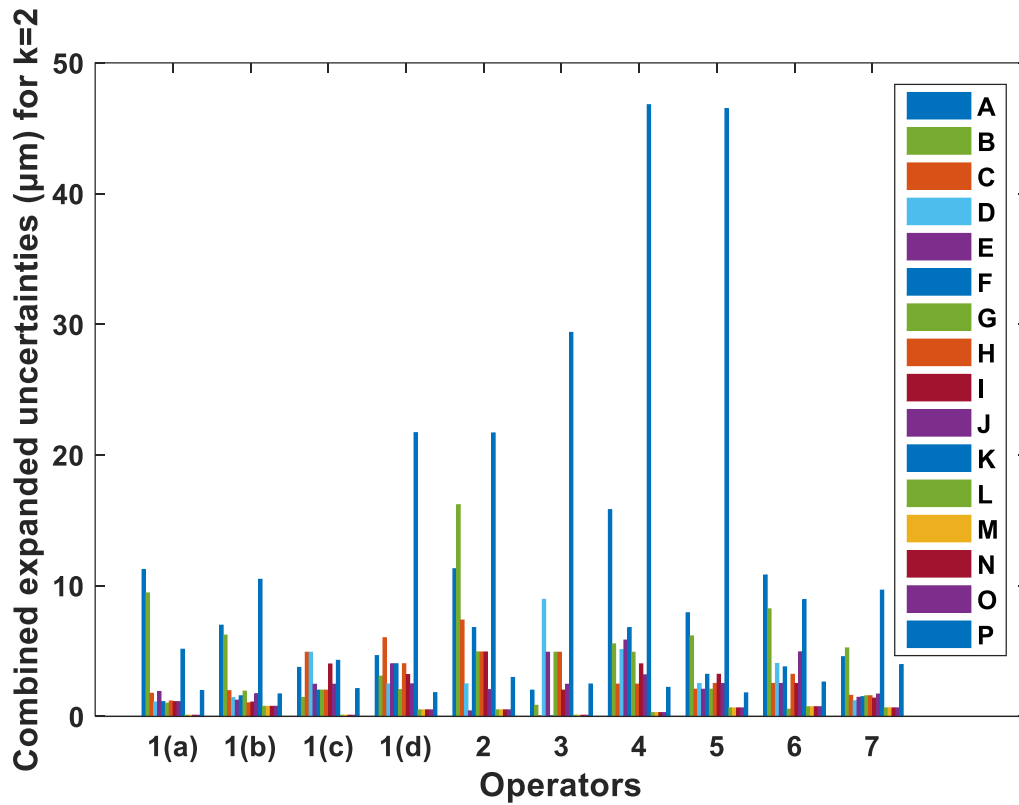


Figure 5.6: Combined expanded uncertainties for G4 from hard gauging.

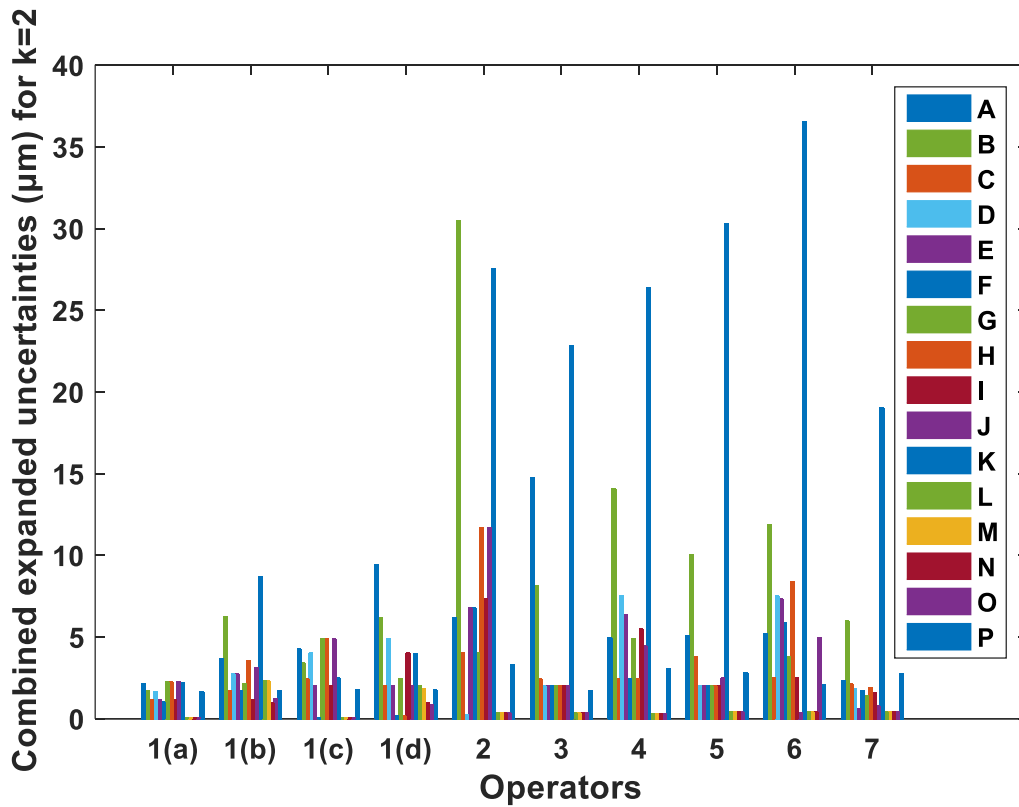


Figure 5.7: Combined expanded uncertainties for G6 from hard gauging.

Hard gauging provided high measurement uncertainties mainly due to the errors associated with the measurement instruments, the measurement environment, and the operator performing the measurements.

5.3 Equator - CMM Compare

The absolute performance of the CMM and the repeatability of the comparator gauge are crucial for achieving an accurate collaborative calibration of production parts using a calibrated master part [1]. As has been shown in previous chapters, the Renishaw Equator is very repeatable and therefore, using a calibrated CMM, the uncertainty associated with the collaborative calibration is expected to be very small. CMM accuracy is dependent upon the ambient thermal environment in which it operates because thermal effects degrade CMM accuracy. Hence, to ensure accurate comparator measurements, the production of the calibration file required for CMM Compare is performed using a CMM operating in a thermally controlled metrology lab. CMM accuracy is specified in accordance to the ISO 10360 series of standards (see for example [21, 22, 122]), which describe the acceptance tests, the reverification tests, and the interim checks for CMMs. The CMM Compare procedure consists of the following steps:

- i. Obtain a master part from the production parts.
- ii. Generate the required part program on the Equator.
- iii. Edit the part program on the CMM. The part program at this stage should include the commands COMPARE/ON, CAL and COMPARE/OFF.
- iv. Measure the master part using the CMM to produce a calibration file.
- v. Transfer the calibration file to the Equator and edit the part program on the Equator to add the commands COMPARE/ON, CAL and COMPARE/OFF.
- vi. Place the master part on the Equator and run the part program in master mode to produce a master file with reference to the calibration file.
- vii. Run the part program using the master part in measure mode (verification step).
- viii. Remove the master part and replace with the production parts to be measured.

According to Renishaw's equipment instructions for CMM Compare using scanning, there is a requirement to generate more point data from the CMM. In particular, the required minimum ratio of points measured on the CMM is ten for every single point measured on the Equator. In

addition, good measurement practice to maintain accuracy on the CMM is to reduce the part program speeds, accelerations and scan velocity according to the CMM's specification. The calibration file for this study was obtained by a ZEISS CMM located at Renishaw. The fixturing design and methodology were also provided by Renishaw which ensured that the point position variability was minimised across the comparison. The performance of the Equator in CMM Compare mode was evaluated in the same shop floor conditions as the hard-gauging and OMP. This is an uncontrolled environment therefore differences between the conditions is inevitable. A general overview of the experimental setup for the flexible gauging is shown in Figure 5.8. A temperature sample of the master part during repeated measurements is shown in Figure 5.9 (temperature readings were taken every ten seconds).

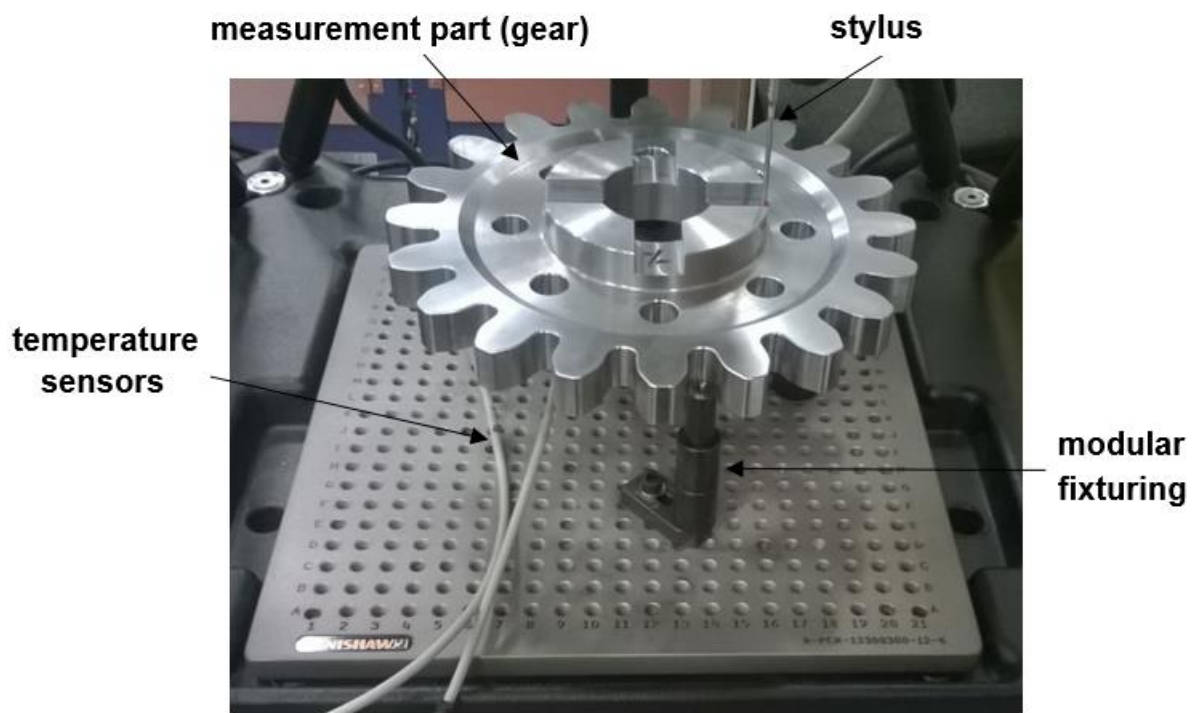


Figure 5.8: Test setup on Equator gauge for CMM Compare method.

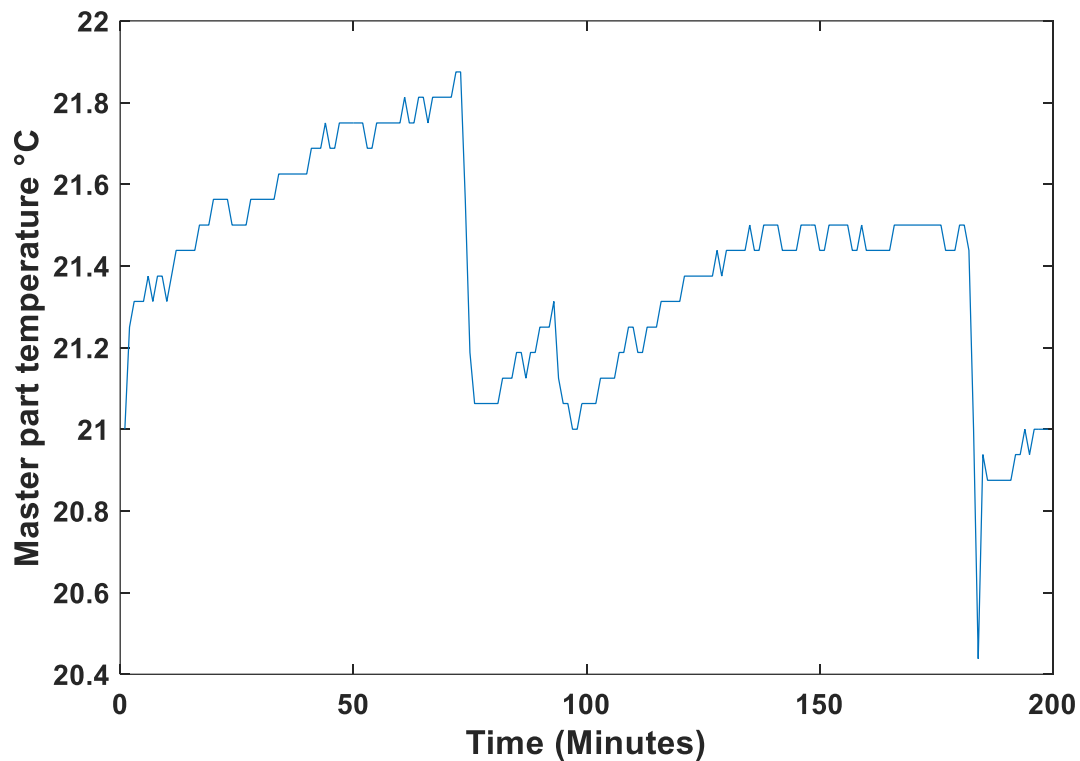


Figure 5.9: Sample of master part temperature.

The Equator combined expanded uncertainties were calculated according to ISO 15530-3:2011 [73]. In particular, the uncertainty contributors considered to calculate the Equator combined expanded uncertainties included: i) the standard uncertainty of the calibrated part (gear 7) estimated by the ten repeated measurements on the gear using the CMM used to produce the calibration file for CMM Compare, ii) the standard uncertainty of the measurement procedure (five repeated measurements after mastering), iii) the standard uncertainty of the systematic error estimated by the ten repeated measurements on the gear 7 using the Equator, iv) and the uncertainty due to the variation of the thermal expansion coefficient of the unknown parts for the size measurements [5, 73, 123]. Figure 5.10 is the bar graph for the Equator combined expanded uncertainties for $k = 2$ and a 95.45% confidence level. As can be seen, the Equator has very small uncertainties despite the shop floor conditions, 24 measurands and 7 parts, with more than 97% of the results being less than just 2 μm .

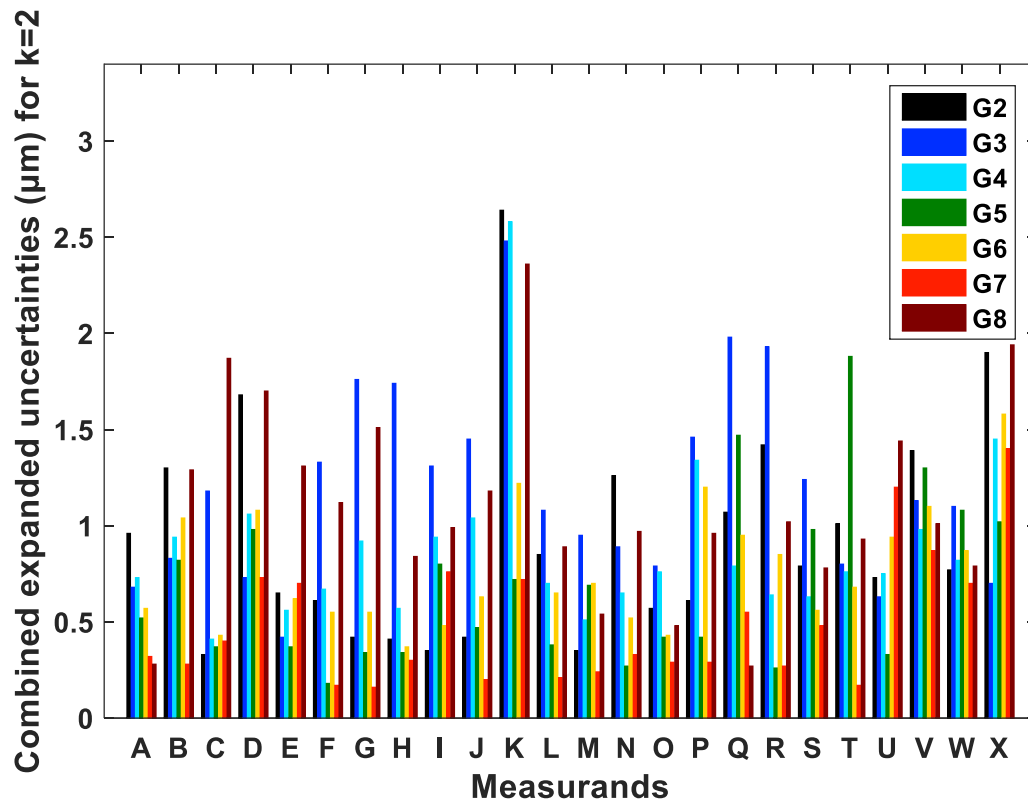


Figure 5.10: Equator combined expanded uncertainties.

5.4 Comparison

This section compares the combined expanded uncertainties obtained from each shop floor inspection approach for $k = 2$ and a 95.45% confidence level and their residuals calculated by the difference between the shop floor dimensional measurement systems mean values and the CMM results/estimates for each measurand. Figures 5.11-5.17 compare the combined expanded uncertainties obtained from each inspection approach.

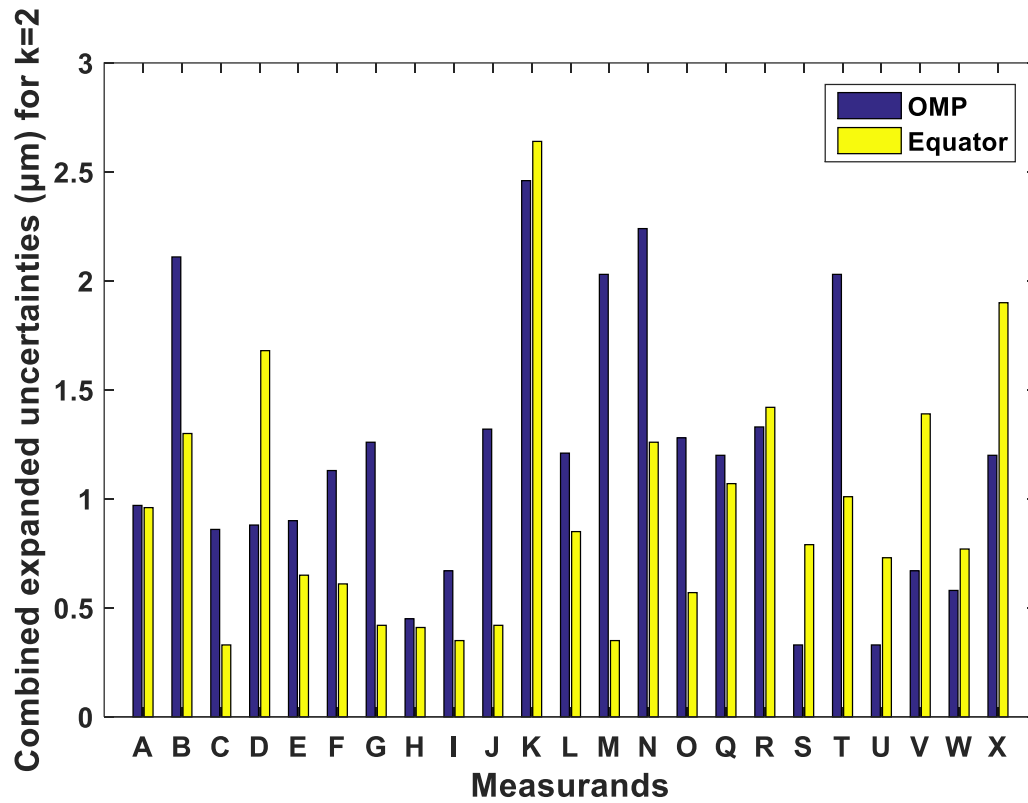


Figure 5.11: Comparison between OMP and Equator uncertainties for G2.

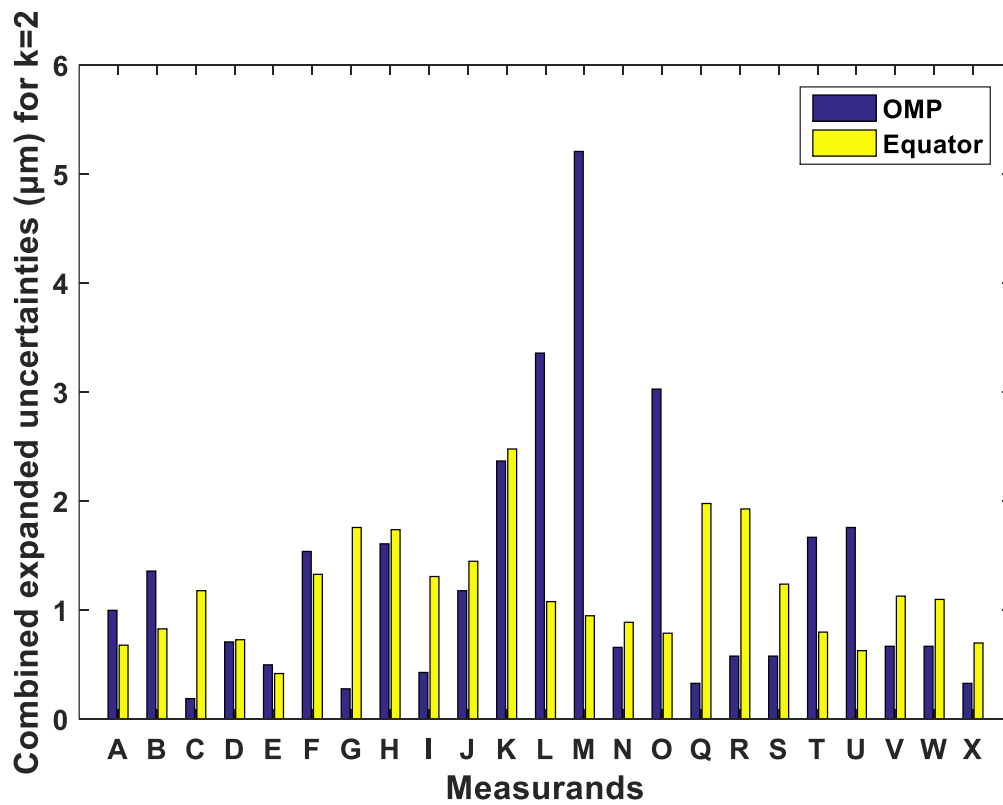


Figure 5.12: Comparison between OMP and Equator uncertainties for G3.

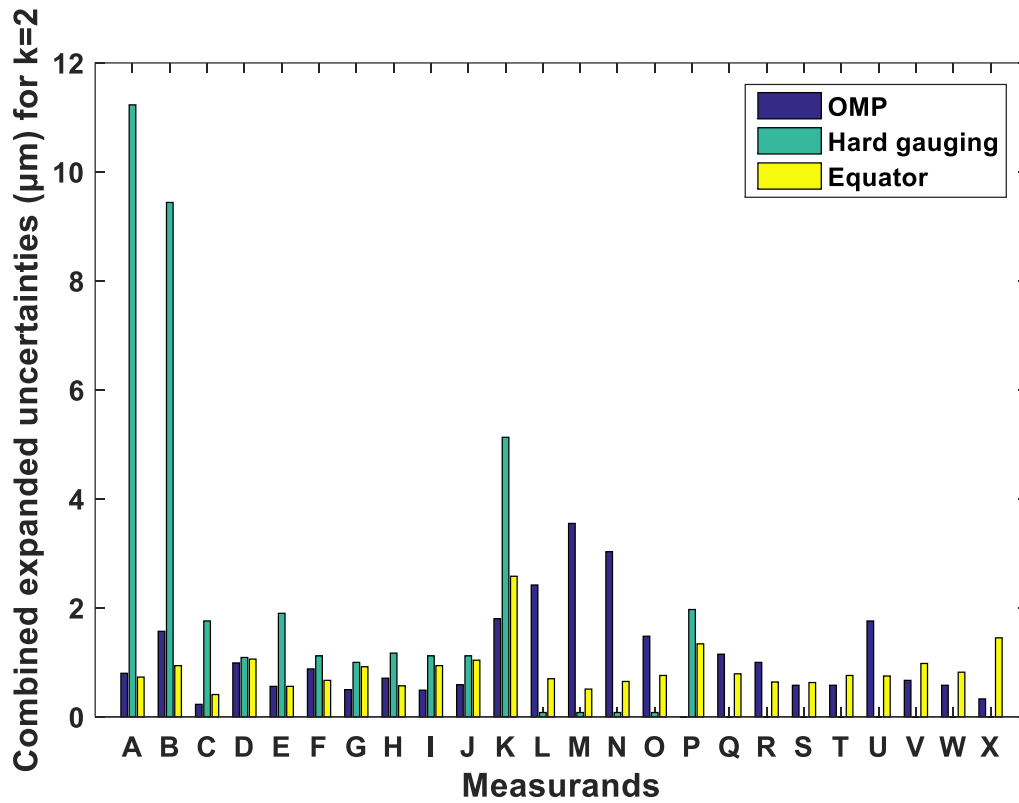


Figure 5.13: Comparison between OMP, hard gauging and Equator uncertainties for G4.

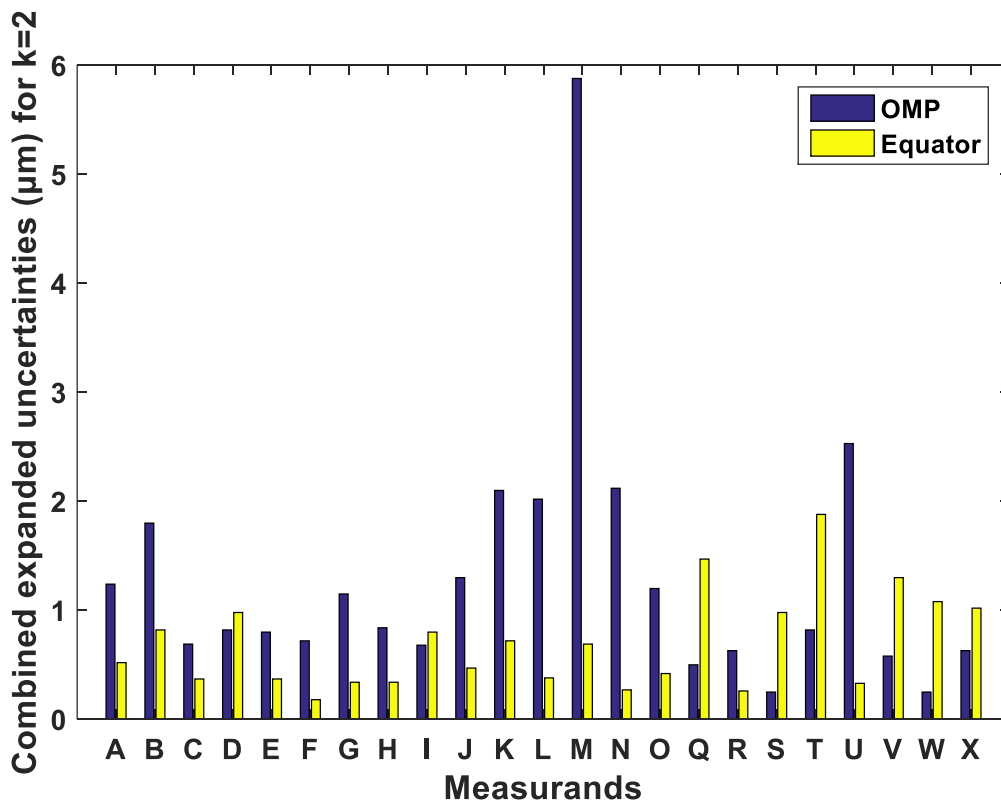


Figure 5.14: Comparison between OMP and Equator uncertainties for G5.

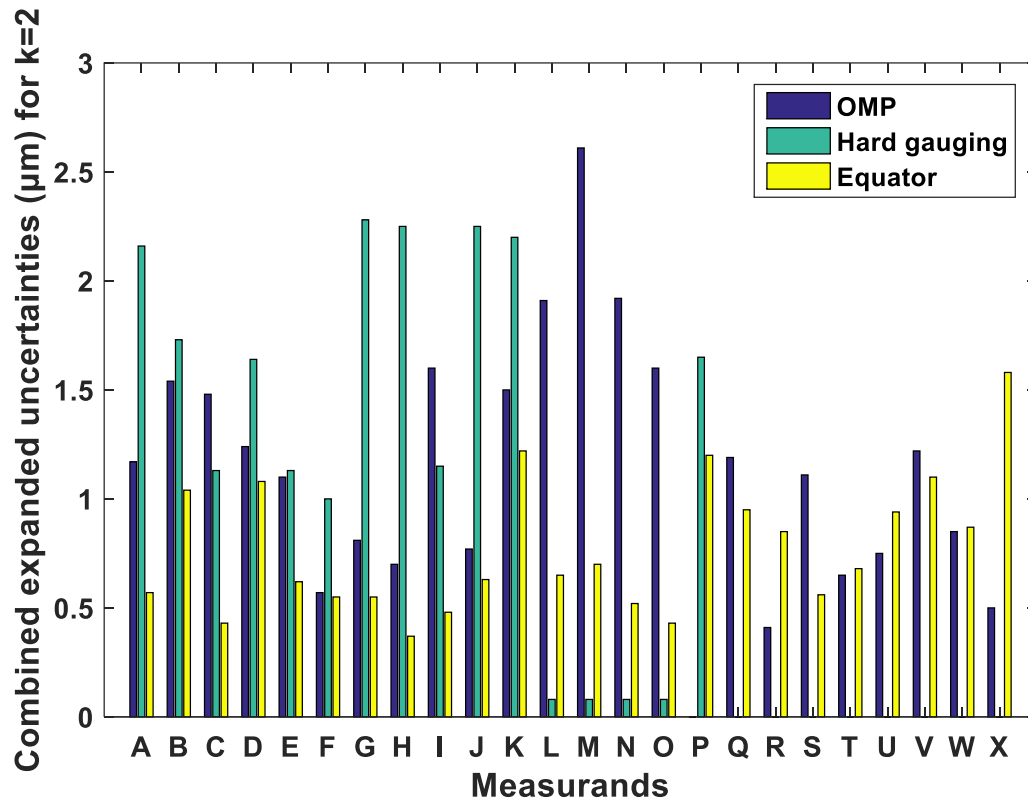


Figure 5.15: Comparison between OMP, hard gauging and Equator uncertainties for G6.

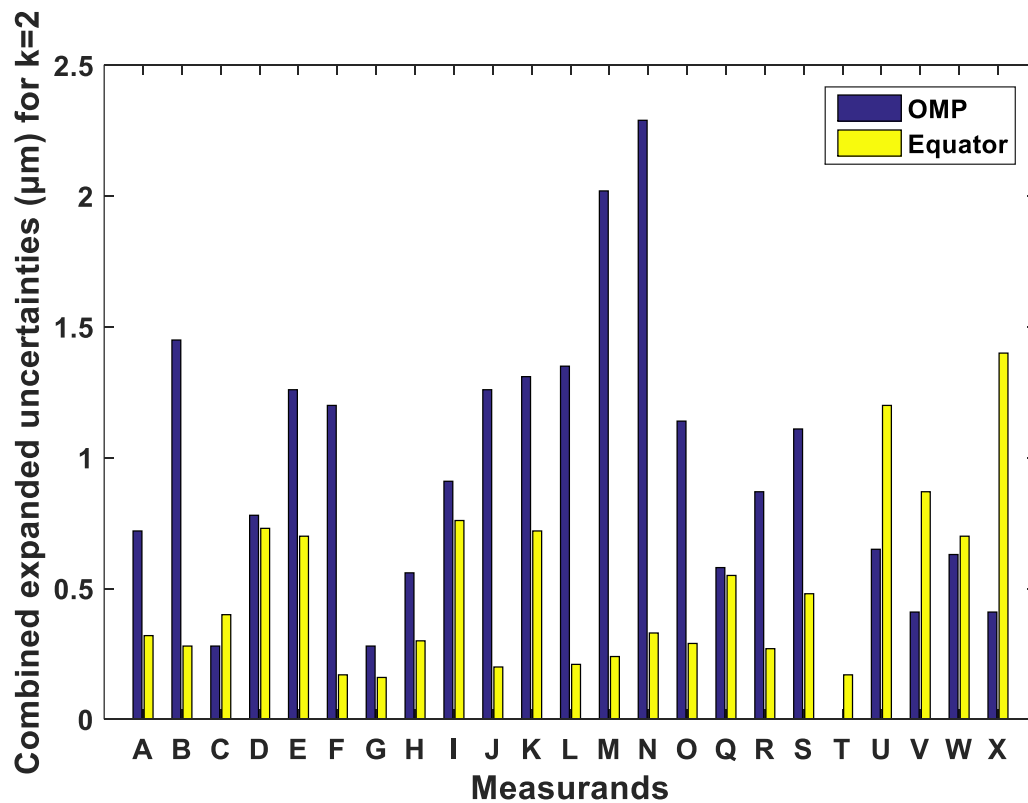


Figure 5.16: Comparison between OMP and Equator uncertainties for G7.

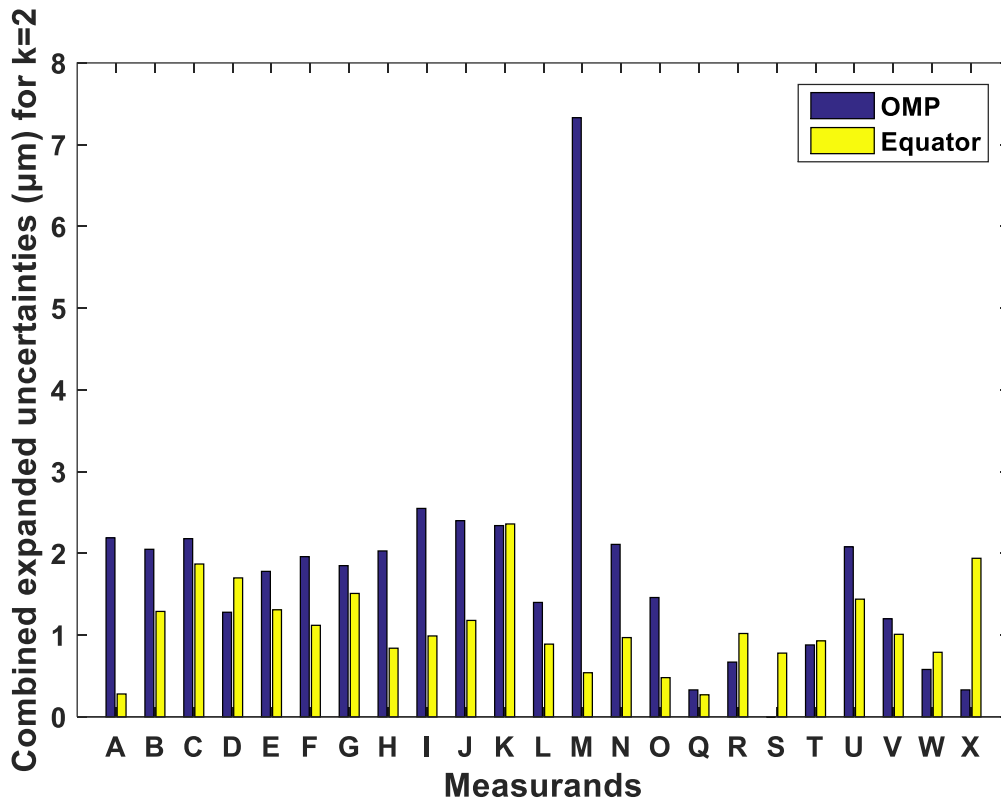


Figure 5.17: Comparison between OMP and Equator uncertainties for G8.

Based on Figures 5.11-5.17, it can be concluded that hard gauging and OMP provided higher measurement uncertainties than automated flexible gauging for most measurands. The Equator combined expanded uncertainties were less than 2 µm for all the measurands and measurement parts apart from the measurand K (PCD) for the parts G2, G3, G4 and G8, which were about 2.5 µm. OMP provided high uncertainties for the measurand M (width of x-slots 4-1) especially for the measurement parts G3, G5 and G8. Hard gauging (1st operator for 20 repetitions at low temperatures) provided much higher uncertainties for measurand A, B and K for G4 than G6 though those measurements were performed at the same temperature conditions and from the same operator. Figures 5.18-5.24 compare the residuals as calculated by the ‘reference’ CMM values.

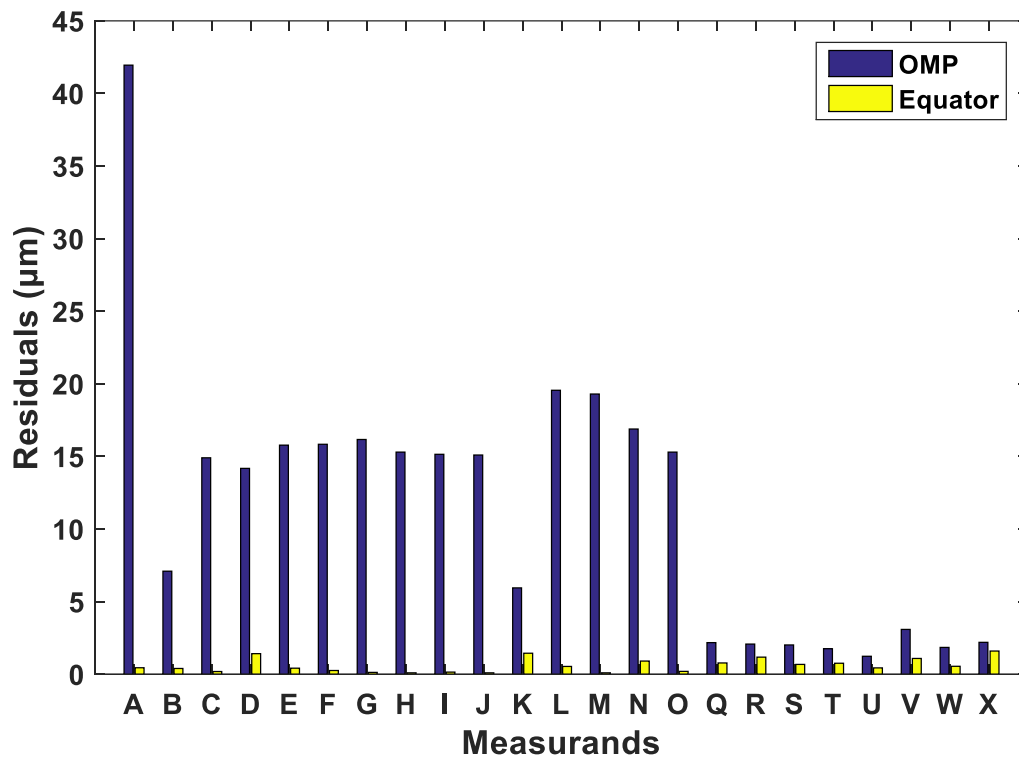


Figure 5.18: Comparison between OMP and Equator residuals for G2.

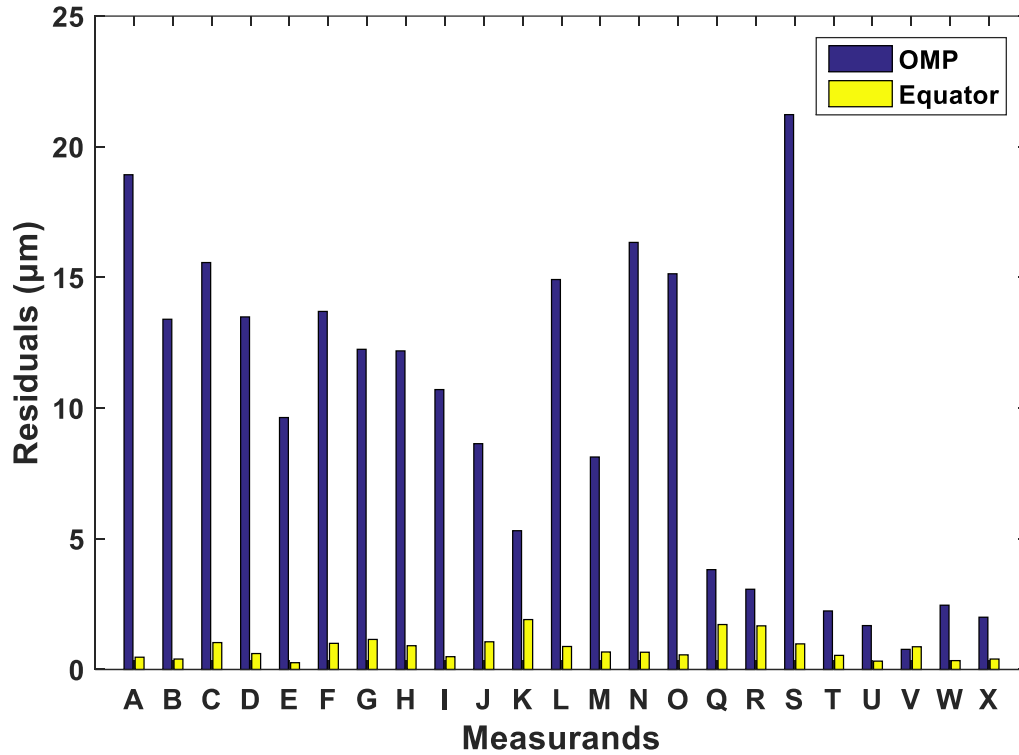


Figure 5.19: Comparison between OMP and Equator residuals for G3.

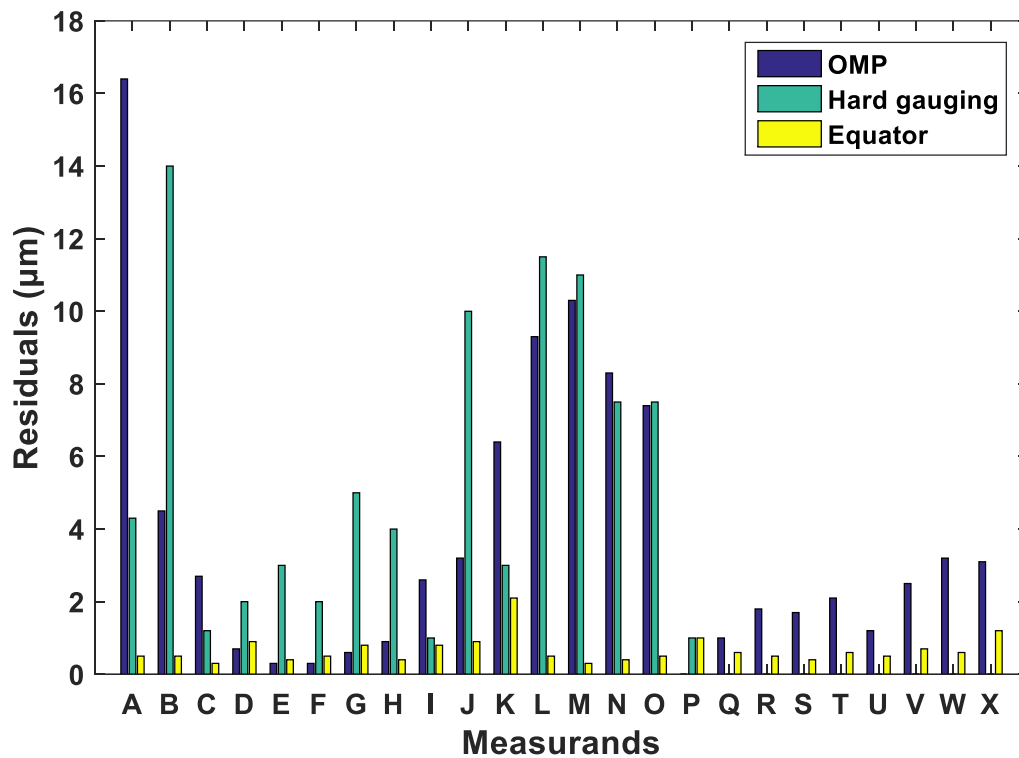


Figure 5.20: Comparison between OMP, hard gauging and Equator residuals for G4.

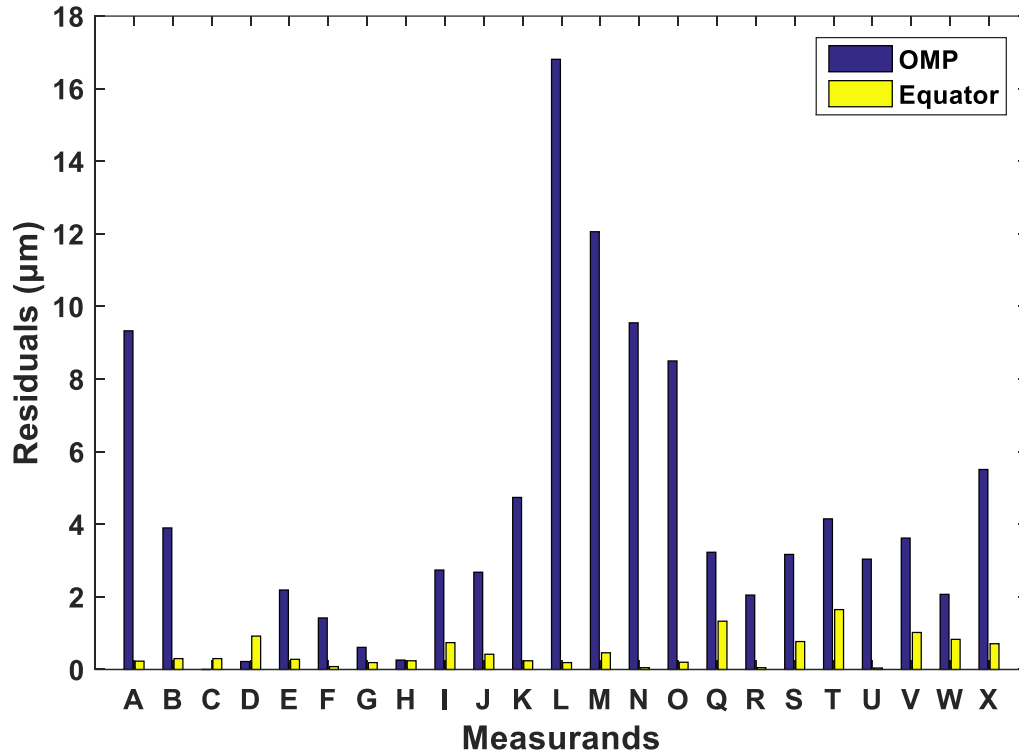


Figure 5.21: Comparison between OMP and Equator residuals for G5.

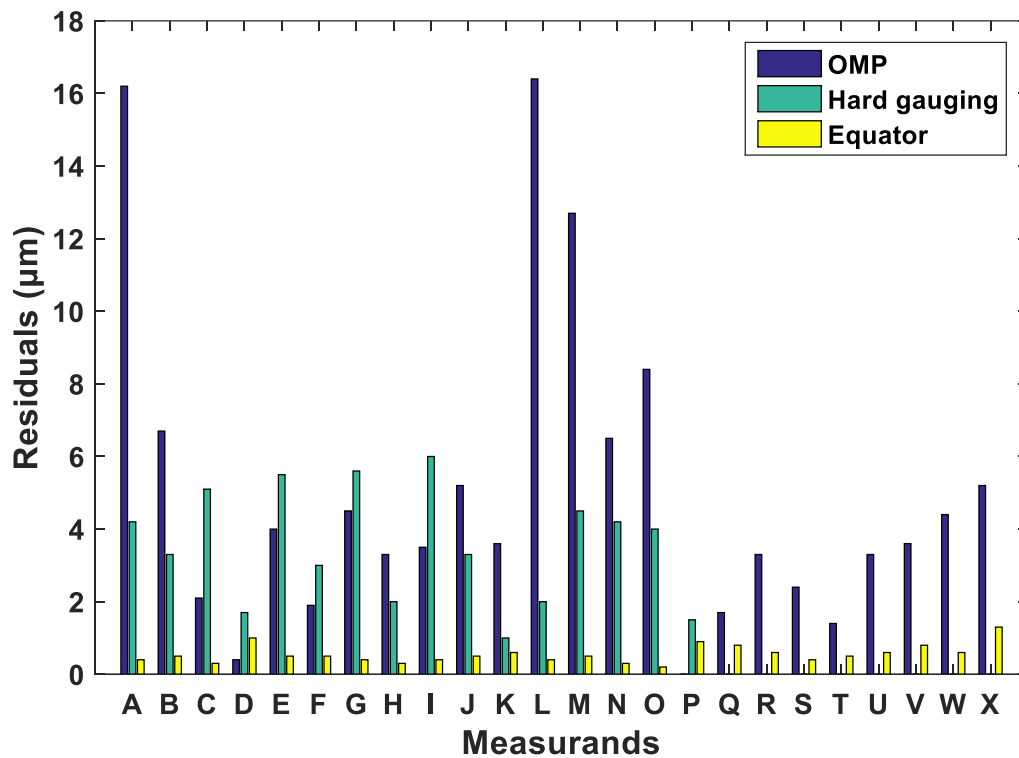


Figure 5.22: Comparison between OMP, hard gauging and Equator residuals for G6.

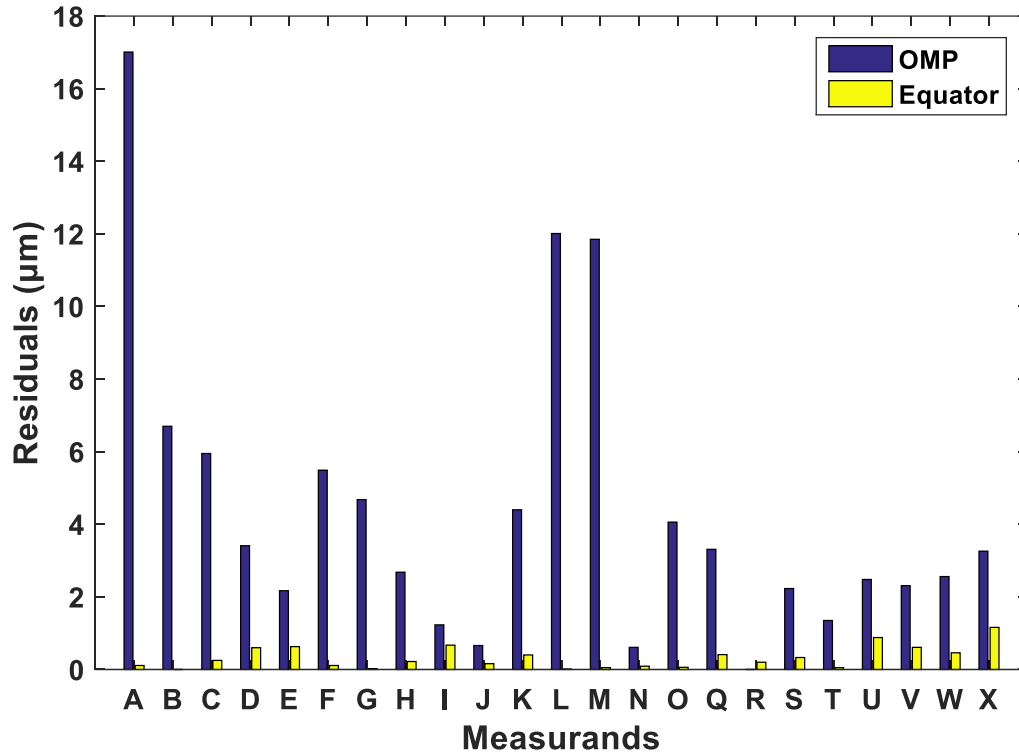


Figure 5.23: Comparison between OMP and Equator residuals for G7.

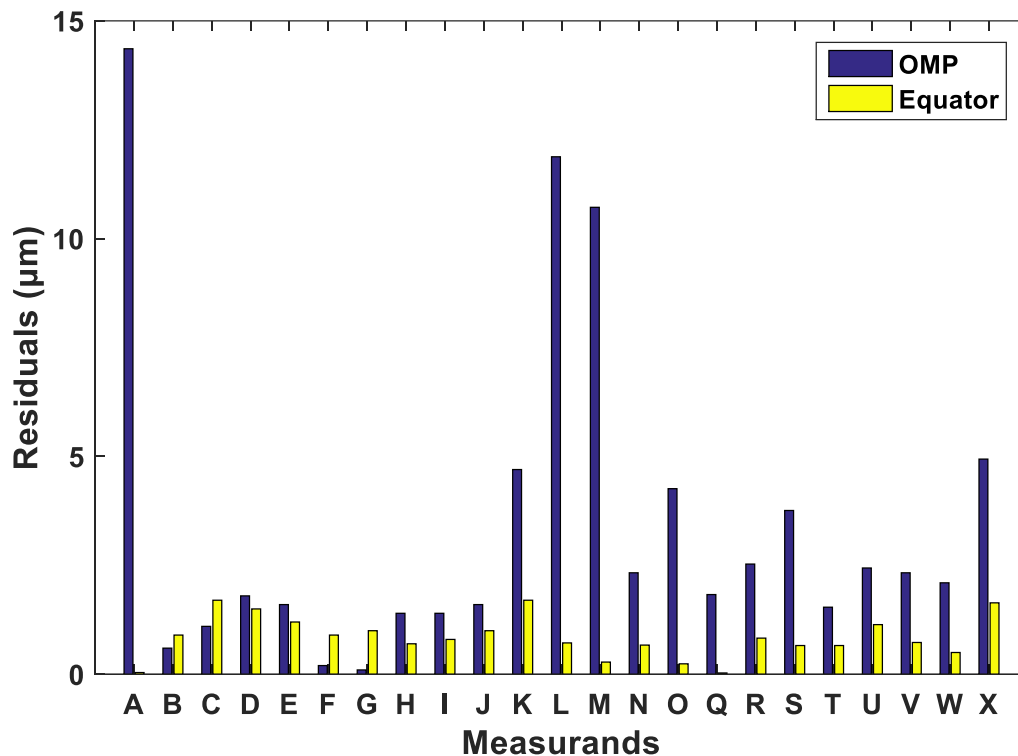


Figure 5.24: Comparison between OMP and Equator residuals for G8.

As can be seen from Figures 5.18-5.24, the Equator residuals are very small compared to the OMP and hard gauging residuals. The OMP and hard gauging results are subject to both random and systematic effects. Therefore, the evaluation of measurement uncertainty for these inspection approaches requires considerable efforts for valid measurement uncertainty estimates. Regarding the measurement time, in comparison to the Equator, OMP needed more than twice the time to complete the inspection and hard gauging was also very time consuming but a direct comparison cannot be made in this case since hard gauging was restricted to evaluating only a certain number of measurands due to the fundamental metrological limitations. Also, the inspection time for hard gauging was dependent on the operator. It is also worth mentioning that the Equator employed in CMM Compare requires repeatable part fixturing in order to achieve accurate results with low measurement uncertainties. The standard uncertainty associated with the fixturing repeatability must be significantly small, depending on the accuracy requirements and the measurement task. The same fixturing arrangement should also be used to produce the calibration file using the CMM. In total, compared to hard gauging (1st operator for 20 repetitions at low temperatures) and OMP, the Equator residuals and combined uncertainties are much smaller. Therefore, it can be concluded that such a flexible gauge employing the CMM Compare method can achieve highly repeatable

measurements which are traceable to national standards through the CMM calibration of the master part.

5.5 Summary

The aim of this chapter was to implement different shop floor inspection approaches and compare the measurement uncertainties obtained from each one. The dimensional inspection approaches included hard gauging, OMP, and automated flexible gauging. Different measurement results were obtained, as expected, due to the various error sources associated with the measurement environment (workshop conditions), measurement strategy, and measurement/gauging systems themselves. The measurement results have illustrated that traditional inspection methods such as OMP and hard gauging can lead to significant residual values and high measurement uncertainties. On the other hand, a PKM-based flexible gauge employed in a production environment in CMM Compare can achieve measurement results close to that obtained by a CMM located in a temperature controlled environment. Immediately after mastering, the comparator measurement uncertainty is mainly dependent on the accuracy of the CMM used to measure the master part and fixturing repeatability. If the fixturing variability is significant, then, the comparative analysis of the metrology data is unreliable because the comparison process involves a point-to-point comparison between the master part data and the measured part data.

Chapter 6

A Bayesian Approach to Evaluate Uncertainty associated with Comparative Coordinate Measurement

The aim of this chapter is to provide a statistical characterisation of a Renishaw Equator employed in comparator mode using small prior sample sizes. This solution can avoid executing large experimental designs thus providing a practical solution to robust statistical analysis for complex CMSs in industrial situations where the acquisition of large data sets is not practical. While the work focused on the Equator, it would be equally applicable and advantageous to other CMSs where unsystematic effects are dominant. Coordinate measurements in comparator mode benefit from the fact that many of the systematic effects associated with the measurement system cancel out through the principle of mastering. The process of mastering involves the measurement of a master part, using the measurement routine produced to measure the test parts, to calibrate the comparator system. Markov chains are suitable for modelling the performance characterised by probability distributions. Therefore, methods such as MCMC are required to provide summary information about these distributions. In this thesis, the Gibbs sampler is employed to produce a finite sample from the posterior. It is illustrated that estimating uncertainty associated with comparative coordinate measurement according to Bayesian principles offers significant advantages in terms of cost and reliability.

6.1 Modelling comparator measurement uncertainty

Given an accurately calibrated master artefact, the accuracy of comparative measurement depends mainly on the random effects associated with the comparator system and the drift of behaviour of the comparator system from its state at the time of the last measurement of the master artefact. Therefore, we can assume that comparator measurements can be modelled as

$$x_i = \alpha + e + \epsilon_i, \quad \epsilon_i \in N(0, \sigma^2), \quad (6.1)$$

where α is the unknown true value of the measurand, e is a fixed offset associated with the comparator, and ϵ_i is a random effect with unknown variance σ^2 . Variations in the differential thermal expansion between the part under test and gauging machine are difficult to predict and intermittent re-mastering is required to manage environmental effects. Regular re-mastering can significantly reduce or even eliminate the effects due to environment drift. In this chapter, we exam the influence of environmental effects in comparator mode through a statistical analysis gathered in repeatability and reproducibility (R&R) conditions.

Although a CMS that employs the comparator principle can account for the influence of systematic effects associated with the measurement system, the statistical characterisation of the repeatability component in comparator measurement can be determined in an R&R study. Another issue is the unknown time-interval required for managing efficiently the re-mastering process. The variability of the environmental conditions will determine the frequency at which the comparator system is calibrated. Due to the complexity and unpredictability of the environment changes and the kinematic behaviour of the instrument, a deterministic error model of the system parameters is not feasible. Instead we provide a statistical characterisation and use Bayesian methods to achieve posterior distribution of the statistical parameters. These posterior distributions can then be used to present the performance of the comparator system.

As has been discussed in previous chapters, the Equator gauge provides two main compare methods; the CMM Compare and the Golden Compare. The CMM Compare does not require a reference master part to calibrate the Equator as with Golden Compare. With CMM Compare, a test part produced close to drawing nominals can be used as a master part and is first calibrated on an accurate CMS such as a CMM in order to generate a calibration (.cal) file. The calibration file is then transferred to the Equator and read during mastering to enable the individual points of master data set to be compared with that of test data sets. Therefore, with CMM Compare, the calibrated absolute accuracy of the CMM located in a temperature controlled environment can be transferred to the shop floor to provide calibrated traceability to Equator measurements. The Golden Compare differs from the CMM Compare in that there is no requirement to first calibrate the master part on a CMM. However, this compare method requires a reference master part to calibrate the Equator and assumes that the master part is produced to drawing nominals. Therefore, with Golden Compare, any deviation of master part to drawing nominals will be included in the measurements. The most accurate method of using an Equator flexible gauge is the CMM Compare. However, in both cases, the measurement uncertainty for a given

production part will inherit uncertainty from the calibration of the master part [1, 31]. In particular, for Golden Compare, the uncertainty component associated with the calibration of the master part can be found from the calibration certificate of the calibrated part, while for CMM Compare from the task-specific uncertainty evaluation of CMM measurement. However, for both cases, this uncertainty contributor can be considered as a systematic effect and shall be considered in the overall uncertainty budget. Hence, consider an open system with four variables, as shown in Figure 6.1. The dependent variable is the comparator measurement uncertainty while the independent variables affecting the unknown quantity of interest are the environmental and random effects, and the uncertainty component brought-in from the calibration of the master part.

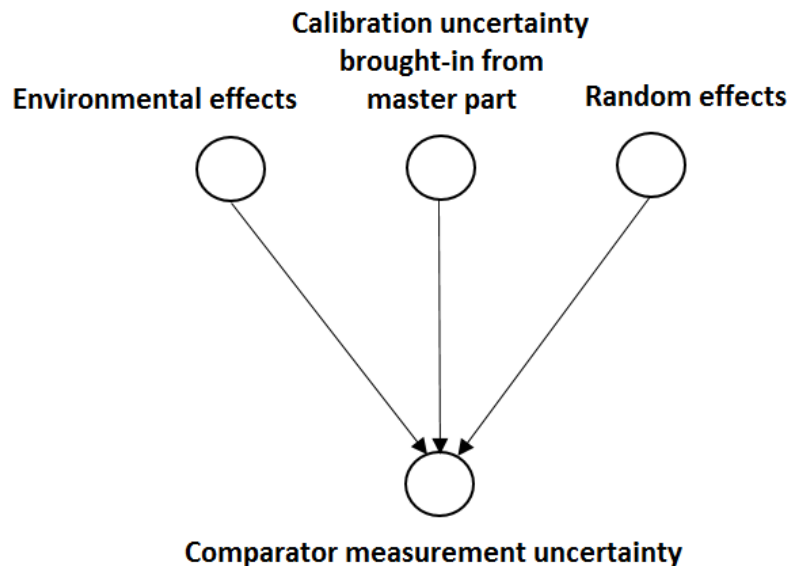


Figure 6.1: Comparator measurement uncertainty contributors.

The environmental effects can be ignored only when measuring immediately after mastering and their variability is negligible, or when measuring under temperature controlled conditions. Random effects can be decreased by repeated measurements. Therefore, the standard uncertainty associated with the measurement procedure generally accounts for these effects. In particular, the expanded uncertainty of the comparator measurement, U , can be calculated according to ISO 15530-3:2011 [73] (see Equation 2.10).

Now, suppose we wish to obtain an estimate y of the measurand Y and the standard uncertainty associated with the measurement procedure as defined by $s(\bar{x}) = \frac{s}{\sqrt{n}}$ where \bar{x} is the sample mean value, s is the sample standard deviation and n is the number of repeated measurements [5]. Classical uncertainty evaluation techniques require a relatively large number of repeated measurements to achieve reliable measurement uncertainty statements. When dealing with a small data set that follows a Gaussian distribution, the GUF recommends the t -distribution approach though the information on the parent PDF cannot be inferred from few repeated measurements.

6.2 Experimental comparator measurements

Experimental work was performed using the Renishaw Equator operating in Golden Compare and a specific manufactured part, as shown in Figure 6.2, used to validate the developed probabilistic model for different types of measurement. As has been mentioned in the previous chapters, the Equator is equipped with the SP25 3-axis analogue scanning probe. The SP25M (25 mm diameter scanning probe with scanning and touch-trigger modules) comprises two sensors in a single housing in order to function either as a scanning probe or as a touch-trigger probe. The machine is constructed with a parallel kinematic constraint mechanism to improve repeatability and reduce inertial effects when working for long periods of time and/or at high working speeds [111]. This device can be positioned next to the manufacturing equipment on the shop floor for close-to-manufacturing measurement and for fully automated applications; automated workcells with manufacturing equipment, robots, and comparator gauges. Therefore, in order to obtain realistic comparator measurements, angular misalignments (part misalignment from rotation between master and measure coordinate frames) were applied under changeable environmental effects (see chapter 3). The stylus used is a typical 21 mm long stylus with stainless steel stem and a 5 mm diameter ruby ball. After mastering, ten repeated measurements were performed in scanning mode without re-mastering for each angular misalignment applied; no offset by tilt in any direction, 2.5 mm offset by tilt along z -axis, 3 mm offset by tilt along y -axis, and the resulting 3D angular misalignment with the simultaneous combination of both. The scanning speed used was 100 mm/s, which is the maximum recommended for the specific Equator. In total, 40 measurement results were determined for each measurand. Table 6.1 shows the measurands considered for this work. A general overview of the experimental setup is shown in Figure 6.2.

Table 6.1: Measurands for probabilistic modelling.

Measurands	
A	Diameter of right circle (20 mm)
B	Diameter of left circle (45 mm)
C	Overall length (214.193 mm)
D	Top plane flatness
E	Circularity of right circle
F	Circularity of left circle

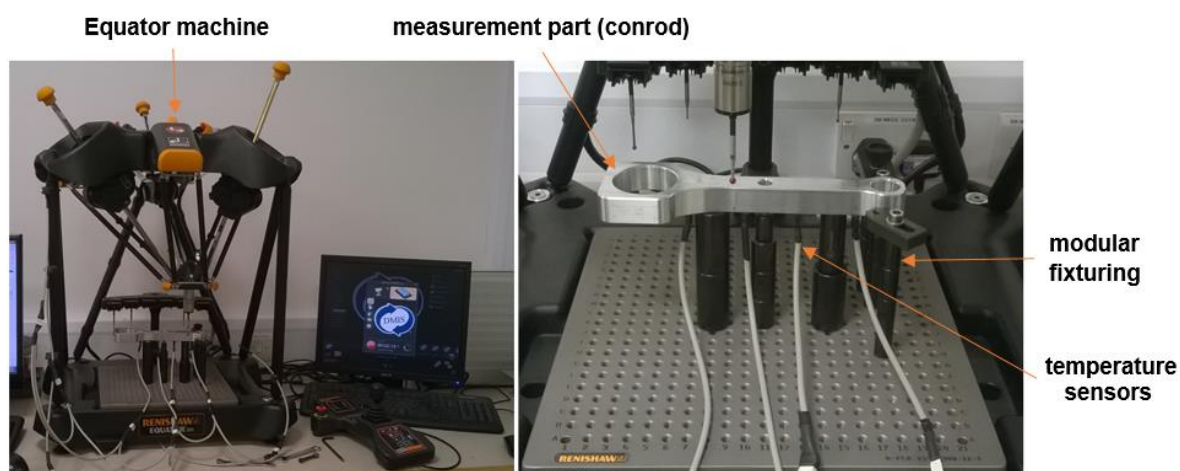


Figure 6.2: Test setup on Renishaw Equator flexible gauge.

6.3 Bayesian framework

The basis for inference in computational Bayesian statistics is the algorithms used to draw random samples from the true posterior, even when only the unnormalized posterior is known [49, 124]. The posterior distribution is the conditional probability distribution of the unknown parameters, given the observed data. Whereas in likelihood inference, where the joint likelihood function is not a probability density, in Bayesian inference the posterior is always a probability density, conditional on the available data. For this reason, the mean of the posterior distribution can be used as the estimate of the unknown parameter of interest since the posterior mean minimizes the mean squared deviation [125]. The sampling algorithms may be based on direct methods or MCMC methods [48]. Algorithms based on direct methods such as acceptance-rejection-sampling are inefficient, particularly, for high-dimensional parameter

spaces. Therefore, they are mainly used as a small step in Gibbs sampler, which is one of the most widely used MCMC methods. MCMC sampling is based on sophisticated algorithms that set up a Markov chain (see Appendix B) that has the posterior distribution as its long-run (limiting) distribution so that a random draw from the Markov chain can be equivalent to a random draw from the posterior. Common MCMC sampling algorithms are the Metropolis sampler, the Metropolis-Hastings sampler which is a generalization of the Metropolis algorithm, and the Gibbs sampler which is a special case of the Metropolis-Hastings algorithm where proposal distributions are the posterior conditionals and the acceptance rate is always one and thus, there is no wasted computation. In this thesis, the Gibbs sampler [126] was used to obtain a MCMC sample from the posterior distribution.

Let $\boldsymbol{\theta} = (\theta_1, \dots, \theta_N)$ denote unobservable vector quantities and $\boldsymbol{y} = (y_1, \dots, y_n)$ denote the observed data. Then, the joint PDF (or joint probability mass function in the case of discrete $\boldsymbol{\theta}$) is given by [49]:

$$p(\boldsymbol{\theta}, \boldsymbol{y}) = p(\boldsymbol{\theta})p(\boldsymbol{y} | \boldsymbol{\theta}), \quad (6.2)$$

where $p(\boldsymbol{\theta})$ is the prior distribution and $p(\boldsymbol{y} | \boldsymbol{\theta})$ is the likelihood. Using Bayes' rule, the posterior density can be determined by:

$$p(\boldsymbol{\theta} | \boldsymbol{y}) = \frac{p(\boldsymbol{\theta}, \boldsymbol{y})}{p(\boldsymbol{y})} = \frac{p(\boldsymbol{\theta})p(\boldsymbol{y} | \boldsymbol{\theta})}{p(\boldsymbol{y})}, \quad (6.3)$$

where $p(\boldsymbol{y})$ is the marginal or prior predictive distribution given by:

$$p(\boldsymbol{y}) = \int p(\boldsymbol{\theta})p(\boldsymbol{y} | \boldsymbol{\theta}) d\boldsymbol{\theta}. \quad (6.4)$$

With fixed \boldsymbol{y} , the factor $p(\boldsymbol{y})$ can be considered a constant and thus, it can be omitted. Therefore, the posterior can be expressed in the unscaled form as *posterior* proportional to *prior* times *likelihood*:

$$p(\boldsymbol{\theta} | \boldsymbol{y}) \propto p(\boldsymbol{\theta})p(\boldsymbol{y} | \boldsymbol{\theta}). \quad (6.5)$$

Even though the formula of unnormalized posterior does not give the posterior density $p(\boldsymbol{\theta} | \boldsymbol{y})$ exactly, it gives its shape by the prior times the likelihood. Based on the observed data \boldsymbol{y} , future data $\tilde{\boldsymbol{y}}$ can be generated e.g. using Monte Carlo simulation. The distribution of $\tilde{\boldsymbol{y}}$, conditional on \boldsymbol{y} , $p(\tilde{\boldsymbol{y}} | \boldsymbol{y})$, is called the posterior predictive distribution that can be written as:

$$\begin{aligned}
 p(\tilde{\boldsymbol{y}} | \boldsymbol{y}) &= \int p(\tilde{\boldsymbol{y}}, \boldsymbol{\theta} | \boldsymbol{y}) d\boldsymbol{\theta} \\
 &= \int p(\tilde{\boldsymbol{y}} | \boldsymbol{\theta}, \boldsymbol{y}) p(\boldsymbol{\theta} | \boldsymbol{y}) d\boldsymbol{\theta} \\
 &= \int p(\tilde{\boldsymbol{y}} | \boldsymbol{\theta}) p(\boldsymbol{\theta} | \boldsymbol{y}) d\boldsymbol{\theta}
 \end{aligned} \tag{6.6}$$

with the last equality valid since in this model, \boldsymbol{y} and $\tilde{\boldsymbol{y}}$ are conditionally independent given $\boldsymbol{\theta}$.

6.4 Gibbs sampling from the posterior distribution

We begin by considering a model of the form [46, 127]:

$$y_i = \phi(x_i, \boldsymbol{a}) + \epsilon_i, \quad \epsilon_i \in N(0, \sigma^2), \quad i = 1, \dots, n, \tag{6.7}$$

where y_i is the measured response or dependent variable corresponding to accurately known values x_i , $\phi(x_i, \boldsymbol{a})$ is the modelled response with unknown parameters $\boldsymbol{a} = (a_0, a_1, \dots, a_m)^T$ associated with angular misalignments in this case, and ϵ_i represents the random effects drawn from a Gaussian distribution with zero mean and variance σ^2 . Suppose $\phi(x_i, \boldsymbol{a}) = a_0 + a_1 x_i$ or in matrix notation:

$$\boldsymbol{y} = \boldsymbol{X}\boldsymbol{a} + \boldsymbol{\epsilon}, \quad \boldsymbol{\epsilon} \in N(0, \sigma^2 \boldsymbol{I}), \tag{6.8}$$

where \boldsymbol{I} denotes the $n \times n$ identity matrix and \boldsymbol{X} is given by:

$$\mathbf{X} = \begin{bmatrix} 1 & x_{11} & \dots & x_{1m} \\ 1 & x_{21} & \dots & x_{2m} \\ \vdots & \vdots & \ddots & \vdots \\ 1 & x_{n1} & \dots & x_{nm} \end{bmatrix} \quad (6.9)$$

with $m + 1 < n$. Note that, $\mathbf{y} = (y_1, \dots, y_n)^T$ and we assume that $\mathbf{y} \in N(\mathbf{X}\mathbf{a}, \sigma^2\mathbf{I})$. In particular, the “data” in a regression problem comprise both the response variable \mathbf{y} and the predictors \mathbf{X} . Hence, without loss of generality, suppose $p(y_i, x_i | \boldsymbol{\theta}) = p(y_i | x_i, \boldsymbol{\theta})p(x_i | \boldsymbol{\theta})$, $p(y_i | x_i, \boldsymbol{\theta}) = p(y_i | x_i, \boldsymbol{\theta}_{y|x})$, and $p(x_i | \boldsymbol{\theta}) = p(x_i | \boldsymbol{\theta}_x)$, where $\boldsymbol{\theta} = (\boldsymbol{\theta}_{y|x}, \boldsymbol{\theta}_x)^T$ and $\boldsymbol{\theta}_{y|x} = (\mathbf{a}, \sigma^2)$ [128]. Suppose also that $p(\mathbf{y}, \mathbf{X} | \boldsymbol{\theta}) = p(\mathbf{y} | \mathbf{X}, \boldsymbol{\theta}_{y|x})p(\mathbf{X} | \boldsymbol{\theta}_x)$. Therefore, the posterior distribution for $\boldsymbol{\theta}$, given \mathbf{y} and \mathbf{X} , can be written as:

$$p(\boldsymbol{\theta} | \mathbf{y}, \mathbf{X}) \propto p(\boldsymbol{\theta})p(\mathbf{y}, \mathbf{X} | \boldsymbol{\theta}) \quad (6.10)$$

where $p(\boldsymbol{\theta})$ is the prior distribution representing the prior knowledge about $\boldsymbol{\theta}$ and $p(\mathbf{y}, \mathbf{X} | \boldsymbol{\theta})$ is the likelihood. Also, given the assumptions above, and $p(\boldsymbol{\theta}) = p(\boldsymbol{\theta}_{y|x})p(\boldsymbol{\theta}_x) = p(\mathbf{a}, \sigma^2)p(\boldsymbol{\theta}_x)$, then,

$$p(\mathbf{a}, \sigma^2, \boldsymbol{\theta}_x | \mathbf{y}, \mathbf{X}) = p(\mathbf{a}, \sigma^2 | \mathbf{y}, \mathbf{X})p(\boldsymbol{\theta}_x | \mathbf{X}). \quad (6.11)$$

Note that, our interest lies only with $\boldsymbol{\theta}_{y|x}$. The likelihood function for the normal linear model can be written as:

$$p(\mathbf{y}; \mathbf{X}, \mathbf{a}, \sigma^2) = (2\pi\sigma^2)^{-n/2} e^{\left(\frac{-(\mathbf{y}-\mathbf{X}\mathbf{a})^T(\mathbf{y}-\mathbf{X}\mathbf{a})}{2\sigma^2}\right)}. \quad (6.12)$$

Using a conjugate prior density for the parameter vector $\boldsymbol{\theta}_{y|x} = (\mathbf{a}, \sigma^2)^T$, then, the posterior density is:

$$p(\mathbf{a}, \sigma^2 | \mathbf{y}, \mathbf{X}) \propto p(\mathbf{a}, \sigma^2)p(\mathbf{y} | \mathbf{a}, \sigma^2) \quad (6.13)$$

where $p(\mathbf{a}, \sigma^2) = p(\mathbf{a} | \sigma^2)p(\sigma^2)$ is the prior distribution and $p(\mathbf{y} | \mathbf{a}, \sigma^2)$ is the likelihood. Conjugate prior distributions for \mathbf{a} given σ^2 , and σ^2 can be given by:

$$\mathbf{a} \mid \sigma^2 \sim \mathbf{N}(\mathbf{a}_0, \sigma^2 \mathbf{V}_0^{-1}), \quad \sigma^2 \sim \text{IG}(\alpha_0, \beta_0). \quad (6.14)$$

So, the conditional prior density for \mathbf{a} given σ^2 is a multivariate normal density with mean \mathbf{a}_0 and covariance matrix $\sigma^2 \mathbf{V}_0^{-1}$, where \mathbf{V}_0 is a symmetric positive definite matrix of size $(m + 1) \times (m + 1)$, and the prior density for σ^2 is an inverse Gamma density with shape α_0 and scale β_0 . Note that, while the conditional posterior density $p(\mathbf{a} \mid \sigma^2, \mathbf{y}, \mathbf{X})$ is a multivariate normal density, the marginal posterior density $p(\mathbf{a} \mid \mathbf{y}, \mathbf{X})$ is a multivariate t-density given by:

$$p(\mathbf{a} \mid \mathbf{y}, \mathbf{X}) = \int p(\mathbf{a} \mid \sigma^2, \mathbf{y}, \mathbf{X}) p(\sigma^2 \mid \mathbf{y}, \mathbf{X}) d\sigma^2 \quad (6.15)$$

Given different values for α_0 and β_0 , various distributions for σ can be obtained to facilitate the use of prior knowledge. In the case where there is no prior knowledge, then, a possible noninformative prior for this model is given by $p(\mathbf{a}, \sigma^2) \propto 1/\sigma^2$.

The Gibbs sampler was used in MATLAB [129] to draw samples from the unnormalized posterior, $p(\boldsymbol{\theta} \mid \mathbf{y})$. Because our interest lies only with $\boldsymbol{\theta}_{y|x}$, this will be simply denoted by $\boldsymbol{\theta}$. Suppose $y_i \sim \mathbf{N}(\mu_i, \sigma^2)$ where $\mu_i = a_0 + a_1 x_{i1} + \dots + a_m x_{im}$ in order to estimate the uncertainty associated with comparative coordinate measurement influenced by process variations such as angular misalignments in this case while avoiding repeated measurements. To validate the model, various random values were drawn from each data set (see section 6.2). In particular, after performing a normality test for each data set, the measurement data were assigned the Gaussian distribution $\mathbf{y} \sim \mathbf{N}(\boldsymbol{\mu}, \sigma^2)$. Therefore, future measurements from the same process could also be assumed a priori to be Gaussian. To estimate $\boldsymbol{\theta} = (\mu, \sigma^2)$, the posterior predictive distribution of each measurand was approximated by $p(\tilde{\mathbf{y}} \mid \mathbf{y}) \approx \frac{1}{N} \sum_{i=1}^N p(\tilde{\mathbf{y}} \mid \theta_i)$ using Monte Carlo where the sample θ_i was obtained from the posterior distribution $p(\boldsymbol{\theta} \mid \mathbf{y})$ produced via Gibbs sampling. Direct evaluation becomes computationally inefficient as the number parameters increases. Using an improper, reference prior, $p(\mu, \sigma^2) \propto 1/\sigma^2$ then, the conditional posterior for μ is $\mu \mid \sigma^2, \mathbf{y} \sim \mathbf{N}(\bar{y}, \sigma^2/n)$ and the conditional posterior for $1/\sigma^2$ is $1/\sigma^2 \mid \mu, \mathbf{y} \sim \Gamma(n/2, ns_\mu^2/2)$, where \bar{y} is the sample mean, n is the sample size, and s_μ^2 is the sample variance for known μ . The Gibbs sample size, N , was set to 300 in order to ensure that the distribution of the successive values in the sequence $\theta_1, \theta_2, \dots, \theta_N$ converges to the required posterior distribution. To eliminate the effects

associated with the starting values, the burn-in period, which involves the number of samples that are discarded, was set to $N/2$ (half of the total number of samples) though the beginning of the chain accurately represented the posterior [49]. Therefore, there was no need to consider multiple chains since there is no issue about convergence of the Markov chain [47, 48]. Chain thinning, which is a method used to reduce the correlation in simulated Markov chains, it was not required due to the very good mixing properties of the chain. Finally, there was no need to calculate the acceptance probability since it is always one. Figure 6.3 shows a trace plot of Gibbs samples after burn-in for measurand A to illustrate that the accuracy of the method depends on the length of samples. However, the Gibbs sample mean values will always be highly correlated with the prior sample mean values due to the model structure. In this case, the difference between the population mean values and the Bayesian estimates of the mean values was very small ($< 0.1 \mu\text{m}$ for measurands A and B, $< 0.2 \mu\text{m}$ for measurands C and E, and $< 0.4 \mu\text{m}$ for measurands D and F) using different prior random samples for all the measurands.

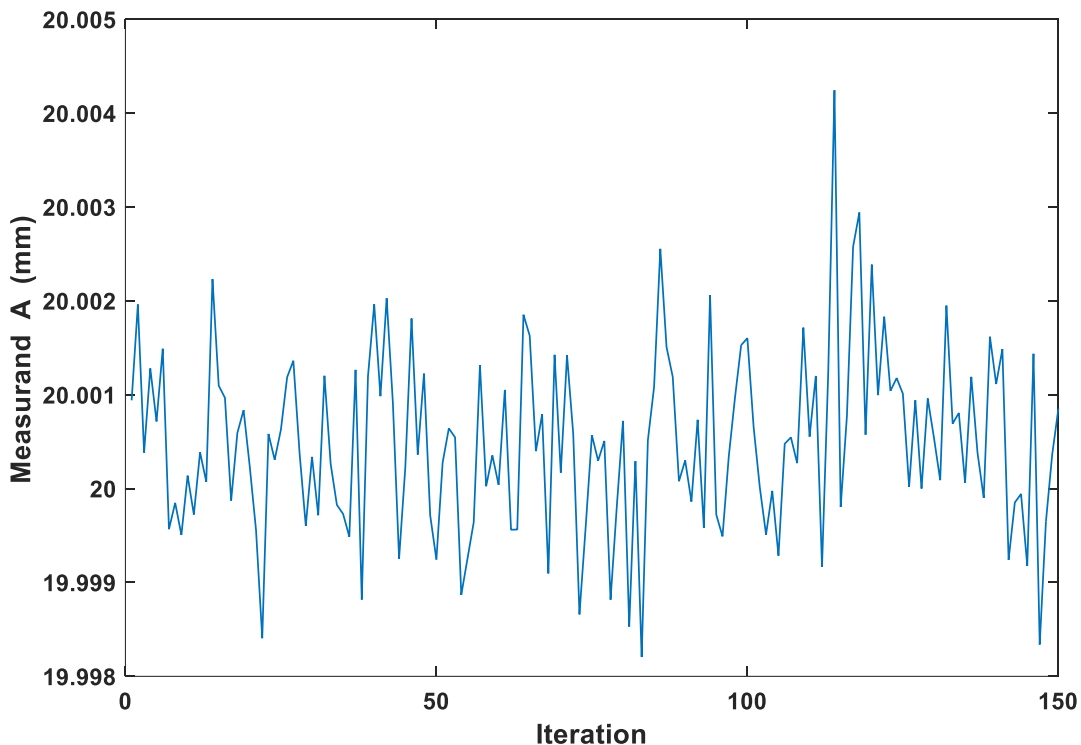


Figure 6.3: Trace plot of the Gibbs sampling chain after burn-in for measurand A.

It can be seen from Figure 6.3 that the Gibbs sampling chain is moving through the space satisfactorily. Figure 6.4 compares the standard uncertainties from the population with the uncertainties calculated by the Bayesian approach using a prior random sample.

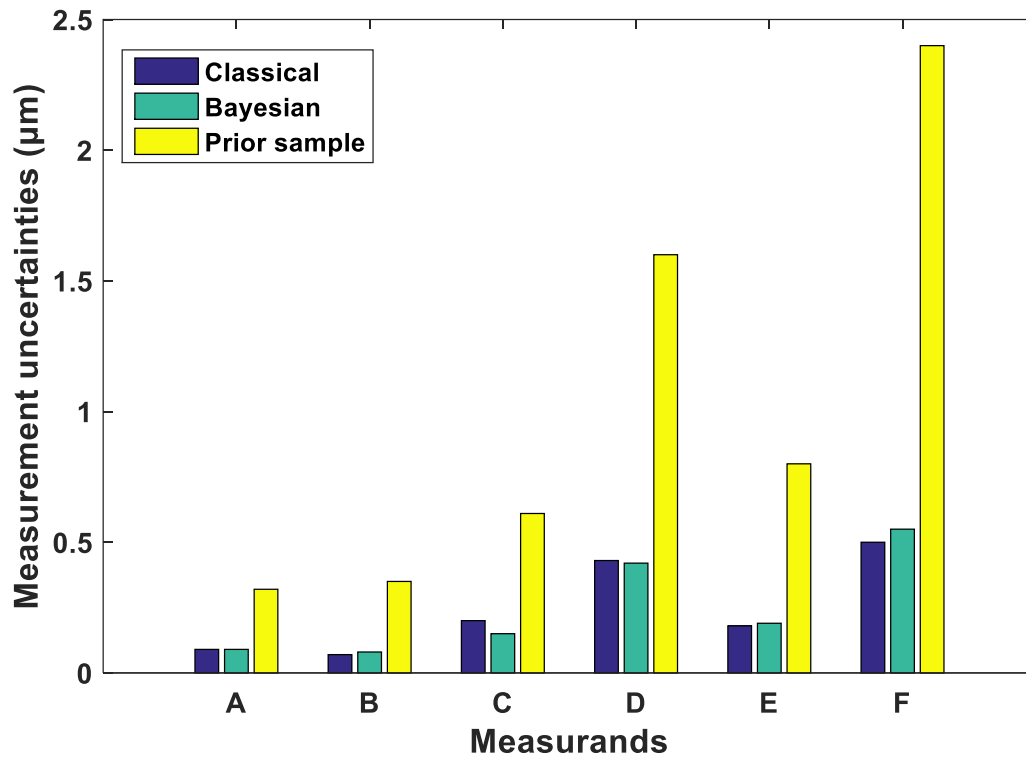


Figure 6.4: Bar graph for standard uncertainties.

As can be seen from Figure 6.4, the Bayesian estimates of the uncertainty values compare well with that of the complete data set for all the measurands. Therefore, estimating uncertainty associated with comparative coordinate measurement according to Bayesian principles can be particularly beneficial especially when large experimental designs are impractical.

6.5 Summary

Recent advances in versatile automated gauging have enabled accurate geometric tolerance assessment on the shop floor. The primary task of this chapter has been to develop a probabilistic model for comparative coordinate measurement and apply a MCMC method to evaluate uncertainty associated with comparative coordinate measurement according to Bayesian principles. In this thesis, the Gibbs sampler, which is a specialized version of the Metropolis-Hastings algorithm, has been employed to draw a random sample from the unnormalized posterior whose distribution approaches the true posterior distribution. This

hybrid algorithm has produced a random sample from the posterior directly so many of the difficulties associated with determining the burn-in period and thinning rate have been avoided. Therefore, this Bayesian sampling approach can be very beneficial for modelling comparator measurement uncertainty, especially, when repeated measurements cannot be performed. Finally, evaluating uncertainty associated with coordinate measurement in absolute mode can also benefit from MCMC methods because they allow for developing more realistic probability models than classical techniques.

Chapter 7

Estimating Point Coordinates and associated Uncertainties using Artificial Intelligence Techniques

CMMs and comparator gauges are complex measuring systems that are widely used in the manufacturing industry for form, size, position, and orientation assessment. In essence, these systems collect a set of individual data points that in practice is often a relatively small sample of an object. Their software then processes these points in order to produce a geometric result or to establish a local coordinate system from datum features. The subject of CMS performance evaluation is a broad and multifaceted one. This chapter is concerned with the uncertainty of measurement in the coordinates of each point within the CMS workzone. Therefore, a novel method for predicting CMS point coordinates and associated uncertainties is developed. This new method is particularly useful when a precise mathematical model for the measurement system is not available and small experimental designs are unavoidable. The proposed method is based on a BRANN model consisting mainly of three inputs and one output. The inputs are: the nominal coordinates; the ambient temperature; and the temperature of the part. The output is the measured (actual) coordinates. An algorithm is developed and implemented before training the BRANN in order to map each nominal coordinate associated with the other inputs to the target coordinate. The method is first implemented in simulated CMM coordinate data and then in actual comparator coordinate data. Most part of this work has been published in [130].

7.1 Motivation and methodology

CMSs such as CMMs are used extensively in manufacturing industry to carry out an inspection with high accuracy. Even though they only measure individual points in space, they are extremely flexible. Their flexibility comes from the software that processes these points in order to produce a geometric result or to establish a local coordinate system from datum features. Every point gathered by a CMM is expressed in terms of its x -, y -, and z - measured coordinates. However, the uncertainty in the x -, y - and z -coordinates of a point in space has a

large influence on the software used to process the coordinate data. Therefore, estimating the uncertainty of the coordinates of each measured point can enable very efficient implementations of geometric element best-fit algorithms [97] and help determine uncertainty contributors associated with a particular axis of the CMM [4].

Classical statistical analysis to estimating uncertainty requires large sample sizes distributed according to a standard distribution such as the multivariate normal distribution. However, in many practical cases, a large amount of data cannot be obtained due to the cost, time, etc. For multivariate measurands such as a set of coordinates, uncertainties are evaluated in terms of variance matrices that can frequently be derived in terms of a measurement system model [96]. Nevertheless, this is not straightforward in the case of CMM measurement due to the complexity of the measurement process and the CMM itself [131]. As a result, the scope of the model is often limited to certain environmental and working conditions. In many applications, when no satisfactory mathematical model can be derived, ANNs are a good alternative predictive modelling approach. ANNs learn from experience rather than by deterministic programming and they provide highly parallel, adaptive models trained only by input-output data. Also, they are able to generalize from given training data to unseen data. However, ANNs cannot be seen as a simple one-answer-fits-all solution, and in many cases misapplication of artificial intelligence (AI) techniques can lead to incorrect results, especially where the ANN model is poorly defined and perturbations are outside the scope of the training sample.

7.1.1 Artificial neural networks

ANNs are computational models that can acquire, store and utilise knowledge gained from experience. They have been inspired by biological neural networks found in humans and can be implemented in either hardware or software. The first model of an artificial neuron called threshold logic unit (TLU) or linear threshold gate (LTG) was proposed by McCulloch and Pitts [132]. The method employed in this thesis uses multi-layer perceptron (MLP) networks though Elman networks will also be employed at the end of this chapter. An MLP network is a feedforward ANN model which consists of one input layer, one output layer, and one or more hidden layers [133]. Each layer includes one or more nodes. Except for the input nodes, each node is a perceptron (neuron) usually with a nonlinear activation function. A typical perceptron is depicted in Figure 7.1.

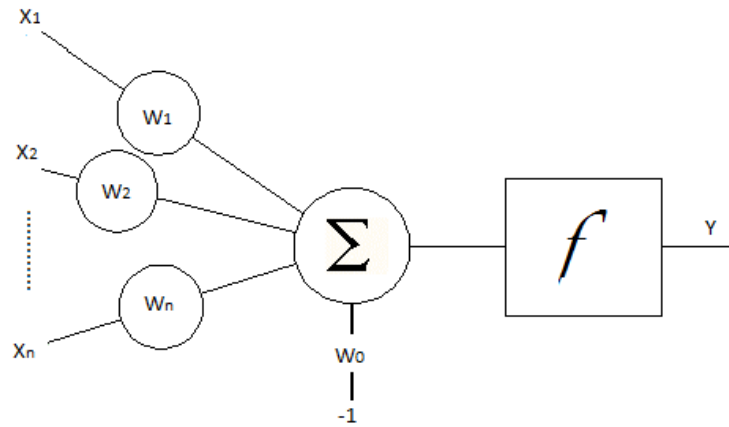


Figure 7.1 A perceptron.

The output of a perceptron can be described by:

$$Y = f\left(\sum_{i=1}^n w_i x_i - w_0\right) \quad (7.1)$$

Where f is usually a nonlinear activation function (e.g. a bipolar sigmoid), w_i is the weight associated with the i^{th} input (x_i), and w_0 is the weight associated with the bias input.

The MLP network is the most common ANN model and is known as a supervised network because it requires a desired output in order to learn. Supervised learning is achieved through use of a training data set, prior to testing on a test data set. An MLP network aims at creating a model that maps the input to the output using historical data. The supervised learning technique utilized by an MLP for training the network is called back-propagation (BP). Determining the number of hidden layers and the number of neurons in each hidden layer is an important task. In most cases, the number of hidden layers, which depends on the complexity of the relationship between the inputs and the outputs, is defined first. The number of hidden neurons usually varies between the number of input neurons and the number of output neurons. Training multiple times will generate different results due to different initial conditions and sampling.

Figure 7.2 shows an MLP network architecture. It contains one input layer with four input nodes, one hidden layer with five neurons, and one output layer with one neuron.

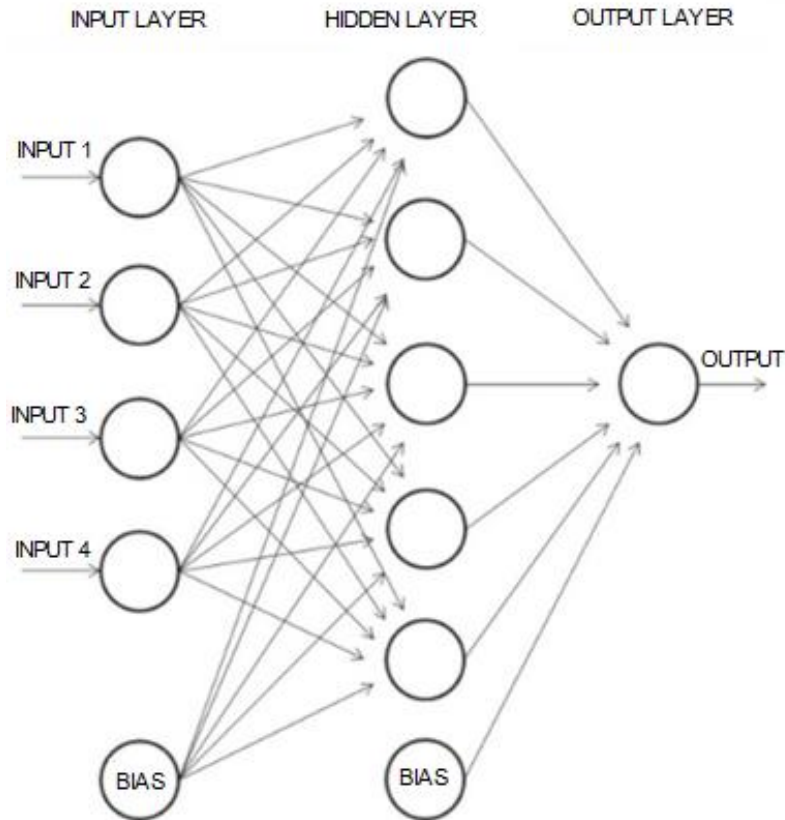


Figure 7.2: An MLP network architecture.

Note that, (a) each node in one layer connects with a certain weight to every node in the following layer, (b) each circle in the hidden and output layer represents a perceptron including a summation unit and an activation function, and (c) the nonlinearity of the activation function will provide the nonlinear characteristic of an ANN.

In this thesis, in order to enhance the ability of ANN to make predictions, the ANN is trained by Bayesian regularization [134]. This approach, which is an improvement of BP, uses statistical techniques so that the trained ANN can use the optimal number of parameters. Bayesian regularization provides better generalization performance than early stopping, especially for small data sets because it uses all the data; it does not require that a validation data set be separate from the training data set. BRANNs avoid overfitting because the regularization pushes unnecessary weights towards zero and offer a simple and usable form of ANN [135].

7.2 CMM measurement case study

Consider that twenty individual data points representing the measured (actual) x -coordinates x_i ranged from 0 to 210 mm in this example are generated according to the model:

$$x_i = x_i^* + e_{a_i} + e_{w_i} + \epsilon_i, \quad \epsilon_i \in N(0, \sigma^2), \quad i = \{1, \dots, 20\}, \quad (7.2)$$

where x_i^* is the nominal x -coordinates, e_{a_i} and e_{w_i} represent systematic effects associated with the ambient temperature and the part temperature, respectively, and ϵ_i represents random effects. Suppose then that ten data sets including twenty actual x -coordinates each are generated according to this model with errors ranged from -10 to 12 μm (temperature values range from 18 to 22°C). Consequently, each data point in each data set is highly correlated to an ambient temperature, a part temperature, and a random, uncorrelated effect.

The multi-layer perceptron (MLP) network shown in Figure 7.3 consists of three input units, five hidden neurons and one output unit. The activation functions for both the hidden and the output layers are tan-sigmoid (tansig) transfer functions to provide the nonlinear characteristic. The three inputs of the network are the vector of nominal coordinates, the vector of ambient temperature data, and the vector of part temperature data while the output (target) is the vector of actual coordinates (displacement). The nominal coordinates are used because they help the ANN to generalize for different measurement tasks across the CMM. The ANN is trained by Bayesian regularization to improve network generalization. To attempt to realize such a model, all the inputs and the output are coded as vectors. An algorithm is developed and implemented before training the ANN in order to map the nominal coordinates associated with the other inputs to the target coordinates. The data has been normalized between -1 and 1, since the Bayesian regularization training algorithm generally works best when the ANN inputs and targets are scaled within that range [135].

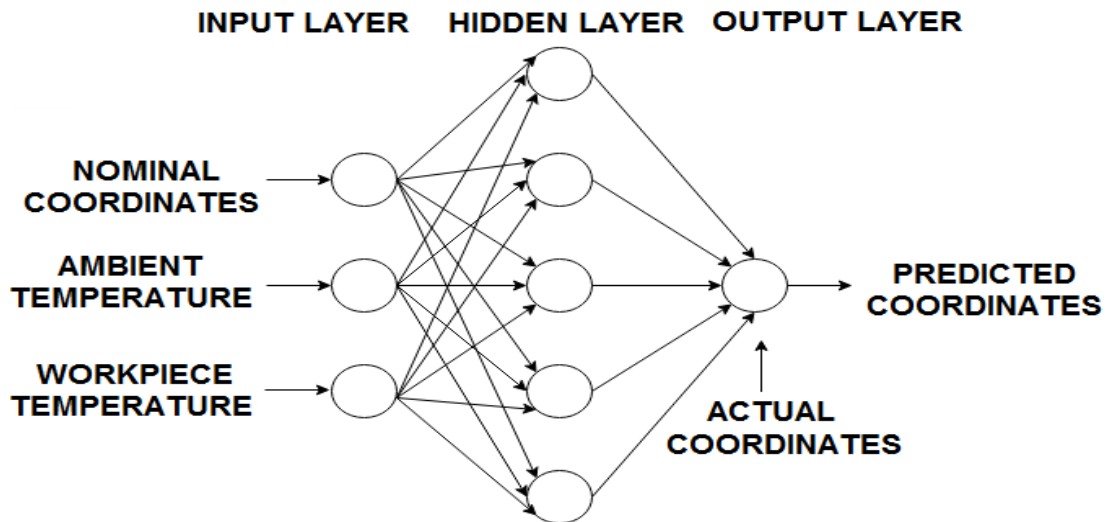


Figure 7.3: The MLP network with five hidden neurons.

7.2.1 Simulation results for CMM case study

By varying the simulations in MATLAB with different numbers of hidden neurons, four different models were developed. The first model consists of five hidden neurons, the second with ten, the third with 20, and the fourth with 40. All the models were trained for a different number of epochs because the training process only needs to be implemented until the errors converge. In order to examine the performance of all the BRANN models on non-training data, another ninety data sets (testing sample) were generated. So, ten simulated data sets were used for training and 90 simulated data sets for testing. This case is particularly important when small sample sizes are available.

The mean squared error (MSE) performance function was used to measure each network's performance. Table 7.1 shows the results obtained from all the developed models; the number of convergence epochs, the network's performance according to the mean of squared errors, and the percentage of improvement in the calculated uncertainty compared to the complete data set.

Table 7.1: Performance of BRANN models.

Models	Number of hidden neurons	Convergence epochs	MSE (mm)	Improvement in accuracy of the uncertainty calculation (%)
1	5	2374	4.65×10^{-5}	83.0
2	10	3744	8.74×10^{-6}	83.0
3	20	3487	1.68×10^{-5}	82.0
4	40	5000	3.28×10^{-5}	83.0

As can be seen from Table 7.1, the minimum MSE is obtained by the second model while all the models provide almost the same variability. In a similar way, the method can be applied to y- and z-coordinates. In addition, by increasing the number of hidden layers to two, the MSE is reduced to a great extent as shown in Table 7.2 and thus, a VCMM can be obtained (see section 2.4.4 for VCMM description). Also, an improvement in the estimated uncertainty is achieved using the predicted variability from the models including two hidden layers. The minimum MSE is obtained by the second model.

Table 7.2: Performance of BRANN models with two hidden layers.

Models	Number of hidden neurons	Convergence epochs	MSE (mm)	Improvement in accuracy of the uncertainty calculation (%)
1	5 – 5	1000	2.89×10^{-6}	83.0
2	10 – 10	1137	2.44×10^{-6}	87.0
3	20 – 20	972	3.13×10^{-6}	87.0
4	40 – 40	1000	4.04×10^{-6}	84.0

7.3 Comparator measurement case study

The aforementioned method could also be extended beyond CMMs to include other measurement systems such as comparator gauges. To validate the performance of the method on comparator gauges, experimental work was performed using the Renishaw Equator operating in Golden Compare and the RESR ring part. The stylus used is a typical 21 mm long stylus with stainless steel stem and a 2 mm diameter ruby ball. After mastering, 80 repeated measurements were performed without re-mastering on the large circle with a nominal diameter of 80 mm using 20 probing points. The number of temperature sensors used as inputs

to the BRANN model in this case study is five. In particular, two temperature sensors were used for the ambient temperature and three for the temperature of the part. Therefore, in this case study, the ANN consists of six input units: a vector of nominal x -coordinates, two vectors of ambient temperature data and three vectors of part temperature data. The output is the vector of measured x -coordinates. A general overview of the experimental setup is shown in Figure 7.4.



Figure 7.4: Test set up on comparator gauge.

7.3.1 Simulation results for comparator case study

To achieve a relatively low MSE value, extensive simulations were performed to find the optimal number of hidden layers and hidden neurons. Therefore, five different models were developed. The first model consists of one hidden layer with ten hidden neurons. The second model consists of two hidden layers with ten hidden neurons each. The third model consists of two hidden layers with five hidden neurons in the first hidden layer and 40 in the second. The fourth model consists of two hidden layers with ten hidden neurons each but different activation functions for the hidden and the output layers. In particular, the activation function for the first hidden layer is linear (purelin) transfer function, the activation function for the second hidden layer is tan-sigmoid (tansig) transfer function and the activation function for the output layer is linear. The fifth model consists of one hidden layer with ten hidden neurons but two different activation functions for the hidden and the output layers. In particular, the activation function for the hidden layer is tan-sigmoid while the activation function for the output layer is linear.

40 data sets were used for training and 40 data sets for testing. Table 7.3 shows the results obtained from all the MLP networks. The minimum MSE is obtained by the fifth model.

Table 7.3: Performance of MLP models for comparator data.

Models	Number of hidden neurons	Convergence epochs	MSE (mm)	Improvement in accuracy of the uncertainty calculation (%)
1	10 – 0	445	7.91×10^{-6}	56.0
2	10 – 10	715	1.23×10^{-5}	56.0
3	5 – 40	258	9.91×10^{-6}	62.0
4	10 – 10	1750	6.96×10^{-6}	59.0
5	10 – 0	2000	6.24×10^{-6}	65.0

Based on Table 7.3, it can be concluded that the method also performs well on experimental coordinate data with a modest decrease in improvement in the calculated uncertainty since the coordinate data have been obtained from an automated comparator gauge employed on the shop floor and thus, random effects are the dominant source of measurement uncertainty.

In addition, Elman networks could be trained to predict the x -coordinates. Elman networks use positive feedback from the hidden layer to construct some form of memory in the network [136]. Different activation functions and number of hidden layers and neurons were tried in effort to find the architectures that would model the comparator coordinate data most effectively. Therefore, three different models were developed. The first model consists of two hidden layers with ten hidden neurons each. The second model consists of one hidden layer with ten hidden neurons. The activation function for the hidden layer is tan-sigmoid while the activation function for the output layer is linear. The third model consists of two hidden layers with ten hidden neurons each but the activation function for the output layer is linear (the activation functions for both hidden layers are tan-sigmoid). Table 7.4 shows the results obtained from all the Elman networks. The minimum MSE is obtained by the second model.

Table 7.4: Performance of Elman models for comparator data.

Models	Number of hidden neurons	Convergence epochs	MSE (mm)	Improvement in accuracy of the uncertainty calculation (%)
1	10 – 10	1280	1.27×10^{-5}	59.0
2	10 – 0	2000	5.81×10^{-6}	62.0
3	10 – 10	1381	6.05×10^{-6}	55.0

7.4 Summary

This chapter has been concerned with the point coordinate uncertainties. Both validation case studies performed have shown that the prediction errors are small according to the MSE and the accuracy of the uncertainty calculation is improved significantly using the predicted variability compared to the uncertainty calculated from the limited/training sample data set. In particular, for validation in the CMM case study, the models were trained using a relatively small sample size of ten data sets to predict the variability of a larger sample size of ninety data sets. The accuracy of the uncertainty calculation was improved by more than 85% using the predicted variability compared to the uncertainty calculated from the limited sample data set. In the comparator case study using actual coordinate data from the Equator, the models were trained using the half of the complete data set and the accuracy of the calculated uncertainty was improved by 65% using the predicted variability compared to the uncertainty calculated from the training sample since random effects dominate in such measurement processes.

Chapter 8

Conclusions and Suggestions for Further Work

This chapter summarises the thesis, draws conclusions, outlines the major contributions of the research performed, and provides suggestions for further work.

8.1 Summary and conclusions

The aims of this thesis were to: i) study the performance of parallel kinematic machine (PKM)-based automatic flexible gauge under various working and environmental conditions and ii) produce novel methods for evaluating uncertainty associated with coordinate measurement in comparator mode.

This first aim was achieved by employing the design of experiments (DOE) approach. Various factors affecting the uncertainty associated with comparative coordinate measurement were investigated using several measurement parts and under different environmental conditions. Also, a statistical model for uncertainty associated with comparative coordinate measurement through analysis of variance (ANOVA) techniques was developed. The experimental designs indicated that the measurement strategy is a significant factor that affects the comparator measurement uncertainty. Other factors such as part misalignment from rotation between master and measure coordinate frames can also affect the comparator measurement uncertainty. In addition, a comparison was made between different shop floor inspection methods including automated flexible gauging, hard gauging, and on-machine probing (OMP).

The second aim involved two parts. The first part was focused on the application of Markov chain Monte Carlo (MCMC) methods in the evaluation of uncertainty associated with comparative coordinate measurement using small data sets. The Gibbs sampler, which is one of the main MCMC methods, was used for performing Bayesian inference. The second was focused on the development of an artificial intelligence (AI)-based method using Bayesian regularized artificial neural networks (BRANNs) to overcome the difficulties associated with

estimating point coordinate uncertainties and improve the assessment of measurement uncertainty in this application.

The following items are the conclusions of this thesis concerning with the performance evaluation of comparator gauge and the development of efficient methods for evaluating uncertainty associated with comparative coordinate measurement:

- The automated comparator gauge under investigation can reduce the influence of systematic effects associated with the measurement system significantly and cope with wide temperature changes in a shop floor environment by re-zeroing the gauging system through the principle of mastering as shown in chapters 3-5.
- The full factorial designs in chapter 3 have revealed that the comparator measurement uncertainties obtained by all the experiments agree with system features under specified conditions. It has also been demonstrated that when the specified conditions are exceeded, the uncertainty associated with comparative coordinate measurement depends on the measurement task, the measurement strategy used, the feature size, and the magnitude and direction of offset angles in relation to the reference axes of the machine. In particular, departures from the specified part fixturing requirement of the versatile gauge have a more significant effect on the uncertainty of length measurement in comparator mode and a less significant effect on the diameter measurement uncertainty for the specific Equator and test conditions.
- The experimental results in chapter 4 have shown that the comparator gauge can achieve highly repeatable measurements under workshop conditions in both discrete-point probing and scanning measuring modes within its whole measuring volume. However, careful consideration of the scanning speed is required for form assessment due to dynamic effects.
- The comparative study between the different dimensional inspection approaches that were studied in this thesis in chapter 5 has shown that an automated flexible gauge employed on the shop floor can achieve very low measurement uncertainties ($< 2 \mu\text{m}$ for more than 97% of the results), especially in comparison to OMP and hard gauges. However, part fixturing repeatability is critical to comparative coordinate measurement because misalignment errors during comparator gauging will lead to inaccurate results.
- A MCMC model has been developed in chapter 6 for uncertainty associated with comparative coordinate measurement. It has been shown that using the Gibbs sampler is

straightforward to obtain a MCMC sample from the posterior distribution and thus, providing reliable uncertainty statements for comparative coordinate measurements influenced by angular misalignments without the need for repeated measurements.

- An AI-based method has been developed in chapter 7 to estimate the uncertainty of measurement in the point coordinates. Small prediction errors were achieved according to the MSE and the accuracy of the uncertainty calculation was improved by more than 85% and by 65% using the predicted variability compared to the uncertainty from the limited/training sample data set for the coordinate measuring machine (CMM) and comparator case study, respectively.

8.2 Contribution to knowledge

Many areas have been identified as giving a significant contribution to knowledge under the scope of this investigation:

- A comprehensive review of the dimensional inspection methods has been conducted. Various key factors affecting the measurement uncertainty were investigated and throughout the thesis, the establishment of the influence of them and their interaction on the comparator measurement uncertainty has been achieved using full factorial designs.
- Dimensional inspection on the shop floor with automated flexible gauges based on parallel kinematic structure has been found to be an efficient solution to fill the gap between CMM measurement and custom hard gauging. This was achieved through a detailed comparison between automated flexible gauges, hard gauges, and OMP on a range of features and operating conditions.
- A statistical model for uncertainty associated with comparative coordinate measurement has been developed using ANOVA techniques. This is applicable to comparative measurement in general, not just the Equator.
- A Bayesian approach through alternating conditional sampling has been produced to evaluate uncertainty associated with comparative coordinate measurement influenced by process variations.
- A new empirical method based on a BRANN model has been developed to predict the variability associated with the CMM and automated comparator coordinate data. The proposed method can be used very straightforwardly to determine uncertainty sources

associated with a particular axis of the CMM when a precise analytical model for the measurement system and/or measurement process is difficult to derive and increase the efficiency of fitting algorithms implemented in CMM and comparator coordinate data while avoiding large experimental designs.

8.3 Suggested further work

- A virtual PKM-based flexible gauge based on Monte Carlo simulation could be developed and integrated in the Renishaw MODUS Equator software for task-specific uncertainty evaluation similar to that available for CMMs using virtual CMM (VCMM).
- Improve the performance of the BRANN models by using more information as inputs to the network and different types of networks, number of hidden neurons, and training algorithms. In addition, integrate the prediction model with geometric element best-fit algorithms to provide task-specific uncertainty statements.
- Application of a combination of the new artificial neural network (ANN)-based method and the Gibbs sampling method to enable highly efficient uncertainty evaluation of CMMs under a variety of operating conditions to facilitate the production of and selection of operating parameters for particular accuracy requirements. This could support decisions for infrastructure designs, whether shop floor coordinate measuring systems (CMSs) can be implemented as well as informing efficient measurement strategies.
- The measuring principle of the Equator gauge is based on the traditional comparison of production parts to a reference master part through software. However, this requires the establishment of a reference master part or the calibration of a production part on an accurate CMS such as a CMM. Therefore, a machine learning model could be developed to predict master part quality using for example machining process monitoring data and Equator metrology data. This will enhance the efficiency of this automated shop floor inspection method in a practical and cost-effective way without the need for kinematic calibration. Hence, shop floor inspection tasks could be executed with the requirement of only a single measuring equipment.

8.4 Refereed papers

- [31] A. B. Forbes, M. Papananias, A. P. Longstaff, S. Fletcher, A. Mengot, and K. Jonas, "Developments in automated flexible gauging and the uncertainty associated with comparative coordinate measurement," in *16th international conference of the european society for precision engineering and nanotechnology*, Nottingham, UK, 2016, pp. 111-112.
- [106] M. Papananias, S. Fletcher, A. P. Longstaff, and A. B. Forbes, "Uncertainty evaluation associated with versatile automated gauging influenced by process variations through design of experiments approach," *Precision Engineering*, vol. 49, pp. 440-455, 2017.
- [119] M. Papananias, S. Fletcher, A. P. Longstaff, A. Mengot, K. Jonas, and A. B. Forbes, "Evaluation of automated flexible gauge performance using experimental designs," in *Laser Metrology and Machine Performance XII, LAMDAMAP*, Wotton-under-Edge, UK, 2017, pp. 45-54.
- [120] M. Papananias, S. Fletcher, A. P. Longstaff, A. Mengot, K. Jonas, and A. B. Forbes, "Modelling uncertainty associated with comparative coordinate measurement through analysis of variance techniques," in *17th International conference of the european society for precision engineering and nanotechnology*, Hannover, Germany, 2017, pp. 407-408.
- [130] M. Papananias, S. Fletcher, A. P. Longstaff, and A. Mengot, "A novel method based on Bayesian regularized artificial neural networks for measurement uncertainty evaluation," in *16th International conference of the european society for precision engineering and nanotechnology*, Nottingham, UK, 2016, pp. 97-98.

References

- [1] A. B. Forbes, A. Mengot, and K. Jonas, "Uncertainty associated with coordinate measurement in comparator mode," in *Laser Metrology and Machine Performance XI, LAMDAMAP*, Huddersfield, UK, 2015, pp. 150-159.
- [2] ISO, "International vocabulary of basic and general terms in metrology (VIM), 3rd ed, International Organization for Standardization," 2004.
- [3] JCGM, "JCGM 200:2012 International vocabulary of metrology - Basic and general concepts and associated terms (VIM), 3rd ed, Joint Committee for Guides in Metrology," 2012.
- [4] S. Phillips, "Performance evaluation," in *RJ Hocken & PH Pereira (Eds.), Coordinate Measuring Machines and Systems*, pp. 183-272, 2011.
- [5] JCGM, "JCGM 100:2008 Evaluation of measurement data - Guide to the expression of uncertainty in measurement (GUM:1995), Joint Committee for Guides in Metrology," 2008.
- [6] S. Bell, *A beginner's guide to uncertainty of measurement*: National Physical Laboratory, 2001.
- [7] F. T. Farago and M. A. Curtis, *Handbook of dimensional measurement*, 4th ed.: Industrial Press Inc, 2007.
- [8] M. P. Groover, *Automation, production systems, and computer-integrated manufacturing*, 3rd ed.: Prentice Hall Press, 2007.
- [9] A. B. Forbes, "Measurement uncertainty and optimized conformance assessment," *Measurement*, vol. 39, pp. 808-814, 2006.
- [10] R. Wilhelm, R. Hocken, and H. Schwenke, "Task specific uncertainty in coordinate measurement," *CIRP Annals-Manufacturing Technology*, vol. 50, pp. 553-563, 2001.
- [11] G. Zhang, "Non-Cartesian coordinate measuring systems," in *RJ Hocken & PH Pereira (Eds.), Coordinate Measuring Machines and Systems*, pp. 467-514, 2011.
- [12] D. González-Madruga, E. Cuesta, J. Barreiro, and A. I. Fernandez-Abia, "Application of a force sensor to improve the reliability of measurement with articulated arm coordinate measuring machines," *Sensors*, vol. 13, pp. 10430-10448, 2013.
- [13] J. Sładek, K. Ostrowska, and A. Gąska, "Modeling and identification of errors of coordinate measuring arms with the use of a metrological model," *Measurement*, vol. 46, pp. 667-679, 2013.

- [14] J. Santolaria, J.-A. Yagüe, R. Jiménez, and J.-J. Aguilar, "Calibration-based thermal error model for articulated arm coordinate measuring machines," *Precision Engineering*, vol. 33, pp. 476-485, 2009.
- [15] X. H. Li, B. Chen, and Z. R. Qiu, "The calibration and error compensation techniques for an Articulated Arm CMM with two parallel rotational axes," *Measurement*, vol. 46, pp. 603-609, 2013.
- [16] A. P. Longstaff, "Methods of evaluation of the positioning capability of Cartesian and non-Cartesian machines," PhD Thesis, University of Huddersfield, 2002.
- [17] M. Papananias, S. Sztendel, and C. Pislaru, "Development of a novel multiBody mechatronic model for five-axis CNC machine tool," in *Laser Metrology and Machine Performance XI, LAMDAMAP*, Huddersfield, UK, 2015, pp. 379-389.
- [18] S. Sztendel, M. Papananias, and C. Pislaru, "Improving the dynamic performance of five-axis CNC machine tool by using the software-in-the-loop (SIL) platform," in *Laser Metrology and Machine Performance XI, LAMDAMAP*, Huddersfield, UK, 2015, pp. 170-180.
- [19] P. Saunders, M. Verma, N. Orchard, and P. Maropoulos, "The application of uncertainty evaluating software for the utilisation of machine tool systems for final inspection," in *Laser Metrology and Machine Performance X, LAMDAMAP*, Cranfield, UK, 2013, pp. 219-228.
- [20] ISO, "ISO 230-10:2016 Test code for machine tools Part 10: Determination of the measuring performance of probing systems of numerically controlled machine tools, International Organization for Standardization," 2016.
- [21] ISO, "ISO 10360-2:2009 Geometrical product specifications (GPS) — Acceptance and reverification tests for coordinate measuring machines (CMM) Part 2: CMMs used for measuring linear dimensions, International Organization for Standardization," 2009.
- [22] ISO, "ISO 10360-5:2010 Geometrical product specifications (GPS) — Acceptance and reverification tests for coordinate measuring machines (CMM) Part 5: CMMs using single and multiple stylus contacting probing systems, International Organization for Standardization," 2010.
- [23] M. Verma, E. Chatzivagiannis, D. Jones, and P. Maropoulos, "Comparison of the measurement performance of high precision multi-axis metal cutting machine tools," *Procedia CIRP*, vol. 25, pp. 138-145, 2014.
- [24] J. Śladek, P. M. Błaszczuk, M. Kupiec, and R. Sitnik, "The hybrid contact–optical coordinate measuring system," *Measurement*, vol. 44, pp. 503-510, 2011.

- [25] F. Li, A. P. Longstaff, S. Fletcher, and A. Myers, "A practical coordinate unification method for integrated tactile–optical measuring system," *Optics and Lasers in Engineering*, vol. 55, pp. 189-196, 2014.
- [26] S. H. Hong, S. B. Kim, H. M. Kwon, and M. K. Lee, "Economic design of screening procedures when the rejected items are reprocessed," *European Journal of Operational Research*, vol. 108, pp. 65-73, 1998.
- [27] I. Lira, "A Bayesian approach to the consumer's and producer's risks in measurement," *Metrologia*, vol. 36, p. 397, 1999.
- [28] R. Hocken, "Measurement integration," in *RJ Hocken & PH Pereira (Eds.), Coordinate Measuring Machines and Systems*, pp. 515-522, 2011.
- [29] W. Jinwen and C. Yanling, "The geometric dynamic errors of CMMs in fast scanning-probing," *Measurement*, vol. 44, pp. 511-517, 2011.
- [30] C. R. Boër, L. M. Tosatti, and K. S. Smith, *Parallel kinematic machines: Theoretical aspects and industrial requirements*: Springer Science & Business Media, 2012.
- [31] A. B. Forbes, M. Papananias, A. P. Longstaff, S. Fletcher, A. Mengot, and K. Jonas, "Developments in automated flexible gauging and the uncertainty associated with comparative coordinate measurement," in *16th international conference of the european society for precision engineering and nanotechnology*, Nottingham, UK, 2016, pp. 111-112.
- [32] A. Weckenmann, M. Knauer, and H. Kunzmann, "The influence of measurement strategy on the uncertainty of CMM-measurements," *CIRP Annals - Manufacturing Technology*, vol. 47, pp. 451-454, 1998.
- [33] J.-P. Kruth, N. Van Gestel, P. Bleys, and F. Welkenhuyzen, "Uncertainty determination for CMMs by Monte Carlo simulation integrating feature form deviations," *CIRP Annals-Manufacturing Technology*, vol. 58, pp. 463-466, 2009.
- [34] ISO/IEC, "ISO/IEC Guide 98-3:2008 Uncertainty of measurement - Part 3: Guide to the expression of Uncertainty in Measurement (GUM:1995), International Organization for Standardization," 2008.
- [35] P. R. G. Couto, J. C. Damasceno, and S. P. de Oliveira, "Monte Carlo simulations applied to uncertainty in measurement," *Theory and Applications of Monte Carlo Simulations*, 2013.
- [36] JCGM, "JCGM 101:2008 Evaluation of measurement data - Supplement 1 to the "Guide to the expression of uncertainty in measurement" - Propagation of distributions using a Monte Carlo method, Joint Committee for Guides in Metrology," 2008.

- [37] A. B. Forbes and J. A. Sousa, "The GUM, Bayesian inference and the observation and measurement equations," *Measurement*, vol. 44, pp. 1422-1435, 2011.
- [38] B. Efron, "Bootstrap methods: Another look at the Jackknife," pp. 1-26, 1979/01 1979.
- [39] B. Efron and R. J. Tibshirani, *An introduction to the bootstrap*: CRC press, 1994.
- [40] J. Shao, "Bootstrap sample size in nonregular cases," *Proceedings of the American Mathematical Society*, vol. 122, pp. 1251-1262, 1994.
- [41] B. Siebert and P. Ciarlini, "Feasibility study of using Bootstrap to compute the uncertainty contribution from few repeated measurements," *Series on Advances in Mathematics for Applied Sciences*, vol. 66, pp. 122-136, 2004.
- [42] M. G. Cox and P. M. Harris, "Measurement uncertainty and traceability," *Measurement Science and Technology*, vol. 17, p. 533, 2006.
- [43] ISO, "ISO 14253-1:2013 Geometrical product specifications (GPS) - Inspection by measurement of workpieces and measuring equipment - Part 1: Decision rules for proving conformity or nonconformity with specifications, International Organization for Standardization," 2013.
- [44] JCGM, "JCGM 106:2012 Evaluation of measurement data - The role of measurement uncertainty in conformity assessment, Joint Committee for Guides in Metrology," 2012.
- [45] A. Forbes, "Approaches to evaluating measurement uncertainty," *International Journal of Metrology and Quality Engineering*, vol. 3, pp. 71-77, 2012.
- [46] A. B. Forbes, "Nonlinear least squares and Bayesian inference," *Advanced Mathematical and Computational Tools in Metrology and Testing, AMCTM VIII*, vol. 78, pp. 104-112, 2009.
- [47] W. R. Gilks, S. Richardson, and D. Spiegelhalter, *Markov chain Monte Carlo in practice*: Chapman & Hall/CRC, 1995.
- [48] A. B. Forbes, "An MCMC algorithm based on GUM Supplement 1 for uncertainty evaluation," *Measurement*, vol. 45, pp. 1188-1199, 2012.
- [49] A. Gelman, J. B. Carlin, H. S. Stern, D. B. Dunson, A. Vehtari, and D. B. Rubin, *Bayesian data analysis*, 3rd ed. vol. 2: Chapman & Hall/CRC, 2014.
- [50] P. H. Pereira, "Cartesian coordinate measuring machines," in *RJ Hocken & PH Pereira (Eds.), Coordinate Measuring Machines and Systems*, pp. 57-79, 2011.
- [51] A. Weckenmann and J. Hoffmann, "Probing systems for coordinate measuring machines," in *RJ Hocken & PH Pereira (Eds.), Coordinate Measuring Machines and Systems*, pp. 93-124, 2011.

- [52] S. Ali, "Probing system characteristics in coordinate metrology," *Measurement Science Review*, vol. 10, pp. 120-129, 2010.
- [53] G. Tomkinson, "Choosing the best probing system for your CMM," *Aircraft Engineering and Aerospace Technology*, vol. 78, 2006.
- [54] D. Flack, "NPL Measurement good practice Guide No. 43: CMM probing," *National Physical Laboratory*, 2001.
- [55] D. A. Swyt and R. J. Hocken, "The international standard of length," in *RJ Hocken & PH Pereira (Eds.), Coordinate Measuring Machines and Systems*, pp. 31-40, 2011.
- [56] D. A. Swyt, "Length and dimensional measurements at NIST," *Journal of Research of the National Institute of Standards and Technology*, vol. 106, p. 1, 2001.
- [57] D. Flack, "NPL Measurement good practice Guide No. 41: CMM measurement strategies," *National Physical Laboratory*, 2001.
- [58] BS, "Geometrical product specifications (GPS) — Geometrical tolerancing — Datums and datum systems (ISO 5459:2011), British Standards Institution," 2011.
- [59] E. Morse, "Specification of design intent - Introduction to dimensioning and tolerancing," in *RJ Hocken & PH Pereira (Eds.), Coordinate Measuring Machines and Systems*, pp. 41-55, 2011.
- [60] P. H. Pereira and R. J. Hocken, "Measurement uncertainty for coordinate measuring systems," in *RJ Hocken & PH Pereira (Eds.), Coordinate Measuring Machines and Systems*, pp. 371-386, 2011.
- [61] BS, "BS 7172:1989 Assessment of position, size and departure from nominal form of geometric features, British Standards Institution," 1989.
- [62] A. Forbes, A. Wilson, P. Saunders, and N. Orchard, "Effect of form errors in datum features on evaluated geometries," in *16th International Congress of Metrology*, 2013.
- [63] P. Pereira and R. Hocken, "Characterization and compensation of dynamic errors of a scanning coordinate measuring machine," *Precision Engineering*, vol. 31, pp. 22-32, 2007.
- [64] Renishaw, "Technical note: The dynamics of co-ordinate measuring machines (CMMs)," *Renishaw plc*, 2003.
- [65] T. E. Ollison, J. M. Ulmer, and R. McElroy, "Coordinate measurement technology: A comparison of scanning versus touch trigger probe data capture," *International Journal of Engineering Research and Innovation*, vol. 4, pp. 60-67, 2012.
- [66] G. Zhang, "Error compensation of coordinate measuring machines," in *RJ Hocken & PH Pereira (Eds.), Coordinate Measuring Machines and Systems*, pp. 319-359, 2011.

- [67] A. M. Abdulshahed, A. P. Longstaff, S. Fletcher, and A. Myers, "Thermal error modelling of machine tools based on ANFIS with fuzzy c-means clustering using a thermal imaging camera," *Applied Mathematical Modelling*, pp. 1837-1852, 2014.
- [68] A. M. Abdulshahed, A. P. Longstaff, and S. Fletcher, "The application of ANFIS prediction models for thermal error compensation on CNC machine tools," *Applied Soft Computing*, vol. 27, pp. 158-168, 2015.
- [69] N. Barakat, M. Elbestawi, and A. Spence, "Kinematic and geometric error compensation of a coordinate measuring machine," *International Journal of Machine Tools and Manufacture*, vol. 40, pp. 833-850, 2000.
- [70] JCGM, "JCGM 102:2011 Evaluation of measurement data - Supplement 2 to the "Guide to the expression of uncertainty in measurement" - Extension to any number of output quantities, Joint Committee for Guides in Metrology," 2011.
- [71] ISO, "ISO 14253-2:2011 Geometrical product specifications (GPS) - Inspection by measurement of workpieces and measuring equipment - Part 2: Guidance for the estimation of uncertainty in GPS measurement, in calibration of measuring equipment and in product verification, International Organization for Standardization " 2011.
- [72] D. Flack, "NPL Measurement good practice Guide No. 42: CMM verification," *National Physical Laboratory*, 2001.
- [73] ISO, "ISO 15530-3:2011 Geometrical product specifications (GPS) - Coordinate measuring machines (CMM): Technique for determining the uncertainty of measurement - Part 3: Use of calibrated workpieces or measurement standards, International Organization for Standardization," 2011.
- [74] E. Trapet and F. Wäldele, "The virtual CMM concept," *Series on Advances in Mathematics for Applied Sciences*, vol. 40, pp. 238-247, 1996.
- [75] S. Phillips, B. Borchardt, D. Sawyer, W. Estler, D. Ward, K. Eberhardt, *et al.*, "The calculation of CMM measurement uncertainty via the method of simulation by constraints," *American Society for Precision Engineering*, vol. 16, pp. 443-446, 1997.
- [76] A. Balsamo, M. Di Ciommo, R. Mugno, B. I. Rebaglia, E. Ricci, and R. Grella, "Evaluation of CMM uncertainty through Monte Carlo simulations," *CIRP Annals - Manufacturing Technology*, vol. 48, pp. 425-428, 1999.
- [77] R. D'Amato, J. Caja, P. Maresca, and E. Gómez, "Use of coordinate measuring machine to measure angles by geometric characterization of perpendicular planes. Estimating uncertainty," *Measurement*, vol. 47, pp. 598-606, 2014.

- [78] S. Osawa, K. Busch, M. Franke, and H. Schwenke, "Multiple orientation technique for the calibration of cylindrical workpieces on CMMs," *Precision Engineering*, vol. 29, pp. 56-64, 2005.
- [79] E. Trapet, M. Franke, F. Haertig, H. Schwenke, F. Waeldele, M. Cox, *et al.*, *Traceability of coordinate measurements according to the method of the virtual measuring machine: Final project report MAT1-CT94-0076, PTB-Report F-35, Parts 1 and 2*, 1999.
- [80] H. M. P. Lobato, "An investigation into coordinate measuring machine task specific measurement uncertainty and automated conformance assessment of airfoil leading edge profiles," PhD Thesis, University of Birmingham, 2012.
- [81] G. E. Box, J. S. Hunter, and W. G. Hunter, *Statistics for experimenters: Design, innovation, and discovery* vol. 2: Wiley-Interscience New York, 2005.
- [82] D. C. Montgomery, *Introduction to statistical quality control*: John Wiley & Sons, 2007.
- [83] J. Antony, *Design of experiments for engineers and scientists*: Elsevier, 2014.
- [84] C. M. Anderson-Cook, C. M. Borror, and D. C. Montgomery, "Response surface design evaluation and comparison," *Journal of Statistical Planning and Inference*, vol. 139, pp. 629-641, 2009.
- [85] G. Box, S. Bisgaard, and C. Fung, "An explanation and critique of Taguchi's contributions to quality engineering," *Quality and Reliability Engineering International*, vol. 4, pp. 123-131, 1988.
- [86] Y. Li, W. Chen, J. Ding, and S. Wu, "Orthogonal robust design method for product quality," in *International Conference on Innovation Management, ICIM'09*, 2009, pp. 120-123.
- [87] E. M. Barini, G. Tosello, and L. De Chiffre, "Uncertainty analysis of point-by-point sampling complex surfaces using touch probe CMMs: DOE for complex surfaces verification with CMM," *Precision Engineering*, vol. 34, pp. 16-21, 2010.
- [88] A. Piratelli-Filho and B. Di Giacomo, "CMM uncertainty analysis with factorial design," *Precision Engineering*, vol. 27, pp. 283-288, 2003.
- [89] C.-X. J. Feng, A. L. Saal, J. G. Salsbury, A. R. Ness, and G. C. S. Lin, "Design and analysis of experiments in CMM measurement uncertainty study," *Precision Engineering*, vol. 31, pp. 94-101, 2007.
- [90] H. Lobato, C. Ferri, J. Faraway, and N. Orchard, "Uncertainty due to experimental conditions in co-ordinate measuring machines," *Proceedings of the Institution of*

- Mechanical Engineers, Part B: Journal of Engineering Manufacture*, vol. 223, pp. 499-509, 2009.
- [91] ISO, "ISO 1101:2012(E) Geometrical product specifications (GPS) - Geometrical tolerancing - Tolerances of form, orientation, location and run-out, International Organization for Standardization," 2012.
- [92] P. B. Dhanish and J. Mathew, "Effect of CMM point coordinate uncertainty on uncertainties in determination of circular features," *Measurement*, vol. 39, pp. 522-531, 2006.
- [93] X.-L. Wen, X.-C. Zhu, Y.-B. Zhao, D.-X. Wang, and F.-L. Wang, "Flatness error evaluation and verification based on new generation geometrical product specification (GPS)," *Precision Engineering*, vol. 36, pp. 70-76, 2012.
- [94] X.-l. Wen, Y.-b. Zhao, D.-x. Wang, and J. Pan, "Adaptive Monte Carlo and GUM methods for the evaluation of measurement uncertainty of cylindricity error," *Precision Engineering*, vol. 37, pp. 856-864, 2013.
- [95] A. B. Forbes, *Least-squares best-fit geometric elements*: National Physical Laboratory, 1989.
- [96] A. Forbes, "Surface fitting taking into account uncertainty structure in coordinate data," *Measurement Science and Technology*, vol. 17, p. 553, 2006.
- [97] A. B. Forbes, "Uncertainty evaluation associated with fitting geometric surfaces to coordinate data," *Metrologia*, vol. 43, pp. S282-S290, 2006.
- [98] I. M. Smith and A. B. Forbes, "Least squares best-fit geometric elements taking into account uncertainty structure," in *16th International Congress of Metrology*, 2013.
- [99] C. Sutton and M. Clarkson, "A general approach to comparisons in the presence of drift," *Metrologia*, vol. 30, p. 487, 1994.
- [100] T. Doiron, "Drift eliminating designs for non-simultaneous comparison calibrations," *Journal of Research-National Institute of Standards and Technology*, vol. 98, pp. 217-217, 1993.
- [101] J. M. Cameron and G. E. Hailes, "Designs for the calibration of small groups of standards in the presence of drift," DTIC Document 1974.
- [102] I. Lira, "Evaluation of cycles of comparison measurements by a least-squares method," *Measurement Science and Technology*, vol. 12, p. 1167, 2001.
- [103] M. Gläser, "Cycles of comparison measurements, uncertainties and efficiencies," *Measurement Science and Technology*, vol. 11, p. 20, 2000.

- [104] J. M. Cameron, M. C. Croarkin, and R. C. Raybold, "Designs for the calibration of standards of mass," *National Bureau of Standards Technical Note 952, Institute for Basic Standards*, 1977.
- [105] Renishaw, "Renishaw Equator gauging system," *Renishaw plc*, 2014.
- [106] M. Papananias, S. Fletcher, A. P. Longstaff, and A. B. Forbes, "Uncertainty evaluation associated with versatile automated gauging influenced by process variations through design of experiments approach," *Precision Engineering*, vol. 49, pp. 440-455, 2017.
- [107] T. Doiron and J. Beers, "The gauge block handbook," *NIST monograph*, vol. 180, pp. 1-143, 2005.
- [108] I. Puertas, C. L. Pérez, D. Salcedo, J. León, R. Luri, and J. Fuertes, "Precision study of a coordinate measuring machine using several contact probes," *Procedia Engineering*, vol. 63, pp. 547-555, 2013.
- [109] R. Hertz and P. Hughes, "Kinematic analysis of a general double-tripod parallel manipulator," *Mechanism and Machine Theory*, vol. 33, pp. 683-696, 1998.
- [110] J.-S. Chen and W.-Y. Hsu, "Design and analysis of a tripod machine tool with an integrated Cartesian guiding and metrology mechanism," *Precision Engineering*, vol. 28, pp. 46-57, 2004.
- [111] Z. M. Bi and Y. Jin, "Kinematic modeling of Exechon parallel kinematic machine," *Robotics and Computer-Integrated Manufacturing*, vol. 27, pp. 186-193, 2011.
- [112] G. Pritschow, "Parallel kinematic machines (PKM)—limitations and new solutions," *CIRP Annals-Manufacturing Technology*, vol. 49, pp. 275-280, 2000.
- [113] BS, "BS 6808-3: 1989 Coordinate measuring machines - Part 3: Code of practice, British Standards Institution," 1989.
- [114] BS, "BS 6808-1: 1987 Coordinate measuring machines - Part 1: Glossary of terms, British Standards Institution," 1987.
- [115] C. Dotson, *Fundamentals of dimensional metrology*, 5th ed.: Cengage Learning, 2015.
- [116] H. Ding, P. J. Scott, and X. Jiang, "A criterion for comparing measurement results and determining conformity with specifications," *Procedia CIRP*, vol. 27, pp. 143-148, 2015.
- [117] J. Pinheiro and D. Bates, *Mixed-effects models in S and S-PLUS*: Springer Science & Business Media, 2006.
- [118] Minitab, "Minitab Inc.," 2017.
- [119] M. Papananias, S. Fletcher, A. P. Longstaff, A. Mengot, K. Jonas, and A. B. Forbes, "Evaluation of automated flexible gauge performance using experimental designs," in

- Laser Metrology and Machine Performance XII, LAMDAMAP*, Wotton-under-Edge, UK, 2017, pp. 45-54.
- [120] M. Papananias, S. Fletcher, A. P. Longstaff, A. Mengot, K. Jonas, and A. B. Forbes, "Modelling uncertainty associated with comparative coordinate measurement through analysis of variance techniques," in *17th International conference of the european society for precision engineering and nanotechnology*, Hannover, Germany, 2017, pp. 407-408.
- [121] G. K. Griffith, *Measuring and gaging geometric tolerances*: Prentice Hall Career and Technology, 1994.
- [122] ISO, "ISO 10360-4:2000 Geometrical product specifications (GPS) — Acceptance and reverification tests for coordinate measuring machines (CMM) Part 4: CMMs used in scanning measuring mode, International Organization for Standardization," 2000.
- [123] J. B. Bryan and T. Doiron, "Temperature fundamentals," in *RJ Hocken & PH Pereira (Eds.), Coordinate Measuring Machines and Systems*, pp. 273-303, 2011.
- [124] D. Gamerman and H. F. Lopes, *Markov chain Monte Carlo: Stochastic simulation for Bayesian inference*: CRC Press, 2006.
- [125] W. M. Bolstad, *Understanding computational Bayesian statistics* vol. 644: John Wiley & Sons, 2010.
- [126] S. Geman and D. Geman, "Stochastic relaxation, Gibbs distributions, and the Bayesian restoration of images," *IEEE Transactions on Pattern Analysis and Machine Intelligence*, pp. 721-741, 1984.
- [127] F. Pavese and A. B. Forbes, *Data modeling for metrology and testing in measurement science*: Springer, 2008.
- [128] S. Jackman, *Bayesian analysis for the social sciences* vol. 846: John Wiley & Sons, 2009.
- [129] Matlab, "MathWorks," 2017.
- [130] M. Papananias, S. Fletcher, A. P. Longstaff, and A. Mengot, "A novel method based on Bayesian regularized artificial neural networks for measurement uncertainty evaluation," in *16th International conference of the european society for precision engineering and nanotechnology*, Nottingham, UK, 2016, pp. 97-98.
- [131] S. Phillips, B. Borchardt, W. Estler, and J. Buttress, "The estimation of measurement uncertainty of small circular features measured by coordinate measuring machines," *Precision Engineering*, vol. 22, pp. 87-97, 1998.

- [132] W. S. McCulloch and W. Pitts, "A logical calculus of the ideas immanent in nervous activity," *The Bulletin of Mathematical Biophysics*, vol. 5, pp. 115-133, 1943.
- [133] S. S. Haykin, *Neural networks and learning machines* vol. 3: Pearson Education Upper Saddle River, 2009.
- [134] D. J. MacKay, "Bayesian interpolation," *Neural Computation*, vol. 4, pp. 415-447, 1992.
- [135] F. Burden and D. Winkler, "Bayesian regularization of neural networks," *Artificial Neural Networks*, pp. 23-42, 2009.
- [136] J. L. Elman, "Finding structure in time," *Cognitive Science*, vol. 14, pp. 179-211, 1990.
- [137] M. J. Evans and J. S. Rosenthal, *Probability and statistics: The science of uncertainty*: Macmillan, 2004.
- [138] S. M. Ross, *Introduction to probability models*: Academic press, 2014.
- [139] W. J. Stewart, *Probability, Markov chains, queues, and simulation: The mathematical basis of performance modeling*: Princeton University Press, 2009.

Appendix A

Renishaw Equator Specifications and Experimental Data

Table A.1: Equator machine specifications.

Working volume	XY ϕ 300 mm, Z 150 mm
Comparison uncertainty	\pm 0.002 mm
Maximum scanning velocity	100 mm/s
Maximum scanning acceleration	1500 mm/s ²
Maximum move velocity	500 mm/s
Maximum move acceleration	2500 mm/s ²
Maximum scanning rate	1000 points/s
Scale resolution	0.0002 mm
Machine electrical supply requirements	24 V DC supplied direct from Equator controller
Probe type	Renishaw 3-axis SP25 analogue scanning probe
Repeatability of piece part in fixture	\pm 1 mm
Fixture plate	305 mm \times 305 mm
Maximum part weight (including fixture plate)	25 kg
Machine dimensions (W \times D \times H)	570 mm \times 500 mm \times 700 mm
Machine weight	25 kg

Table A.2: Operating conditions.

Attitude	Maximum 2000 m
Operating temperature	+10°C to +40°C
Storage temperature	-25°C to +70°C
Relative humidity operating range	Maximum 80% RH at 40°C, non-condensing
Transition voltages	Installation category II
Pollution degree	2

Table A.3: Equator controller specifications and electrical ratings.

Controller electrical supply requirements	100 V AC - 240 V AC \pm 10%, 50 Hz - 60 HZ
Maximum rated power consumption	300 W
Maximum power consumption	190 W
Typical power consumption	100 W
Controller dimensions (W \times D \times H)	130 mm \times 320 mm \times 350 mm
Controller weight	8 kg
Communication with Equator	PCIexpress
User input devices	Keyboard and mouse (USB 2.0)
Display type	VGA monitor
Display resolution	1280 \times 1024
USB hub	2 front, 4 back (USB 2.0)
Ethernet ports	1 \times RJ45 connector

Table A.4: Mean values and associated expanded uncertainties for $k = 2$ from the DOE with the gauge block.

A	B	C	Gauge block length	
			\bar{x} [mm]	U [μm]
1	1	1	100.00081	0.96
2	1	1	100.00003	0.19
1	2	1	99.99994	0.16
2	2	1	99.99979	0.64
1	1	2	99.99987	0.21
2	1	2	99.99954	0.59
1	2	2	99.99960	0.49
2	2	2	100.00016	0.27
1	1	3	99.99981	0.31
2	1	3	100.00035	0.47
1	2	3	99.99964	0.45
2	2	3	100.00032	0.52
1	1	4	99.99964	0.61
2	1	4	100.00014	0.27
1	2	4	99.99983	0.27
2	2	4	99.99968	0.47
1	1	5	99.99934	0.79
2	1	5	100.00054	0.66
1	2	5	99.99898	1.17
2	2	5	99.99932	0.80
1	1	6	99.99898	1.12
2	1	6	99.99950	0.58
1	2	6	99.99859	1.51
2	2	6	99.99973	0.42
1	1	7	99.99811	2.02
2	1	7	99.99911	0.99
1	2	7	99.99823	1.83
2	2	7	99.99922	1.00

See Table 3.1 for notation.

Table A.5: Mean values from the DOE with the conrod part.

A	B	C	Small circle diameter	Medium circle diameter	Large circle diameter	Length distance 1	Length distance 2	Length distance 3
			\bar{x} [mm]	\bar{x} [mm]	\bar{x} [mm]	\bar{x} [mm]	\bar{x} [mm]	\bar{x} [mm]
1	1	1	10.00083	20.00012	44.99980	85.09649	85.09670	170.19320
1	2	1	10.00044	20.00015	45.00015	85.09718	85.09672	170.19390
2	1	1	10.00027	20.00015	45.00009	85.09703	85.09687	170.19391
2	2	1	10.00017	19.99991	45.00007	85.09675	85.09699	170.19371
3	1	1	10.00025	19.99981	45.00029	85.09703	85.09714	170.19418
3	2	1	10.00016	19.99971	44.99982	85.09678	85.09577	170.19256
4	1	1	10.00003	19.99965	44.99983	85.09698	85.09641	170.19337
4	2	1	10.00013	19.99923	44.99961	85.09694	85.09735	170.19431
1	1	2	10.00083	20.00079	45.00004	85.09654	85.09755	170.19410
1	2	2	10.00048	20.00059	45.00024	85.09624	85.09797	170.19421
2	1	2	10.00027	20.00018	44.99999	85.09657	85.09740	170.19396
2	2	2	10.00017	20.00048	45.00033	85.09588	85.09810	170.19399
3	1	2	9.99982	19.99981	44.99993	85.09667	85.09664	170.19331
3	2	2	10.00020	19.99992	44.99967	85.09702	85.09623	170.19325
4	1	2	9.99946	19.99951	44.99902	85.09604	85.09631	170.19238
4	2	2	9.99964	20.00004	44.99946	85.09665	85.09694	170.19357
1	1	3	9.99947	19.99961	45.00064	85.09751	85.09192	170.18942
1	2	3	10.00080	19.99938	45.00112	85.09732	85.09354	170.19085
2	1	3	10.00014	19.99967	45.00084	85.09745	85.09369	170.19113
2	2	3	10.00038	19.99967	45.00082	85.09708	85.09371	170.19078
3	1	3	10.00022	19.99946	45.00129	85.09729	85.09349	170.19080
3	2	3	10.00002	19.99954	45.00037	85.09681	85.09454	170.19137
4	1	3	9.99971	19.99857	44.99997	85.09698	85.09385	170.19082
4	2	3	9.99968	19.99935	44.99981	85.09679	85.09408	170.19085
1	1	4	10.00020	20.00096	44.99956	85.09696	85.09291	170.18984
1	2	4	10.00137	19.99990	44.99918	85.09635	85.09450	170.19083
2	1	4	10.00059	20.00026	45.00211	85.09698	85.09426	170.19125
2	2	4	10.00020	20.00039	44.99970	85.09614	85.09465	170.19078
3	1	4	10.00043	19.99964	44.99949	85.09644	85.09466	170.19110
3	2	4	10.00015	19.99962	45.00019	85.09687	85.09449	170.19136
4	1	4	9.99945	19.99899	44.99922	85.09713	85.09417	170.19130
4	2	4	9.99991	19.99970	44.99912	85.09684	85.09391	170.19075

See Table 3.3 for notation.

Table A.6: Expanded uncertainties for $k = 2$ from the DOE with the conrod part.

A	B	C	Small circle diameter	Medium circle diameter	Large circle diameter	Length distance 1	Length distance 2	Length distance 3
			U [μm]	U [μm]	U [μm]	U [μm]	U [μm]	U [μm]
1	1	1	0.91	0.16	0.28	0.61	0.79	0.38
1	2	1	0.54	0.20	0.22	1.36	0.81	1.04
2	1	1	0.36	0.18	0.19	1.13	1.05	1.13
2	2	1	0.21	0.15	0.15	0.85	1.17	0.88
3	1	1	0.32	0.29	0.39	1.18	1.75	1.81
3	2	1	0.23	0.38	0.27	0.92	0.49	0.68
4	1	1	0.12	0.45	0.22	1.09	0.61	0.53
4	2	1	0.22	0.86	0.50	1.05	1.65	1.60
1	1	2	1.01	0.86	0.10	0.69	1.82	1.35
1	2	2	0.57	0.65	0.33	0.36	2.15	1.38
2	1	2	0.34	0.22	0.05	0.69	1.61	1.23
2	2	2	0.20	0.52	0.41	0.28	2.24	1.15
3	1	2	0.27	0.26	0.17	0.85	0.89	0.49
3	2	2	0.28	0.17	0.42	1.19	0.49	0.60
4	1	2	0.94	0.59	1.14	0.23	0.49	0.85
4	2	2	0.46	0.10	0.65	0.82	1.24	0.83
1	1	3	0.67	0.47	0.79	1.89	4.58	4.10
1	2	3	0.88	0.70	1.20	1.44	2.66	2.41
2	1	3	0.17	0.40	0.94	1.55	2.46	2.03
2	2	3	0.44	0.37	0.87	1.26	2.40	2.40
3	1	3	0.32	0.59	1.41	1.42	2.71	2.47
3	2	3	0.09	0.52	0.47	0.95	1.73	1.87
4	1	3	0.38	1.52	0.10	1.12	2.41	2.47
4	2	3	0.43	0.78	0.28	0.99	2.12	2.44
1	1	4	0.38	1.02	0.49	1.18	3.40	3.67
1	2	4	1.58	0.18	0.91	0.45	1.70	2.29
2	1	4	0.63	0.33	2.18	1.04	1.89	1.89
2	2	4	0.23	0.44	0.38	0.27	1.50	2.37
3	1	4	0.49	0.42	0.61	0.58	1.70	2.28
3	2	4	0.19	0.43	0.30	1.02	1.88	2.08
4	1	4	0.65	1.10	0.87	1.32	2.29	2.27
4	2	4	0.15	0.34	0.97	0.94	2.37	2.56

See Table 3.3 for notation.

Table A.7: Mean values from the DOE for managing re-mastering.

A	B	Small circle diameter	Medium circle diameter	Large circle diameter	Length distance 1	Length distance 2	Length distance 3
		\bar{x} [mm]	\bar{x} [mm]	\bar{x} [mm]	\bar{x} [mm]	\bar{x} [mm]	\bar{x} [mm]
1	1	10.00086	20.00002	45.00006	85.09667	85.09606	170.19275
1	2	10.00014	20.00013	44.99995	85.09670	85.09687	170.19355
2	1	10.00013	19.99998	44.99967	85.09590	85.09709	170.19298
2	2	10.00034	20.00005	45.00003	85.09684	85.09669	170.19353
3	1	10.00020	20.00010	44.99998	85.09708	85.09661	170.19370
3	2	10.00009	20.00009	45.00014	85.09683	85.09697	170.19381
4	1	10.00040	20.00016	45.00027	85.09670	85.09710	170.19379
4	2	10.00021	19.99989	44.99986	85.09699	85.09621	170.19319
5	1	10.00011	20.00088	45.00041	85.09675	85.09819	170.19494
5	2	10.00035	20.00062	45.00078	85.09844	85.09865	170.19708
6	1	10.00136	20.00129	45.00248	85.10173	85.10164	170.20334
6	2	10.00083	20.00164	45.00301	85.10242	85.10307	170.20550
7	1	10.00218	20.00360	45.00586	85.10713	85.10759	170.21473
7	2	10.00220	20.00353	45.00655	85.10881	85.10883	170.21762

See Table 3.5 for notation.

Table A.8: Mean values and associated expanded uncertainties for $k = 2$ from the DOE with the clutch plate.

A	B	Internal diameter		External diameter	
		\bar{x} [mm]	U [μm]	\bar{x} [mm]	U [μm]
1	1	76.99968	0.42	98.39977	0.28
1	2	76.99997	0.19	98.39995	0.16
1	3	77.00019	0.29	98.40027	0.41
1	4	76.99960	0.55	98.39960	0.50
1	5	76.99919	0.93	98.39980	0.26
1	6	76.99933	0.82	98.39987	0.22
1	7	76.99975	0.37	98.39989	0.19
1	8	76.99967	0.41	98.39996	0.13
1	9	76.99972	0.44	98.39998	0.09
2	1	76.99978	0.36	98.39984	0.24
2	2	76.99955	0.53	98.39936	0.76
2	3	76.99976	0.35	98.39974	0.34
2	4	77.00003	0.18	98.39955	0.56
2	5	76.99965	0.47	98.39960	0.49
2	6	76.99981	0.30	98.40016	0.35
2	7	76.99944	0.72	98.39928	0.84
2	8	76.99972	0.36	98.40000	0.07
2	9	77.00021	0.34	98.39997	0.12

See Table 4.1 for notation.

Table A.9: Mean values and associated expanded uncertainties for $k = 2$ from the DOE with the RESR ring.

A	B	C	Large circle diameter		Medium hole diameter		Small hole diameter	
			\bar{x} [mm]	U [μm]	\bar{x} [mm]	U [μm]	\bar{x} [mm]	U [μm]
1	1	1	80.00014	0.22	6.00010	0.15	3.60041	0.50
2	1	1	79.99981	0.24	5.99987	0.18	3.59982	0.27
3	1	1	80.00011	0.14	6.00028	0.34	3.59997	0.13
1	2	1	79.99982	0.23	5.99999	0.04	3.59987	0.17
2	2	1	79.99996	0.08	5.99997	0.08	3.59995	0.12
3	2	1	79.99997	0.10	6.00019	0.24	3.60020	0.29
1	1	2	79.99970	0.34	6.00004	0.08	3.59991	0.14
2	1	2	80.00013	0.17	5.99984	0.22	3.59969	0.38
3	1	2	79.99992	0.12	5.99983	0.29	3.60017	0.25
1	2	2	79.99986	0.21	6.00001	0.04	3.60006	0.09
2	2	2	80.00020	0.24	6.00000	0.04	3.60012	0.17
3	2	2	79.99988	0.19	6.00012	0.18	3.59994	0.12
1	1	3	79.99911	1.02	6.00023	0.25	3.60047	0.52
2	1	3	79.99999	0.05	5.99977	0.27	3.60045	0.52
3	1	3	80.00007	0.11	6.00017	0.24	3.60029	0.38
1	2	3	79.99993	0.12	5.99988	0.15	3.59984	0.22
2	2	3	79.99974	0.29	5.99997	0.06	3.59992	0.14
3	2	3	80.00030	0.41	6.00018	0.23	3.60008	0.14
1	1	4	79.99920	0.87	5.99988	0.16	3.60002	0.07
2	1	4	79.99966	0.38	5.99993	0.14	3.59952	0.55
3	1	4	79.99970	0.34	6.00006	0.14	3.60004	0.22
1	2	4	79.99993	0.13	6.00003	0.05	3.60006	0.11
2	2	4	80.00014	0.18	6.00013	0.17	3.60022	0.28
3	2	4	80.00004	0.11	5.99968	0.38	3.59989	0.20
1	1	5	79.99929	0.93	6.00004	0.07	3.59999	0.09
2	1	5	79.99962	0.45	6.00004	0.08	3.60020	0.26
3	1	5	80.00005	0.08	6.00003	0.11	3.60066	0.81
1	2	5	79.99988	0.17	5.99990	0.13	3.59998	0.08
2	2	5	79.99958	0.51	6.00002	0.05	3.60021	0.25
3	2	5	79.99990	0.17	6.00001	0.06	3.59998	0.09

See Table 4.2 for notation.

Table A.10: Mean values for small-size holes from the DOE concerned with circularity.

A	B	Y_1	Y_2	Y_3	Y_4	Y_5	Y_6
		\bar{x} [mm]					
1	1	0.00100	0.00143	0.00107	0.00121	0.00107	0.00093
2	1	0.00141	0.00144	0.00128	0.00138	0.00176	0.00154
3	1	0.00262	0.00256	0.00273	0.00232	0.00310	0.00283
1	2	0.00126	0.00136	0.00119	0.00106	0.00118	0.00107
2	2	0.00180	0.00229	0.00185	0.00189	0.00229	0.00185
3	2	0.00346	0.00403	0.00353	0.00347	0.00470	0.00389
1	1	0.00118	0.00245	0.00101	0.00096	0.00118	0.00116
2	1	0.00169	0.00187	0.00159	0.00154	0.00159	0.00123
3	1	0.00255	0.00287	0.00275	0.00272	0.00269	0.00298
1	2	0.00135	0.00137	0.00230	0.00238	0.00147	0.00114
2	2	0.00200	0.00234	0.00203	0.00254	0.00236	0.00201
3	2	0.00380	0.00430	0.00366	0.00427	0.00445	0.00364

See Table 4.2 for notation.

Table A.11: Mean values for medium-size holes and large circle from the DOE concerned with circularity.

A	B	Y_7	Y_8	Y_9	Y_{10}	Y_{11}	Y_{12}	Y_{13}
		\bar{x} [mm]						
1	1	0.00128	0.00215	0.00201	0.00149	0.00155	0.00179	0.00216
2	1	0.00197	0.00235	0.00240	0.00221	0.00188	0.00250	0.00318
3	1	0.00326	0.00403	0.00399	0.00375	0.00363	0.00354	0.00531
1	2	0.00186	0.00278	0.00210	0.00154	0.00204	0.00247	0.00200
2	2	0.00262	0.00322	0.00336	0.00310	0.00267	0.00302	0.00297
3	2	0.00419	0.00568	0.00460	0.00472	0.00409	0.00428	0.00589
1	1	0.00173	0.00155	0.00138	0.00149	0.00126	0.00181	0.00252
2	1	0.00237	0.00245	0.00206	0.00250	0.00181	0.00223	0.00289
3	1	0.00310	0.00349	0.00353	0.00348	0.00328	0.00349	0.00479
1	2	0.00250	0.00188	0.00195	0.00219	0.00237	0.00177	0.00205
2	2	0.00281	0.00292	0.00300	0.00289	0.00279	0.00267	0.00272
3	2	0.00427	0.00462	0.00524	0.00503	0.00419	0.00440	0.00546

See Table 4.2 for notation.

Table A.12: Expanded uncertainties for $k = 2$ for small-size holes from the DOE concerned with circularity.

A	B	Y_1	Y_2	Y_3	Y_4	Y_5	Y_6
		$U [\mu m]$					
1	1	1.08	1.57	1.15	1.31	1.15	1.02
2	1	1.52	1.64	1.38	1.49	1.88	1.70
3	1	2.72	2.82	2.99	2.57	3.43	3.10
1	2	1.31	1.43	1.26	1.13	1.28	1.13
2	2	1.89	2.40	1.95	2.01	2.41	2.04
3	2	3.66	4.23	3.68	3.62	4.94	4.02
1	1	1.27	2.75	1.11	1.02	1.30	1.29
2	1	1.86	2.00	1.72	1.67	1.71	1.36
3	1	2.77	3.14	2.99	2.89	2.86	3.18
1	2	1.46	1.45	2.45	2.73	1.57	1.21
2	2	2.12	2.47	2.13	2.76	2.48	2.11
3	2	4.01	4.51	3.86	4.61	4.68	3.81

See Table 4.2 for notation.

Table A.13: Expanded uncertainties for $k = 2$ for medium-size holes and large circle from the DOE concerned with circularity.

A	B	Y_7	Y_8	Y_9	Y_{10}	Y_{11}	Y_{12}	Y_{13}
		$U [\mu m]$						
1	1	1.38	2.40	2.20	1.64	1.70	1.94	2.55
2	1	2.13	2.55	2.60	2.36	1.96	2.73	3.70
3	1	3.45	4.28	4.26	4.00	3.82	3.74	5.95
1	2	2.02	3.10	2.30	1.61	2.23	2.64	2.24
2	2	2.85	3.37	3.64	3.26	2.86	3.25	3.45
3	2	4.40	6.07	4.77	5.01	4.31	4.46	6.65
1	1	1.98	1.70	1.51	1.66	1.38	2.09	2.66
2	1	2.55	2.68	2.19	2.68	1.96	2.37	3.40
3	1	3.32	3.68	3.69	3.72	3.51	3.66	5.23
1	2	2.81	2.01	2.08	2.33	2.61	1.87	2.23
2	2	3.09	3.11	3.18	3.05	3.01	2.82	3.11
3	2	4.56	4.87	5.61	5.36	4.44	4.55	6.26

See Table 4.2 for notation.

Table A.14: OMP combined expanded uncertainties for $k = 2$.

Measurands	G2	G3	G4	G5	G6	G7	G8
	$U [\mu m]$						
A	0.97	1.00	0.80	1.24	1.17	0.72	2.19
B	2.11	1.36	1.57	1.80	1.54	1.45	2.05
C	0.86	0.19	0.23	0.69	1.48	0.28	2.18
D	0.88	0.71	0.99	0.82	1.24	0.78	1.28
E	0.90	0.50	0.56	0.80	1.10	1.26	1.78
F	1.13	1.54	0.88	0.72	0.57	1.20	1.96
G	1.26	0.28	0.50	1.15	0.81	0.28	1.85
H	0.45	1.61	0.71	0.84	0.70	0.56	2.03
I	0.67	0.43	0.49	0.68	1.60	0.91	2.55
J	1.32	1.18	0.59	1.30	0.77	1.26	2.40
K	2.46	2.37	1.80	2.10	1.50	1.31	2.34
L	1.21	3.36	2.42	2.02	1.91	1.35	1.40
M	2.03	5.21	3.55	5.88	2.61	2.02	7.33
N	2.24	0.66	3.03	2.12	1.92	2.29	2.11
O	1.28	3.03	1.48	1.20	1.60	1.14	1.46
Q	1.20	0.33	1.15	0.50	1.19	0.58	0.33
R	1.33	0.58	1.00	0.63	0.41	0.87	0.67
S	0.33	0.58	0.58	0.25	1.11	1.11	0.00
T	2.03	1.67	0.58	0.82	0.65	0.00	0.88
U	0.33	1.76	1.76	2.53	0.75	0.65	2.08
V	0.67	0.67	0.67	0.58	1.22	0.41	1.20
W	0.58	0.67	0.58	0.25	0.85	0.63	0.58
X	1.20	0.33	0.33	0.63	0.50	0.41	0.33

See Table 5.1 for notation.

Table A.15: Hard gauging combined expanded uncertainties for $k = 2$ from operator 1 for G4.

Measurands	1(a)	1(b)	1(c)	1(d)
	$U [\mu\text{m}]$	$U [\mu\text{m}]$	$U [\mu\text{m}]$	$U [\mu\text{m}]$
A	11.23	6.97	3.74	4.64
B	9.44	6.21	1.44	3.07
C	1.76	1.96	4.90	6.01
D	1.09	1.43	4.90	2.48
E	1.90	1.23	2.45	4.02
F	1.12	1.57	2.00	4.02
G	1.00	1.92	2.00	2.04
H	1.17	1.03	2.00	4.02
I	1.12	1.09	4.00	3.19
J	1.12	1.73	2.45	2.48
K	5.13	10.48	4.28	21.70
L	0.08	0.76	0.08	0.49
M	0.08	0.76	0.08	0.49
N	0.08	0.76	0.08	0.49
O	0.08	0.76	0.08	0.49
P	1.97	1.71	2.12	1.81

See Tables 5.1-5.3 for notation.

Table A.16: Hard gauging combined expanded uncertainties for $k = 2$ from operators 2-7 for G4.

Measurands	2	3	4	5	6	7
	$U [\mu\text{m}]$					
A	11.29	2.00	15.81	7.92	10.81	4.56
B	16.19	0.84	5.54	6.15	8.22	5.23
C	7.36	0.02	2.46	2.07	2.51	1.60
D	2.48	8.94	5.10	2.51	4.04	1.19
E	0.41	4.90	5.83	2.07	2.51	1.45
F	6.79	0.02	6.79	3.21	3.78	1.50
G	4.92	4.90	4.90	2.07	0.54	1.57
H	4.92	4.90	2.46	2.51	3.21	1.57
I	4.92	2.00	4.01	3.21	2.51	1.39
J	2.04	2.45	3.17	2.51	4.93	1.70
K	21.68	29.37	46.79	46.50	8.93	9.65
L	0.49	0.08	0.28	0.64	0.73	0.64
M	0.49	0.08	0.28	0.64	0.73	0.64
N	0.49	0.08	0.28	0.64	0.73	0.64
O	0.49	0.08	0.28	0.64	0.73	0.64
P	2.97	2.47	2.21	1.79	2.62	3.96

See Tables 5.1-5.3 for notation.

Table A.17: Hard gauging combined expanded uncertainties for $k = 2$ from operator 1 for G6.

Measurands	1(a)	1(b)	1(c)	1(d)
	$U [\mu m]$	$U [\mu m]$	$U [\mu m]$	$U [\mu m]$
A	2.16	3.67	4.28	9.44
B	1.73	6.26	3.41	6.17
C	1.13	1.71	2.45	2.01
D	1.64	2.75	4.00	4.90
E	1.13	2.77	2.00	2.01
F	1.00	1.68	0.07	0.20
G	2.28	2.11	4.90	2.46
H	2.25	3.55	4.90	0.20
I	1.15	1.16	2.00	4.00
J	2.25	3.09	4.90	2.01
K	2.20	8.71	2.48	3.99
L	0.08	2.32	0.08	1.99
M	0.08	2.31	0.08	1.82
N	0.08	0.99	0.08	0.95
O	0.08	1.20	0.08	0.82
P	1.65	1.69	1.79	1.79

See Tables 5.1-5.3 for notation.

Table A.18: Hard gauging combined expanded uncertainties for $k = 2$ from operators 2-7 for G6.

Measurands	2	3	4	5	6	7
	$U [\mu m]$					
A	6.20	14.72	4.95	5.09	5.22	2.32
B	30.47	8.14	14.04	10.05	11.87	5.97
C	4.01	2.46	2.46	3.76	2.47	2.12
D	0.22	2.01	7.49	2.03	7.49	1.85
E	6.79	2.01	6.33	2.03	7.36	0.61
F	6.79	2.01	2.46	2.03	5.84	1.68
G	4.01	2.01	4.90	2.03	3.76	1.40
H	11.66	2.01	2.46	2.03	8.37	1.88
I	7.35	2.01	5.48	2.03	2.47	1.57
J	11.66	2.01	4.48	2.47	0.34	0.77
K	27.51	22.85	26.37	30.31	36.54	19.05
L	0.36	0.33	0.31	0.42	0.41	0.42
M	0.36	0.33	0.31	0.42	0.41	0.42
N	0.36	0.33	0.31	0.42	0.41	0.42
O	0.36	0.33	0.31	0.42	4.92	0.42
P	3.30	1.70	3.03	2.83	2.10	2.72

See Tables 5.1-5.3 for notation.

Table A.19: Equator combined expanded uncertainties for $k = 2$.

Measurands	G2	G3	G4	G5	G6	G7	G8
	$U [\mu m]$						
A	0.96	0.68	0.73	0.52	0.57	0.32	0.28
B	1.30	0.83	0.94	0.82	1.04	0.28	1.29
C	0.33	1.18	0.41	0.37	0.43	0.40	1.87
D	1.68	0.73	1.06	0.98	1.08	0.73	1.70
E	0.65	0.42	0.56	0.37	0.62	0.70	1.31
F	0.61	1.33	0.67	0.18	0.55	0.17	1.12
G	0.42	1.76	0.92	0.34	0.55	0.16	1.51
H	0.41	1.74	0.57	0.34	0.37	0.30	0.84
I	0.35	1.31	0.94	0.80	0.48	0.76	0.99
J	0.42	1.45	1.04	0.47	0.63	0.20	1.18
K	2.64	2.48	2.58	0.72	1.22	0.72	2.36
L	0.85	1.08	0.70	0.38	0.65	0.21	0.89
M	0.35	0.95	0.51	0.69	0.70	0.24	0.54
N	1.26	0.89	0.65	0.27	0.52	0.33	0.97
O	0.57	0.79	0.76	0.42	0.43	0.29	0.48
P	0.61	1.46	1.34	0.42	1.20	0.29	0.96
Q	1.07	1.98	0.79	1.47	0.95	0.55	0.27
R	1.42	1.93	0.64	0.26	0.85	0.27	1.02
S	0.79	1.24	0.63	0.98	0.56	0.48	0.78
T	1.01	0.80	0.76	1.88	0.68	0.17	0.93
U	0.73	0.63	0.75	0.33	0.94	1.20	1.44
V	1.39	1.13	0.98	1.30	1.10	0.87	1.01
W	0.77	1.10	0.82	1.08	0.87	0.70	0.79
X	1.90	0.70	1.45	1.02	1.58	1.40	1.94

See Table 5.1 for notation.

Table A.20: CMM results for the comparative study.

Measu- rands	G2	G3	G4	G5	G6	G7	G8
	$x [mm]$						
A	49.9652	49.9713	49.9773	49.9656	49.9722	49.9968	49.9879
B	99.9382	100.0140	100.0120	100.0153	99.9827	100.0067	99.9786
C	16.0182	16.0115	16.0022	15.9971	15.9919	16.0154	16.0020
D	16.0176	16.0111	16.0010	15.9982	15.9953	16.0142	16.0020
E	16.0188	16.0095	16.0020	15.9970	15.9915	16.0137	16.0020
F	16.0182	16.0070	16.0000	15.9978	15.9930	16.0124	16.0015
G	16.0186	16.0055	16.0000	15.9962	15.9894	16.0112	16.0000
H	16.0182	16.0060	16.0000	15.9968	15.9920	16.0102	16.0000
I	16.0182	16.0050	16.0020	15.9948	15.9920	16.0092	16.0000
J	16.0182	16.0038	15.9980	15.9953	15.9907	16.0083	16.0010
K	128.9935	128.9944	128.9940	128.9956	128.9960	128.9984	128.9945
L	20.0268	20.0122	20.0125	20.0041	19.9990	20.0103	20.0078
M	20.0267	20.0131	20.0120	20.0044	19.9995	20.0117	20.0087
N	20.0202	20.0096	20.0075	20.0006	19.9942	20.0079	20.0042
O	20.0198	20.0107	20.0075	20.0002	19.9940	20.0094	20.0057
P	0.0578	0.0833	0.0678	0.0764	0.0855	0.0707	0.0955
Q	0.0040	0.0050	0.0035	0.0045	0.0040	0.0048	0.0031
R	0.0039	0.0046	0.0038	0.0036	0.0048	0.0023	0.0043
S	0.0038	0.0227	0.0042	0.0048	0.0045	0.0043	0.0053
T	0.0045	0.0035	0.0041	0.0056	0.0037	0.0029	0.0033
U	0.0034	0.0031	0.0040	0.0073	0.0062	0.0048	0.0054
V	0.0044	0.0031	0.0043	0.0061	0.0056	0.0038	0.0041
W	0.0034	0.0043	0.0052	0.0040	0.0058	0.0037	0.0036
X	0.0045	0.0037	0.0049	0.0071	0.0075	0.0043	0.0061

See Table 5.1 for notation.

Table A.21: OMP and Equator residuals for G2 and G3.

Measurands	Residuals for G2		Residuals for G3	
	OMP [μm]	Equator [μm]	OMP [μm]	Equator [μm]
A	41.95	0.45	18.93	0.47
B	7.10	0.40	13.40	0.40
C	14.91	0.19	15.57	1.03
D	14.18	1.42	13.49	0.61
E	15.78	0.42	9.64	0.26
F	15.84	0.26	13.70	1.00
G	16.17	0.13	12.25	1.15
H	15.30	0.10	12.19	0.91
I	15.15	0.15	10.71	0.49
J	15.10	0.10	8.64	1.06
K	5.95	1.45	5.31	1.91
L	19.56	0.54	14.92	0.88
M	19.30	0.10	8.13	0.67
N	16.89	0.91	16.34	0.66
O	15.30	0.20	15.14	0.56
Q	2.18	0.78	3.82	1.72
R	2.08	1.18	3.07	1.67
S	2.02	0.68	21.23	0.98
T	1.76	0.76	2.24	0.54
U	1.24	0.44	1.68	0.32
V	3.09	1.09	0.77	0.87
W	1.85	0.55	2.46	0.34
X	2.20	1.60	2.00	0.40

See Table 5.1 for notation.

Table A.22: OMP, hard gauging, and Equator residuals for G4.

Measurands	Residuals for G4		
	OMP [μm]	Hard gauging [μm]	Equator [μm]
A	16.40	4.30	0.50
B	4.50	14.00	0.50
C	2.70	1.20	0.30
D	0.70	2.00	0.90
E	0.30	3.00	0.40
F	0.30	2.00	0.50
G	0.60	5.00	0.80
H	0.90	4.00	0.40
I	2.60	1.00	0.80
J	3.20	10.00	0.90
K	6.40	3.00	2.10
L	9.30	11.50	0.50
M	10.30	11.00	0.30
N	8.30	7.50	0.40
O	7.40	7.50	0.50
P	-	1.00	1.00
Q	1.00	-	0.60
R	1.80	-	0.50
S	1.70	-	0.40
T	2.10	-	0.60
U	1.20	-	0.50
V	2.50	-	0.70
W	3.20	-	0.60
X	3.10	-	1.20

See Table 5.1 for notation.

Table A.23: OMP and Equator residuals for G5.

Measurands	Residuals for G5	
	OMP [μm]	Equator [μm]
A	9.33	0.23
B	3.90	0.30
C	0.00	0.30
D	0.22	0.92
E	2.19	0.28
F	1.42	0.08
G	0.61	0.19
H	0.26	0.24
I	2.74	0.74
J	2.68	0.42
K	4.74	0.24
L	16.81	0.19
M	12.06	0.46
N	9.55	0.05
O	8.50	0.20
Q	3.23	1.33
R	2.05	0.05
S	3.17	0.77
T	4.15	1.65
U	3.04	0.04
V	3.62	1.02
W	2.07	0.83
X	5.51	0.71

See Table 5.1 for notation.

Table A.24: OMP, hard gauging, and Equator residuals for G6.

Measurands	Residuals for G6		
	OMP [μm]	Hard gauging [μm]	Equator [μm]
A	16.20	4.20	0.40
B	6.70	3.30	0.50
C	2.10	5.10	0.30
D	0.40	1.70	1.00
E	4.00	5.50	0.50
F	1.90	3.00	0.50
G	4.50	5.60	0.40
H	3.30	2.00	0.30
I	3.50	6.00	0.40
J	5.20	3.30	0.50
K	3.60	1.00	0.60
L	16.40	2.00	0.40
M	12.70	4.50	0.50
N	6.50	4.20	0.30
O	8.40	4.00	0.20
P	-	1.50	0.90
Q	1.70	-	0.80
R	3.30	-	0.60
S	2.40	-	0.40
T	1.40	-	0.50
U	3.30	-	0.60
V	3.60	-	0.80
W	4.40	-	0.60
X	5.20	-	1.30

See Table 5.1 for notation.

Table A.25: OMP and Equator residuals for G7 and G8.

Measurands	Residuals for G7		Residuals for G8	
	OMP [μm]	Equator [μm]	OMP [μm]	Equator [μm]
A	17.01	0.11	14.36	0.04
B	6.70	0.00	0.60	0.90
C	5.95	0.25	1.10	1.70
D	3.41	0.60	1.80	1.50
E	2.17	0.63	1.60	1.20
F	5.49	0.11	0.20	0.90
G	4.68	0.02	0.10	1.00
H	2.68	0.22	1.40	0.70
I	1.23	0.67	1.40	0.80
J	0.66	0.16	1.60	1.00
K	4.40	0.40	4.70	1.70
L	12.01	0.01	11.88	0.72
M	11.85	0.05	10.72	0.28
N	0.61	0.09	2.33	0.67
O	4.06	0.06	4.26	0.24
Q	3.31	0.41	1.83	0.03
R	0.00	0.20	2.53	0.83
S	2.23	0.33	3.76	0.66
T	1.35	0.05	1.54	0.66
U	2.48	0.88	2.44	1.14
V	2.31	0.61	2.33	0.73
W	2.56	0.46	2.10	0.50
X	3.26	1.16	4.94	1.64

See Table 5.1 for notation.

Table A.26: Testing, training, and MLP model 1 standard uncertainties for the comparator.

Probing points	Testing sample standard uncertainties [μm]	Training sample standard uncertainties [μm]	MLP model 1 standard uncertainties [μm]
1	0.07	0.35	0.00
2	0.09	0.40	0.25
3	0.16	0.35	0.18
4	0.24	0.47	0.08
5	0.21	0.41	0.24
6	0.21	0.45	0.12
7	0.36	0.62	0.17
8	0.27	0.45	0.13
9	0.24	0.40	0.14
10	0.10	0.36	0.17
11	0.06	0.32	0.00
12	0.11	0.31	0.18
13	0.18	0.44	0.13
14	0.21	0.40	0.12
15	0.19	0.33	0.17
16	0.20	0.43	0.15
17	0.36	0.66	0.25
18	0.42	0.53	0.08
19	0.22	0.55	0.17
20	0.10	0.41	0.27

See Table 7.3 for notation.

Table A.27: MLP model 2, 3, and 4 standard uncertainties for the comparator.

Probing points	MLP model 2 standard uncertainties [μm]	MLP model 3 standard uncertainties [μm]	MLP model 4 standard uncertainties [μm]
1	0.00	0.00	0.24
2	0.35	0.11	0.24
3	0.36	0.20	0.22
4	0.30	0.20	0.20
5	0.30	0.16	0.20
6	0.28	0.31	0.20
7	0.28	0.43	0.23
8	0.18	0.37	0.24
9	0.18	0.28	0.26
10	0.17	0.13	0.28
11	0.00	0.00	0.27
12	0.17	0.13	0.29
13	0.19	0.29	0.27
14	0.19	0.39	0.26
15	0.31	0.45	0.25
16	0.26	0.34	0.23
17	0.24	0.15	0.23
18	0.28	0.19	0.23
19	0.36	0.21	0.23
20	0.37	0.12	0.26

See Table 7.3 for notation.

Table A.28: MLP model 5 and Elman model 1 standard uncertainties for the comparator.

Probing points	MLP model 5 standard uncertainties [μm]	Elman model 1 standard uncertainties [μm]
1	0.28	0.00
2	0.28	0.30
3	0.24	0.31
4	0.22	0.38
5	0.21	0.40
6	0.20	0.29
7	0.21	0.35
8	0.19	0.26
9	0.18	0.24
10	0.18	0.19
11	0.16	0.00
12	0.18	0.20
13	0.19	0.23
14	0.20	0.26
15	0.22	0.38
16	0.22	0.30
17	0.24	0.39
18	0.25	0.40
19	0.26	0.35
20	0.30	0.33

See Tables 7.3 and 7.4 for notation.

Table A.29: Elman model 2 and 3 standard uncertainties for the comparator.

Probing points	Elman model 2 standard uncertainties [μm]	Elman model 3 standard uncertainties [μm]
1	0.20	0.14
2	0.21	0.14
3	0.18	0.12
4	0.16	0.12
5	0.16	0.14
6	0.15	0.15
7	0.19	0.19
8	0.19	0.22
9	0.21	0.25
10	0.25	0.33
11	0.23	0.32
12	0.25	0.32
13	0.23	0.29
14	0.21	0.23
15	0.20	0.20
16	0.19	0.18
17	0.19	0.16
18	0.19	0.15
19	0.20	0.14
20	0.21	0.15

See Table 7.4 for notation.

Appendix B

Discrete-time Markov chains

A Markov chain is a particular type of stochastic process that satisfies the Markov property [137, 138]. It requires a finite set \mathcal{S} of possible states and transition probabilities p_{ij} whose collection $\{p_{ij} : i, j \in \mathcal{S}\}$ satisfies $p_{ij} \geq 0$ for all $i, j \in \mathcal{S}$, and

$$\sum_{j \in \mathcal{S}} p_{ij} = 1$$

for each $i \in \mathcal{S}$. A Markov chain is mathematically described by:

$$P(X_{n+1} = j \mid X_n = i) = p_{ij} \quad (\text{B.1})$$

for any positive integer n and any $i, j \in \mathcal{S}$. The Markov property requires that:

$$P(X_{n+1} = j \mid X_n = i, X_{n-1} = i_{n-1}, \dots, X_0 = i_0) = p_{ij} \quad (\text{B.2})$$

for all n and all $i, j, i_0, \dots, i_{n-1} \in \mathcal{S}$. The probability of any particular sequence of future states can be computed by:

$$P(X_0 = i_0, X_1 = i_1, \dots, X_n = i_n) = P(X_0 = i_0) p_{i_0 i_1} \cdots p_{i_{n-1} i_n}. \quad (\text{B.3})$$

Assuming that the initial state X_0 is equal to some i_0 then:

$$P(X_1 = i_1, \dots, X_n = i_n \mid X_0 = i_0) = p_{i_0 i_1} \cdots p_{i_{n-1} i_n}. \quad (\text{B.4})$$

The n -step transition probabilities are defined by:

$$r_{ij}(n) = P(X_n = j \mid X_0 = i) \tag{B.5}$$

and can be calculated using the Chapman-Kolmogorov equation [139]:

$$r_{ij}(n) = \sum_{k \in S} r_{ik}(n-1)p_{kj} \tag{B.6}$$

for $n > 1$, and all i, j starting with $r_{ij}(1) = p_{ij}$. Asserting that for every state j , $r_{ij}(n)$ approaches a limiting value π_j which is independent of i , then, π_j is called the steady-state probability of j because for large n , $\pi_j \approx P(X_n = j)$. The steady-state probabilities π_j form a probability distribution on the state space, which is called the stationary distribution of the chain, because they sum to 1.